

A MODEL FOR THE RIGID BODY MOTIONS OF SKEW BRIDGES

Thesis by

Emmanuel Maragakis

In Partial Fulfillment of the Requirements

for the Degree of

Doctor of Philosophy

California Institute of Technology

Pasadena, California

(Submitted December 21, 1984)

1985

© 1984

Emmanuel Maragakis

All Rights Reserved

ACKNOWLEDGMENTS

I wish to express my sincere appreciation and gratitude to my research advisor, Professor Paul C. Jennings, first of all for suggesting the research topic and then for providing guidance, encouragement, understanding, and many valuable suggestions during the course of this study and in the preparation of this thesis. I am also thankful to the entire faculty of Civil Engineering and Applied Mechanics of Caltech for the excellent instruction I received and for the helpful discussion of some of the problems which were encountered.

The financial support provided by the National Science Foundation and the California Institute of Technology throughout my graduate studies is gratefully appreciated.

Special thanks are due to Miss Jeanie Pratt for her conscientious and skillful work during the typing of this thesis and to Mrs. Kim Jeffrey for her help with the illustrations.

My sincere thanks to all my friends and, particularly, to Costas Chazapis for his valuable help during the preparation of this thesis.

I want to extend my heartfelt appreciation to my wife, Mary, for her love, patience, and understanding which were very crucial for the completion of this work and to my newborn son, Antonios, for the numerous moments of joy and relaxation he offered me during the last five months of my effort.

Finally, I wish to dedicate this thesis wholeheartedly to my parents, Antonios and Dimitra Maragakis, who have done so much for me during my whole life. Without their continuous moral and economic support, their inspiration, and their encouragement, this thesis may never have been written.

ABSTRACT

This thesis investigates the rigid body motions of skew bridges, concentrating on the in-plane translational and rotational displacements of the bridge deck induced by impact between the deck and the abutments. Experience in the San Fernando Earthquake of February 9, 1971 demonstrates that this feature is particularly important for skew bridges.

A simple model, in which the bridge deck is represented by a rigid rod restricted by column and abutment springs is examined first. This model illustrates the mechanism by which in-plane rotational vibrations is triggered after the closure of the gap between the bridge deck and the abutment. It also shows that the force-deflection relations of the columns and the abutments are particularly important features for the response of the bridge. Methods for the exact and approximate estimation of the elastic stiffness of elastically founded, tapered bridge columns with octagonal cross section are presented next. The methods are applied to a bridge used later as an example. In addition, the yielding of the columns is examined and the force-deflection relations for bending about two orthogonal axes are estimated.

The abutments are treated as rigid bodies and the soil embankments as Winkler Foundations with elastic spring constants increasing with depth. For the examination of the yielding of soil the Rankine theory is used. Based on these assumptions an approximate force-deflection relation for the abutments is constructed.

The response of a more complicated bridge model applied to a bridge near Riverside, California is examined at the end of the thesis and examples of the results are given. This model, in which the bridge deck

is still represented as a rigid rod, has three in-plane degrees of freedom: two orthogonal displacements and a rotation, and is capable of capturing many of the more important features of the nonlinear, yielding response of skew bridges during strong earthquake shaking.

TABLE OF CONTENTS

ACKNOWLEDGMENTS.....	ii
ABSTRACT.....	iii
CHAPTER 1: INTRODUCTION.....	1
1.1. BACKGROUND ON THE SEISMIC RESPONSE OF BRIDGES.....	1
1.2. STATEMENT OF THE PROBLEM.....	2
1.3. EXAMPLES OF SKEW BRIDGES WHICH SHOWED ROTATION OF THEIR DECKS DURING RECENT EARTHQUAKES.....	3
1.4. ORGANIZATION OF THE THESIS.....	7
CHAPTER 2: A SIMPLE MODEL FOR THE RIGID BODY ROTATIONS OF SKEW BRIDGES.....	9
2.1. INTRODUCTION.....	9
2.2. MOTIONS AND DISTORTIONS OF A BRIDGE DECK.....	9
2.3. THE MODEL.....	11
2.4. EXCITATION-GEOMETRY AND FORCES OF THE MODEL.....	13
2.5. EQUATIONS OF MOTION.....	16
2.6. PARAMETERS OF IMPORTANCE.....	18
2.7. EXAMPLE OF RESPONSE.....	20
2.8. EFFECTS OF THE VARIATION OF PARAMETERS.....	26
2.8.1. Rod with Restoring Springs Close to the Center of Mass.....	26
2.8.1.1. Effects of the Angle of Skewness.....	26
2.8.1.2. Effects of the Abutment Stiffness.....	32
2.8.1.3. Effects of the Abutment Gap.....	43
2.8.2. Deck with Widely Spaced Columns.....	53
2.9. GENERAL CONCLUSIONS AND REMARKS.....	58
CHAPTER 3: ELASTIC STIFFNESS OF BRIDGE COLUMNS WITH PARABOLIC FLARES.....	61
3.1. INTRODUCTION.....	61

3.2.	EQUATIONS AND BOUNDARY CONDITIONS FOR A BERNOULLI-EULER BEAM.....	63
3.3.	STIFFNESS OF A BRIDGE COLUMN WITH OCTAGONAL CROSS SECTION AND PARABOLIC FLARE AT THE TOP AND FOUNDATION SPRINGS AT THE BOTTOM.....	65
3.3.1.	Equations of a Tapered Column with Foundation Springs.....	65
3.3.2.	General Expressions for the Geometric Properties of the Parabolic Flare of the Column with Octagonal Cross Sections.....	73
3.3.3.	Evaluation of the Integrals L_1^Y , L_2^Y , and L_3^Y in the Case of a Parabolic Flare with Octagonal Cross Sections.....	77
3.3.4.	Evaluation of the Integrals L_1^X , L_2^X , and L_3^X in the Case of a Parabolic Flare with Octagonal Cross Sections.....	89
3.3.5.	Summary of the Basic Steps for the Analytical Evaluation of the Stiffness.....	90
3.4.	APPROXIMATE ESTIMATION OF THE STIFFNESS OF A TAPERED COLUMN.....	91
3.4.1.	Estimation of the Stiffness for Bending about the Y Direction.....	91
3.4.2.	Estimation of the Stiffness for Bending about the X Direction.....	96
3.5.	EXAMPLE.....	96
3.5.1.	Analytical Solution of the Problem.....	98
3.5.2.	Approximate Solution of the Problem.....	103
3.5.3.	Yielding of the Column along the Two Directions of Bending.....	106
3.5.3.1.	Estimation of the Ultimate Bending Moments.....	110
3.5.3.2.	Construction of the Force-Deflection Diagrams for Bending.....	110
CHAPTER 4:	ESTIMATION OF THE EQUIVALENT ABUTMENT STIFFNESS.....	113
4.1.	INTRODUCTION.....	113
4.2.	PRELIMINARY CONCEPTS.....	114

4.2.1. Abutments.....	114
4.2.2. Geostatic Stresses in the Soil.....	114
4.2.3. Rankine Theory.....	116
4.2.4. Active Thrust and Passive Resistance.....	119
4.3. BASIC ASSUMPTIONS.....	121
4.4. ESTIMATION OF THE EQUIVALENT ABUTMENT STIFFNESS.....	123
4.4.1. Statement of the Problem.....	123
4.4.2. Solution of the Problem in the Case of Winkler Foundation.....	123
4.4.3. Yielding of Regions of the Two Soil Deposits.....	128
4.4.3.1. Yielding of the Regions of Deposit 1.....	128
4.4.3.2. Yielding of the Regions of Deposit 2.....	132
4.4.4. Estimation of the Equivalent Abutment Stiffness in the General Case.....	136
4.5. EXAMPLE.....	143
4.6. SOLUTION OF THE PROBLEM IN THE CASE OF DISCRETE SPRINGS....	148
CHAPTER 5:	153
5.1. INTRODUCTION.....	153
5.2. THE MODEL.....	154
5.3. FORCES.....	158
5.3.1. Column Forces.....	158
5.3.2. Pad Forces.....	159
5.3.3. Abutment Forces.....	160
5.4. EQUATIONS OF MOTION.....	161
5.5. EXAMPLE OF RESPONSE.....	164
5.5.1. Estimation of the Parameters.....	166
5.5.2. Cases Examined.....	172
CHAPTER 6: SUMMARY AND CONCLUSIONS.....	197

REFERENCES.....	204
APENDICES.....	208
A. ESTIMATION OF ULTIMATE BENDING MOMENTS.....	208
B. EVALUATION OF FOUNDATION SPRING CONSTANTS AND SOIL PROPERTIES.....	215

CHAPTER 1

INTRODUCTION

1.1 BACKGROUND ON THE SEISMIC RESPONSE OF HIGHWAY BRIDGES

The 1971 San Fernando Earthquake revealed the vulnerability of highway bridges to earthquake loadings and, thus, presented a major turning point in the development of research on the seismic response of freeway structures. Actually, prior to the San Fernando Earthquake, very little damage was observed worldwide to reinforced concrete bridges as a direct result of earthquake shaking. According to Imbsen, Nutt and Penzien (Ref. 2) the damage to bridges prior to the San Fernando Earthquake had been caused by:

- (i) Tilting, settlement and overturning of substructures,
- (ii) Displacement of supports and anchor bolt breakage, and
- (iii) Settlement of approach fills and wingwall damage.

More specifically, in California from 1933 until 1971, eleven separate earthquakes ranging in magnitude from 5.4 to 7.7 on the Richter scale affected approximately 1,000 bridges. However, none of these bridges was close to the area of intense shaking and the total amount of damage was about \$100,000. In the case of the San Fernando Earthquake, many bridges were located within the zone of the intense shaking and the resulting damage was approximately \$6,500,000 for this earthquake alone (Ref. 3).

As a result of the San Fernando Earthquake, there has been an increased public awareness of the seriousness of the earthquake hazard to highway bridges. A reflection of this concern was the recognition of the need for extensive research in order to provide engineers with information about designing highway bridges that are more earthquake resistant. Thus, immediately following the San Fernando Earthquake,

research efforts were initiated to develop new seismic design criteria taking into account the vibrational properties of the bridge elements and the soil (Ref. 4). The result of these efforts was the formation of the basis for a new national seismic bridge design code (Ref. 4). In addition, publication of many research results provided explanations for the observed behavior of individual bridges during earthquakes (especially the San Fernando Earthquake) or predicted the seismic response of particular bridges (Refs. 2 and 8).

These research efforts paved the way for significant advances during the last decade in the design and construction of seismic resistant bridges. However, in view of the complexity of the problem, significant gaps still remain in the understanding of the vibrational response of highway structures; and numerous aspects of the problem remain still unexplored. The solution of these problems requires the continuation of both analytical and experimental research.

1.2 STATEMENT OF THE PROBLEM

One of the observations from damage to freeway structures caused by the San Fernando earthquake was that several moderate span bridges with relatively large skew angles showed a tendency to rotate in a horizontal plane in a direction that increased their skewness (Refs. 5, 6, and 7). The same behavior was later observed during the recent Coalinga Earthquake of May 1983. In the San Fernando Earthquake this susceptibility of skewed bridges to rotational displacements caused, in some cases, severe damage to columns and abutments. The damage to bridges was relatively minor during the Coalinga Earthquake.

It has been concluded (Ref. 5) that this rotation was a direct result of the interaction between the structure and the approach fill,

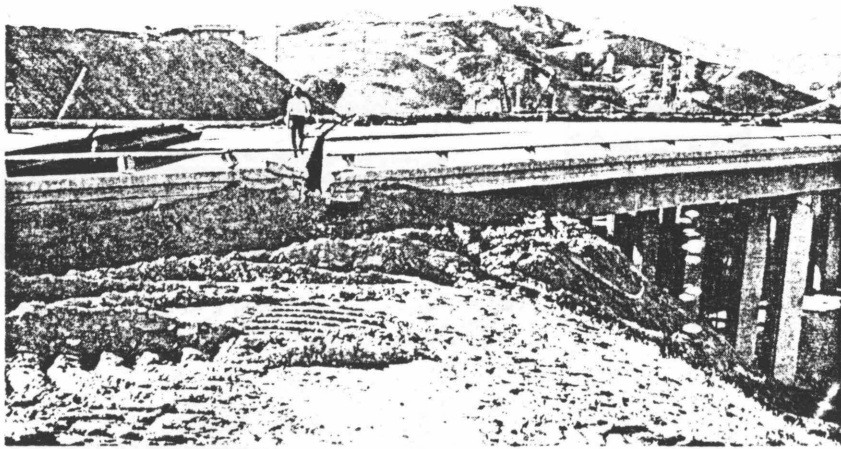
and it was suggested that research on this phenomenon was required. This is the subject of this thesis which has as its purpose the investigation of the in-plane rotational vibrations of short span skew highway bridges, including the effects of interaction with the abutments.

1.3 EXAMPLES OF SKEW BRIDGES WHICH SHOWED ROTATION OF THEIR DECKS DURING RECENT EARTHQUAKES

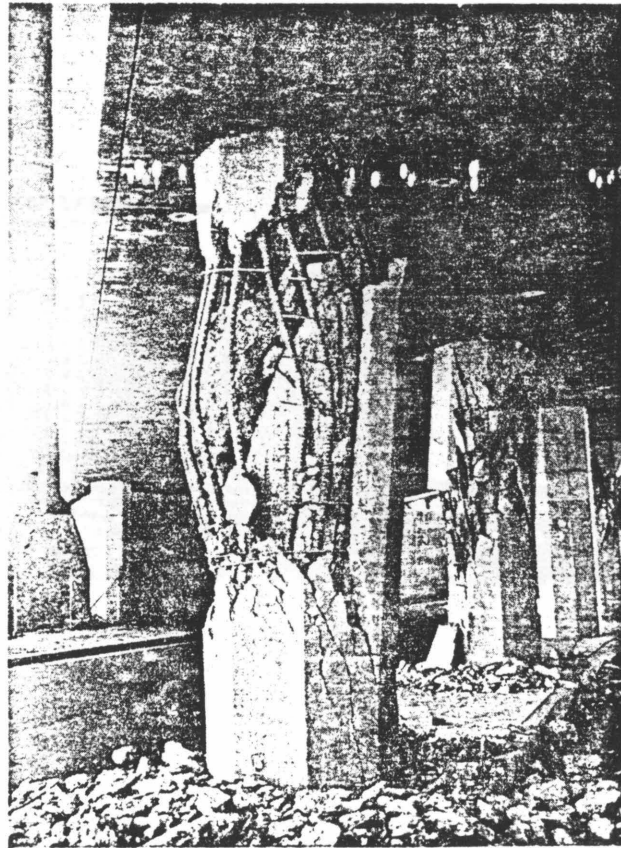
Some of the bridges that were highly susceptible to in-plane, rotational displacements and which suffered extensive damage during the San Fernando Earthquake include the following.

a. The San Fernando Road Overhead (Refs. 5 and 6) The two San Fernando Road Overhead bridges, part of the Golden State-Foothill Freeway interchange, are seven-span skew structures that carry the Golden State Freeway over the San Fernando Road and the Southern Pacific Railroad. The central spans over the railroad were constructed of both steel and precast prestressed concrete girders. The other spans are of reinforced concrete box construction. The structure suffered collapse of the simply-supported steel girder spans. It seems probable that the steel girders fell from their steel bearings and then, with the onset of large horizontal deformation, the girder span rotated in a horizontal plane by the pounding at skew joints until some of the girders slipped free from the piers. In Fig. 1.1a one can see the permanent set of the bridge in the direction of increasing skewness.

b. Northbound Truck Route Undercrossing (Refs. 5 and 6) This bridge, which is also part of the Golden State-Foothill Freeway interchange is a three-span continuous concrete box bridge approximately 225 feet long. It has large angles of skewness at each abutment. The bridge rotated in a horizontal plane about the western end resulting in



a



b

FIG. 1.1 DAMAGE TO HIGHWAY BRIDGES DUE TO ROTATION OF THEIR DECKS DURING THE SAN FERNANDO EARTHQUAKE

- a. San Fernando Road Overhead
- b. Foothill Blvd. Undercrossing

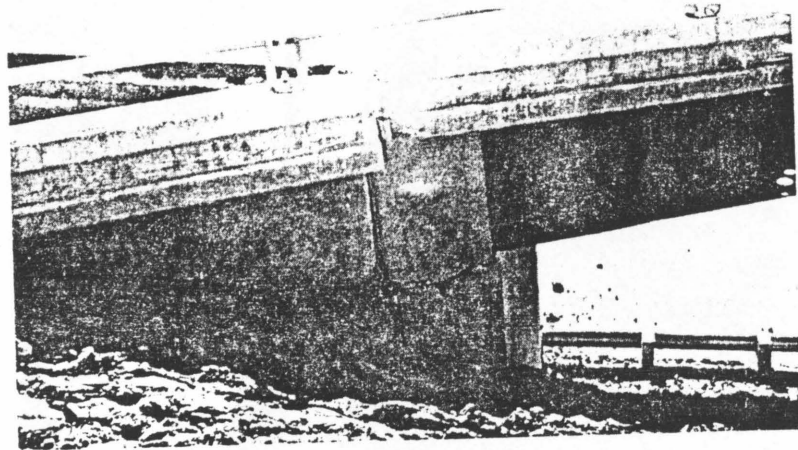
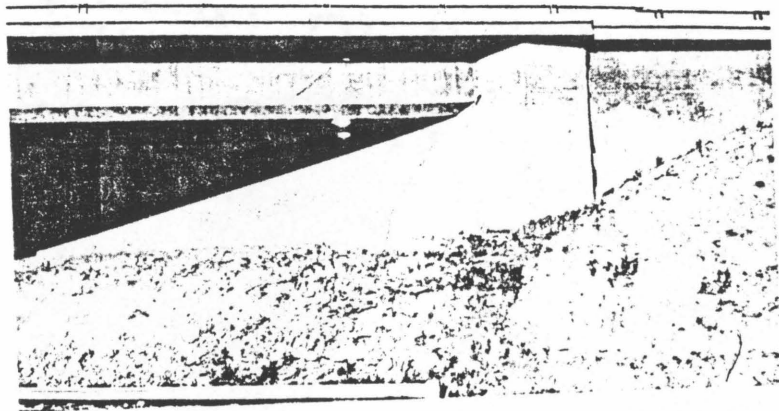


FIG. 1.2 DAMAGE TO HIGHWAY BRIDGES DUE TO ROTATION
OF THEIR DECKS DURING THE SAN FERNANDO
EARTHQUAKE
Northbound Truck Route Undercrossing

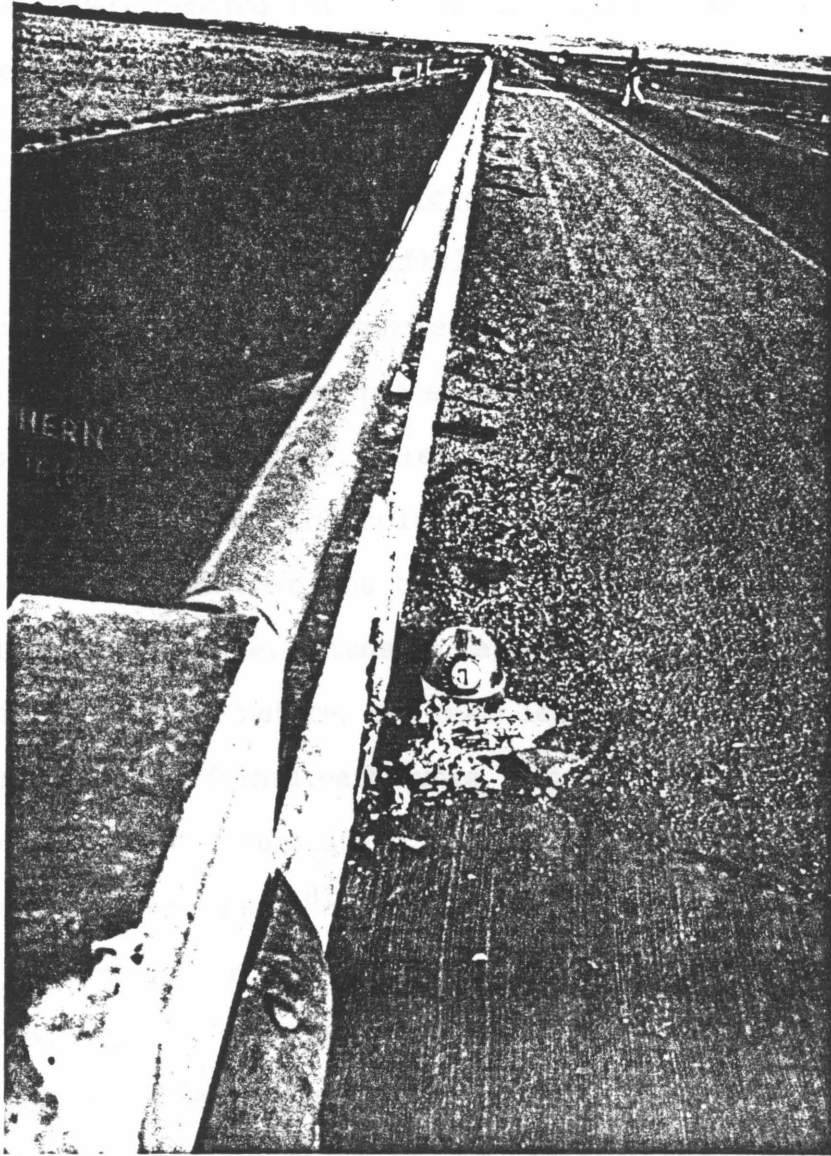


FIG. 1.3 DAMAGE TO HIGHWAY BRIDGE DUE TO ROTATION
OF ITS DECK DURING THE 1983 COALINGA
EARTHQUAKE

a large permanent displacement of the superstructure at the eastern abutment and severe bending failures at the tops of the columns in the eastern pier. Pictures of the damage to this bridge are shown in Fig. 1.2.

c. Foothill Boulevard Undercrossing (Refs. 5 and 6) This structure, which is part of the Foothill Freeway Bridges, is a pair of four-span continuous reinforced concrete box girder skewed bridges. The bridge rotated in the horizontal plane, and a permanent offset of about four inches in the direction of increasing skewness was observed at the abutments. The damage to the columns of this bridge is shown in Fig. 1.1b. It appeared that the bridge rotated at about the third column, which did not suffer extensive damage.

Damage of a similar nature, but much less intense, occurred during the 1983 Coalinga, California earthquake. Fig 1.3 shows the rotation of the skew bridge where Interstate 5 crosses the railroad near Coalinga (The bridge is marked 5.FRE 8⁸¹). The bridge experienced a rotational deflection of about one inch, which was accompanied by minor spalling of the reinforced concrete railing wall.

1.4 ORGANIZATION OF THE THESIS

This thesis has been divided into six chapters. Chapter 1 is a general introduction with a brief history of the research on the seismic response of bridges and a statement of the problem to be studied in the thesis. Chapter 2 presents the examination of a simple model for the rigid body motions of skew bridges. The relatively stiff bridge deck is modeled as a rigid body. The identification of the important parameters and their effects on the response of the model are the principal features of this chapter. Two of the most important elements in the

nonlinear response of skew bridges are believed to be the bridge columns and the abutments. Chapters 3 and 4 present methods for the estimation of the yielding force-deflection relations for the bridge columns and abutments, respectively. Examples of the applications of the methods are included in both chapters. Chapter 5 introduces a more detailed model in the dynamics of skew bridges. The model includes the nonlinear effect of the abutments, expansion gaps, yielding of the columns, and elastometric pads. This chapter also presents some examples of the earthquake response of a mathematical model based on the Nichols Road Overcrossing (Bridge #56-725 near Riverside, California). Chapter 6 includes a summary of the thesis and some conclusions based on the research.

Mathematical notations have been defined where they first appear, while some formulas and details of the solutions of some examples appear in the appendices.

CHAPTER 2

A SIMPLE MODEL FOR THE RIGID BODY ROTATIONS OF SKEW BRIDGES

2.1 INTRODUCTION

The purpose of this chapter is to develop and analyze a simple model which captures the basic features of the complicated rigid body motions of a skew bridge.

In the first part of the chapter, the possible distortions of a bridge deck are described. Then a simple model of a skew bridge is proposed and the simplified assumptions on which the model is based are discussed. Following next is the derivation of the equations of motion of the model along with the identification and discussion of the important parameters. Finally, the kinematic mechanism of the model is described, the effects of several parameters on the dynamic response of the model are examined, and some conclusions are drawn concerning more detailed modeling of skew bridges.

2.2 MOTIONS AND DISTORTIONS OF A BRIDGE DECK

Basically, there are six principal types of motion of a bridge deck relative to the ground of concern here; these are shown in Fig. 2.1 and include:

- a. Rigid body longitudinal translation during which the deck translates longitudinally as a rigid body,
- b. Rigid body lateral translation where the deck translates laterally as a rigid body,
- c. Rigid body rotation about a vertical axis during which the deck rotates in its own plane,

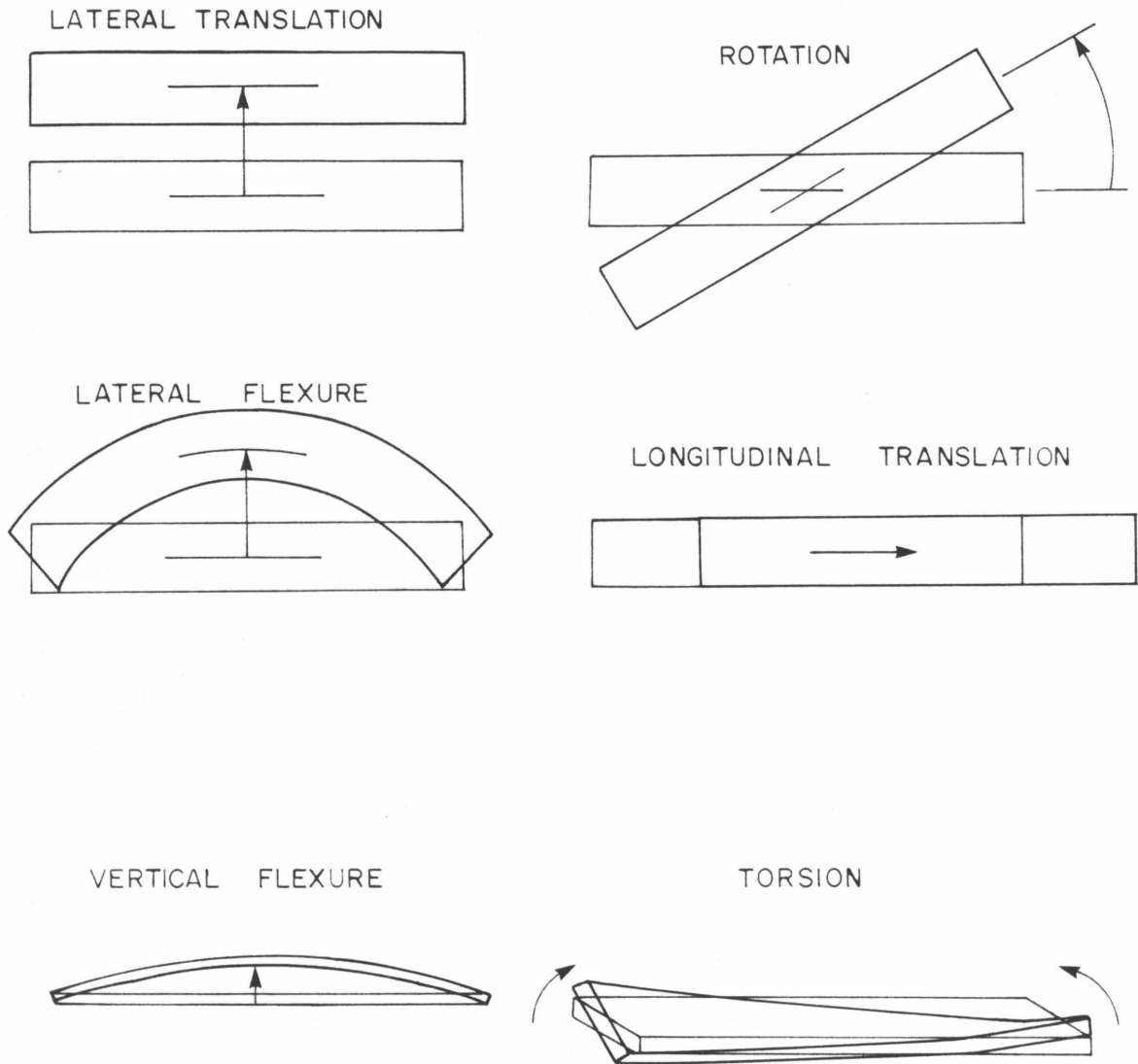


FIG. 2.1 POSSIBLE TYPES OF DISTORTION OF A BRIDGE DECK
RELATIVE TO THE GROUND

- d. Vertical flexure during which the deck bends in a vertical plane,
- e. Lateral flexure in which the deck bends in its plane, and
- f. Torsional distortion during which the deck is twisted about an axis parallel to the centerline of the roadway.

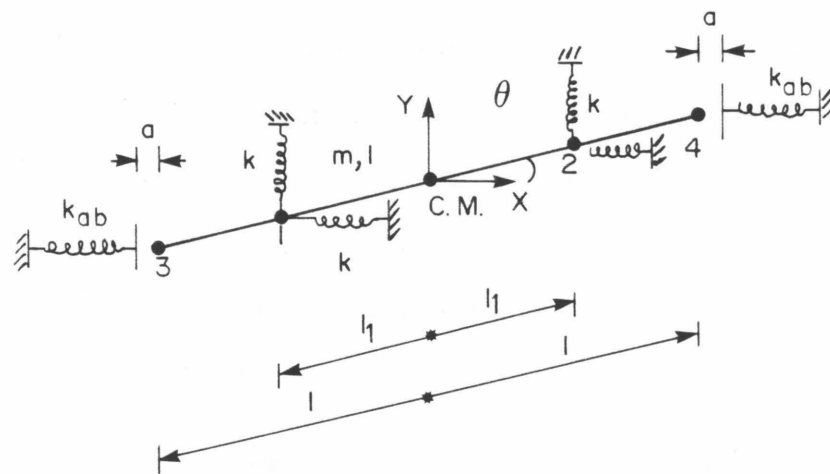
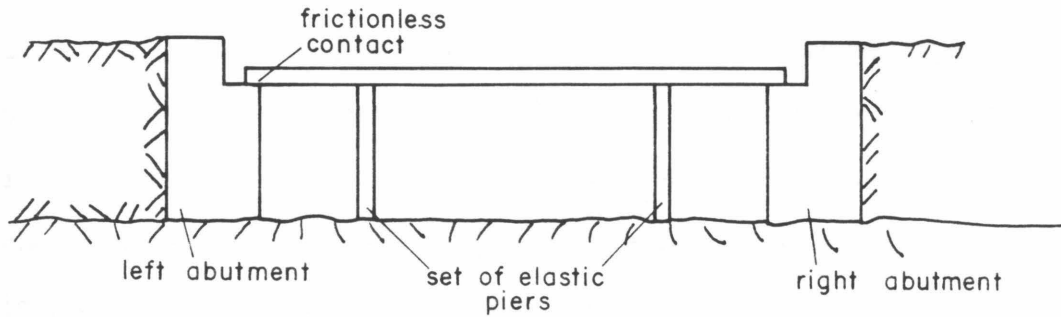
2.3 THE MODEL

The most basic assumption on which the model is based is the rigidity of the bridge deck. Thus, the deck is represented as a one-dimensional rigid bar having the mass and length of the real deck. Consequently, the model is capable of capturing only rigid body motions a, b and c. Motions d, e and f will be neglected.

For simplicity, the model is assumed to be undamped; and the only lateral resisting mechanisms taken into account are the bridge piers and the abutments.

Each set of piers is idealized by two linearly elastic springs. One spring is directed in the longitudinal direction and resists distortions of type a and one spring is directed in the lateral direction and resists distortions of type b. The two springs are assumed to have equal stiffness, k , which can be estimated from the properties of the piers.

It is also assumed that there are two sets of piers symmetrically located with respect to the center of mass of the deck. Thus, the resulting model is symmetric with respect to both the longitudinal axis, X , and the lateral axis, Y . The inclusion of only two sets of piers in the model restricts it to the case of moderate span bridges. The rotational resistance of the model comes from the moments of the pier



X longitudinal direction

a abutment gap

Y lateral direction

θ angle of skewness

k pier springs

m mass of the deck

k_{ab} .. abutment springs

I mass moment of inertia of the deck

FIG. 2.2 SIMPLIFIED MODEL OF A SKEW BRIDGE

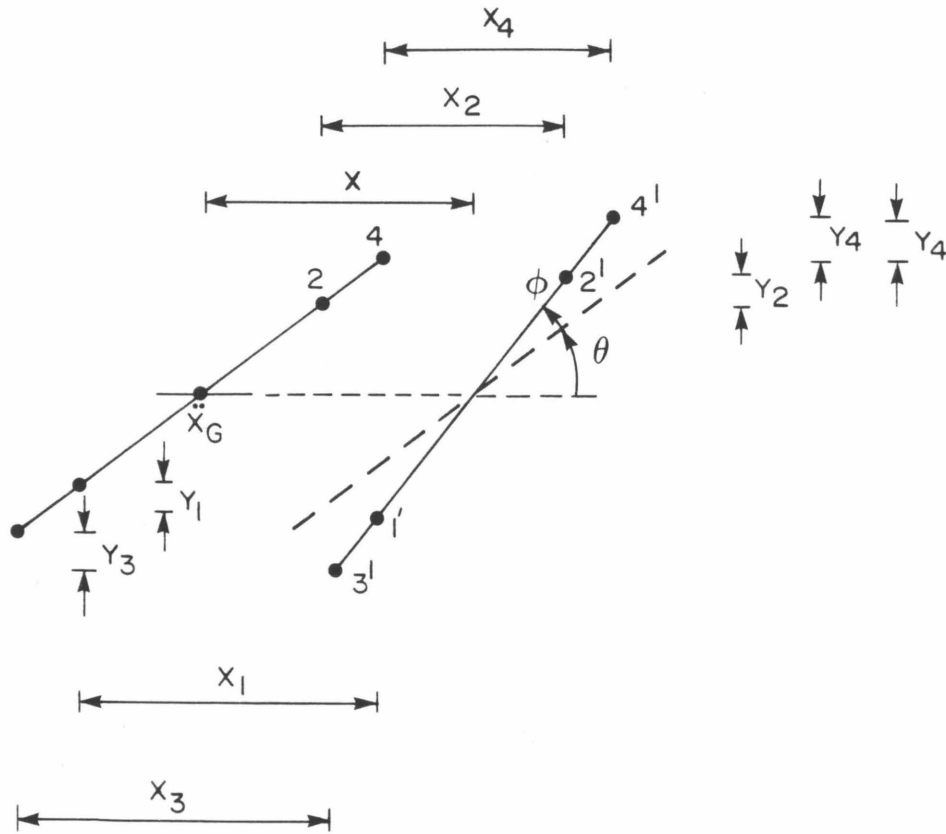
springs generated by rotation about the center of mass of the deck. No other form of rotational resistance is included.

Each abutment is represented by a gap in the longitudinal direction, which, in practice, is used to allow thermal expansion of the bridge deck and a linearly elastic spring of stiffness k_{ab} also oriented in the longitudinal direction. The values of the length of the gap and the stiffness of the spring are the same for both abutments, so symmetry is preserved. The contact between the deck and the abutments is assumed to be frictionless. Finally, the bridge is assumed to be skew at angle θ with respect to the longitudinal direction. The model is illustrated in Fig. 2.2.

Summarizing the above assumptions, we can see that, basically, the model is a rigid bar supported by springs with a gap at each end where springs modeling the abutment are located. The model has considerable symmetry, but the skewness of the deck with respect to the abutments means that longitudinal motion large enough to close the abutment gaps will induce rotation.

2.4 EXCITATION - GEOMETRY AND FORCES OF THE MODEL

To simplify the equations of motion, we assume that the only excitation is ground motion directed along the longitudinal X-axis. This assumption, combined with the symmetry of the model, leads to motion of the center of mass only along the X-axis. All the other points of the deck can move in the Y direction only as a result of rotation in the X, Y plane if such rotation occurs. Therefore, the model has two degrees of freedom: longitudinal translation and rotation in the X, Y plane.



Longitudinal Displacements

$$X_1 = X + l_1 \sin \theta \phi$$

$$X_2 = X - l_1 \sin \theta \phi$$

$$X_3 = X + l \sin \theta \phi$$

$$X_4 = X - l \sin \theta \phi$$

Lateral Displacements

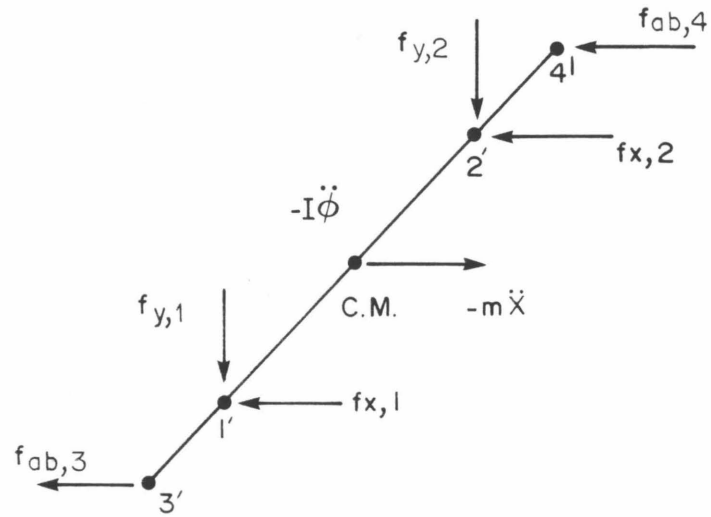
$$Y_1 = -l_1 \cos \theta \phi$$

$$Y_2 = l_1 \cos \theta \phi$$

$$Y_3 = -l \cos \theta \phi$$

$$Y_4 = l \cos \theta \phi$$

FIG. 2.3 GEOMETRY OF THE MODEL FOR SMALL DISPLACEMENTS



$$f_{x,1} = k(x + l_1 \sin \theta \phi)$$

$$f_{y,1} = -k l_1 \cos \theta \phi$$

$$f_{x,2} = k(x - l_1 \sin \theta \phi)$$

$$f_{y,2} = k l_1 \cos \theta \phi$$

$$f_{ab,4} = b_4 k_{ab} (x - l \sin \theta \phi - a)$$

$$f_{ab,3} = b_3 k_{ab} (x + l \sin \theta \phi + a)$$

$$b_4 = \begin{cases} 1 & \text{if } x_4 > a \\ 0 & \text{otherwise} \end{cases}$$

$$b_3 = \begin{cases} 1 & \text{if } x_3 < -a \\ 0 & \text{otherwise} \end{cases}$$

FIG. 2.4 FORCES IMPOSED ON THE MOVING DECK

The geometry needed for the model includes expressions for the displacements of points 1, 2, 3, and 4 of the deck as functions of X and ϕ . These expressions are presented in detail in Fig. 2.3. The equations were derived based on the assumption of small displacements and small angles of rotation ($\sin \phi \approx \phi$, $\cos \phi \approx 1$). The displacements of every point are measured with respect to the initial position of the point with positive displacements occurring in the positive direction of the corresponding coordinate axis.

The forces which are exerted on the deck during its motion come from the piers, the abutment, and the inertia of the deck itself. The forces of the piers and the abutments are calculated as the reactions of linearly elastic springs. It should be pointed out that abutment forces at points 3 and 4 of the deck occur only when the left or right gaps, respectively, are closed. To account for this, coefficients b_3 and b_4 are introduced into the equations. These coefficients take the values of 1 or 0 depending on the closure of the gaps. The forces which act on the deck are given in detail in Fig. 2.4.

2.5 EQUATIONS OF MOTION

The equations of motion are derived using Newton's second law written about the center of gravity.

$$\Sigma F_x = m\ddot{x} \quad (2.1)$$

$$\Sigma M = I\ddot{\phi} \quad (2.2)$$

From (2.1) and the expression of the forces provided in Fig. 2.4, one gets:

$$\begin{aligned} -f_{x,1} - f_{x,2} - f_{ab,4} - f_{ab,3} - m\ddot{x}_G &= m\ddot{x} \quad \text{or} \\ -k(x + l_1 \sin \theta \phi) - k(x - l_1 \sin \theta \phi) - b_4 k_{ab}(x - l \sin \theta \phi - a) \\ - b_3 k_{ab}(x + l \sin \theta \phi + a) - m\ddot{x}_G &= m\ddot{x} \end{aligned} \quad (2.3)$$

From equation (2.3), one can find the first equation of motion.

$$\begin{aligned}
 x + \frac{2k + (b_3 + b_4)k_{ab}}{m} X + \frac{b_3 - b_4}{m} k_{ab} l \sin\theta\phi \\
 + \frac{b_3 - b_4}{m} k_{ab} a = - X_G
 \end{aligned} \quad (2.4)$$

Similarly, equation (2.2) gives:

$$\begin{aligned}
 -f_{x,1} l_1 \sin(\theta + \phi) + f_{y,1} l_1 \cos(\theta + \phi) + f_{x,2} l_1 \sin(\theta + \phi) - \\
 f_{y,2} l_1 \cos(\theta + \phi) + f_{ab,4} l \sin(\theta + \phi) - f_{ab,3} l \sin(\theta + \phi) = I\phi
 \end{aligned}$$

or

$$\begin{aligned}
 -k(x + l_1 \sin\theta\phi) l_1 (\sin\theta + \phi \cos\theta) - k l_1 \cos\theta\phi l_1 (\cos\theta - \phi \sin\theta) + \\
 + k(x - l_1 \sin\theta\phi) l_1 (\sin\theta + \phi \cos\theta) - k l_1 \cos\theta\phi (\cos\theta - \phi \sin\theta) + \\
 + b_4 k_{ab} (x - l \sin\theta\phi - a) l (\sin\theta + \phi \cos\theta) - \\
 - b_3 k_{ab} (x + l \sin\theta\phi + a) l (\sin\theta + \phi \cos\theta) = I\phi
 \end{aligned} \quad (2.5)$$

From (2.5), after carrying out the algebra and neglecting the second order terms, one finds the second equation of motion:

$$\begin{aligned}
 \phi + \frac{1}{I} [2k l_1^2 \sin^2\theta + k_{ab} l^2 (b_3 + b_4) \sin^2\theta + (b_3 + b_4) k_{ab} l \cos\theta a + \\
 2k l_1^2 \cos^2\theta] \phi + \frac{1}{I} (b_3 - b_4) k_{ab} l \sin\theta X + \\
 + \frac{1}{I} (b_4 + b_3) k_{ab} a l \sin\theta = 0
 \end{aligned} \quad (2.6)$$

Let $\omega^2 = \frac{k}{m}$ (2.7)

(Note that the small amplitude frequency of the rod is

$$f_x = \sqrt{\frac{2k}{m}} = \sqrt{2\omega_x}$$

Let γ be the nondimensional ratio of the abutment stiffness k_{ab} to the pier stiffness k :

$$k_{ab} = \gamma k \quad (2.8)$$

Note also that the mass moment of inertia, I , of the node modeling the deck is given by:

$$I = \frac{ml^2}{3} \quad (2.9)$$

The combination of (2.4), (2.6), (2.7), (2.8), (2.9) gives:

$$\begin{aligned} \ddot{X} + [2 + (b_3 + b_4)\gamma] \frac{2}{X} \dot{X} + (b_3 - b_4)\gamma \sin\theta \omega_X^2 \phi + \\ (b_3 - b_4)\gamma a \omega_X^2 = X_G \end{aligned} \quad (2.10)$$

$$\begin{aligned} \ddot{\phi} + [6 \frac{l_1}{l^2} \sin^2\theta + 3\gamma(b_3 + b_4)\sin^2\theta + 3\gamma(b_3 + b_4) \frac{a}{l} \cos\theta \\ + 6 \frac{l_1^2}{l^2} \cos^2\theta] \omega_X^2 \phi + 3(b_3 - b_4)\gamma \frac{\sin\theta}{l} \omega_X^2 X \\ + 3(b_3 + b_4)\gamma \frac{a}{l} \sin\theta \omega_X^2 = 0 \end{aligned} \quad (2.11)$$

where b_3 and b_4 are defined in Fig. 2.4. In order to find the response of the model to a given ground input acceleration \ddot{X}_G , the system of nonlinear coupled differential equation (2.10), (2.11) has to be solved. For this purpose, a computer program was written using the method of Runge-Kutta Gill for solving the equation.

2.6 PARAMETERS OF IMPORTANCE

The most important parameters involved in the model are:

a. The Angle of Skewness Since the primary purpose is to investigate the response of skew bridges, it is clearly important to

understand how variations in θ affect the response of the model. In application, the values of θ are usually between 10° and 60° .

b. The Abutment Stiffness k_{ab} As mentioned in the introduction of the thesis, the behavior of skew bridges during strong earthquake shaking is believed to be strongly controlled by the interaction between the bridge deck and the approach fill. The abutment stiffness models the reaction of the soil upon the bridge deck after the gap closes. Consequently, it will be very important to understand its influence on the response of the model.

There is no generally accepted method for calculating the value of the abutment stiffness. However, the geometry of most bridges indicates that the abutment stiffness is higher than the stiffness of an individual bridge column. Thus, the factor γ which relates k_{ab} to the pier stiffness is taken to be greater than one (values of $\gamma = 1, \gamma = 2, \gamma = 5, \gamma = 10$ will be examined).

c. The Abutment Gap a This is the other parameter of the model which is related to the degree of interaction between the deck and the soil. Larger gaps imply less contact between the deck and the abutment springs. Consequently, the degree of interaction between the bridge deck and the soil will decrease with an increase in the gap. The gap at the abutment is intended to allow thermal expansion of the bridge deck. When the gap exists, its size is typically 1 to 2 inches.

d. The Location of the Columns The distance l_1 defines the position of the columns with respect to the center of the deck (see Fig. 2.2). It will be useful to examine cases in which the columns are located near the center of mass of the deck and cases in which the columns are close to the ends of the deck. In actuality, there are bridges with columns

located very close to the center of the bridge deck (l_1 approaches zero). However, in the model under consideration, the only rotational resistance of the deck results from the resisting moments of the pier springs with respect to its center of mass. Therefore, it would be unrealistic to examine values of l_1 too close to zero as the deck would have almost zero torsional resistance.

e. The Small Amplitude Longitudinal Frequency Several tests on bridges have indicated that the small amplitude, longitudinal frequency of small span bridges is within the range of 2 to $5H_z$ (Ref. 36). Since, in this model, structural elements of the bridge other than the piers are neglected, it is reasonable to consider a small value for the frequency. Thus, a representative value of $2H_z$ was chosen. (This value corresponds to $\omega_x = 8.89$ rad/sec).

f. The Input Excitation It is expected that the character of the excitation will affect the response of the model so that no general conclusions about earthquake response can be drawn unless the response to many ground motions is examined. However, since the purpose of this chapter is essentially to illustrate the nature of the problem, in the following paragraphs only the response of the model to one particular excitation will be analyzed. The excitation consists of the 10 most important seconds of the Imperial Valley earthquake of October 15, 1979 (Imperial County Services Building Free-Field Site N O2 E).

2.7 EXAMPLE OF RESPONSE

Assume that the following values are assigned to the parameters of the model.

$$l = 40\text{m}, l_1 = 12\text{m}, \theta = 40^\circ, a = 0.025\text{m}, \gamma = 2, \omega_x = 8.89 \text{ rad/sec}$$

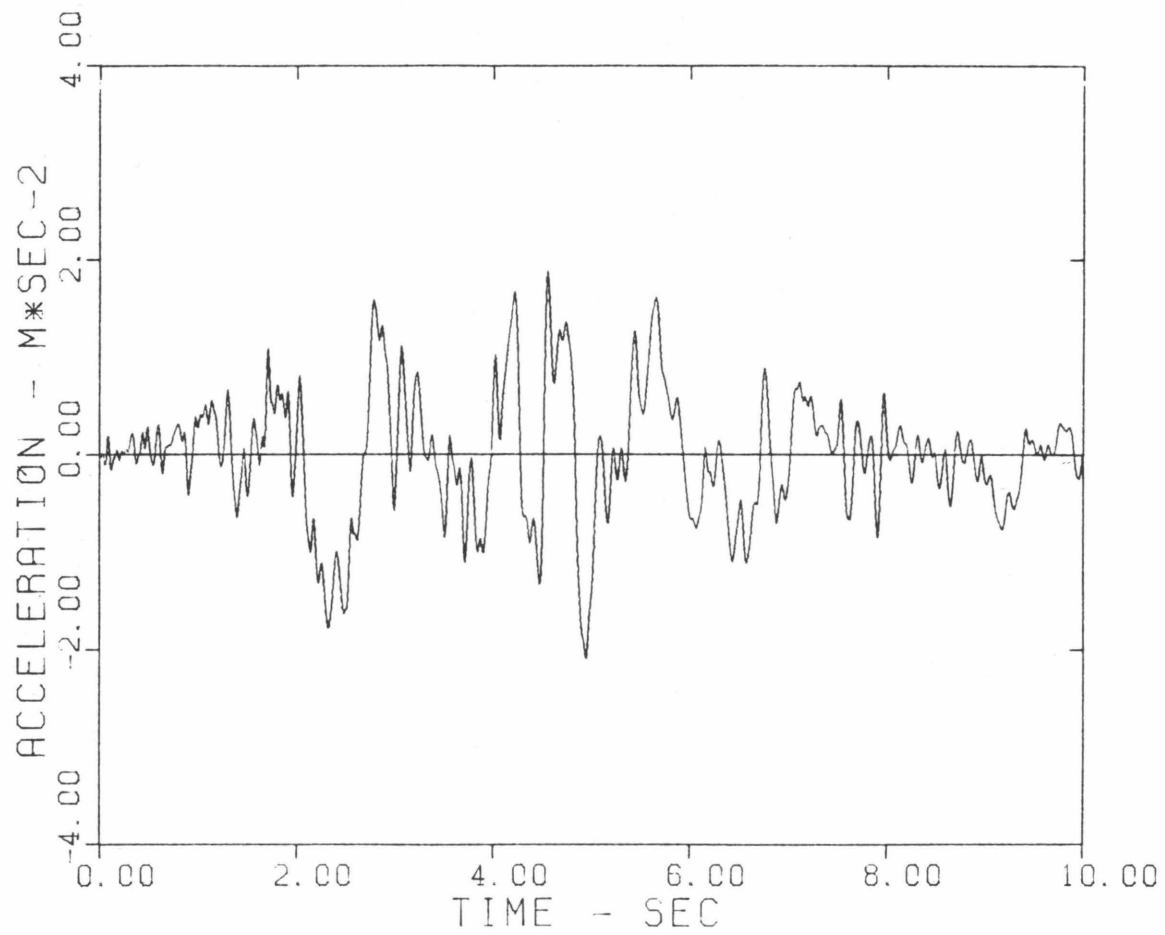


FIG. 2.5 THE TEN MOST IMPORTANT SECONDS OF THE IMPERIAL VALLEY EARTHQUAKE, OCTOBER 15, 1979 (IMPERIAL COUNTY SERVICES BUILDING, FREE-FIELD SITE N O2 E)

At the beginning of the response to the ground motion, the model behaves like a simple degree of freedom oscillator excited along the X-direction. The gaps at both ends of the rod remain open and no rotational vibrations are triggered since the moments of all the restoring forces which act on the deck cancel. So, since $\phi = 0$, the displacements of the center of mass and of points 3 and 4 are identical.

The first impact between the deck and the abutment springs takes place at the left end (point 3) at about 4.2 seconds from the beginning of the excitation (see Fig. 2.6b). Since the moment of the reaction force of the left abutment spring is not counterbalanced by the moment of any other force, rotational vibrations are induced and the deck starts rotating in a positive direction (see Fig. 2.7a), which is in agreement with the direction of the moment from the left abutment. The impact between the deck and the left abutment spring ends when the displacement X_3 becomes larger than -0.025m . But, soon after that, the right gap closes; and an impact between the deck and the right abutment springs occurs, which lasts until the displacement X_4 becomes smaller than 0.025m (Fig. 2.6b). In this way, several impacts between the deck and either the left or the right abutment occur. In the example, all the impacts occur when the displacements X_3 or X_4 exceed the corresponding dotted lines (see Fig. 2.6b and Fig. 2.7a). Between two consecutive impacts, no abutment force is acting on the rod since both gaps are opened.

The consequences of the rotational vibrations induced by the impacts are:

(i) Coupling between the longitudinal translation X and the rotation ϕ occurs; and, as a result, the displacements X_3 and X_4 start

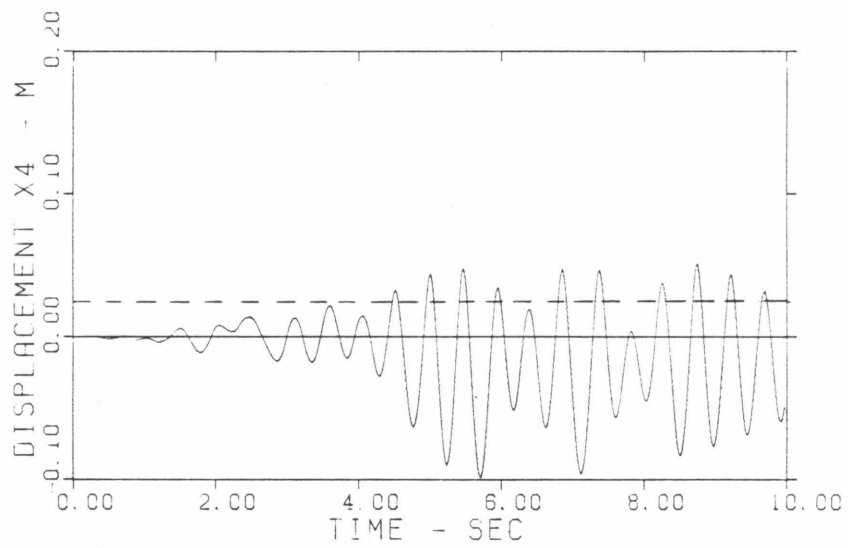
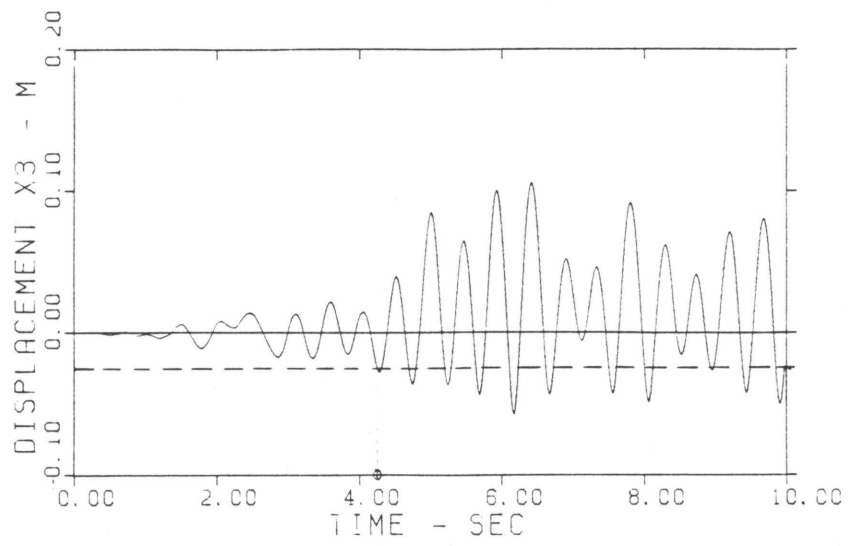


FIG. 2.6 EXAMPLE RESPONSE OF THE MODEL, X_3 and X_4 MOTIONS

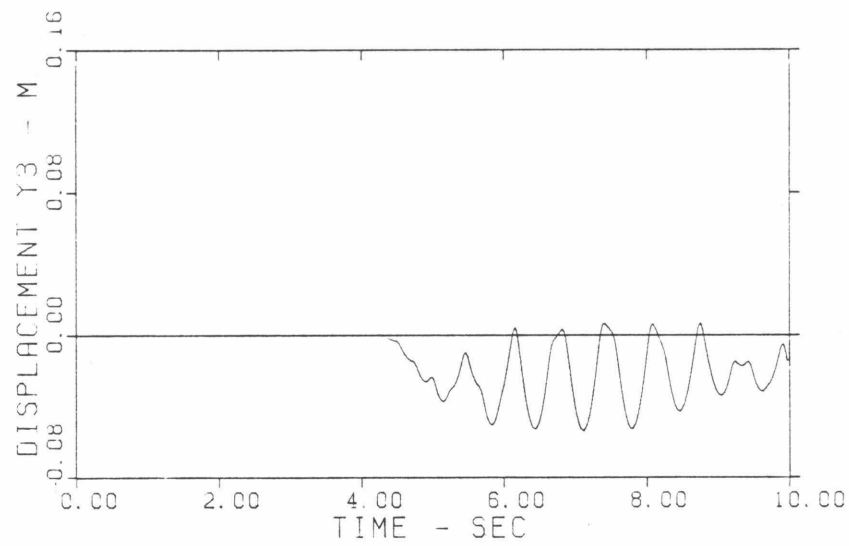
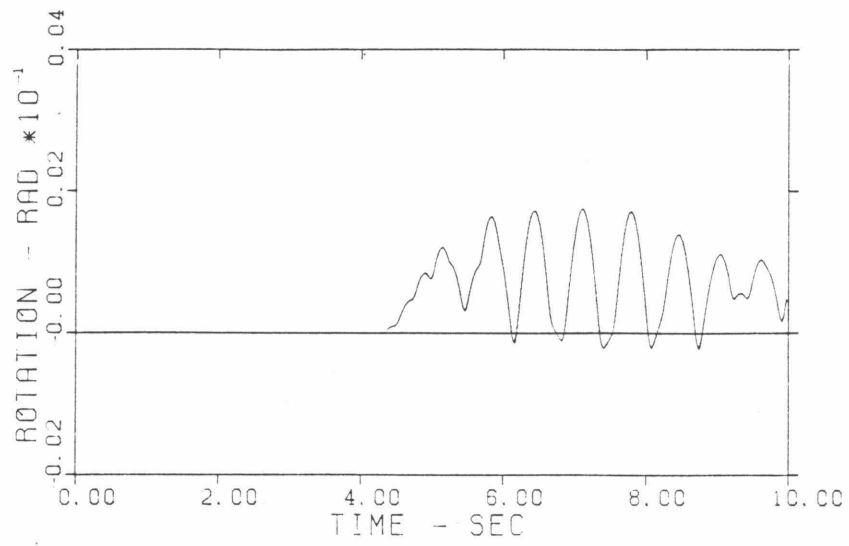


FIG. 2.7 EXAMPLE RESPONSE OF THE MODEL, ϕ AND Y_3 MOTIONS

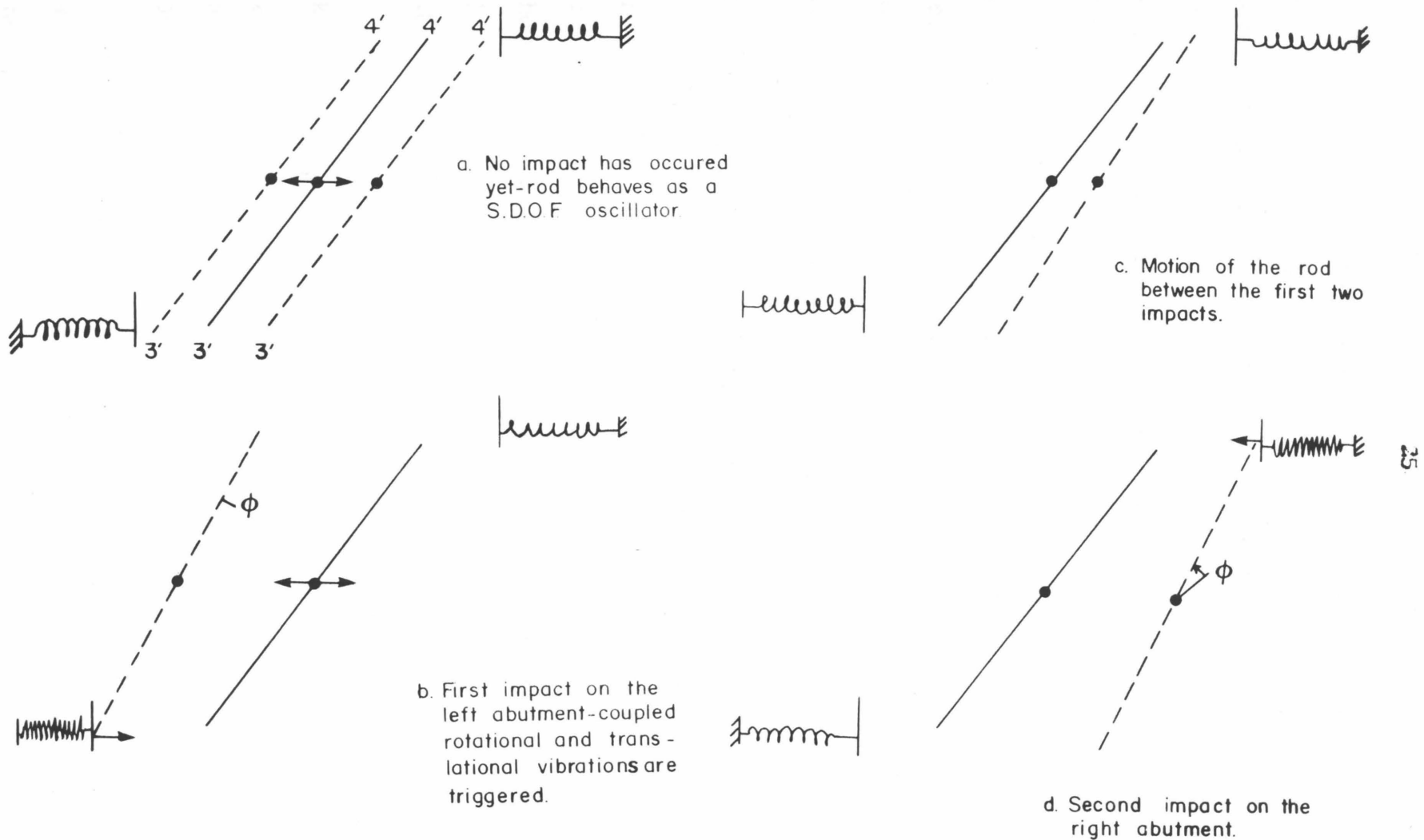


FIG. 2.8 THE PHASES OF THE MOTION BETWEEN THE FIRST TWO IMPACTS

differing from each other and from the displacement X of the center of mass. In fact, a positive rotation of the deck will result in additional positive and negative displacements of the points 3 and 4, respectively. This can be seen in Fig. 2.6b and Fig. 2.7a and can be explained by the relation between X_3, X, ϕ and X_4, X, ϕ shown in Fig. 2.3.

(ii) The ends of the deck move in the Y -direction after the first closure of the gap. However, due to the symmetry of the model, the center of mass of the rod does not move in the Y -direction even after rotational vibrations are triggered.

2.8 EFFECTS OF THE VARIATION OF THE PARAMETERS

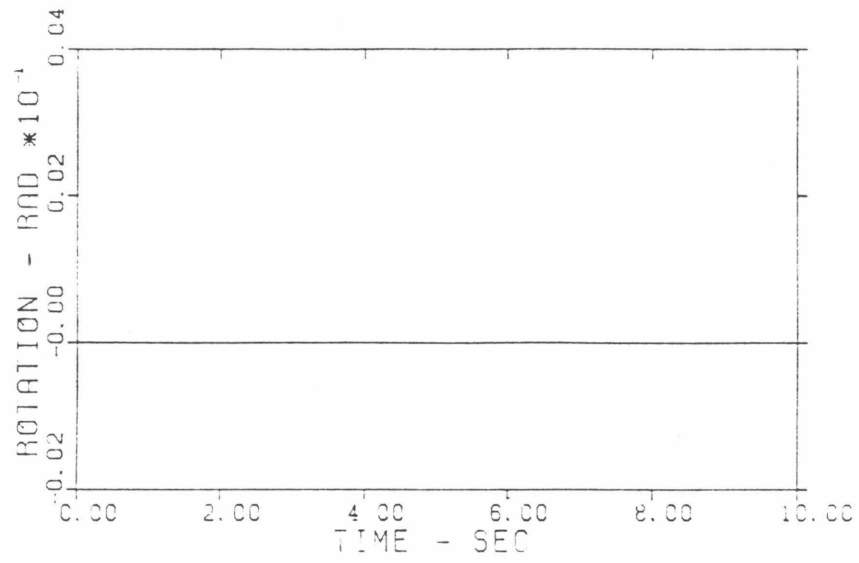
2.8.1 Rod With Restoring Springs Close to the Center of Mass

Assume that the total length of the bridge deck is 80m ($l = 40m$) and that the columns are located at a distance $l_1 = 8m$ from the center of mass of the deck. This results in a ratio $l_1/l = 0.2$, which is thought to be a representative value for the case of columns located close to the center of mass of the deck.

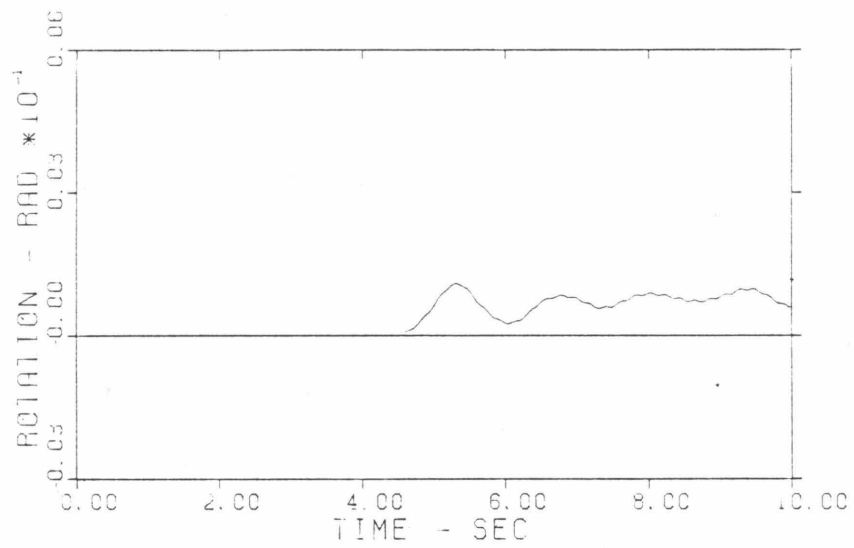
2.8.1.1. Effects of the Angle of Skewness

To investigate the effects of the variation of the angle of skewness, the other parameters are fixed: $\gamma = 2$, $a = 0.025m$, $\omega_x = 8.89 \text{ rad/sec}$. The range of skewness is taken to be between $\theta = 0$ and $\theta = 60^\circ$; and the response of the model to values of $\theta = 0, 5^\circ, 10^\circ, 20^\circ, 40^\circ$, and 60° is investigated.

In Figs. 2.9 - 2.11, the rotational responses of the model to the 1979 El Centro excitation for several values of the initial angle of skewness are shown. From these figures, the following conclusions can

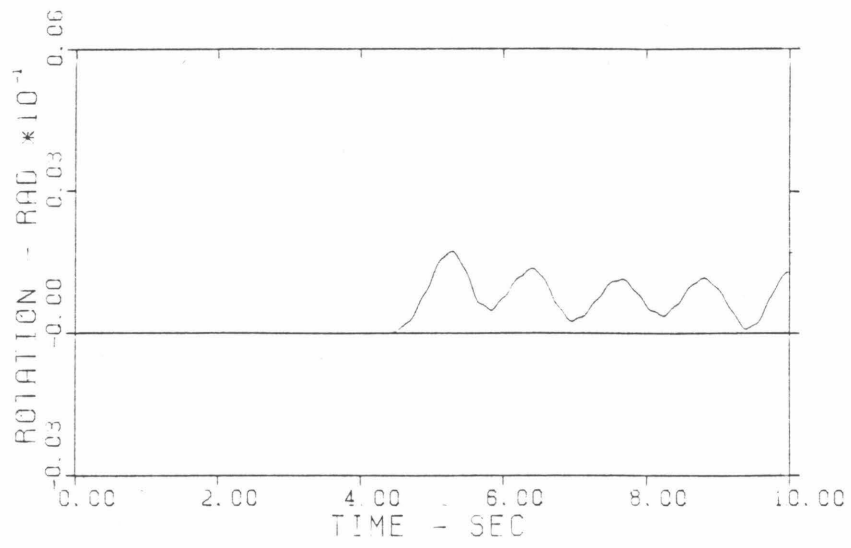


a

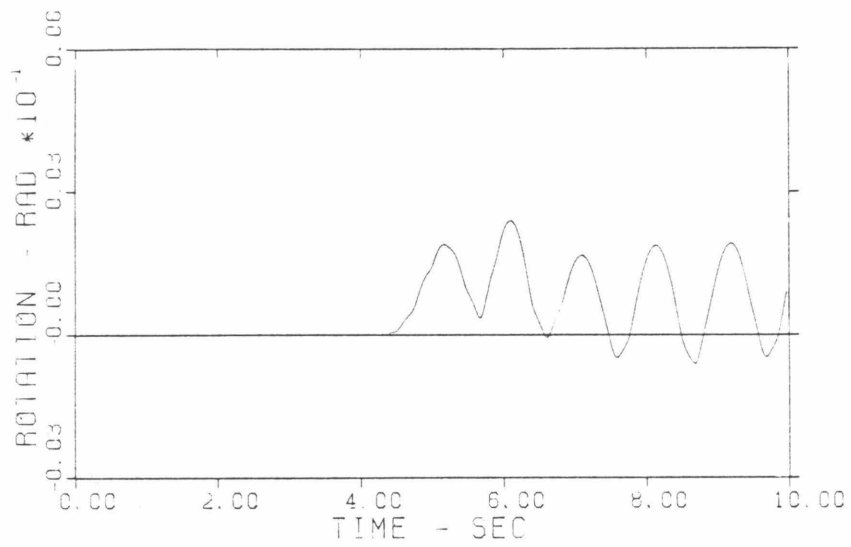


b

FIG. 2.9 EFFECTS OF VARIATION OF SKEWNESS, θ
a. $\theta = 0$ b. $\theta = 5^\circ$

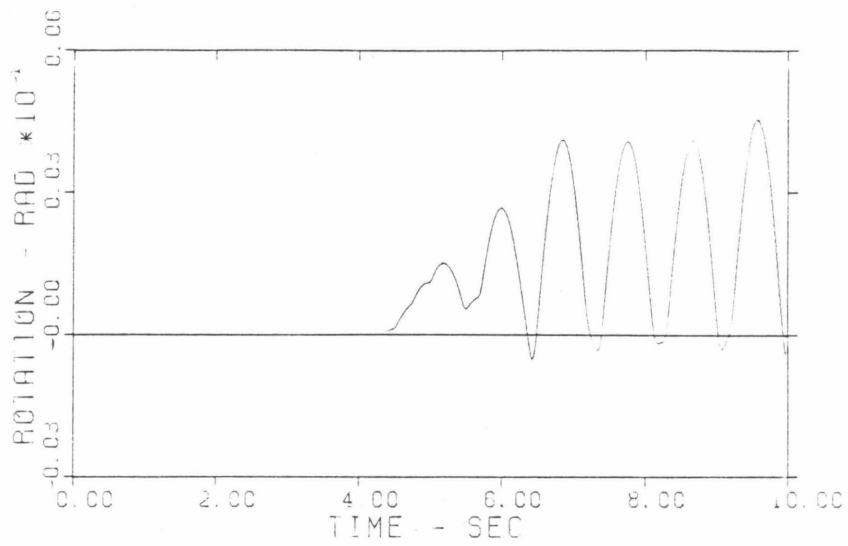


a

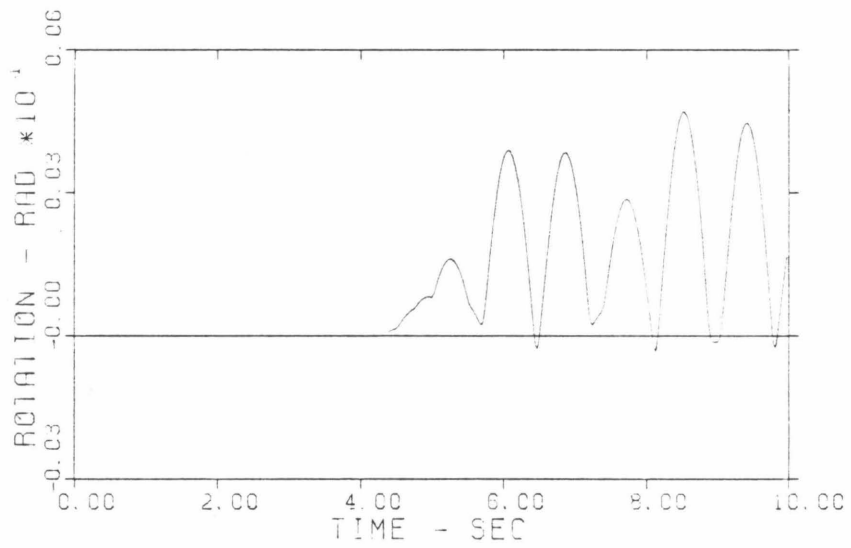


b

FIG. 2.10 EFFECTS OF VARIATION OF SKEWNESS,
a. $\theta = 10^\circ$ b. $\theta = 20^\circ$



a



b

FIG. 2.11 EFFECTS OF VARIATION OF SKEWNESS, θ
 a. $\theta = 40^\circ$ b. $\theta = 60^\circ$

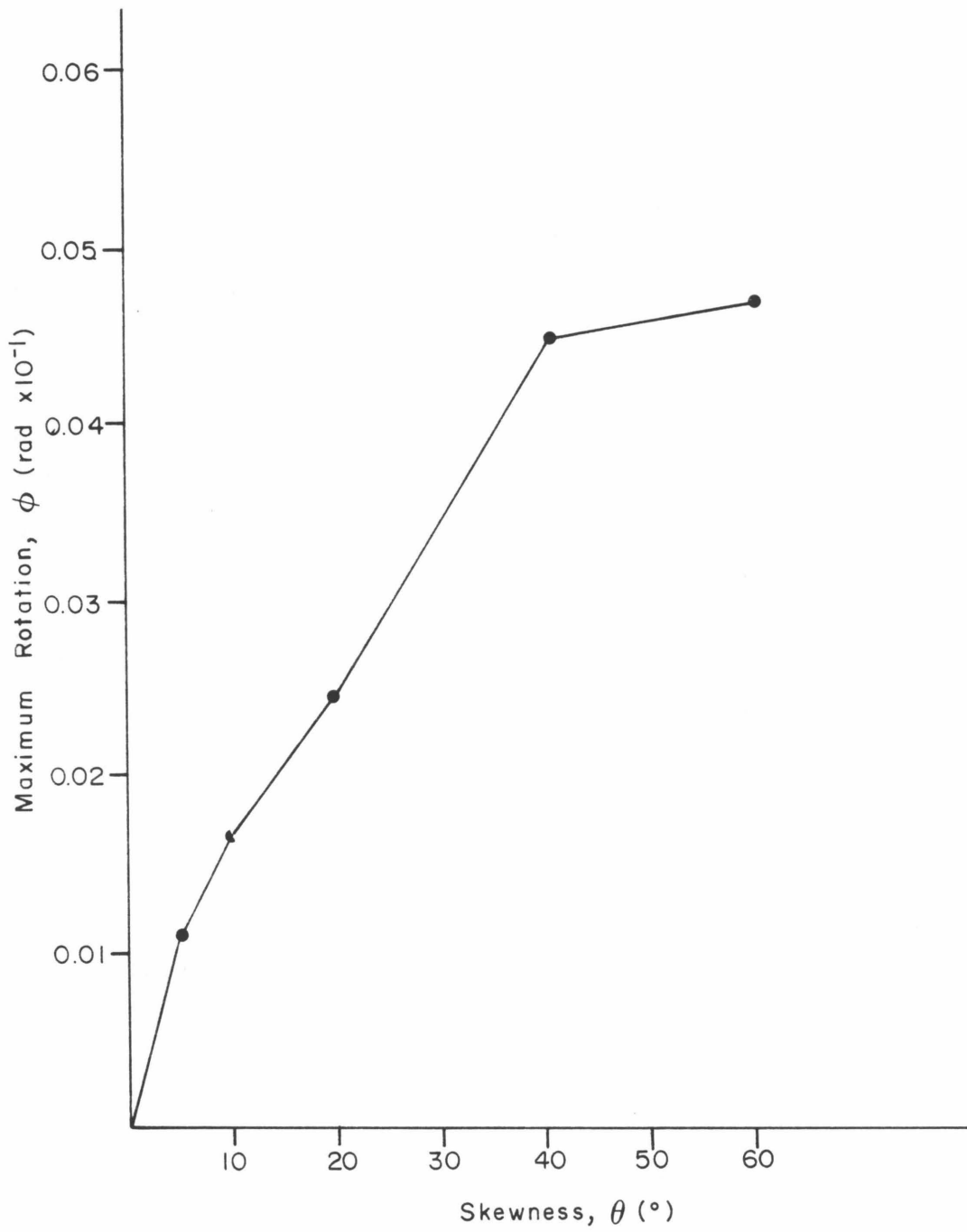


FIG. 2.12 VARIATION OF MAXIMUM ROTATIONAL RESPONSE, ϕ , WITH SKEWNESS, θ

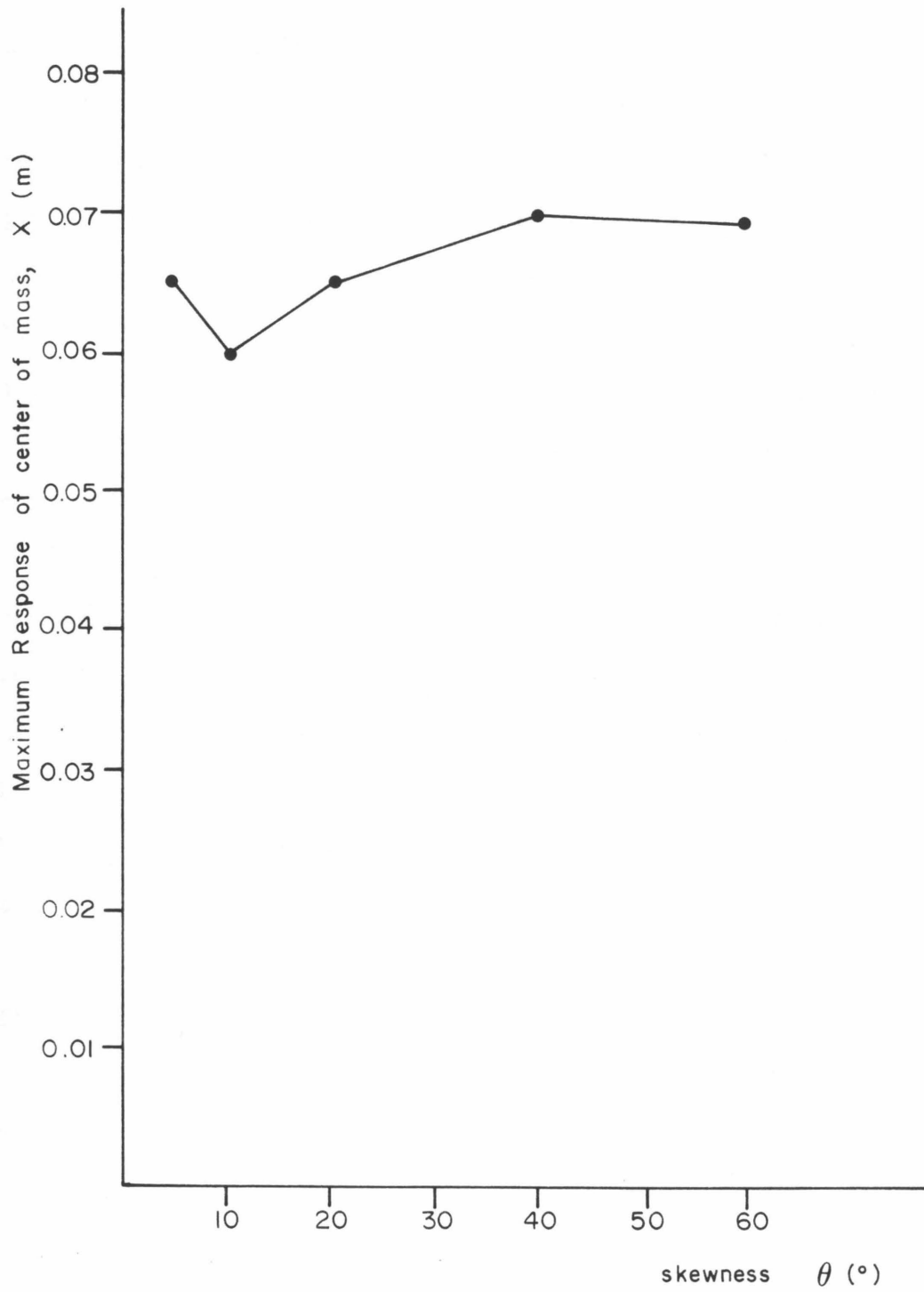


FIG. 2.13 VARIATION OF MAXIMUM MOTION OF THE CENTER OF MASS, X , WITH SKEWNESS, θ

be drawn:

a. The response is more sensitive to initial changes in the angle of skewness (from 0 to 10°) than to later ones (from 40° to 60°). This can also be seen in Fig. 2.12.

b. The overall appearance of the response depends upon the frequency of the impacts between the deck and the abutment springs and upon the rotational frequency of the deck. One can observe that the deck rotates primarily in the positive direction. Particularly for $\theta = 5^\circ$ and 10° , no negative rotation occurs. This happens because the deck hits the abutment springs before its rotation becomes negative.

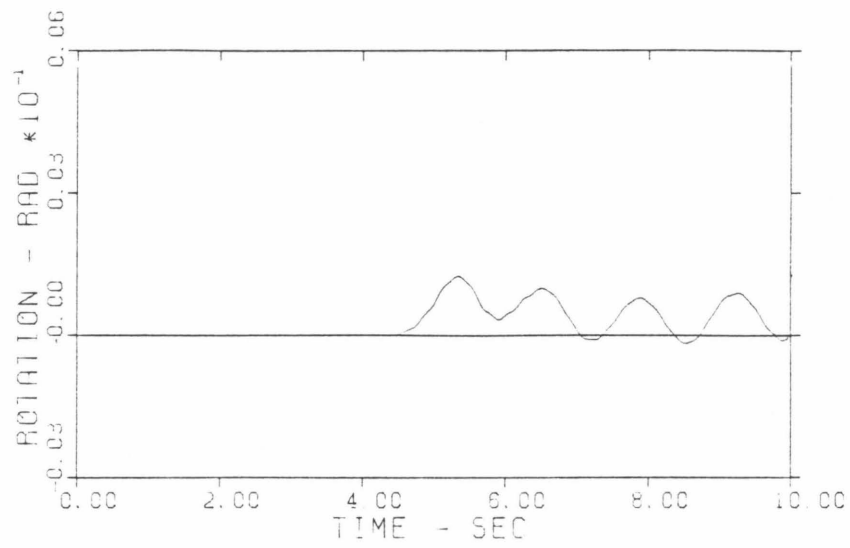
c. The maximum rotational response has a tendency to increase with an increase in the angle of skewness.

d. As shown in Fig. 2.13, the response of the center of mass is not substantially affected by variations of the angle of skewness.

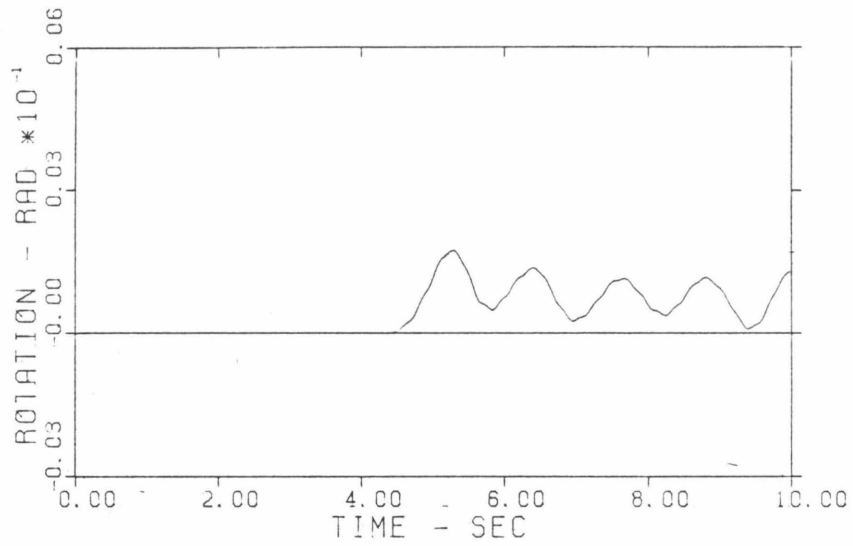
2.8.1.2. Effects of the Abutment Stiffness

To investigate the effects of the abutment stiffness, the response of the model for various values of the parameter γ has to be examined. The values of γ considered are: $\gamma = 1$, $\gamma = 2$, $\gamma = 5$, $\gamma = 10$. The values of ω_x and a remain fixed at 8.89 rad/sec and $0.025m$, respectively; while, for purposes of further investigation of the effects of the angle of skewness on the coupling between the X and ϕ motions, two values of θ will be examined: $\theta = 10^\circ$ and $\theta = 40^\circ$. Thus, the cases under consideration are:

<u>Case 1</u>		<u>Case 2</u>	
$\theta = 10^\circ$		$\theta = 40^\circ$	
$\omega_x = 8.89$	$\gamma = 1,2,5,10$	$\omega_x = 8.89$	$\gamma = 1,2,5,10$
$a = 0.025$		$a = 0.025$	

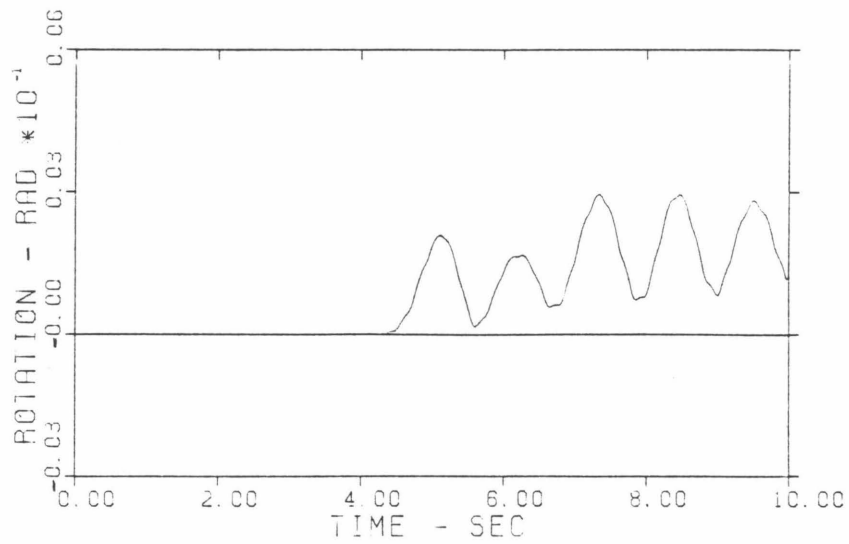


a

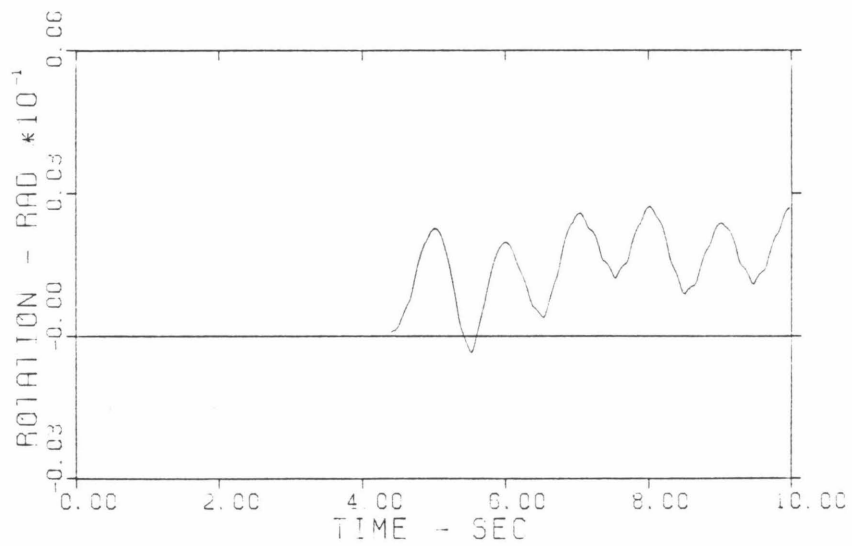


b

FIG. 2.14 EFFECTS OF THE VARIATION OF ABUTMENT STIFFNESS, γ ,
FOR $\theta = 10^\circ$
a. $\gamma = 1$ b. $\gamma = 2$

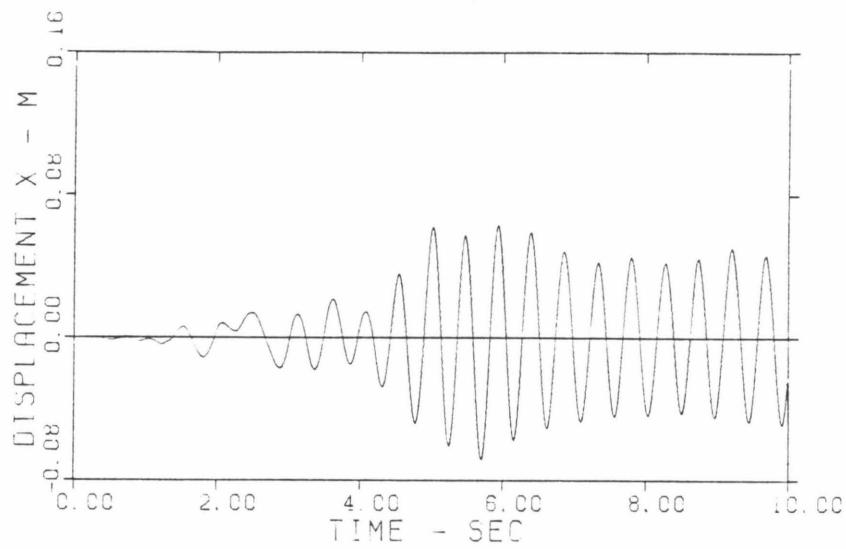


a

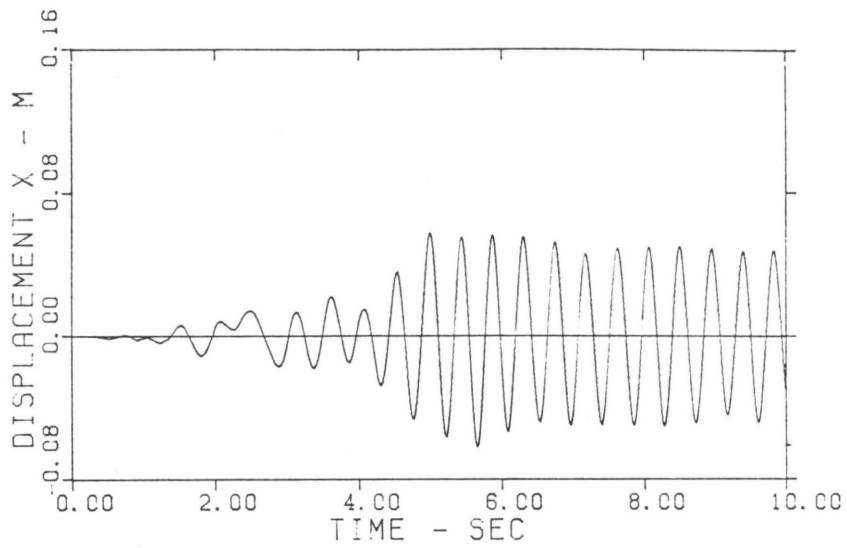


b

FIG. 2.15 EFFECTS OF THE VARIATION OF ABUIMENT STIFFNESS, γ ,
FOR $\theta = 10^\circ$
a. $\gamma = 5$ b. $\gamma = 10$

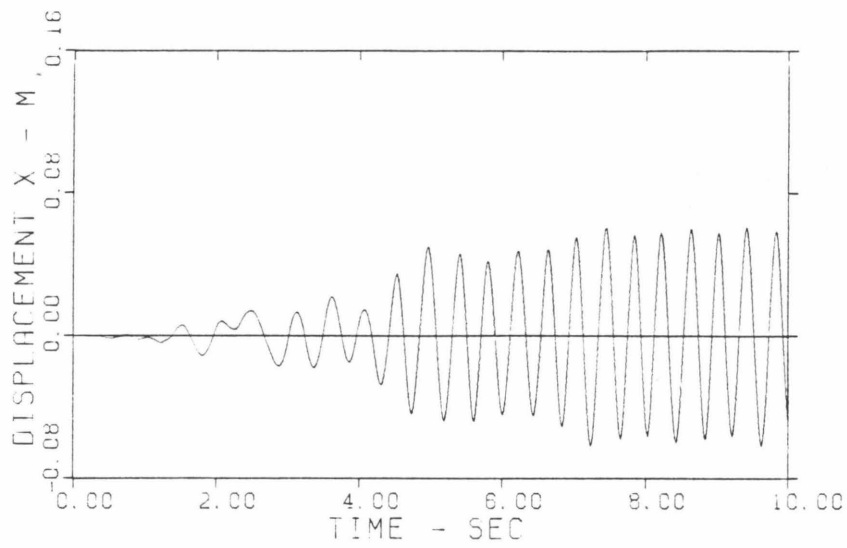


a

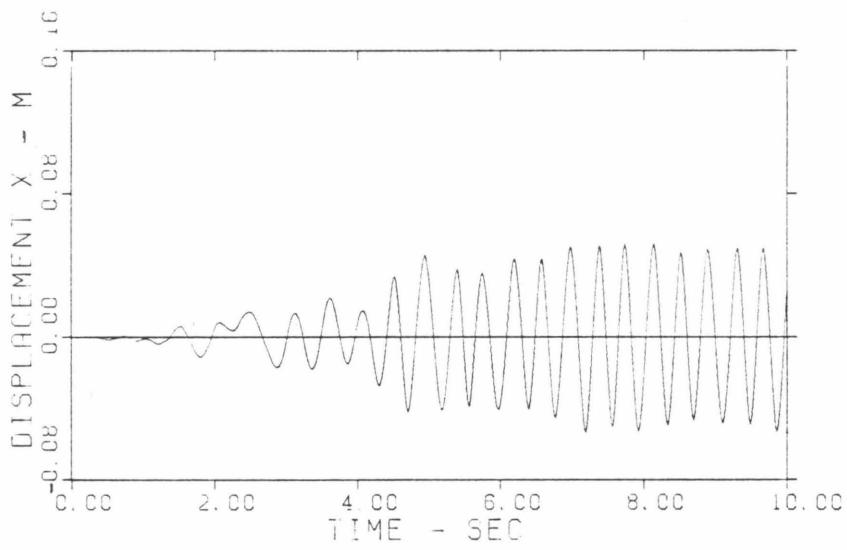


b

FIG. 2.16 EFFECTS OF THE VARIATION OF ABUIMENT STIFFNESS, γ ,
FOR $\theta = 10^\circ$
a. $\gamma = 1$ b. $\gamma = 2$

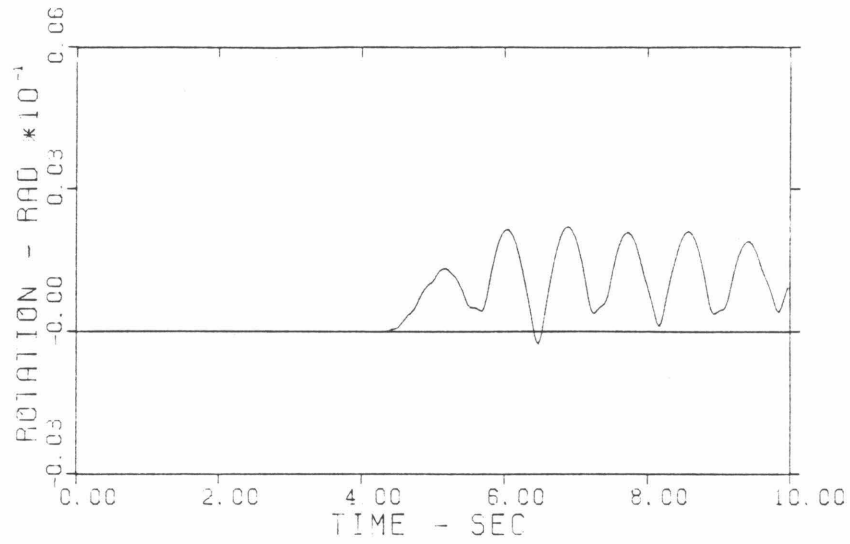


a

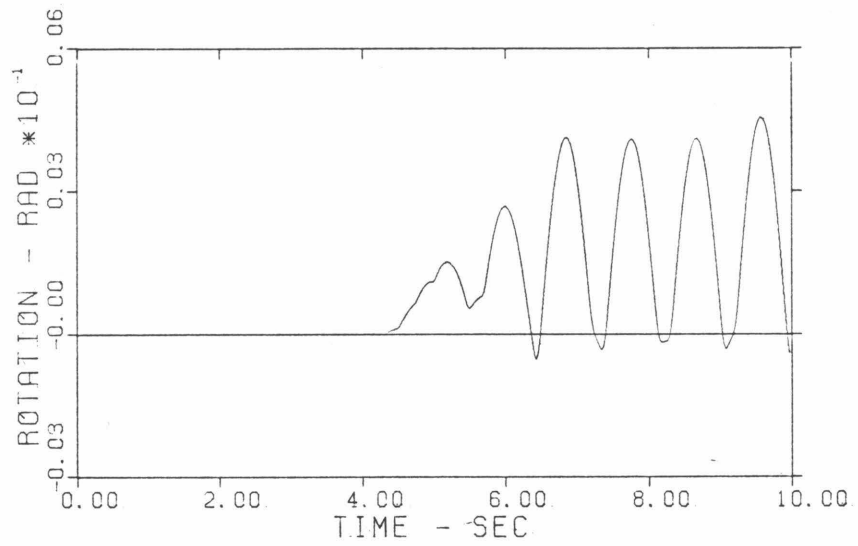


b

FIG. 2.17 EFFECTS OF THE VARIATION OF ABUIMENT STIFFNESS, γ ,
 FOR $\theta = 10^\circ$
 a. $\gamma = 5$ b. $\gamma = 10$

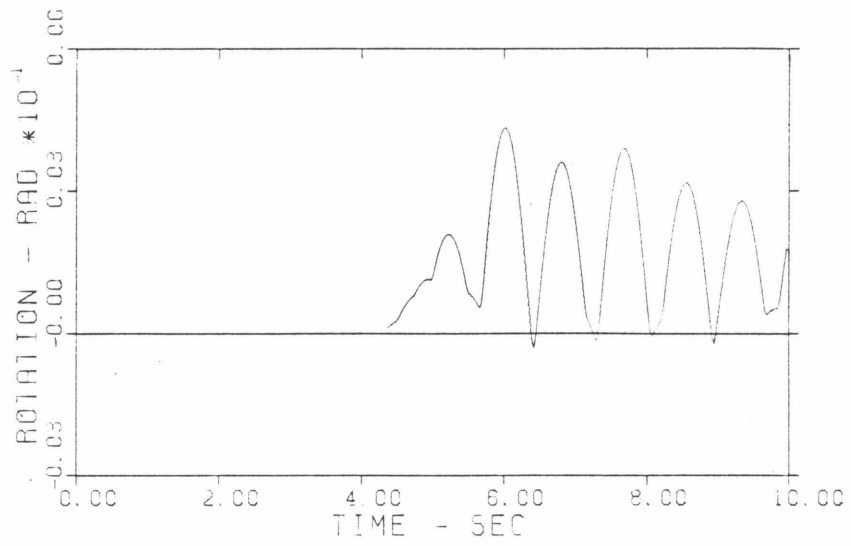


a

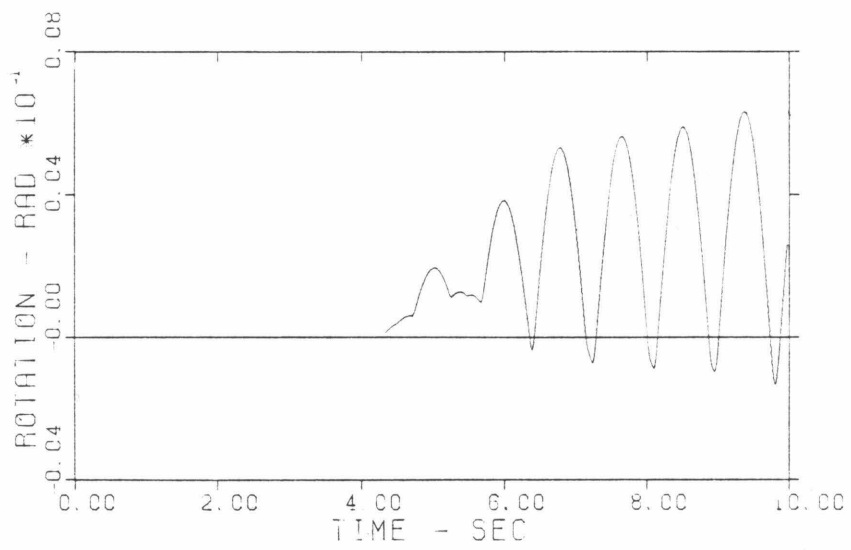


b

FIG. 2.18 EFFECTS OF THE VARIATION OF ABUTMENT STIFFNESS, γ ,
 FOR $\theta = 40^\circ$
 a. $\gamma = 1$ b. $\gamma = 2$

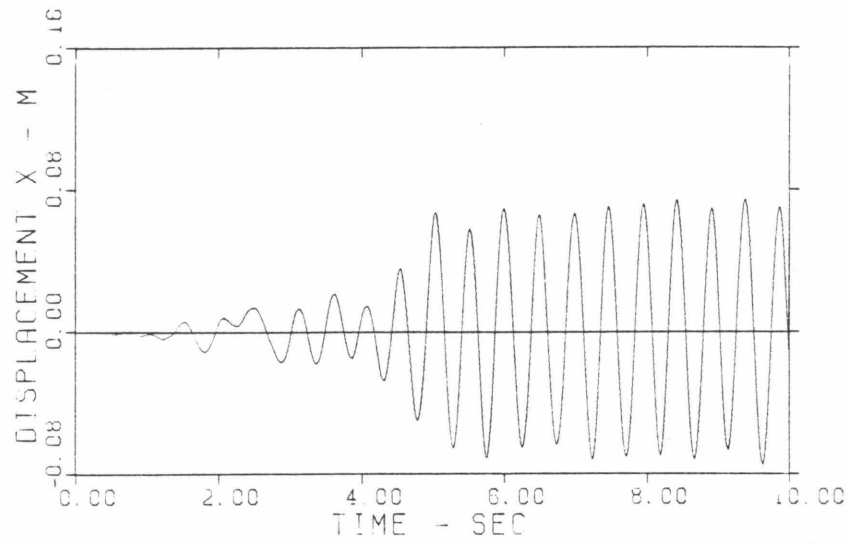


a

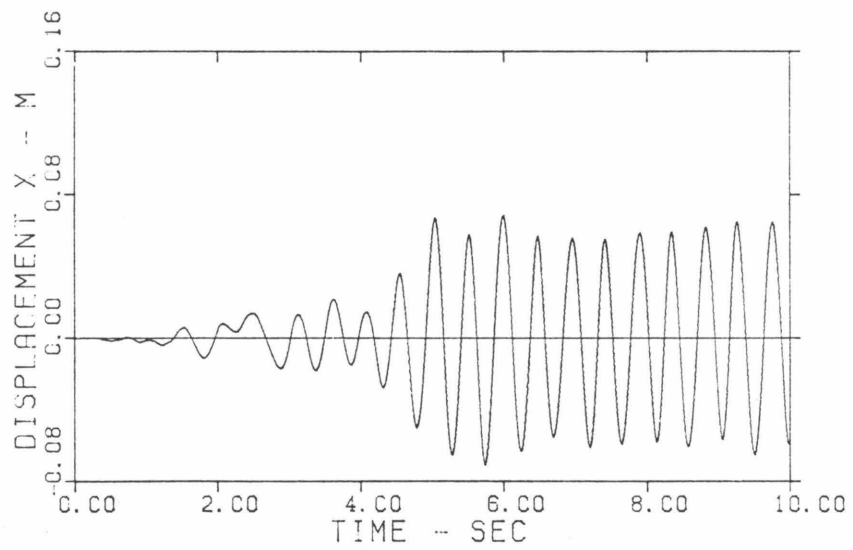


b

FIG. 2.19 EFFECTS OF THE VARIATION OF ABUIMENT STIFFNESS, γ ,
 FOR $\theta = 40^\circ$
 a. $\gamma = 5$ b. $\gamma = 10$

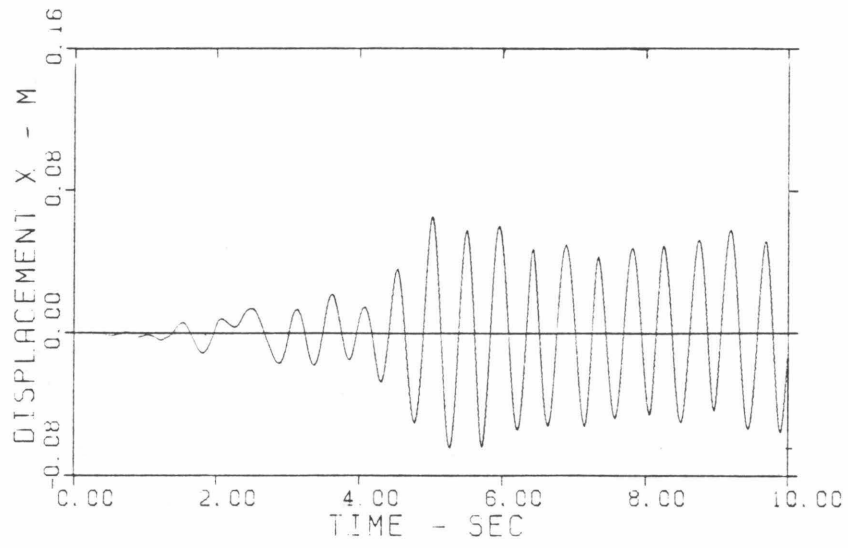


a

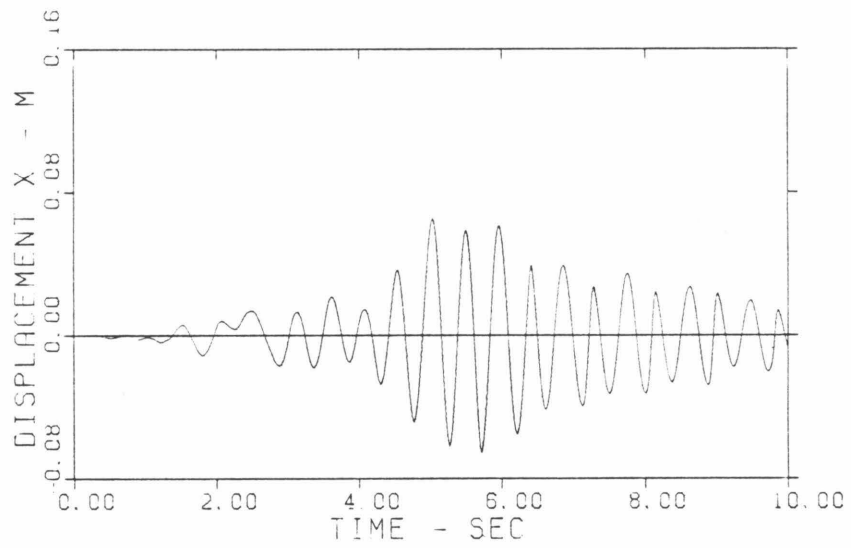


b

FIG. 2.20 EFFECTS OF THE VARIATION OF ABUIMENT STIFFNESS, γ ,
 FOR $\theta = 40^\circ$
 a. $\gamma = 1$ b. $\gamma = 2$



a



b

FIG. 2.21 EFFECTS OF THE VARIATION OF ABUTMENT STIFFNESS, γ ,
 FOR $\theta = 40^\circ$
 a. $\gamma = 5$ b. $\gamma = 10$

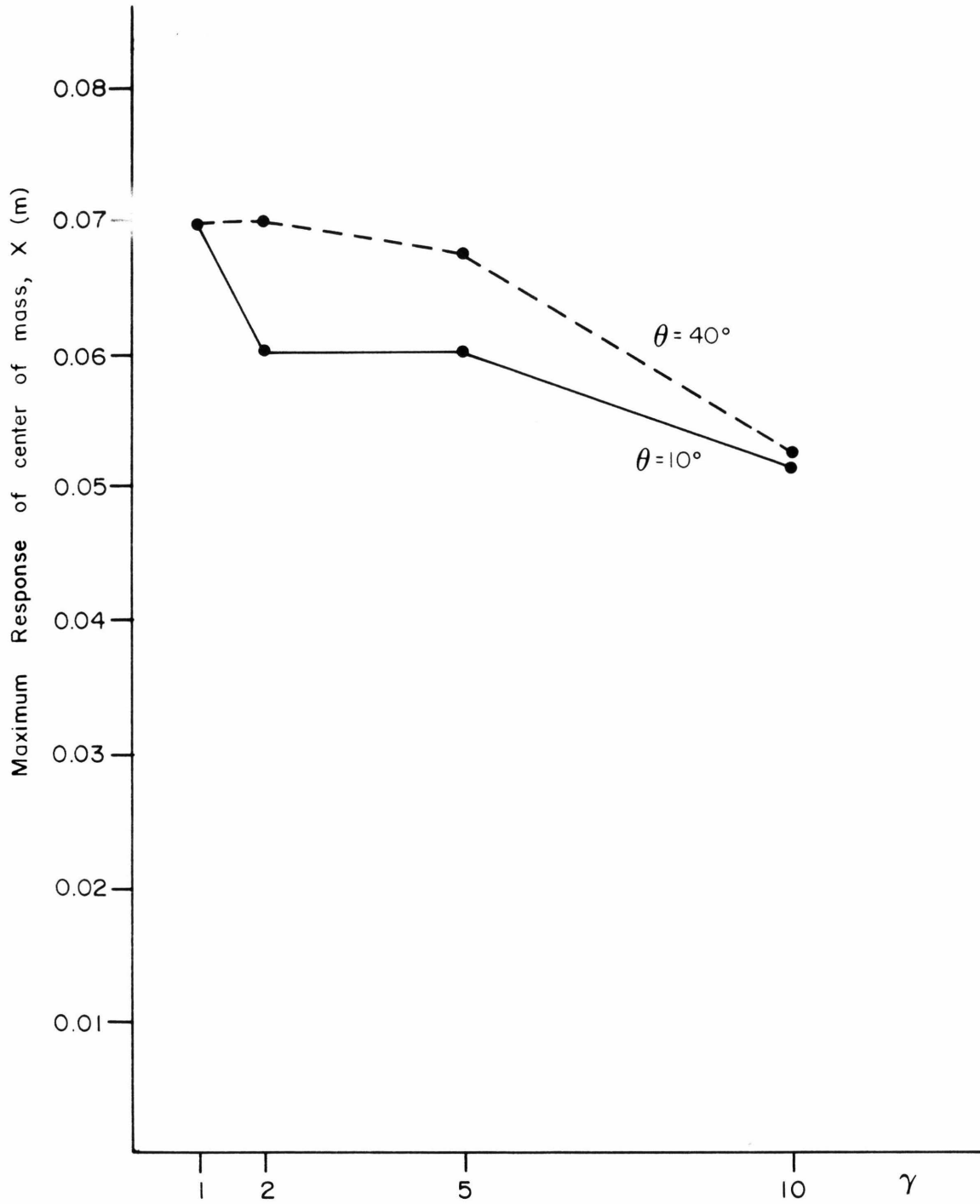
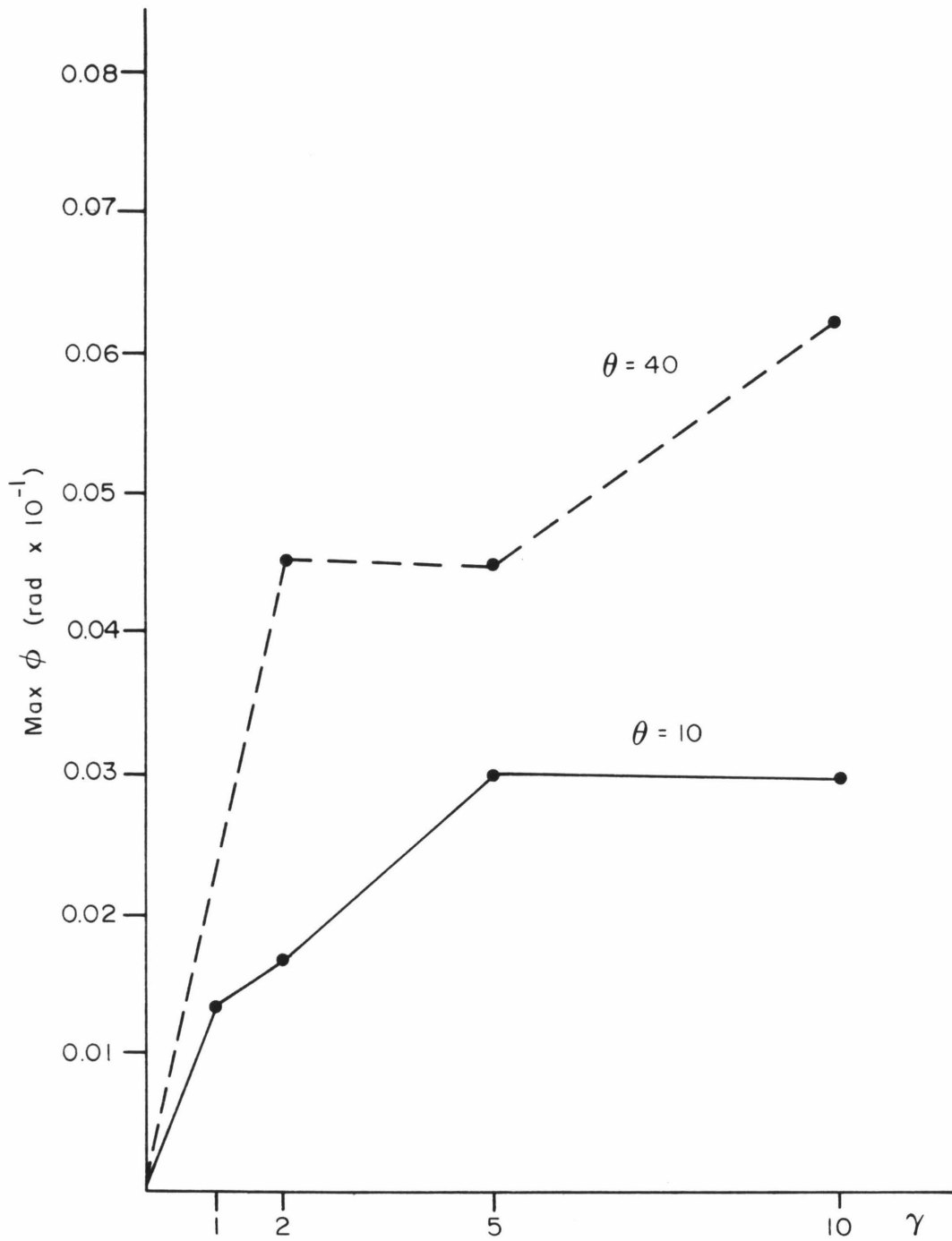


FIG. 2.22 VARIATION OF THE MAXIMUM DISPLACEMENT OF THE CENTER OF THE DECK, X , WITH ABUTMENT STIFFNESS, γ

FIG. 2.23 VARIATION OF MAXIMUM ϕ WITH γ

Figs. 2.14 - 2.17 show the responses of the model in case 1, while Figs. 2.18 - 2.21 show the responses of the model in case 2. From these figures, as well as from Fig. 2.22 and 2.23, one can see that:

- a. The maximum displacement along the X-axis of the center of mass of the rod decreases with an increase in γ ;
- b. The maximum rotation of the rod increases with γ ;
- c. The obviously different overall appearance of the responses in the two cases reveals once more the effect of the initial angle of skewness on the coupling between the translational and rotational motions.

2.8.1.3 Effects of the Abutment Gap

For the investigation of the effects of the gap on the response of the model, the values of θ , γ , and ω_x will remain fixed at 40° , 5 and 8.89 rad/sec, respectively. As was mentioned earlier, the typical range of actual gaps is 0-2" (0-5cm). But, for purposes of better understanding of the role of the gap, values outside of that range will also be examined.

In Fig. 2.24, the response of the deck when the gap is open (i.e. the deck never hits the abutment springs) is shown. In this case, the deck behaves like a single degree of freedom oscillator excited in the X-direction; there is no rotational motion. The maximum displacement of the rod in the X-direction when the gap is open is slightly over 0.09m. So, if the gap is 0.09m, the deck lightly hits the abutment springs; and the induced rotational vibrations are not strong (Fig. 2.27b). In Figs. 2.25 - 2.30, one can see the rotational response of the deck for several values of the gap. From these figures, as well as from Figs. 2.31 and 2.32, the following conclusions can be drawn:

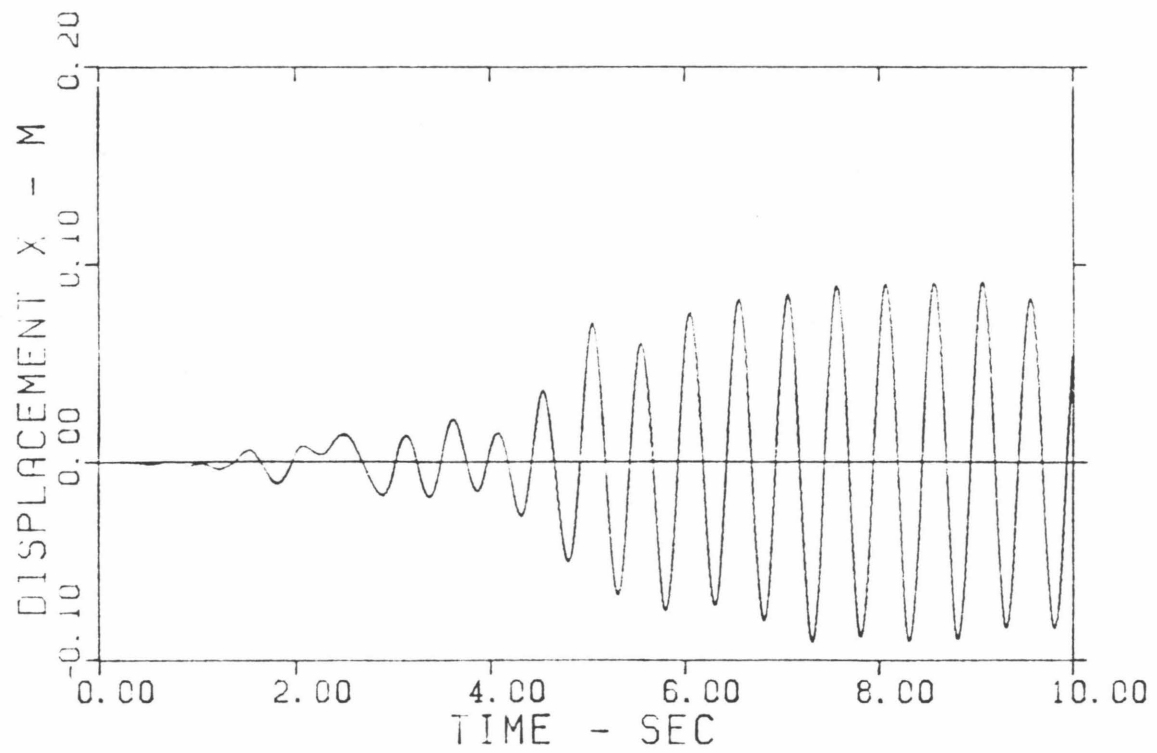
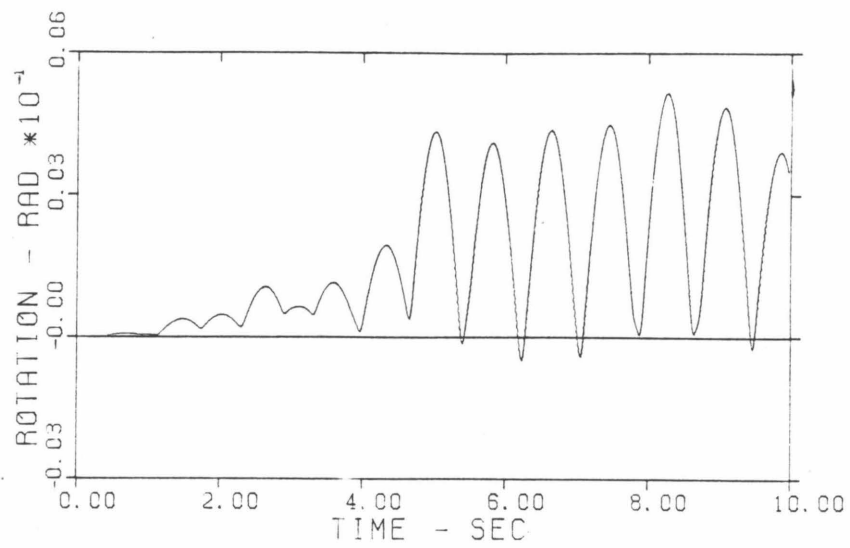
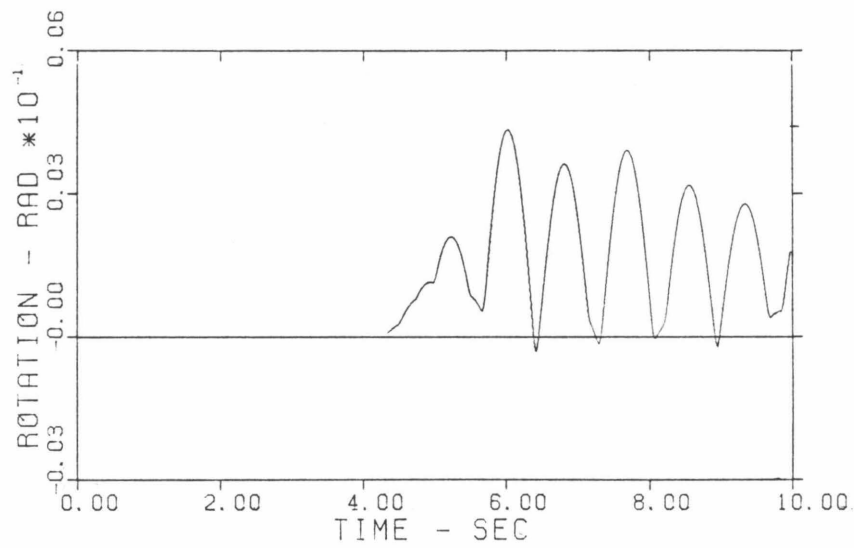


FIG. 2.24 LONGITUDINAL RESPONSE OF THE CENTER OF MASS OF THE DECK FOR THE GAP, $a = \infty$



a



b

FIG. 2.25 EFFECTS OF THE VARIATION OF GAP WIDTH, a , UPON THE ROTATIONAL RESPONSE

a. $a = 0\text{m}$

b. $a = 0.025\text{m}$

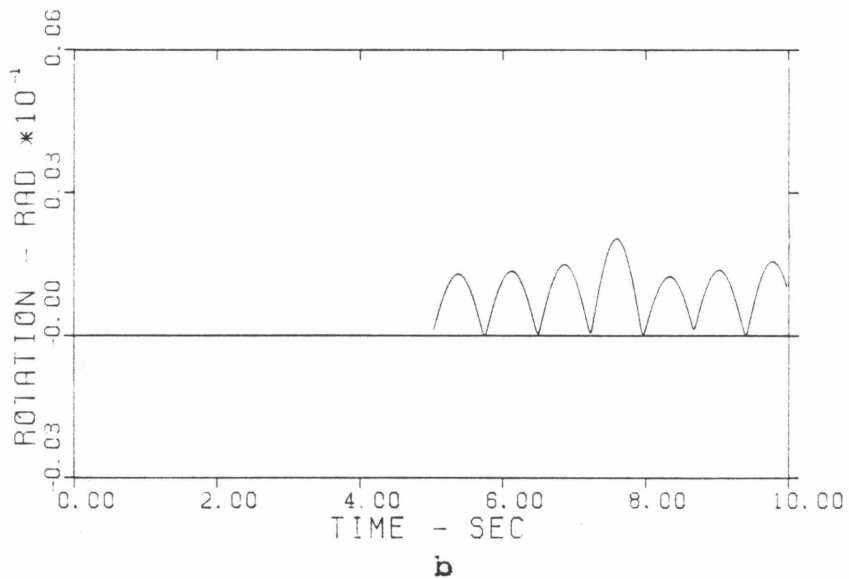
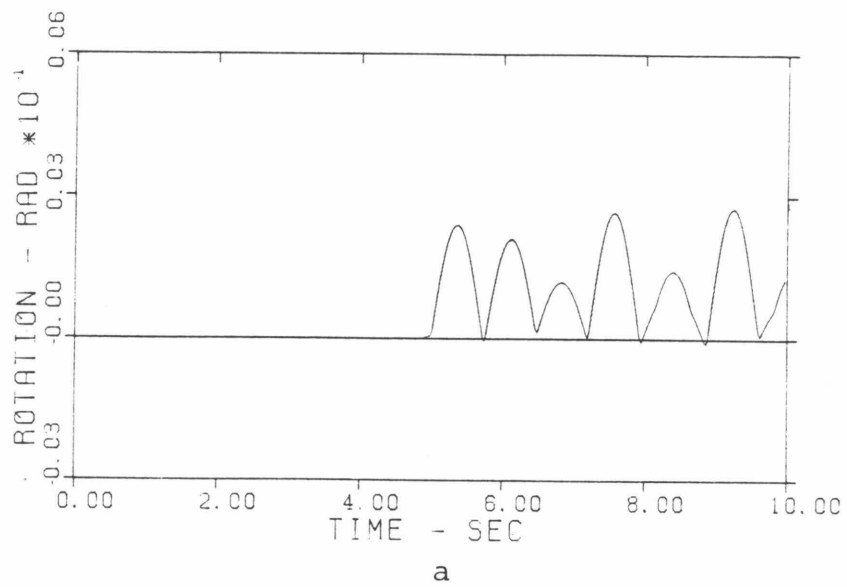
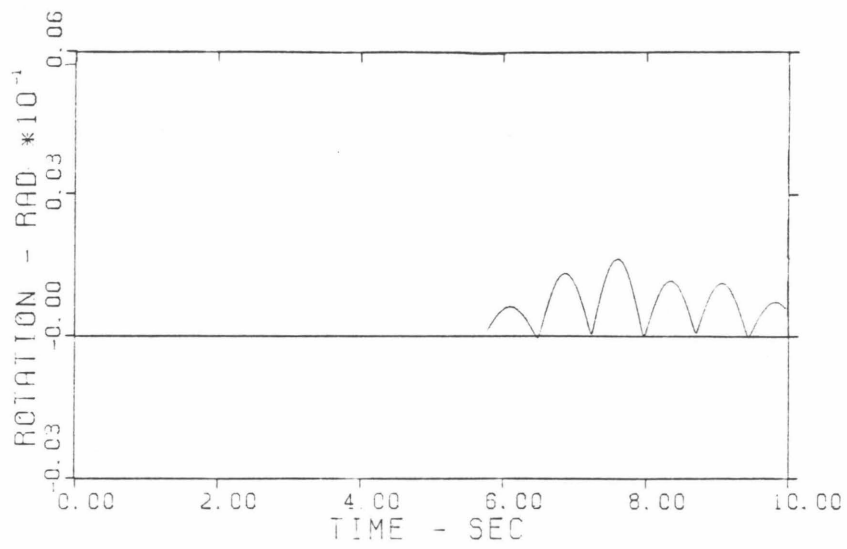
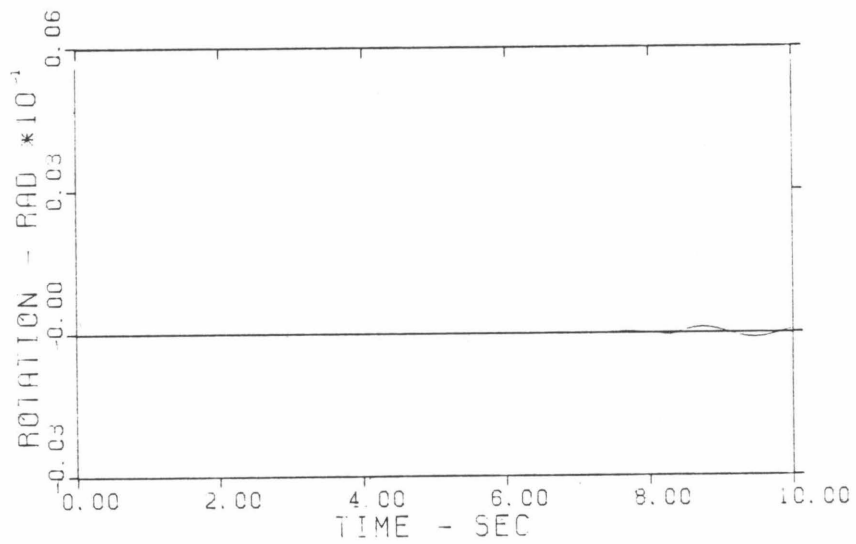


FIG. 2.26 EFFECTS OF THE VARIATION OF GAP WIDTH, a , UPON THE ROTATIONAL RESPONSE
a. $a = 0.05\text{m}$ b. $a = 0.06\text{m}$



a

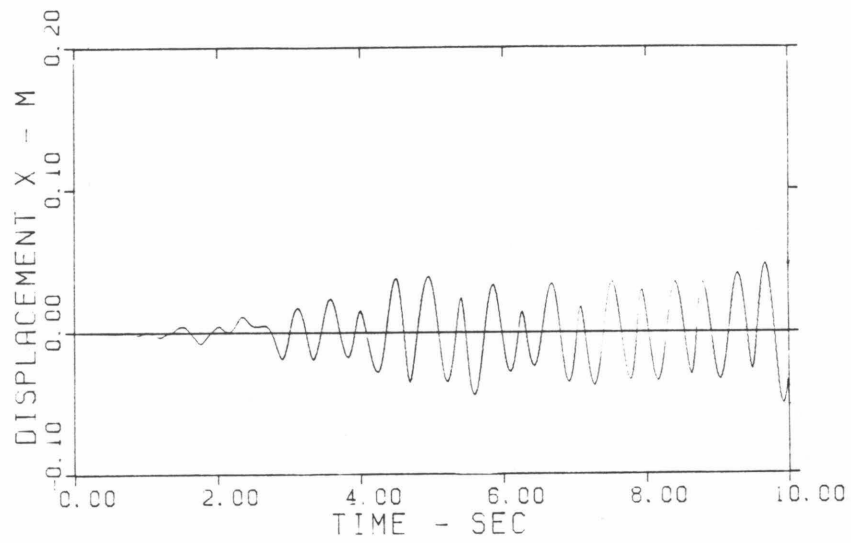


b

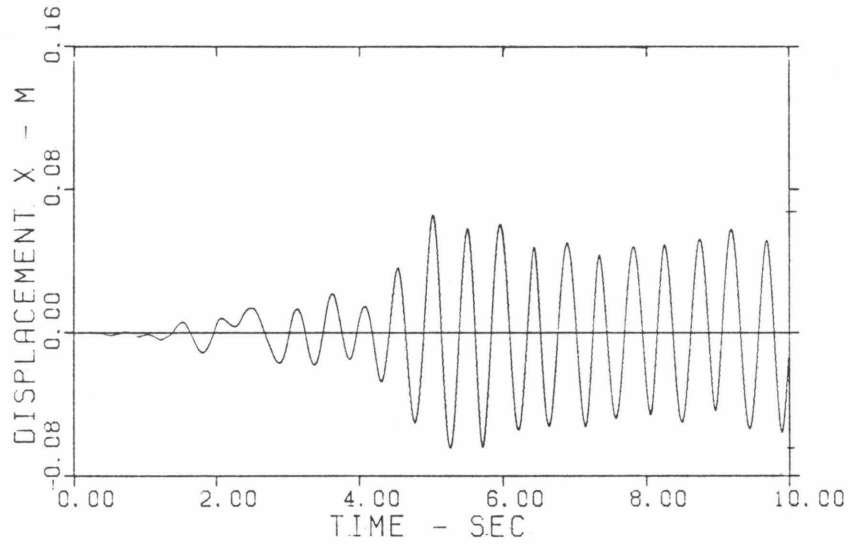
FIG. 2.27 EFFECTS OF THE VARIATION OF GAP WIDTH, a , UPON THE ROTATIONAL RESPONSE

a. $a = 0.07$

b. $a = 0.09$

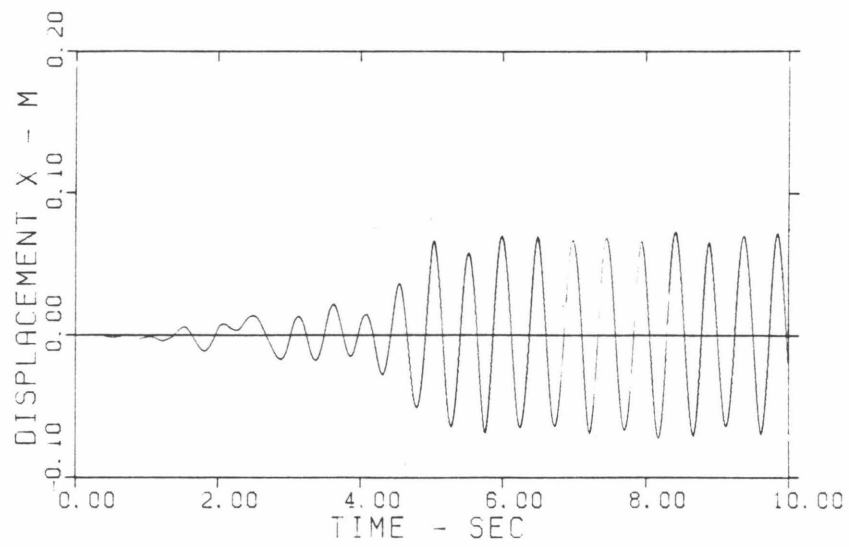


a

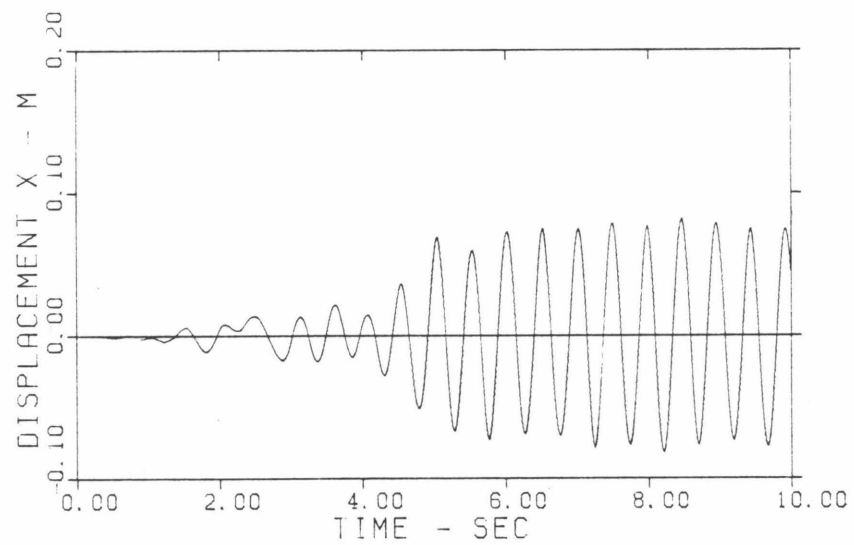


b

FIG. 2.28 EFFECTS OF THE VARIATION OF GAP WIDTH, a , UPON THE LONGITUDINAL RESPONSE OF THE CENTER OF MASS OF THE DECK
a. $a = 0$ b. $a = 0.025$



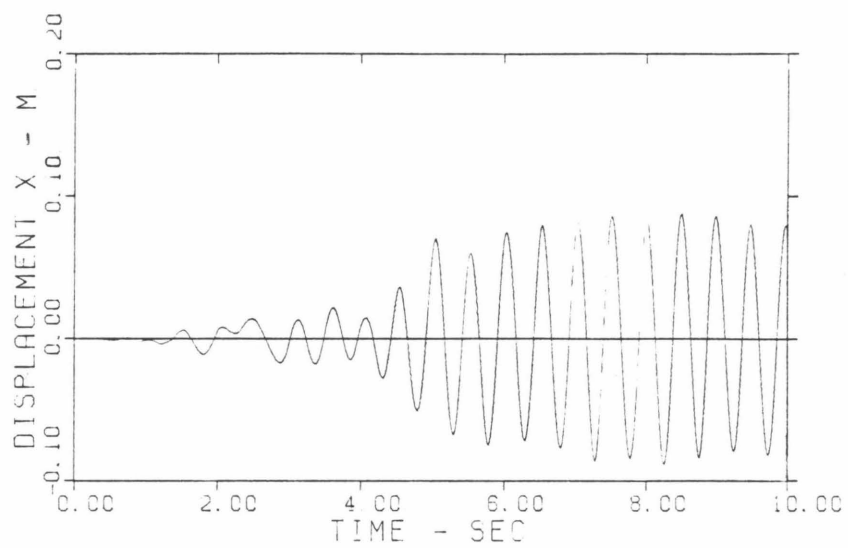
a



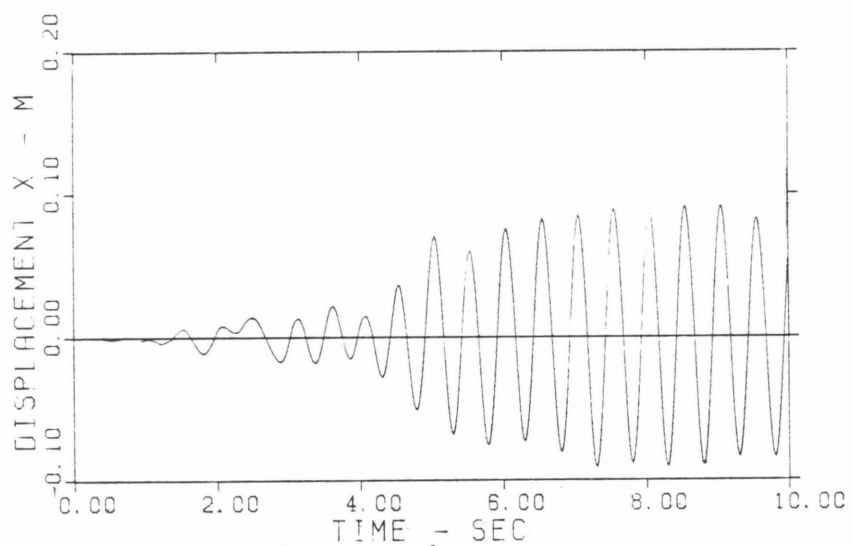
b

FIG. 2.29 EFFECTS OF THE VARIATION OF GAP WIDTH, a , UPON THE LONGITUDINAL RESPONSE OF THE CENTER OF MASS OF THE DECK

a. $a = 0.05$ b. $a = 0.06$



a



b

FIG. 2.30 EFFECTS OF THE VARIATION OF GAP WIDTH, a , UPON THE LONGITUDINAL RESPONSE OF THE CENTER OF MASS OF THE DECK

a. $a = 0.07$ b. $a = 0.09$

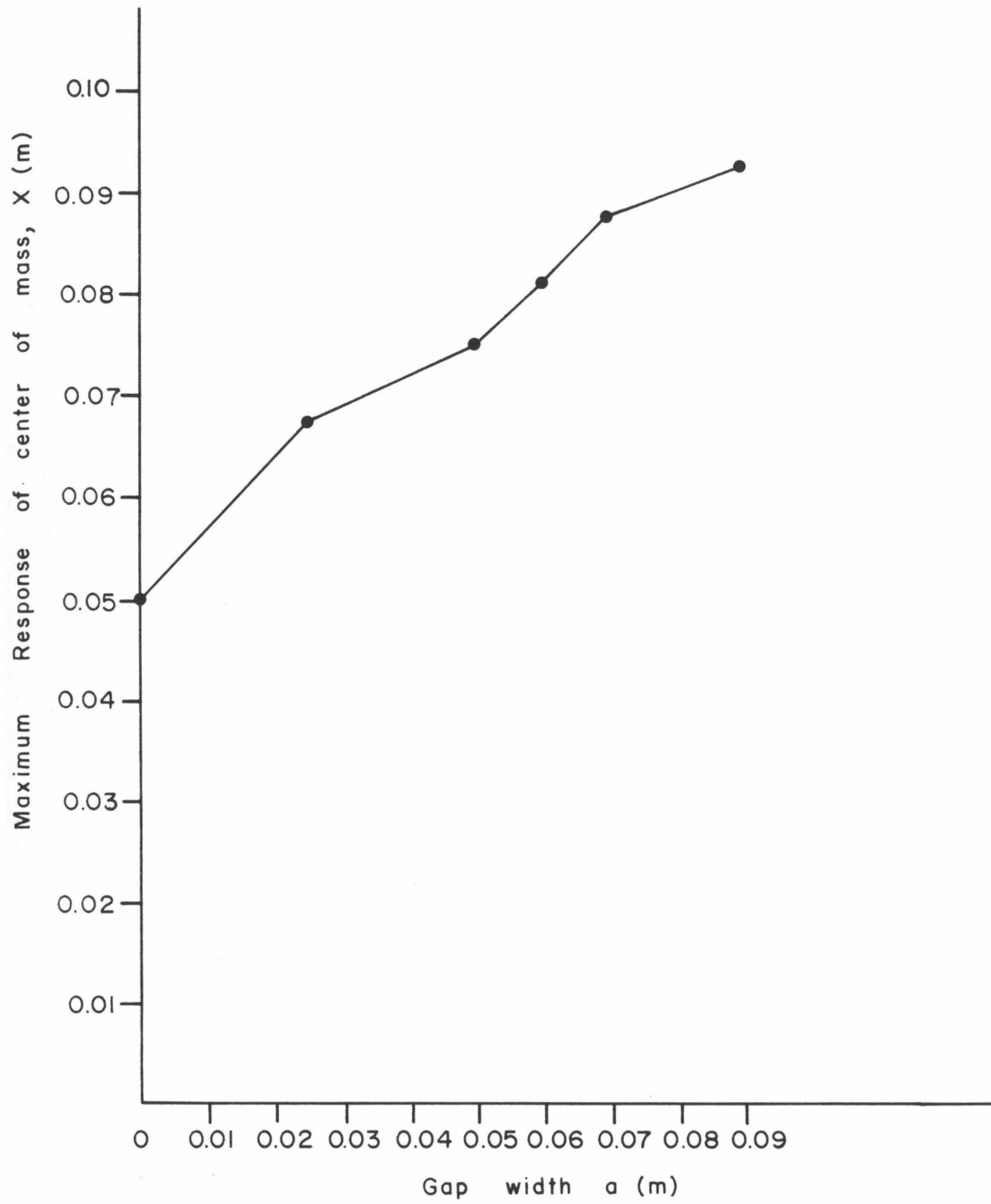


FIG. 2.31 VARIATION OF MAXIMUM LONGITUDINAL RESPONSE WITH GAP WIDTH

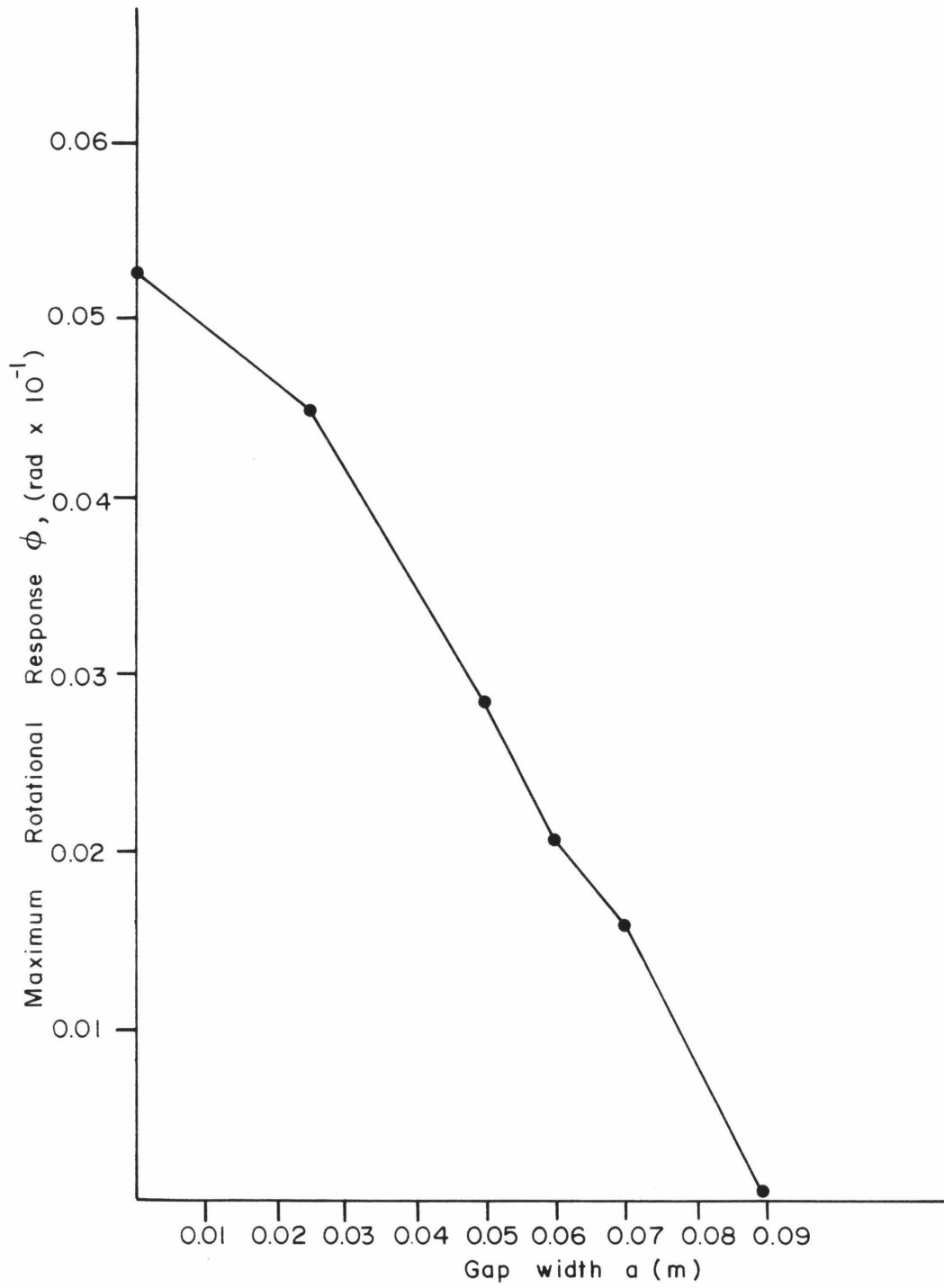


FIG. 2.32 VARIATION OF MAXIMUM ROTATIONAL RESPONSE WITH GAP WIDTH, a

a. The duration of the rotational motions increases as the gap decreases because of earlier impact between the deck and the abutment springs;

b. The maximum rotation decreases as the gap width, a , increases;

c. The maximum displacement in the X-direction of the center of mass of the bridge increases as a increases. This was expected since the bigger the gap, the smaller the reaction force of the abutment spring.

2.8.2. Deck with Widely-Spaced Columns

In the preceding paragraphs, the effects of variations of the initial angle of skewness, the abutment stiffness, and the gap were examined for a case in which the columns were located relatively close to the center of mass of the deck. Because the purpose of the chapter is primarily to illustrate the general nature of the response of the skew bridges, it was decided not to repeat the same calculations for the case in which the columns were located relatively far away from the center of mass.

It will be useful, however, to examine the effects of the location of the restoring springs of the columns on the response of the model. To do this, the values of $l_1/l = 1$ (restoring springs at the ends of the deck) and $l_1/l = 0.6$ (intermediate position of the restoring springs) are examined with values of a , γ and ω_x fixed at 0.025, 5, and 8.89, respectively. The responses of the model for the two values of the ratio l_1/l are shown in Figs. 2.33 - 2.36. Comparing results for these values of l_1/l with those for the initially examined value of $l_1/l = 0.2$, one can draw the following conclusions about the effects of the location of the restoring springs.

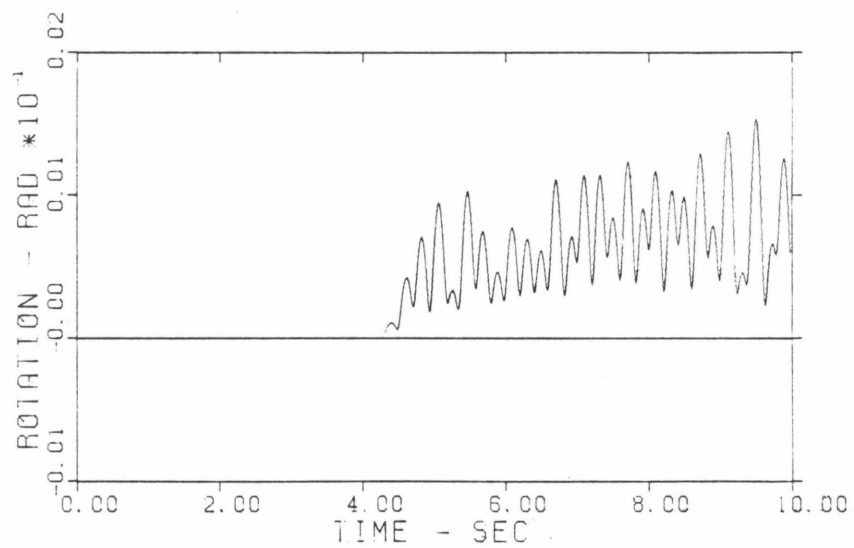
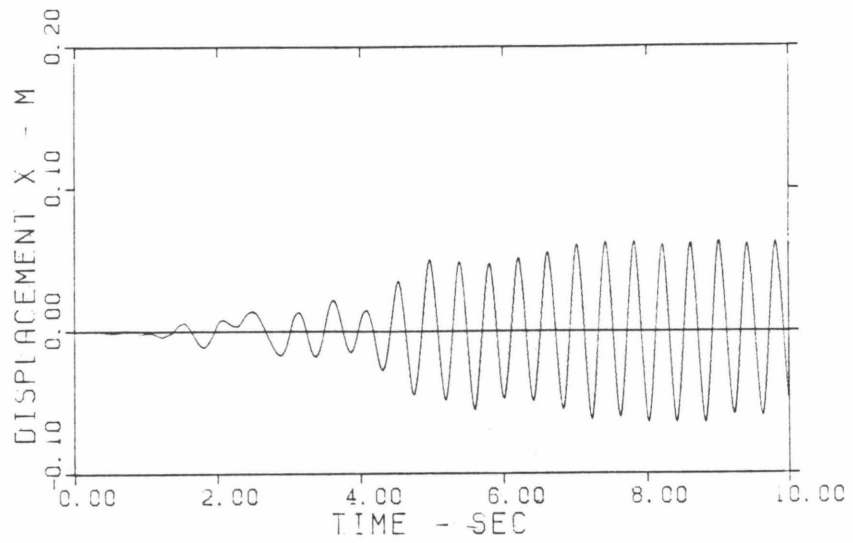


FIG. 2.34 EFFECTS OF THE VARIATION OF COLUMN LOCATION, l_1/l ,
 $\theta = 40^\circ$ AND $l_1/l = 0.6$

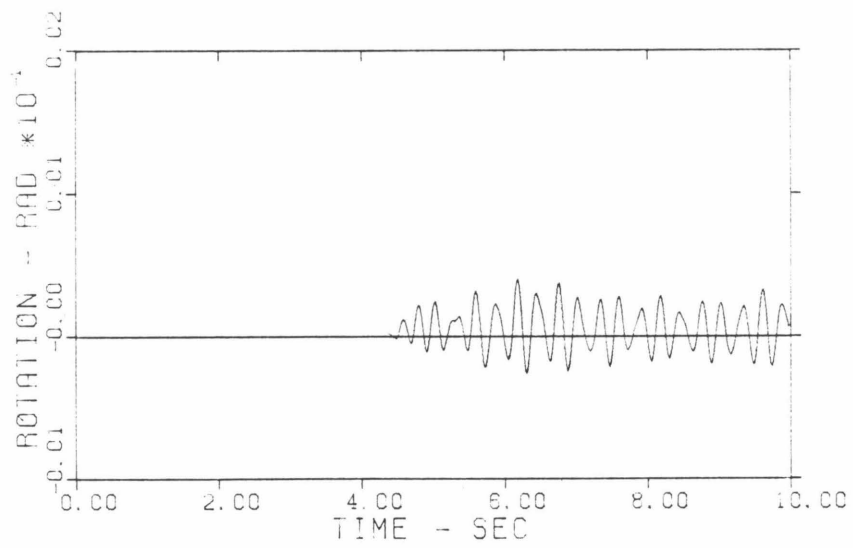
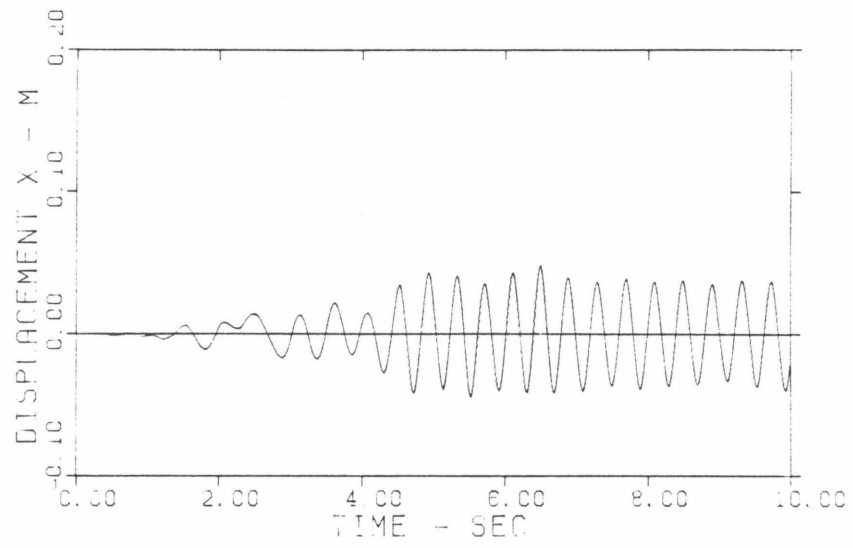


FIG. 2.35 EFFECTS OF THE VARIATION OF COLUMN LOCATION, l_1/l ,
 $\theta = 10^\circ$ AND $l_1/l = 1$

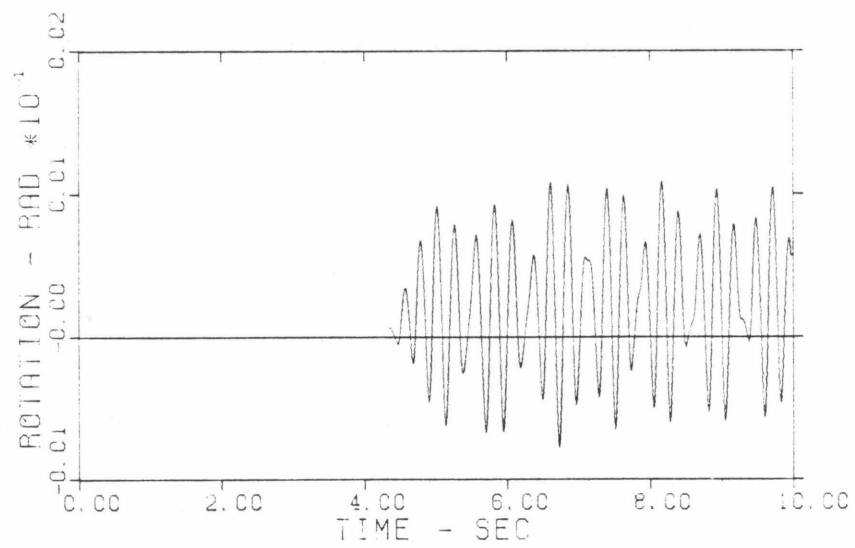
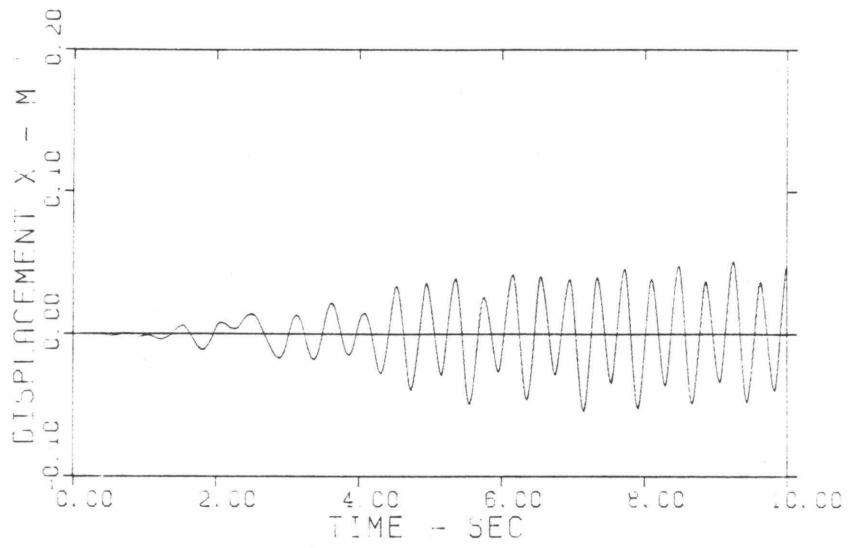


FIG. 2.36 EFFECTS OF THE VARIATION OF COLUMN LOCATION, l_1/l ,
 $\theta = 40^\circ$ AND $l_1/l = 1$

a. As expected, the period of the rotational vibrations of the deck increases as the restoring springs approach the center of mass. On the other hand, if $l_1/l = 1$, the rotational response exhibits relatively high frequencies. In a real bridge, these frequencies could cause substantial flexural deformations (which are neglected in the present analysis) in the plane of rotation.

b. The maximum rotation of the deck decreases as the restoring springs approach the ends of the deck. Again, this change is anticipated because of the increased rotational resistance.

c. Changes in l_1/l result in changes of the dynamic characteristics of the system as reflected in changes in the degree of coupling between the $X-\phi$ motions and in the appearance of the responses.

2.9 GENERAL CONCLUSIONS AND REMARKS

In the preceding paragraphs, some special conclusions were drawn concerning the kinematic mechanisms of the model and its response to an accelerogram from the 1979 Imperial Valley earthquake. In this section, some general conclusions concerning the behavior of the model are presented.

a. The model which was examined in this chapter is capable of illustrating the kinematics of planar, rigid body rotation of the decks of skew bridges including the interaction between the deck and the abutment. Therefore, it can be used as a basis for more detailed modeling of the earthquake response of skew bridges.

b. The model, in the form in which it was developed in this chapter, cannot capture the details of the rigid body response of skew bridges since many simplifications were made (perfect symmetry was

assumed; all the springs were considered linearly elastic; the rotational resistance of the columns was ignored; and any pads were completely neglected). Therefore, the results which were found are only qualitative.

c. In spite of the simplifications that have been made, the model exhibited a complicated behavior, particularly because of the coupling between the X and ϕ motions which occur after impact between the deck and the abutment springs.

d. Most of the parameters of the model seem to be easily identifiable from the geometric and material properties of the bridge. A notable exception is the abutment stiffness. In this case, there is no standard method for determining the required force-deflection behavior. Under these circumstances, it is important to know how sensitive the results are to estimates of the abutment stiffness. Table 2.1 was made based on the results of section 8.1.2 in order to compare the change in γ with the corresponding changes in the maximum rotation and the maximum translation of the center of mass. From this table, one can see that, in most cases, the percentage of change of the parameters of response X and ϕ is substantially less than the corresponding percentages of change of γ . Thus, taking into consideration the other simplifications of the model, one can conclude that a reasonable, simplified method will be accurate enough for the estimation of the abutment stiffness.

TABLE 2.1

Comparison of changes of relative abutment stiffness, γ , with the changes of maximum rotation, ϕ , and maximum translation, X.

θ	Change of γ		Change of γ (%)	Change of Maximum Rotation, ϕ (%)	Change of Maximum Translation, X (%)
	From	To			
10	1	2	100	3.8	14
10	1	5	400	138	14
10	1	10	800	137	25
10	2	5	150	72	0
10	2	10	400	71	13
10	5	10	100	0	13
40	1	2	100	80	0
40	1	5	400	79	3.5
40	1	10	900	140	24
40	2	5	150	0	3.5
40	2	10	400	38	24
40	5	10	100	37	22

CHAPTER 3

ELASTIC STIFFNESS OF BRIDGE COLUMNS WITH PARABOLIC FLARES

3.1 INTRODUCTION

As was shown in Chapter 2, one of the most important parameters of the simple bridge model is the elastic column stiffness, defined as the force required to deflect the top of the column by a unit displacement. In that chapter, the analysis was elastic; and, therefore, the elastic stiffness of the bridge columns alone was sufficient. However, for a more complicated model in which the yielding of the columns will play an important role, a complete force-deflection relation for the columns will be required including both elastic and postelastic stiffnesses. It is believed to be important for the subsequent analysis to have characterizations of the force-deflection relations in both directions of bending.

In order to represent the nonlinear force-deflection relation in a given direction, the following parameters are needed.

a. The initial elastic stiffness For the estimation of the initial column stiffness three things are important:

- (i) The types of deformations which are taken into account,
- (ii) The conditions at the two ends of the columns (boundary conditions), and
- (iii) The geometry of the bridge columns.

In the case of a typical bridge column, the length to depth ratio is large; and, therefore, the bending deformations are large compared to those caused by shear. Consequently, the shearing deformations can be neglected; and the columns can be modeled as beam-columns using Bernoulli-Euler beam theory. As far as the boundary conditions of the

column beams are concerned, it is reasonable to assume that the column is built into the bridge deck at the upper end and has rotational and translational springs at the bottom which account for the effects of the soil. If the foundation conditions are such that these springs can be considered to be infinitely large, then the resulting model of the bridge column is a bending beam built in at both ends. Finally, the geometry depends on the particular column. Columns with uniform cross sections simplify the solution of the problem; whereas, columns with variable cross sections make it more difficult.

b. The yielding levels The ultimate capacity of a concrete column at a given point depends primarily on the cross sectional properties (geometric and reinforcement) of the column at that point and can be estimated by standard methods (Ref. 47).

c. The postelastic stiffness This is the stiffness of the column after its first yielding at the bottom or top cross section. It can be evaluated from the same beam model by properly readjusting the boundary conditions.

The purpose of this chapter is to provide a method for calculating the required force-deflection diagrams of a bridge column. The analysis focuses on the case of columns with parabolic flares at their tops since the bridge which will be used as an illustrative model (Nichols Road Overcrossing - Riverside County, California) has this type of columns. Although a reasonably accurate method would be enough for the purposes of modeling followed in this research, it was found during the analysis of the problem that an exact solution for the initial elastic stiffness of the parabolically flared columns could be provided. Thus, the presentation of this chapter was expanded in order to include this

solution. The solution is presented in the second part of the chapter following an introduction in which the basic points of Bernoulli-Euler bending beam theory are presented. In the third part of the chapter, an alternate solution of the same problem is provided. This solution is approximate, but it is more general in the sense that it can treat columns with any type of flare. This solution is based on the representation of the flare by a sequence of beams of uniform cross section. Finally, the application of the two methods to the case of the columns of the Nichols Road Overcrossing is presented. Also, in the last part of the chapter, the yielding of the columns in the two directions is examined.

3.2 EQUATIONS AND BOUNDARY CONDITIONS FOR A BERNULLI-EULER BEAM

Consider the beam shown in Fig. 3.1. The governing equations for the static case are:

$$\left. \begin{aligned} \frac{d^2}{dz^2} \left(EI(z) \frac{d^2 w(z)}{dz^2} \right) &= 0 & (3.1a) \\ M(z) &= EI(z) \frac{d^2 w(z)}{dz^2} & (3.1b) \\ Q(z) &= - \frac{dM(z)}{dz} & (3.1c) \end{aligned} \right\} (3.1)$$

where:

E is the modulus of elasticity of the material of the beam;

$I(z)$ is the moment of inertia of the cross section of the beam which, for the general case, is a function of z ;

$w(z)$, $M(z)$, and $Q(z)$ are the displacement, bending moment, and shear force, respectively.

In the case of a beam of uniform cross section ($I(z) = \text{constant}$), the

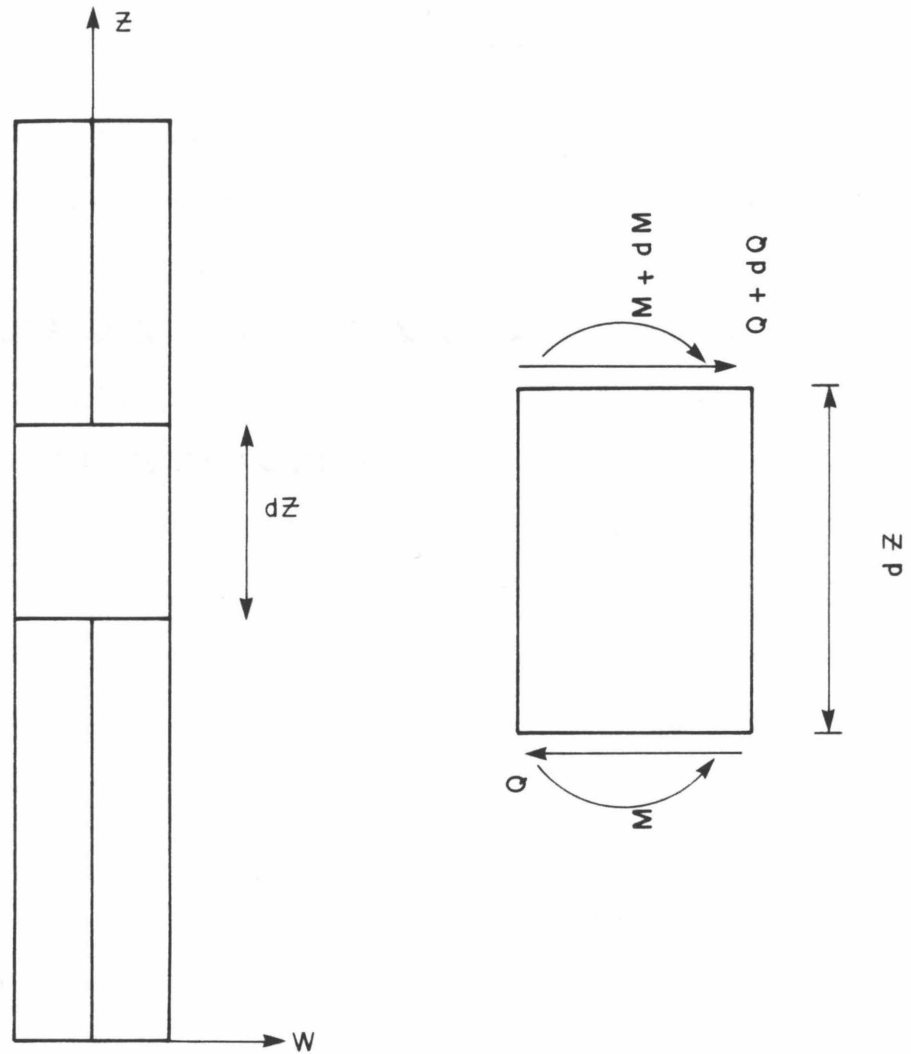


FIG. 3.1 BERNOULLI-EULER BENDING BEAM

above equations reduce to:

$$\frac{d^4w(z)}{dz^4} = 0 \quad (3.2a)$$

$$M(z) = EI \frac{d^2w(z)}{dz^2} \quad (3.2b)$$

$$Q(z) = - \frac{dM(z)}{dz} \quad (3.2c)$$

} (3.2)

In addition to the governing differential equations, the specification of boundary conditions is required. For the case of a bridge column, the most common boundary conditions are shown in Table 3.1.

3.3 STIFFNESS OF A BRIDGE COLUMN WITH OCTAGONAL CROSS SECTION AND PARABOLIC FLARE AT THE TOP AND FOUNDATION SPRINGS AT THE BOTTOM

3.3.1 Equations of a Tapered Column with Foundation Springs

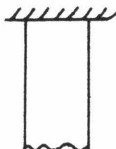
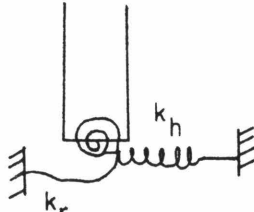
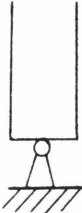
Consider the tapered bridge column shown in Fig. 3.2. The column is fixed at the top; at the bottom, it has torsional foundation springs k^{ZX} and k^{ZY} resisting rotation in the Z-X and Z-Y planes, respectively, and translational foundation springs k_h^X and k_h^Y resisting displacements in the X and Y directions, respectively.

This column can be considered as consisting of two beams. Beam 1 with length h_1 has a uniform cross section and, consequently, a constant moment of inertia while beam 2 with length h_2 has a variable cross section; consequently, its moment of inertia is a function of the position of the cross section. The system of the two beams along with the coordinate systems used in the analysis is shown in Fig. 3.2.

Estimation of the stiffness for in-plane bending

Assume that a unit displacement $X_L^* = 1$ along the X-axis is imposed at the top of the column. Then the equations of each of the two beams

TABLE 3.1 COMMON BOUNDARY CONDITIONS FOR BRIDGE COLUMNS

Type of Boundary	Sketch of Boundary	Boundary Conditions
Fixed end		$[W(Z)]_{\text{end}} = 0$ (displacement = 0) $[W'(Z)]_{\text{end}} = 0$ (slope = 0)
Pinned Bottom end with horizontal and torsional springs		$[EI(Z) \frac{d^2W(Z)}{dz^2}]_{\text{end}} = k_r [W'(Z)]_{\text{end}}$ $[\frac{d}{dz} (EI(Z) \frac{d^2W(Z)}{dz^2})]_{\text{end}} = -k_h [W(Z)]_{\text{end}}$
Pinned end		$[W(Z)]_{\text{end}} = 0$ (displacement = 0) $[EI(Z) \frac{d^2W(Z)}{dz^2}]_{\text{end}} = 0$ (moment = 0)

are the following:

Beam 1 (see formulas 3.2)

$$\frac{d^4W_1(z_1)}{dz_1^4} = 0 \quad (3.3)$$

The solution of (3.3) has the general form:

$$W_1(z_1) = A_1^Y + B_1^Y z_1 + C_1^Y z_1^2 + D_1^Y z_1^3 \quad (3.4)$$

By using (3.4), (3.2b) and (3.2c) one gets:

*For an arbitrary $X_t \neq 1$, the expressions for the displacement, shearing forces, and bending moments should be multiplied by X_t .

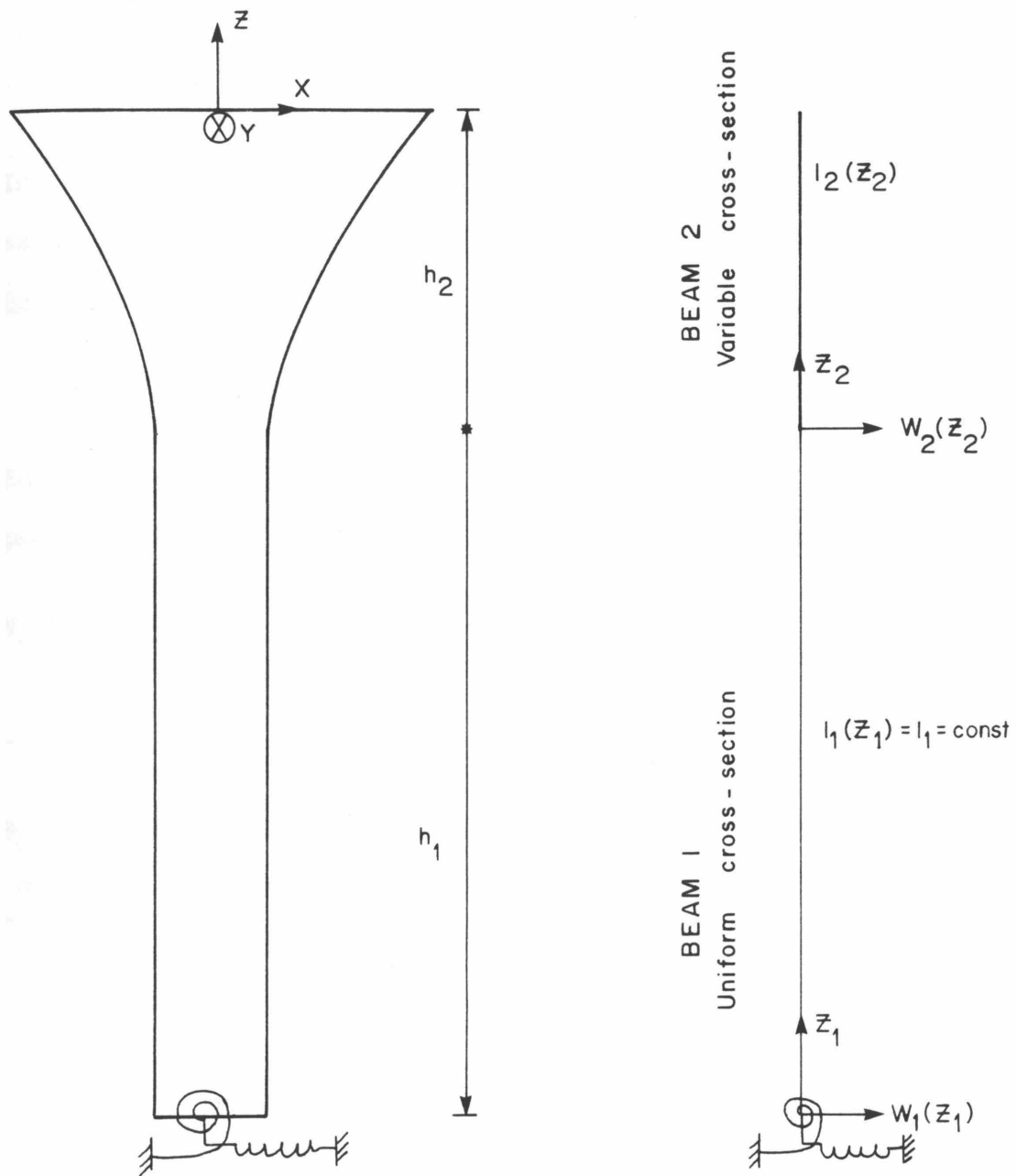


FIG. 3.2 TAPERED BRIDGE COLUMN

$$\frac{dW_1(z_1)}{dz_1} = B_1^Y + 2C_1^Y z_1 + 3D_1^Y z_1^2 \quad (3.5)$$

$$M_1^Y(z_1) = EI_1^Y(2C_1^Y + 6D_1^Y z_1) \quad (3.6)$$

$$Q_1^Y(z_1) = -6EI_1^Y D_1^Y \quad (3.7)$$

In the above equations, the superscript "Y" denotes bending about the Y-axis.

Beam 2 (see formulas 3.1)

$$\frac{d^2}{dz_2^2} (EI_2^Y(z_2) \frac{d^2 w_2(z_2)}{dz_2^2}) = 0 \quad (3.8)$$

Equation (3.8) can be solved by using the method of variation of parameters (Ref. 45). The solution has the final form:

$$\begin{aligned} W_2(z_2) = & D_2^Y + C_2^Y z_2 + \frac{z_2}{E} \int \left(\frac{A_2^Y}{I_2^Y(z_2)} + \frac{B_2^Y z_2}{I_2^Y(z_2)} \right) dz_2 \\ & - \frac{1}{E} \int \left(\frac{z_2 A_2^Y}{I_2^Y(z_2)} + \frac{B_2^Y z_2^2}{I_2^Y(z_2)} \right) dz_2 \end{aligned} \quad (3.9)$$

By combining (3.9), (3.1b) and (3.1c), one gets:

$$\frac{dW_2(z_2)}{dz_2} = C_2^Y + \frac{1}{E} \int \left(\frac{A_2^Y}{I_2^Y(z_2)} + \frac{B_2^Y z_2}{I_2^Y(z_2)} \right) dz_2 \quad (3.10)$$

$$M_2^Y(z_2) = A_2^Y + B_2^Y z_2 \quad (3.11)$$

$$Q_2^Y(z_2) = -B_2^Y \quad (3.12)$$

From equation (3.12) and the definition of the stiffness of the column, it is obvious that the unknown stiffness is the coefficient $-B_2^Y$.

Boundary conditions (see Table 3.1)

$$\text{Beam 1: (i) } EI_1^Y \frac{d^3 w_1(z_1)}{dz_1^3} \Big|_{z_1=0} = -k_h^X w_1(z_1) \Big|_{z_1=0} \quad (3.13)$$

From (3.13) and (3.4) to (3.7), one gets:

$$6EI_1^Y D_1^Y = -k_r^X A_1 \quad (3.14)$$

$$(ii) \quad EI_1^Y \frac{d^2 w_1(z_1)}{dz_1^2} \Big|_{z_1=0} = k_r^{ZX} \frac{dw_1(z_1)}{dz_1} \Big|_{z_1=0} \quad (3.15)$$

Using (3.15) and (3.4) to (3.7) yields:

$$2EI_1^Y C_1^Y = k_r^{ZX} B_1^Y \quad (3.16)$$

$$\text{Beam 2: (i) } w_2(h_2) = 1 \quad (3.17)$$

Combining (3.17) and (3.9) gives:

$$D_2^Y + C_2^Y h_2 + \frac{h_2}{E} \left[\int_{z_2=h_2} \left(\frac{A_2^Y}{I_2^Y(z_2)} + \frac{B_2^Y z_2}{I_2^Y(z_2)} \right) dz_2 \right] -$$

$$\frac{1}{E} \left[\int_{z_2=h_2} \left(\frac{z_2 A_2^Y}{I_2^Y(z_2)} + \frac{B_2^Y z_2^2}{I_2^Y(z_2)} \right) dz_2 \right] = 1 \quad (3.18)$$

$$(ii) \quad \frac{dw_2(z_2)}{dz_2} \Big|_{z_2=h_2} = 0 \quad (3.19)$$

From (3.19) and (3.10):

$$C_2^Y + \frac{1}{E} \left[\int_{z_2=h_2} \left(\frac{A_2^Y}{I_2^Y(z_2)} + \frac{B_2^Y z_2}{I_2^Y(z_2)} \right) dz_2 \right] = 0 \quad (3.20)$$

Conditions of continuity at the connection of the beams

At the connection between Beam 1 and Beam 2, the following continuity conditions must be satisfied:

(i) Continuity of displacements:

$$w_1(z_1) \Big|_{z_1=h_1} = w_2(z_2) \Big|_{z_2=0} \quad (3.21)$$

Applying (3.4), (3.9) and (3.21) produces:

$$A_1^Y + B_1^Y h_1 + C_1^Y h_1^2 + D_1^Y h_1^3 =$$

$$D_2^Y - \frac{1}{E} \left[\int \left(\frac{z_2 A_2^Y}{I_2^Y(z_2)} + \frac{B_2^Y z_2^2}{I_2^Y(z_2)} \right) dz_2 \right]_{z_2=0} \quad (3.22)$$

(ii) Continuity of slopes:

$$\left. \frac{dW_1(z_1)}{dz_1} \right|_{z_1=h_1} = \left. \frac{dW_2(z_2)}{dz_2} \right|_{z_2=0} \quad (3.23)$$

Using (3.5) and (3.10), (3.23) becomes:

$$B_1^Y + 2C_1^Y h_1 + 3D_1^Y h_1^2 =$$

$$C_2^Y + \frac{1}{E} \left[\int \left(\frac{A_2^Y}{I_2^Y(z_2)} + \frac{B_2^Y z_2}{I_2^Y(z_2)} \right) dz_2 \right]_{z_2=0} \quad (3.24)$$

(iii) Continuity of moments:

$$\left. M_1^Y(z_1) \right|_{z_1=h_1} = \left. M_2^Y(z_2) \right|_{z_2=0} \quad (3.25)$$

Combining (3.25) with (3.6) and (3.11) gives:

$$EI_1^Y (2C_1^Y + 6D_1^Y h_1) = A_2^Y \quad (3.26)$$

(iv) Continuity of shears:

$$\left. Q_1^Y(z_1) \right|_{z_1=h_1} = \left. Q_2^Y(z_2) \right|_{z_2=0} \quad (3.27)$$

Using (3.7) and (3.12), (3.27) reduces to

$$6EI_1^Y D_1^Y = B_2^Y \quad (3.28)$$

Equations (3.14), (3.16), (3.18), (3.20), (3.22), (3.24), (3.26) and (3.28) form a system of eight equations in the eight unknowns A_1^Y, \dots, D_1^Y and A_2^Y, \dots, D_2^Y . After making the necessary algebraic manipulations and the substitutions defined by equation (3.29) below, the system takes the final form (3.30) (see page 72).

$$L_1^Y = \int \frac{1}{I_2^Y(z_2)} dz_2 \quad (3.29a)$$

$$L_2^Y = \int \frac{z_2}{I_2^Y(z_2)} dz_2 \quad (3.29b)$$

$$L_3^Y = \int \frac{z_2^2}{I_2^Y(z_2)} dz_2 \quad (3.29c)$$

$$L_1^Y \Big|_{h_2} = \left[\int \frac{1}{I_2^Y(z_2)} dz_2 \right]_{z_2=h_2} ,$$

$$L_1^Y \Big|_0 = \left[\int \frac{1}{I_2^Y(z_2)} dz_2 \right]_{z_2=0}$$

$$L_2^Y \Big|_{h_2} = \left[\int \frac{z_2}{I_2^Y(z_2)} dz_2 \right]_{z_2=h_2} ,$$

$$L_2^Y \Big|_0 = \left[\int \frac{z_2}{I_2^Y(z_2)} dz_2 \right]_{z_2=0}$$

$$L_3^Y \Big|_{h_2} = \left[\int \frac{z_2^2}{I_2^Y(z_2)} dz_2 \right]_{z_2=h_2} ,$$

$$L_3^Y \Big|_0 = \left[\int \frac{z_2^2}{I_2(z_2)} dz_2 \right]_{z_2=0}$$

(3.29)

$$\begin{bmatrix}
 k_h^X & 0 & 0 & 6EI_1^h & 0 & 0 & 0 & 0 \\
 0 & -k_r^{XZ} & 2EI_1^Y & 0 & 0 & 0 & 0 & 0 \\
 0 & 0 & 0 & 0 & \frac{1}{E}(h_2L_1^Y|h_2 - L_2^Y|h_2) & \frac{1}{E}(h_2L_2^Y|h_2 - L_3^Y|h_2) & h_2 & 1 \\
 0 & 0 & 0 & 0 & \frac{1}{E}L_1^Y|h_2 & \frac{1}{E}L_2^Y|h_2 & 1 & 0 \\
 1 & h_1 & h_1^2 & h_1^3 & \frac{1}{E}L_2^Y|_O & \frac{1}{E}L_3^Y|_O & 0 & -1 \\
 0 & 1 & 2h_1 & 3h_1^2 & -\frac{1}{E}L_1^Y|_O & -\frac{1}{E}L_2^Y|_O & -1 & 0 \\
 0 & 0 & 2EI_1^Y & 6EI_1^Yh_1 & -1 & 0 & 0 & 0 \\
 0 & 0 & 0 & -6EI_1^Y & 0 & 1 & 0 & 0
 \end{bmatrix}
 \begin{bmatrix}
 A_1^Y \\
 B_1^Y \\
 C_1^Y \\
 D_1^Y \\
 A_2^Y \\
 B_2^Y \\
 C_2^Y \\
 D_2^Y
 \end{bmatrix}
 =
 \begin{bmatrix}
 0 \\
 1 \\
 1 \\
 0 \\
 0 \\
 0 \\
 0 \\
 0
 \end{bmatrix}$$

(3.30)

It is obvious that, in order to solve the system (3.30), the indefinite integrals L_1^Y , L_2^Y , and L_3^Y have to be evaluated.

Estimation of the stiffness for out-of-plane bending

Following a similar procedure, one finds that the problem is reduced again to the evaluation of the integrals L_1^X , L_2^X , and L_3^X , which are defined by the relations (3.31) and the solution of the system (3.32) (Note that the superscript X denotes bending about the X-axis).

$$\left. \begin{aligned} L_1^X &= \int \frac{1}{I_2^X(z_2)} dz_2 & (3.31a) \\ L_2^X &= \int \frac{z_2}{I_2^X(z_2)} dz_2 & (3.31b) \\ L_3^X &= \int \frac{z_2^2}{I_2^X(z_2)} dz_2 & (3.31c) \end{aligned} \right\} (3.31)$$

3.3.2 General Expressions for the Geometric Properties of the Parabolic Flare of the Column with Octagonal Cross Section

Consider the parabolic flare of the bridge column of total length h_2 as shown in Fig. 3.3. From this figure, it is clear that the dimension which varies parabolically as a function of the position of the cross section is r_1 . Thus:

$$r_1 = \frac{z_2^2}{4k} \quad (3.33)$$

where k is the constant in the equation of the parabolic flare, which can be determined from the value of r_1 at the top of the cross section (r_1^t):

$$k = \frac{h_2^2}{4r_1^t} \quad (3.34)$$

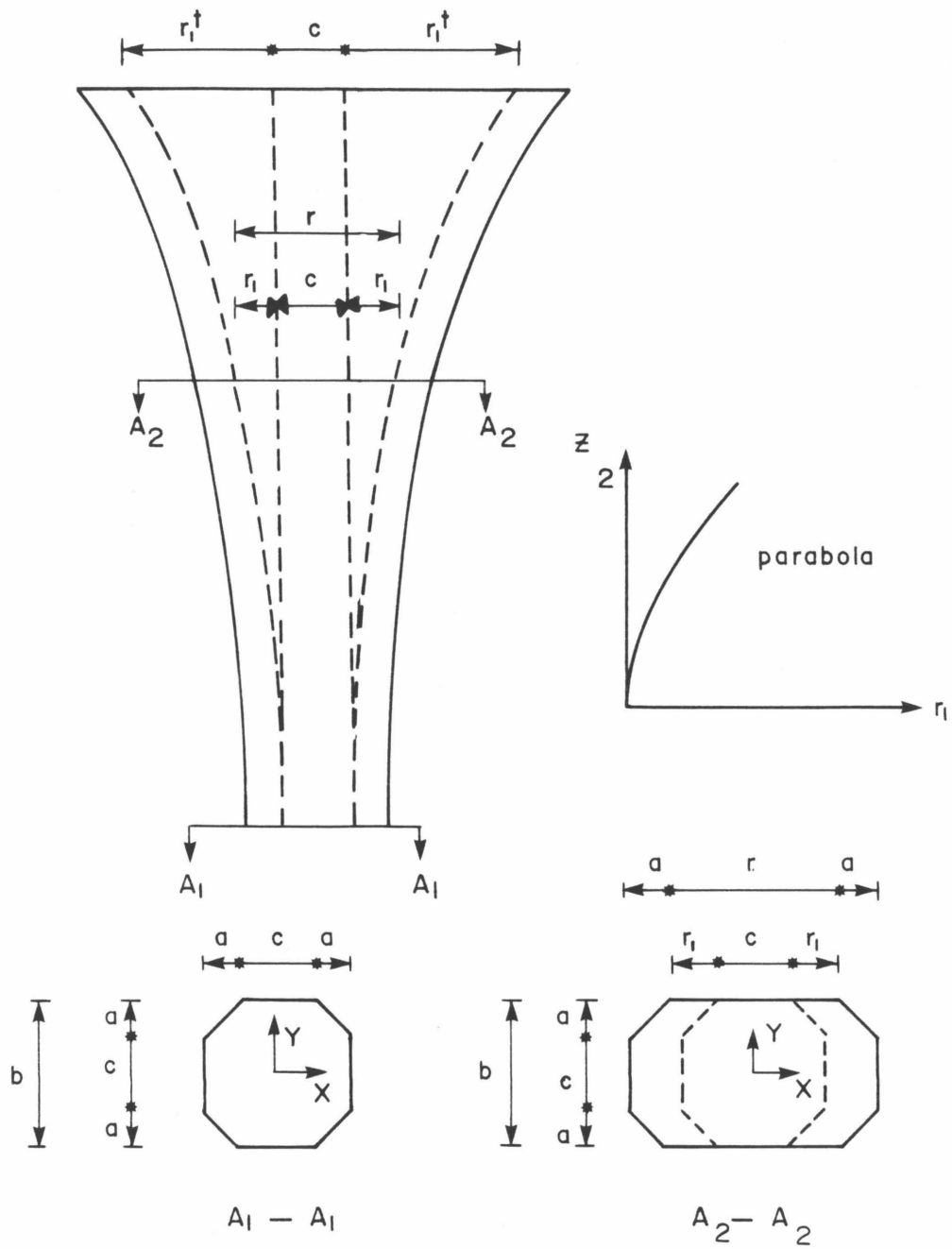


FIG. 3.3 PARABOLIC FLARE WITH OCTAGONAL CROSS SECTION

$$\begin{bmatrix}
 k_h^Y & 0 & 0 & 6EI_1^X & 0 & 0 & 0 & 0 \\
 0 & -k^{YZ} & 2EI_1^X & 0 & 0 & 0 & 0 & 0 \\
 0 & 0 & 0 & 0 & \frac{1}{E}(h_2L_1^X|_{h_2} - L_2^X|_{h_2}) & \frac{1}{E}(h_2L_2^X|_{h_2} - L_3^X|_{h_2}) & h_2 & 1 \\
 0 & 0 & 0 & 0 & \frac{1}{E}L_1^X|_{h_2} & \frac{1}{E}L_2^X|_{h_2} & 1 & 0 \\
 1 & h_1 & h_1^2 & h_1^3 & \frac{1}{E}L_2^X|_0 & \frac{1}{E}L_3^X|_0 & 0 & -1 \\
 0 & 1 & 2h_1 & 3h_1^2 & -\frac{1}{E}L_1^X|_0 & -\frac{1}{E}L_2^X|_0 & -1 & 0 \\
 0 & 0 & 2EI_1^X & 6EI_1^Xh_1 & -1 & 0 & 0 & 0 \\
 0 & 0 & 0 & -6EI_1^X & 0 & 1 & 0 & 0
 \end{bmatrix}
 \begin{bmatrix}
 A_1^X \\
 B_1^X \\
 C_1^X \\
 D_1^X \\
 A_2^X \\
 B_2^X \\
 C_2^X \\
 D_2^X
 \end{bmatrix}
 =
 \begin{bmatrix}
 0 \\
 0 \\
 1 \\
 0 \\
 0 \\
 0 \\
 0 \\
 0
 \end{bmatrix}$$

(3.32)

Also, the following geometric relations can be easily derived from Fig. 3.3:

$$r = c + 2r_1 = c + 2 \frac{z_2^2}{4k} \quad (3.35)$$

Moment of inertia for bending about the Y-axis:

$$I_2^Y(z_2) = \frac{(c + 2\frac{z_2^2}{4k} + 2a)^3 b}{12} - 4 \left[\frac{a^4}{36} + \frac{a^2}{2} \left(\frac{a}{3} + \frac{c}{2} + \frac{z_2^2}{4k} \right)^2 \right] \quad (3.36)$$

Moment of inertia for bending about the X-axis:

$$I_2^X(z_2) = \frac{b^3 (c + 2\frac{z_2^2}{4k} + 2a)}{12} - 4 \left[\frac{a^4}{36} + \frac{a^2}{2} \left(\frac{a}{3} + \frac{b-2a}{2} \right)^2 \right] \quad (3.37)$$

After carrying out all the necessary algebra, the general expressions for the moments of inertia reduce to:

$$I_2^Y(z_2) = \alpha_1^Y z_2^6 + \alpha_2^Y z_2^4 + \alpha_3^Y z_2^2 + \alpha_4^Y \quad (3.38a)$$

$$I_2^X(z_2) = \alpha_1^X z_2^2 + \alpha_2^X \quad (3.38b)$$

}
⋮

$$\begin{aligned}
 \text{where: } \alpha_1^Y &= \frac{b}{96k^3} ; \quad \alpha_2^Y = \frac{(c+2a)b}{16k^2} - \frac{a^2}{8k^2} \\
 \alpha_3^Y &= \frac{(c+2a)^2b}{8k} - \frac{a^2}{k} \left(\frac{a}{3} + \frac{c}{2} \right) , \\
 \alpha_4^Y &= \frac{(c+2a)^3b}{12} - \frac{a^4}{9} - 2a^2 \left(\frac{a}{3} + \frac{c}{2} \right)^2 \\
 \alpha_1^X &= \frac{b^3}{24k} \\
 \alpha_2^X &= \frac{cb^3}{12} + \frac{ab^3}{6} - \frac{a^4}{9} - 2a^2 \left(\frac{a}{3} + \frac{b-2a}{2} \right)^2
 \end{aligned}
 \tag{3.38}$$

3.3.3 Evaluation of the Integrals L_1^Y , L_2^Y , and L_3^Y in the case of a Parabolic Flare with Octagonal Cross Section

Combining the relations (3.29a) to (3.29c) with (3.38a), the integrals to be evaluated can be expressed by the following general relations:

$$\begin{aligned}
 L_1^Y &= \int \frac{1}{\alpha_1^Y z_2^6 + \alpha_2^Y z_2^4 + \alpha_3^Y z_2^2 + \alpha_4^Y} dz_2 & (3.39a) \\
 L_2^Y &= \int \frac{z_2}{\alpha_1^Y z_2^6 + \alpha_2^Y z_2^4 + \alpha_3^Y z_2^2 + \alpha_4^Y} dz_2 & (3.39b) \\
 L_3^Y &= \int \frac{z_2^2}{\alpha_1^Y z_2^6 + \alpha_2^Y z_2^4 + \alpha_3^Y z_2^2 + \alpha_4^Y} dz_2 & (3.39c)
 \end{aligned}
 \tag{3.39}$$

To evaluate the integrals, the roots of the denominator must be examined.

Consider the equation:

$$I_2^Y(z_2) = \alpha_1^Y (z_2^6 + \frac{\alpha_2^Y}{\alpha_1^Y} z_2^4 + \frac{\alpha_3^Y}{\alpha_1^Y} z_2^2 + \frac{\alpha_4^Y}{\alpha_1^Y}) = 0 \quad (3.40)$$

By making the substitution $z_2^2 = S$ in (3.40) and noting that $\alpha_1^Y \neq 0$, one gets:

$$P(S) = S^3 + \frac{\alpha_2^Y}{\alpha_1^Y} S^2 + \frac{\alpha_3^Y}{\alpha_1^Y} S + \frac{\alpha_4^Y}{\alpha_1^Y} = 0 \quad (3.41)$$

The analytic expressions of the roots of (3.41) are given by the following relations (Ref. 47):

Roots

$$S_1 = A + B - \frac{\alpha_2^Y}{3\alpha_1^Y} \quad (3.42a)$$

$$S_2 = -1/2 (A + B) + \frac{i\sqrt{3}}{2} (A - B) - \frac{\alpha_2^Y}{3\alpha_1^Y} \quad (3.42b) \quad (3.42)$$

$$S_3 = -1/2 (A + B) - \frac{i\sqrt{3}}{2} (A - B) - \frac{\alpha_2^Y}{3\alpha_1^Y} \quad (3.42c)$$

where:

$$A = \sqrt[3]{-\frac{\lambda}{2} + \sqrt{\frac{\lambda^2}{4} + \frac{\mu}{27}}} \quad (3.43)$$

$$B = \sqrt[3]{-\frac{\lambda}{2} - \sqrt{\frac{\lambda^2}{4} + \frac{\mu}{27}}}$$

$$\lambda = \frac{1}{27} \left[2 \left(\frac{\alpha_2^Y}{\alpha_1^Y} \right)^3 - 9 \frac{\alpha_2^Y \alpha_3^Y}{(\alpha_1^Y)^2} + 27 \frac{\alpha_4^Y}{\alpha_1^Y} \right]$$

$$\mu = \frac{1}{3} \left[3 \frac{\alpha_3^Y}{\alpha_1^Y} - \left(\frac{\alpha_2^Y}{\alpha_1^Y} \right)^2 \right]$$

From relations (3.42) and (3.43), it follows that there are three cases

for the roots of (3.41):

Case (i) $-\frac{\lambda^2}{4} + \frac{\mu^2}{27} > 0$, (3.41) has one real root and two conjugate complex roots.

Case (ii) $-\frac{\lambda^2}{4} + \frac{\mu^3}{27} = 0$, (3.41) has three real roots; two, at least, equal.

Case (iii) $-\frac{\lambda^2}{4} + \frac{\mu^3}{27} < 0$, (3.41) has three real, unequal roots.

It is important to note that, in all three cases, the real root(s) of (3.41) have to be negative, because, if S_i is a positive real root of (3.41), then $Z_i = S_i > 0$ will be a positive real root of (3.40); this, however, has no physical meaning since the moment of inertia must be positive.

Case (i)

Let $S_1 = A + B - \frac{\alpha^{\frac{Y}{2}}}{3\alpha_1^{\frac{Y}{2}}}$ be the real root of (3.41).

Since $S_1 < 0$, one can write:

$$S_1 = A + B - \frac{\alpha^{\frac{Y}{2}}}{3\alpha_1^{\frac{Y}{2}}} = -t_1^2$$

where:

(3.44)

$$t_1 = \sqrt{\left| A + B - \frac{\alpha^{\frac{Y}{2}}}{3\alpha_1^{\frac{Y}{2}}} \right|} = \sqrt{|S_1|}$$

Then, the moment of inertia $I_2^Y(Z_2)$ can be written as a product of a

quatic and a quadratic polynomial in the following way:

$$I_2^Y(Z_2) = \alpha_1^Y (Z_2^2 + t_1^2) (LZ_2^4 + KZ_2^2 + M) \quad (3.45)$$

The coefficients L , K , and M can be evaluated easily by equating the coefficients of the same order terms in equations (3.38a) and (3.45):

$$L = 1$$

$$K = -\frac{1}{\alpha_1^Y} (\alpha_2^Y + \alpha_1^Y S_1) \quad (3.46)$$

$$M = -\frac{\alpha_4^Y}{S_1 \alpha_1^Y}$$

Consider now the polynomial $R(Z_2) = Z_2^4 + KZ_2^2 + M$, which, by the transformation $Z_2^2 = S$, can be written as: $R(S) = S^2 + KS + M$. Let $\Delta = K^2 - 4M$ be the discriminant of $R(S)$. Since Case (i) is being examined, the polynomial $R(S)$ has two complex conjugate roots; and, therefore, $\Delta < 0$. The two roots of $R(S)$ are given by the relations

$$S_2 = \alpha + i\beta$$

$$S_3 = \alpha - i\beta$$

$$(3.47)$$

$$\alpha = -\frac{K}{2}, \quad \beta = \frac{-4}{2}$$

Using polar coordinates, the roots can be expressed as follows:

$$\rho = |S_2| = |S_3| = \sqrt{\alpha^2 + \beta^2}$$

$$\phi = \phi_2 = -\phi_3 \quad -\pi < \phi < \pi \quad (\text{principal argument})$$

$$\cos \phi_2 = \frac{\alpha}{\rho}, \quad \sin \phi_2 = \frac{\beta}{\rho}, \quad \cos \phi_3 = \frac{\alpha}{\rho}, \quad \sin \phi_3 = -\frac{\beta}{\rho} \quad (3.48)$$

$$S_2 = \rho(\cos \phi_2 + i \sin \phi_2) = \rho(\cos \phi + i \sin \phi)$$

$$S_3 = \rho(\cos \phi_3 + i \sin \phi_3) = \rho(\cos \phi - i \sin \phi)$$

By using the polar representation of S_2 and S_3 , one can find the four

roots of $R(Z_2)$ from application of the relation for the n^{th} root of a complex number.

$$W_n = r(\cos\theta + i \sin\theta)$$

where

(3.49)

$$W_n = \sqrt[n]{r} \left(\cos \frac{\theta + 2k\pi}{n} + i \sin \frac{\theta + 2k\pi}{n} \right) \quad (k = 0, 1, \dots, n-1)$$

This gives:

$$\begin{aligned}
 z_2^2 = S_2 \rightarrow & \left\{ \begin{aligned} z_{2,1} &= \sqrt{\rho} \left[\cos \frac{\phi}{2} + i \sin \frac{\phi}{2} \right] \\ z_{2,2} &= \sqrt{\rho} \left[\cos \frac{\phi + 2\pi}{2} + i \sin \frac{\phi + 2\pi}{2} \right] = \\ & -\sqrt{\rho} \left[\cos \frac{\phi}{2} + i \sin \frac{\phi}{2} \right] \end{aligned} \right. \\
 z_2^2 = S_3 \rightarrow & \left\{ \begin{aligned} z_{2,3} &= \sqrt{\rho} \left[\cos \frac{\phi}{2} - i \sin \frac{\phi}{2} \right] \\ z_{2,4} &= \sqrt{\rho} \left[\cos \frac{-\phi + 2\pi}{2} + i \sin \frac{-\phi + 2\pi}{2} \right] = \\ & -\sqrt{\rho} \left[\cos \frac{\phi}{2} - i \sin \frac{\phi}{2} \right] \end{aligned} \right. \quad (3.50)
 \end{aligned}$$

With this result, the polynomial $R(Z_2)$ can be written as the product of four first order polynomials as follows:

$$R(z_2) = (z_2 - z_{2,1})(z_2 - z_{2,3})(z_2 - z_{2,2})(z_2 - z_{2,4}) \text{ or}$$

$$R(z_2) = [z_2 - \sqrt{\rho} \left(\cos \frac{\phi}{2} + i \sin \frac{\phi}{2} \right)]$$

$$[z_2 - \sqrt{\rho} \left(\cos \frac{\phi}{2} - i \sin \frac{\phi}{2} \right)] [z_2 + \sqrt{\rho} \left(\cos \frac{\phi}{2} + i \sin \frac{\phi}{2} \right)]$$

$$[z_2 + \sqrt{\rho} \left(\cos \frac{\phi}{2} - i \sin \frac{\phi}{2} \right)] \quad (3.51)$$

After carrying out the algebra in (3.51), one can express the polynomial $R(z_2)$ as a product of two irreducible quadratic polynomials with real coefficients:

$$R(z_2) = (z_2^2 - 2z_2\sqrt{\rho} \cos \frac{\phi}{2} + \rho) (z_2^2 + 2z_2\sqrt{\rho} \cos \frac{\phi}{2} + \rho) \quad (3.52)$$

Combining equations (3.45) and (3.52), the moment of inertia can be factored into three irreducible quadratic factors with real coefficients:

$$I_2^Y(z_2) = \alpha_1^Y (z_2^2 + t_1^2) (z_2^2 - 2z_2\sqrt{\rho} \cos \frac{\phi}{2} + \rho)$$

$$(z_2^2 + 2z_2\sqrt{\rho} \cos \frac{\phi}{2} + \rho) \quad (3.53)$$

Consider now the fraction:

$$\begin{aligned}
 F(Z_2) &= \frac{1}{I_2^Y(Z_2)} = \\
 &= \frac{1}{\alpha_1^Y (z_2^2 + t_1^2) (z_2^2 - 2z_2 \sqrt{\rho} \cos \frac{\phi}{2} + \rho) (z_2^2 + 2z_2 \sqrt{\rho} \cos \frac{\phi}{2} + \rho)} \quad (3.54)
 \end{aligned}$$

The above fraction can be broken into partial fractions as follows

(Ref. 48):

$$\begin{aligned}
 F(Z_2) &= \frac{1}{\alpha_1^Y} \left(\frac{X_1 Z_2 + X_2}{z_2^2 + t_1^2} + \frac{X_3 Z_2 + X_4}{z_2^2 - 2z_2 \sqrt{\rho} \cos \frac{\phi}{2} + \rho} + \right. \\
 &\quad \left. \frac{X_5 Z_2 + X_6}{z_2^2 + 2z_2 \sqrt{\rho} \cos \frac{\phi}{2} + \rho} \right) \quad (3.55)
 \end{aligned}$$

By combining (3.54) and (3.55) and equating coefficients, one produces the system of equations shown in (3.56). The solution of this system determines the coefficients X_1, X_2, \dots, X_6 . Therefore, the expression of $F(Z_2)$ as a sum of partial fractions [see (3.55)] is completely defined by solving the system (3.56). Next, return to the integrals L_1^Y, L_2^Y , and L_3^Y . By combining relations (3.39) and (3.55), the following

$$\begin{bmatrix}
 1 & 0 & 1 & 0 & 1 & 0 \\
 0 & 1 & 2\sqrt{\rho} \cos \frac{\phi}{2} & 1 & -2\sqrt{\rho} \cos \frac{\phi}{2} & 1 \\
 2(1-2\cos^2 \frac{\phi}{2}) & 0 & \rho + t_1^2 & 2\sqrt{\rho} \cos \frac{\phi}{2} & t_1^2 + \rho & -2\sqrt{\rho} \cos \frac{\phi}{2} \\
 0 & 2\rho(1-2\cos^2 \frac{\phi}{2}) & 2t_1^2 \sqrt{\rho} \cos \frac{\phi}{2} & \rho + t_1^2 & -2t_1^2 \sqrt{\rho} \cos \frac{\phi}{2} & t_1^2 + \rho \\
 \rho^2 & 0 & \rho t_1^2 & 2t_1^2 \sqrt{\rho} \cos \frac{\phi}{2} & \rho t_1^2 & -2t_1^2 \sqrt{\rho} \cos \frac{\phi}{2} \\
 0 & \rho^2 & 0 & \rho t_1^2 & 0 & \rho t_1^2
 \end{bmatrix}
 \begin{bmatrix}
 x_1 \\
 x_2 \\
 x_3 \\
 x_4 \\
 x_5 \\
 x_6
 \end{bmatrix}
 =
 \begin{bmatrix}
 0 \\
 0 \\
 0 \\
 0 \\
 0 \\
 1
 \end{bmatrix}$$

(3.56)

expressions for the above integrals can be obtained.

$$\begin{aligned}
 L_1^Y &= \frac{1}{\alpha_1^Y} (X_1 H_2 + X_2 H_1 + X_3 H_4 + X_4 H_3 + X_5 H_6 + X_6 H_5) \\
 L_2^Y &= \frac{1}{\alpha_1^Y} (X_1 H_7 + X_2 H_2 + X_3 H_8 + X_4 H_4 + X_5 H_9 + X_6 H_6) \\
 L_3^Y &= \frac{1}{\alpha_1^Y} (X_1 H_{10} + X_2 H_7 + X_3 H_{11} + X_4 H_8 + X_5 H_{12} + X_6 H_9)
 \end{aligned} \tag{3.57}$$

where:

$$\begin{aligned}
 H_1 &= \int \frac{1}{z_2^2 + t_1^2} dz_2 \\
 H_2 &= \int \frac{z_2}{z_2^2 + t_1^2} dz_2 \\
 H_3 &= \int \frac{1}{z_2^2 - 2z_2 \sqrt{\rho} \cos \frac{\phi}{2} + \rho} dz_2 \\
 H_4 &= \int \frac{z_2}{z_2^2 - 2z_2 \sqrt{\rho} \cos \frac{\phi}{2} + \rho} dz_2 \\
 H_5 &= \int \frac{1}{z_2^2 + 2z_2 \sqrt{\rho} \cos \frac{\phi}{2} + \rho} dz_2 \\
 H_6 &= \int \frac{z_2}{z_2^2 + 2z_2 \sqrt{\rho} \cos \frac{\phi}{2} + \rho} dz_2
 \end{aligned} \tag{3.58}$$

$$\begin{aligned}
 H_7 &= \int \frac{z_2^2}{z_2^2 + t_1^2} dz_2 \\
 H_8 &= \int \frac{z_2^2}{z_2^2 - 2z_2\sqrt{\rho} \cos \frac{\phi}{2} + \rho} dz_2 \\
 H_9 &= \int \frac{z_2^2}{z_2^2 + 2z_2\sqrt{\rho} \cos \frac{\phi}{2} + \rho} dz_2
 \end{aligned}
 \tag{3.58} \text{ cont.}$$

These integrals can all be evaluated using standard integral tables.

$$\begin{aligned}
 H_1 &= \frac{1}{t_1} \operatorname{arctg} \frac{z_2}{t_1} \\
 H_2 &= \frac{1}{2} \ln(z_2^2 + t_1^2) \\
 H_3 &= \frac{1}{\sqrt{(1 - \cos^2 \frac{\phi}{2})}} \operatorname{arctg} \frac{z_2 - \sqrt{\rho} \cos \frac{\phi}{2}}{\sqrt{\rho} (1 - \cos^2 \frac{\phi}{2})}
 \end{aligned}
 \tag{3.59}$$

$$\begin{aligned}
H_4 &= \frac{1}{2} \ln(z_2^2 - 2z_2 \sqrt{\rho} \cos \frac{\phi}{2} + \rho) + \\
&\frac{\cos \frac{\phi}{2}}{\sqrt{1 - \cos^2 \frac{\phi}{2}}} \operatorname{arctg} \frac{z_2 - \sqrt{\rho} \cos \frac{\phi}{2}}{\sqrt{\rho (1 - \cos^2 \frac{\phi}{2})}} \\
H_5 &= \frac{1}{\sqrt{\rho (1 - \cos^2 \frac{\phi}{2})}} \operatorname{arctg} \frac{\sqrt{\rho} \cos \frac{\phi}{2} + z_2}{\sqrt{\rho (1 - \cos^2 \frac{\phi}{2})}} \\
H_6 &= \frac{1}{2} \ln(z_2^2 + 2z_2 \sqrt{\rho} \cos \frac{\phi}{2} + \rho) - \\
&\frac{\cos \frac{\phi}{2}}{\sqrt{1 - \cos^2 \frac{\phi}{2}}} \operatorname{arctg} \frac{\sqrt{\rho} \cos \frac{\phi}{2} + z_2}{\sqrt{\rho (1 - \cos^2 \frac{\phi}{2})}} \\
H_7 &= z_2 - t_1 \operatorname{arctg} \frac{z_2}{t_1} \\
H_8 &= z_2 + \sqrt{\rho} \cos \frac{\phi}{2} \ln(z_2^2 - 2z_2 \sqrt{\rho} \cos \frac{\phi}{2} + \rho) + \\
&\frac{2\rho \cos^2 \frac{\phi}{2} - \rho}{\sqrt{\rho (1 - \cos^2 \frac{\phi}{2})}} \operatorname{arctg} \frac{-\sqrt{\rho} \cos \frac{\phi}{2} + z_2}{\sqrt{\rho (1 - \cos^2 \frac{\phi}{2})}} \\
H_9 &= z_2 - \sqrt{\rho} \cos \frac{\phi}{2} \ln(z_2^2 + 2z_2 \sqrt{\rho} \cos \frac{\phi}{2} + \rho) +
\end{aligned} \tag{3.59}$$

$$\begin{aligned}
& \frac{2\rho \cos^2 \frac{\phi}{2} - \rho}{\sqrt{\rho(1 - \cos^2 \frac{\phi}{2})}} \operatorname{arctg} \frac{z_2 + \sqrt{\rho} \cos \frac{\phi}{2}}{\sqrt{\rho(1 - \cos^2 \frac{\phi}{2})}} \\
H_{10} &= \frac{z_2^2}{2} - \frac{t_1^2}{2} \ln(z_2^2 + t_1^2) \\
H_{11} &= \frac{z_2^2}{2} + 2\sqrt{\rho} \cos \frac{\phi}{2} z_2 + \\
& \frac{4\rho \cos^2 \frac{\phi}{2} - \rho}{2} \ln(z_2^2 - 2z_2 \sqrt{\rho} \cos \frac{\phi}{2} + \rho) + \\
& \cos \frac{\phi}{2} (4\rho \cos^2 \frac{\phi}{2} - 3\rho) \frac{1}{\sqrt{1 - \cos^2 \frac{\phi}{2}}} \operatorname{arctg} \frac{-\sqrt{\rho} \cos \frac{\phi}{2} + z_2}{\sqrt{\rho(1 - \cos^2 \frac{\phi}{2})}} \\
H_{12} &= \frac{z_2^2}{2} - 2\sqrt{\rho} \cos \frac{\phi}{2} z_2 + \\
& \frac{4\rho \cos^2 \frac{\phi}{2} - \rho}{2} \ln(z_2^2 + 2z_2 \sqrt{\rho} \cos \frac{\phi}{2} + \rho) - \\
& \cos \frac{\phi}{2} (4\rho \cos^2 \frac{\phi}{2} - 3\rho) \frac{1}{\sqrt{1 - \cos^2 \frac{\phi}{2}}} \operatorname{arctg} \frac{\sqrt{\rho} \cos \frac{\phi}{2} + z_2}{\sqrt{\rho(1 - \cos^2 \frac{\phi}{2})}}
\end{aligned} \tag{3.59} \text{ cont.}$$

Combination of relations (3.59), (3.58), (3.57) results in the determination of the elements of the coefficient matrix in the system (3.30).

Case (iii)

Let S_1 , S_2 , and S_3 be the three unequal roots of (3.41). Since all of them are negative, one can write:

$$\left. \begin{aligned} S_1 &= -t_1^2 \\ S_2 &= -t_2^2 \\ S_3 &= -t_3^2 \end{aligned} \right\} (3.60)$$

Then, the moment of inertia $I_2^Y(z_2)$ can be factorized in the following way:

$$I_2^Y(z_2) = \alpha_1^Y (z_2^2 + t_1^2) (z_2^2 + t_2^2) (z_2^2 + t_3^2) \quad (3.61)$$

The steps that have to be followed after the factorization of $I_2^Y(z_2)$ are quite similar to the ones followed in Case (i). The fraction $F(z_2) =$

$\frac{1}{I_2^Y(z_2)}$ has to be broken into partial fractions, which will result in

expressions for the integrals L_1^Y , L_2^Y , and L_3^Y in terms of integrals like H_1 , H_2 , and H_7 .

3.3.4 Evaluation of the Integrals L_1^X , L_2^X , and L_3^X in the Case of a Parabolic Flare with Octagonal Cross Section

Combining relations (3.31a) to (3.31c) with (3.38b), one can see that the integrals to be evaluated can be expressed by the following general relations:

$$L_1^X = \int \frac{1}{\alpha_1^X z_2^2 + \alpha_2^X} dz_2 \quad (3.62a)$$

$$L_2^X = \int \frac{z_2}{\alpha_1^X z_2^2 + \alpha_2^X} dz_2 \quad (3.62b) \quad (3.62)$$

$$L_3^X = \int \frac{z_2^2}{\alpha_1^X z_2^2 + \alpha_2^X} dz_2 \quad (3.62c)$$

The above integrals can be evaluated easily:

$$L_1^X = \frac{1}{\alpha_1^X} \frac{1}{\sqrt{\frac{\alpha_2^X}{\alpha_1^X}}} \operatorname{arctg} \frac{z_2}{\sqrt{\frac{\alpha_2^X}{\alpha_1^X}}} \quad (3.63)$$

$$L_2^X = \frac{1}{\alpha_1^X} \frac{1}{2} \ln \left(z_2^2 + \frac{\alpha_2^X}{\alpha_1^X} \right)$$

$$L_3^X = \frac{1}{\alpha_1^X} z_2 - \frac{1}{\alpha_1^X} \sqrt{\frac{\alpha_2^X}{\alpha_1^X}} \operatorname{arctg} \frac{z_2}{\sqrt{\frac{\alpha_2^X}{\alpha_1^X}}}$$

It should be clear from the above analysis that the method presented can be used for any column with variable cross section provided that the moments of inertia can be expressed by equations (3.38a) and (3.38b).

3.3.5 Summary of the Basic Steps for the Analytic Evaluation of the Stiffness

Because of the extent of the previous analysis, it seems appropriate to summarize the steps needed to apply the results to a particular case.

a. Bending about the Y-axis - Case (i)

1. Find t_1 , K , and M from formulas (3.44) and (3.46), respectively.
2. Find α , β , ρ , and ϕ by using relations (3.47) and (3.48).
3. Calculate the elements of the matrix in system (3.56); solve the system and find the coefficients X_1, X_2, \dots, X_6 .
4. By using equation (3.59), evaluate the integrals H_1, \dots, H_9 at the required points ($Z_2 = 0, Z_2 = h_2$).

5. Use formula (3.57) to evaluate L_1^Y , L_2^Y , and L_3^Y at the required points ($Z_2 = 0$, $Z_2 = h_2$).
6. Calculate the elements of the matrix in system (3.30) and solve it. The value of $-B_2^Y$ is the desired stiffness.

b. Bending about the X-axis

1. By using equation (3.63), evaluate the integrals L_1^X , L_2^X , and L_3^X at the required points ($Z_2 = 0$, $Z_2 = h_2$).
2. Calculate the elements of the matrix in the system (3.32) and solve it. The value of $-B_2^X$ is the required stiffness.

3.4 APPROXIMATE ESTIMATION OF THE STIFFNESS OF A TAPERED COLUMN

The analysis in this section is intended to provide an alternative approach to the problem of finding the elastic stiffness of a tapered column. The approach is less accurate but more general than that developed in the previous section.

Consider again the column shown in Fig. 3.2. This column can be approximated by a sequence of bending beams, each one having a constant moment of inertia equal to the average moment of the corresponding section of the column. This representation of the column is shown in Fig. 3.4.

3.4.1 Estimation of the Stiffness for Bending About the Y-Direction

Assume that a unit displacement $X^t = 1$ along the X-axis is imposed at the top of the column. The deflection of the k^{th} beam is governed by the equation:

$$\frac{d^4 w_k(z_k)}{dz_k^4} = 0 \quad (3.64)$$

The solution of (3.64) has the general form:

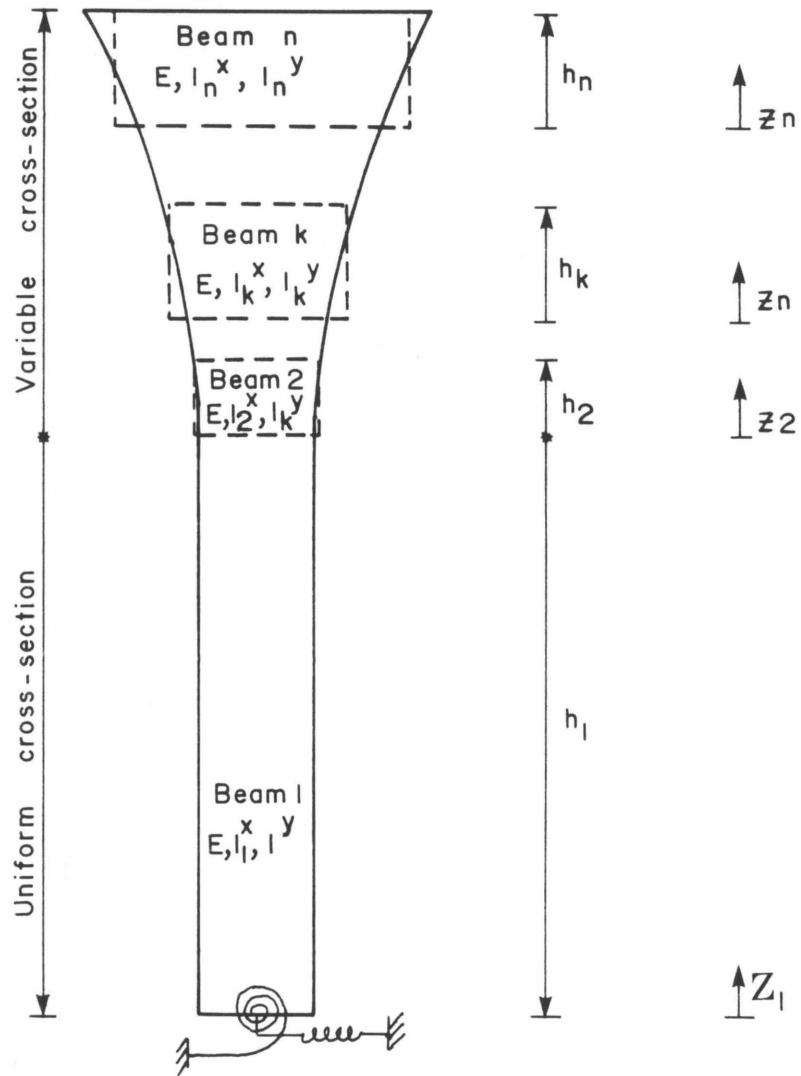


FIG. 3.4 APPROXIMATE REPRESENTATION OF A TAPERED COLUMN

$$w_k(z_k) = A_k^Y + B_k^Y z_k + C_k^Y z_k^2 + D_k^Y z_k^3 \quad (3.65)$$

By using (3.4), (3.2b), and (3.2c), one gets:

$$\frac{dw_k(z_k)}{dz_k} = B_k^Y + 2C_k^Y z_k + 3D_k^Y z_k^2 \quad (3.66)$$

$$M_k^Y(z_k) = EI_k^Y (2C_k^Y + 6D_k^Y z_k) \quad (3.67)$$

$$Q_k^Y(z_k) = -6EI_k^Y D_k^Y \quad (3.68)$$

The response of each beam is fully described by four coefficients. Considering all the n beams, the total number of the unknown coefficients is $4n$. The equations required to estimate the $4n$ unknowns arise from the boundary conditions and the conditions of continuity at the connections between the beams.

Boundary conditions

$$\text{Beam 1: (i) } EI_1^Y \frac{d^3 w_1(z_1)}{dz_1^3} \Big|_{z_1=0} = -k_h^X w_1(z_1) \Big|_{z_1=0}$$

$$\text{or } 6EI_1 D_1 = -k_h^X A_1 \quad (3.69)$$

$$\text{(ii) } EI_1^Y \frac{d^2 w_1(z_1)}{dz_1^2} \Big|_{z_1=0} = k_r^{ZX} \frac{dw_1(z_1)}{dz_1} \Big|_{z_1=0}$$

$$\text{or } 2EI_1 C_1 = k_r^{ZX} B_1 \quad (3.70)$$

$$\text{Beam } n: \text{ (i) } w_n(z_n) \Big|_{z_n=h_n} = 1 \text{ or}$$

$$A_n^Y + B_n^Y h_n + C_n^Y h_n^2 + D_n^Y h_n^3 = 1 \quad (3.71)$$

$$(ii) \quad \left. \frac{dw_n(z_n)}{dz_n} \right|_{z_n = h_n} = 0 \quad \text{or}$$

$$B_n + 2C_n h_n + 3D_n h_n^2 = 0 \quad (3.72)$$

Equations of continuity at the connection between the k^{th} and $k^{\text{th}} + 1$ beams

$$(i) \quad w_k(z_k) \Big|_{z_k = h_k} = w_{k+1}(z_{k+1}) \Big|_{z_{k+1} = 0} \quad \text{or}$$

$$A_k^Y + B_k^Y h_k + C_k^Y h_k^2 + D_k^Y h_k^3 = A_{k+1} \quad (3.73)$$

$$(ii) \quad \left. \frac{dw_k(z_k)}{dz_k} \right|_{z_k = h_k} = \left. \frac{dw_{k+1}(z_{k+1})}{dz_{k+1}} \right|_{z_{k+1} = 0} \quad \text{or}$$

$$B_k^Y + 2C_k^Y h_k + 3D_k^Y h_k^2 = B_{k+1}^Y \quad (3.74)$$

$$(iii) \quad M_k^Y(z_k) \Big|_{z_k = h_k} = M_{k+1}^Y(z_{k+1}) \Big|_{z_{k+1} = 0} \quad \text{or}$$

$$2EI_k^Y C_k^Y + 6EI_k^Y h_k D_k^Y = 2EI_{k+1}^Y C_{k+1}^Y \quad (3.75)$$

$$(iv) \quad Q_k^Y(z_k) \Big|_{z_k = h_k} = Q_{k+1}^Y(z_{k+1}) \Big|_{z_{k+1} = 0} \quad \text{or}$$

$$EI_k^Y D_k^Y = EI_{k+1}^Y D_{k+1}^Y \quad (3.76)$$

By writing equations similar to equations (3.73) to (3.76) for the $n-1$ connections between two consecutive beams, one can find a set of $4(n-1)$ equations which, combined with the four boundary conditions, leads to a system of $4n$ equations with $4n$ unknown coefficients. This system has the following general form:

$$\begin{bmatrix}
 k_h^X & 0 & 0 & 6EI_1^Y & 0 & 0 & 0 & 0 & \dots & 0 & 0 & \dots & 0 & 0 & 0 & 0 \\
 0 & -k_r^{ZX} & 2EI_1^Y & 0 & 0 & 0 & 0 & 0 & \dots & 0 & 0 & \dots & 0 & 0 & 0 & 0 \\
 0 & 0 & 0 & 0 & 0 & 0 & 0 & 0 & \dots & 0 & 0 & \dots & 1 & h_n & h_n^2 & h_n^3 \\
 0 & 0 & 0 & 0 & 0 & 0 & 0 & 0 & \dots & 0 & 0 & \dots & 0 & 1 & 2h_n & 3h_n^2 \\
 1 & h_1 & h_1^2 & h_1^3 & -1 & 0 & 0 & 0 & \dots & 0 & 0 & \dots & 0 & 0 & 0 & 0 \\
 0 & 1 & 2h_1 & 3h_1^2 & 0 & -1 & 0 & 0 & \dots & 0 & 0 & \dots & 0 & 0 & 0 & 0 \\
 0 & 0 & 2EI_1^Y & 6EI_1^Y h_1 & 0 & 0 & -2EI_2^Y & 0 & \dots & 0 & 0 & \dots & 0 & 0 & 0 & 0 \\
 0 & 0 & 0 & EI_1^Y & 0 & 0 & 0 & -EI_2^Y & \dots & 0 & 0 & \dots & 0 & 0 & 0 & 0 \\
 \vdots & & & & & & & & & & & & & & & & \\
 \dots & & & & & & & & & & & & & -1 & 0 & 0 & 0 \\
 \dots & & & & & & & & & & & & & 0 & -1 & 0 & 0 \\
 \dots & & & & & & & & & & & & & 0 & 0 & -2EI_n^Y & 0 \\
 \dots & & & & & & & & & & & & & 0 & 0 & 0 & -EI_n^Y
 \end{bmatrix}
 \begin{bmatrix}
 A_1^Y \\
 B_1^Y \\
 C_1^Y \\
 D_1^Y \\
 A_2^Y \\
 B_2^Y \\
 C_2^Y \\
 D_2^Y \\
 \vdots \\
 A_n^Y \\
 B_n^Y \\
 C_n^Y \\
 D_n^Y
 \end{bmatrix}
 =
 \begin{bmatrix}
 0 \\
 0 \\
 1 \\
 0 \\
 0 \\
 0 \\
 0 \\
 0 \\
 \vdots \\
 0 \\
 0 \\
 0 \\
 0
 \end{bmatrix}$$

(3.77)

By solving the above system, the unknown coefficients can be determined. The unknown stiffness will be given by the product $6EI_n^Y D_n^Y$ (see equation 3.68).

3.4.2 Estimation of the Stiffness for Bending About the X-Direction

The procedure which has to be followed in this case is exactly like that just described with superscript Y replaced by superscript X.

3.5 EXAMPLE

Consider the concrete column shown in Fig. 3.5. The dimensions are those of the columns of the Nichols Road Overcrossing (bridge No. 56-725) located in Riverside County, California. This column has a uniform cross section up to a height of 4.85m followed by a parabolic flare which has a total length of 3.66m. Based on the drawings of Fig. 3.5, the following values can be assigned to the geometric parameters of the problem:

$$\begin{aligned} h_1 &= 4.85\text{m}, & h_2 &= 3.66\text{m} \\ a &= 0.36\text{m}, & c &= 0.5\text{m}, & b &= 1.22 \\ r_1^t &= 0.605\text{m}, & I_1 &= 0.147\text{m}^4 & k &= 5.5 \end{aligned}$$

The value of $E = 2.4 \times 10^6 \text{ t/m}^2$ will be used for the modulus of elasticity of the concrete. The soil is considered to be stiff and with properties taken from Table B.2 of Appendix B. The values of the soil-springs can be estimated by the formulas provided in Table B.1 of Appendix B. Using the footings of the example, the following values of the soil springs are obtained:

$$\begin{aligned} k_h^X &= k_h^Y = 4.85 \times 10^5 \text{ t/m} \\ k_r^{ZX} &= k_r^{ZY} = 5.87 \times 10^6 \text{ tm/rad} \end{aligned}$$

From formulas (3.38c) and (3.38d), the coefficients $\alpha_1^Y, \dots, \alpha_4^Y$ and $\alpha_1^X,$

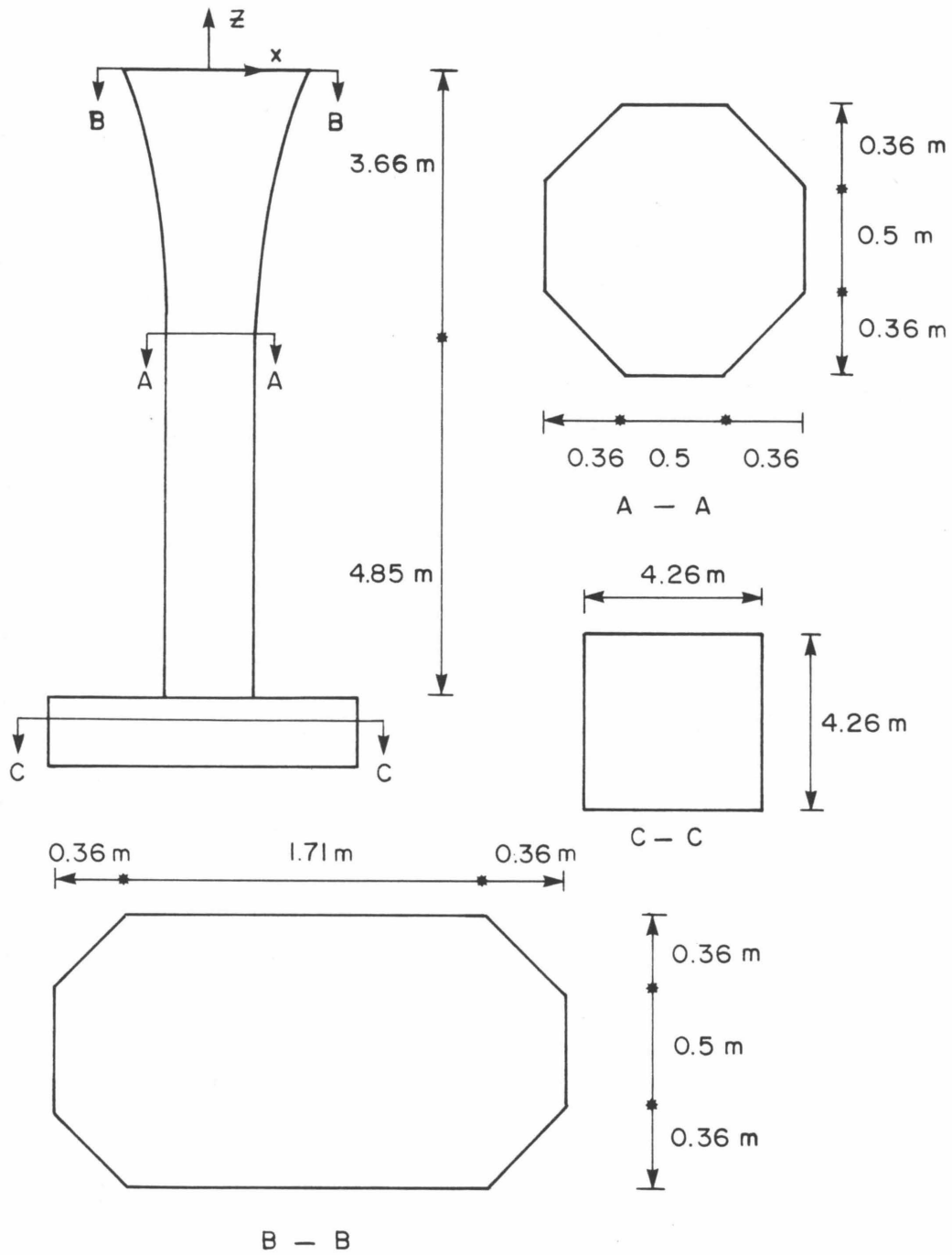


FIG. 3.5 DIMENSIONS OF THE EXAMPLE COLUMN (NICHOLS ROAD OVER-CROSSING, RIVERSIDE COUNTY, CALIFORNIA)

α_2^X can be found:*

$$\alpha_1^Y = 7.638 \times 10^{-5}$$

$$\alpha_2^Y = 2.540 \times 10^{-3}$$

$$\alpha_3^Y = 3.255 \times 10^{-2}$$

$$\alpha_4^Y = 1.473 \times 10^{-1}$$

$$\alpha_1^X = 1.376 \times 10^{-2}$$

$$\alpha_2^X = 1.473 \times 10^{-1}$$

So, the moments of inertia of the parabolic flare have the following forms:

$$I_2^Y(z_2) = 7.638 \times 10^{-5} z_2^6 + 2.540 \times 10^{-3} z_2^4 + 3.255 \times 10^{-2} z_2^2 + 1.473 \times 10^{-1}$$

$$I_2^X(z_2) = 1.376 \times 10^{-2} z_2^2 + 1.473 \times 10^{-1} \quad \text{for } 0 \leq z_2 \leq 3.66$$

3.5.1 Analytical Solution of the Problem

(i) Stiffness for bending about the Y-direction

From formula (3.41), one finds:

$$\lambda = -74.0$$

$$\mu = 58.2$$

Note that $\frac{\lambda^2}{4} + \frac{\mu^3}{27} = 8688 > 0$; therefore, case (i) applies.

Following the steps outlined in part a of section 3.3.5 yields:

1. $S_1 = -9.9$, $t_1 = 3.1$, $K = 23.4$, $M = 195.6$

2. $\alpha = -11.7$, $\beta = 7.7$

$\rho = 14.0$, $\phi = 146.8$

3. The system (3.56) becomes:

$$\begin{bmatrix} 1 & 0 & 1 & 0 & 1 & 0 \\ 0 & 1 & 2.1 & 1 & -2.1 & 1 \\ 24.4 & 0 & 23.4 & 2.1 & 23.4 & -2.1 \\ 0 & 23.4 & 21 & 23.4 & -21.1 & 23.4 \\ 195.5 & 0 & 137.9 & 21.1 & 137.9 & -21.1 \\ 0 & 195.5 & 0 & 137.9 & 0 & 137.9 \end{bmatrix} \begin{bmatrix} X_1 \\ X_2 \\ X_3 \\ X_4 \\ X_5 \\ X_6 \end{bmatrix} = \begin{bmatrix} 0 \\ 0 \\ 0 \\ 0 \\ 0 \\ 1 \end{bmatrix}$$

*Intermediate results presented in this example are given to four significant figures while final results are rounded to three significant figures.

Solving the above system produces the following values for the coefficients X_1, X_2, \dots, X_6 :

$$X_1 = 0$$

$$X_4 = -0.008677$$

$$X_2 = 0.01735$$

$$X_5 = -0.0000012$$

$$X_3 = 0.0000012$$

$$X_6 = -0.008677$$

4. TABLE 3.2: VALUES OF INTEGRALS AT $Z_2 = 0, Z_2 = 3.66\text{m}$

Integral	At $Z_2 = 0$	At $Z_2 = 3.66$
H_1	0	0.27
H_2	1.14	1.57
H_3	-0.08	0.17
H_4	1.23	1.67
H_5	0.08	0.26
H_6	1.23	1.50
H_7	0	0.95
H_8	3.77	4.8
H_9	-3.77	-3.16
H_{10}	-11.28	-8.81
H_{11}	-9.17	-6.44
H_{12}	-9.17	-7.59

5.

$$L_1^Y \Big|_{Z_2 = 0} = 0$$

$$L_1^Y \Big|_{Z_2 = 3.66} = 13.25$$

$$L_2^Y \Big|_{Z_2 = 0} = -19.97$$

$$L_2^Y \Big|_{Z_2 = 3.66} = -3.60$$

$$L_3^Y \Big|_{Z_2 = 0} = -5.38 \times 10^{-7}$$

$$L_3^Y \Big|_{Z_2 = 3.60} = 30.82$$

6. The system (3.30) becomes:

$$\begin{bmatrix}
 4.85 \times 10^5 & 0 & 0 & 2.116 \times 10^6 & 0 & 0 & 0 & 0 \\
 0 & -5.87 \times 10^6 & 7.05 \times 10^5 & 0 & 0 & 0 & 0 & 0 \\
 0 & 0 & 0 & 0 & 21.7 \times 10^{-6} & -18.33 \times 10^{-6} & 3.66 & 1 \\
 0 & 0 & 0 & 0 & 5.52 \times 10^{-6} & -1.50 \times 10^{-6} & 1 & 0 \\
 1 & 4.85 & 23.52 & 114.084 & -8.31 \times 10^{-6} & 0 & 0 & -1 \\
 0 & 1 & 9.7 & 70.56 & 0 & 8.31 \times 10^{-6} & -1 & 0 \\
 0 & 0 & 7.05 \times 10^5 & 10.25 \times 10^6 & -1 & 0 & 0 & 0 \\
 0 & 0 & 0 & -2.116 \times 10^6 & 0 & 1 & 0 & 0
 \end{bmatrix}
 \begin{bmatrix}
 A_1^Y \\
 B_1^Y \\
 C_1^Y \\
 D_1^Y \\
 A_2^Y \\
 B_2^Y \\
 C_2^Y \\
 D_2^Y
 \end{bmatrix}
 =
 \begin{bmatrix}
 0 \\
 0 \\
 1 \\
 0 \\
 0 \\
 0 \\
 0 \\
 0
 \end{bmatrix}$$

Solution of the above system of equations gives the unknown coefficients:

$$A_1^Y = 0.023$$

$$A_2^Y = -15934.8$$

$$B_1^Y = 0.007$$

$$B_2^Y = -11344.94$$

$$C_1^Y = 0.006$$

$$C_2^Y = 0.071$$

$$D_1^Y = -0.005$$

$$D_2^Y = 0.878$$

The stiffness of the column is equal to the absolute value of B_2^Y ,

$$k^Y = 11340 \text{ t/m} \quad (3.78)$$

Stiffness for bending about the X-direction

$$1. \quad L_1^X \Big|_0 = 0$$

$$L_1^X \Big|_{3.66} = 18.7$$

$$L_2^X \Big|_0 = 86.17$$

$$L_2^X \Big|_{3.66} = 115.7$$

$$L_3^X \Big|_0 = 0$$

$$L_3^X \Big|_{3.66} = 65.95$$

2. The system (3.32) becomes:

$$\begin{bmatrix}
 4.85 \times 10^5 & 0 & 0 & 2.119 \times 10^6 & 0 & 0 & 0 & 0 & 0 \\
 0 & -5.87 \times 10^6 & 7.05 \times 10^5 & 0 & 0 & 0 & 0 & 0 & 0 \\
 0 & 0 & 0 & 0 & -19.68 \times 10^{-6} & 148.9 \times 10^{-6} & 3.66 & 1 & 0 \\
 0 & 0 & 0 & 0 & 7.78 \times 10^{-6} & 48.19 \times 10^{-6} & 1 & 0 & 0 \\
 1 & 4.85 & 23.5225 & 114.1 & 35.9 \times 10^{-6} & 0 & 0 & -1 & 0 \\
 0 & 1 & 9.7 & 70.57 & 0 & -35.9 \times 10^{-6} & -1 & 0 & 0 \\
 0 & 0 & 7.05 \times 10^5 & 10.27 \times 10^6 & -1 & 0 & 0 & 0 & 0 \\
 0 & 0 & 0 & -2.11 \times 10^6 & 0 & 1 & 0 & 0 & 0
 \end{bmatrix}
 \begin{bmatrix}
 A_1^X \\
 B_1^X \\
 C_1^X \\
 D_1^X \\
 A_2^X \\
 B_2^X \\
 C_2^X \\
 D_2^X
 \end{bmatrix}
 =
 \begin{bmatrix}
 0 \\
 0 \\
 1 \\
 0 \\
 0 \\
 0 \\
 1 \\
 0
 \end{bmatrix}$$

Solution of the above system gives:

$$\begin{aligned} A_1^X &= 0.0173 & A_2^X &= -8497.361 \\ B_1^X &= 0.0055 & B_2^X &= -8360.965 \\ C_1^X &= 0.0457 & C_2^X &= 0.47 \\ D_1^X &= -0.004 & D_2^X &= 0.3611 \end{aligned}$$

The stiffness in this case is:

$$k^X = 8360 \text{ t/m} \quad (3.78)$$

3.5.2 Approximate Solution of the Problem

To illustrate the use of the approximate method for determination of the stiffness, the simple case in which the parabolic flare is represented by a simple beam of uniform cross section is chosen. Thus, the total number of beams involved is $n = 2$. The geometric parameters of each beam are shown in Fig. 3.6.

Bending about Y-axis

For $n = 2$, the system (3.77) takes the following general form:

$$\begin{bmatrix} k_h^X & 0 & 0 & 6EI_1^Y & 0 & 0 & 0 & 0 \\ 0 & -k^{ZX} & 2EI_1^Y & 0 & 0 & 0 & 0 & 0 \\ 0 & 0 & 0 & 0 & 1 & h_2 & h^2 & h_2^3 \\ 0 & 0 & 0 & 0 & 0 & 1 & 2h_2 & 3h_2^2 \\ 1 & h_1 & h^2 & h_1^3 & -1 & 0 & 0 & 0 \\ 0 & 1 & 2h_1 & 3h_1^2 & 0 & -1 & 0 & 0 \\ 0 & 0 & 2EI_1^Y & 6EI_1^Y h_1 & 0 & 0 & -2EI_2^Y & 0 \\ 0 & 0 & 0 & EI_1^Y & 0 & 0 & 0 & -EI_2^Y \end{bmatrix} \begin{bmatrix} A_1^Y \\ B_1^Y \\ C_1^Y \\ D_1^Y \\ A_2^Y \\ B_2^Y \\ C_2^Y \\ D_2^Y \end{bmatrix} = \begin{bmatrix} 0 \\ 0 \\ 1 \\ 0 \\ 0 \\ 0 \\ 0 \\ 0 \end{bmatrix}$$

Substituting the numerical values of the parameters,

$$\begin{bmatrix}
 4.85 \times 10^5 & 0 & 0 & 21.19 \times 10^5 & 0 & 0 & 0 & 0 \\
 0 & -5.87 \times 10^6 & 7.05 \times 10^5 & 0 & 0 & 0 & 0 & 0 \\
 0 & 0 & 0 & 0 & 1 & 3.66 & 13.4 & 49.003 \\
 0 & 0 & 0 & 0 & 0 & 1 & 7.32 & 40.18 \\
 1 & 4.85 & 23.52 & 114.08 & -1 & 0 & 0 & 0 \\
 0 & 1 & 9.7 & 70.57 & 0 & -1 & 0 & 0 \\
 0 & 0 & 7.05 \times 10^5 & 102.7 \times 10^5 & 0 & 0 & -1.88 \times 10^6 & 0 \\
 0 & 0 & 0 & 3.53 \times 10^5 & 0 & 0 & 0 & -0.943 \times 10^6
 \end{bmatrix}
 \begin{bmatrix}
 A_1^Y \\
 B_1^Y \\
 C_1^Y \\
 D_1^Y \\
 A_2^Y \\
 B_2^Y \\
 C_2^Y \\
 D_2^Y
 \end{bmatrix}
 =
 \begin{bmatrix}
 0 \\
 0 \\
 1 \\
 0 \\
 0 \\
 0 \\
 0 \\
 0
 \end{bmatrix}$$

(3.77a)

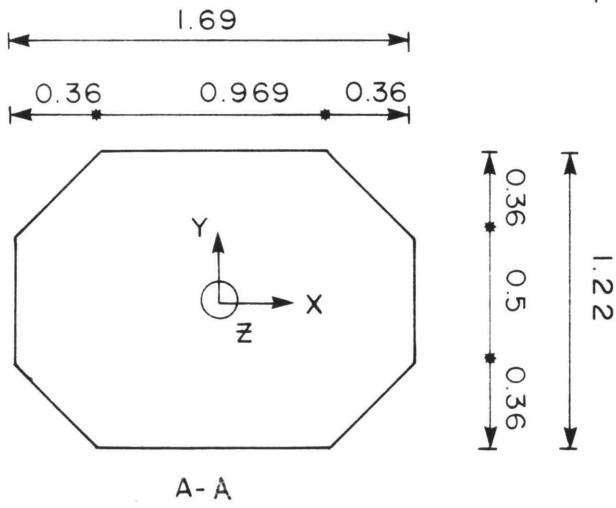
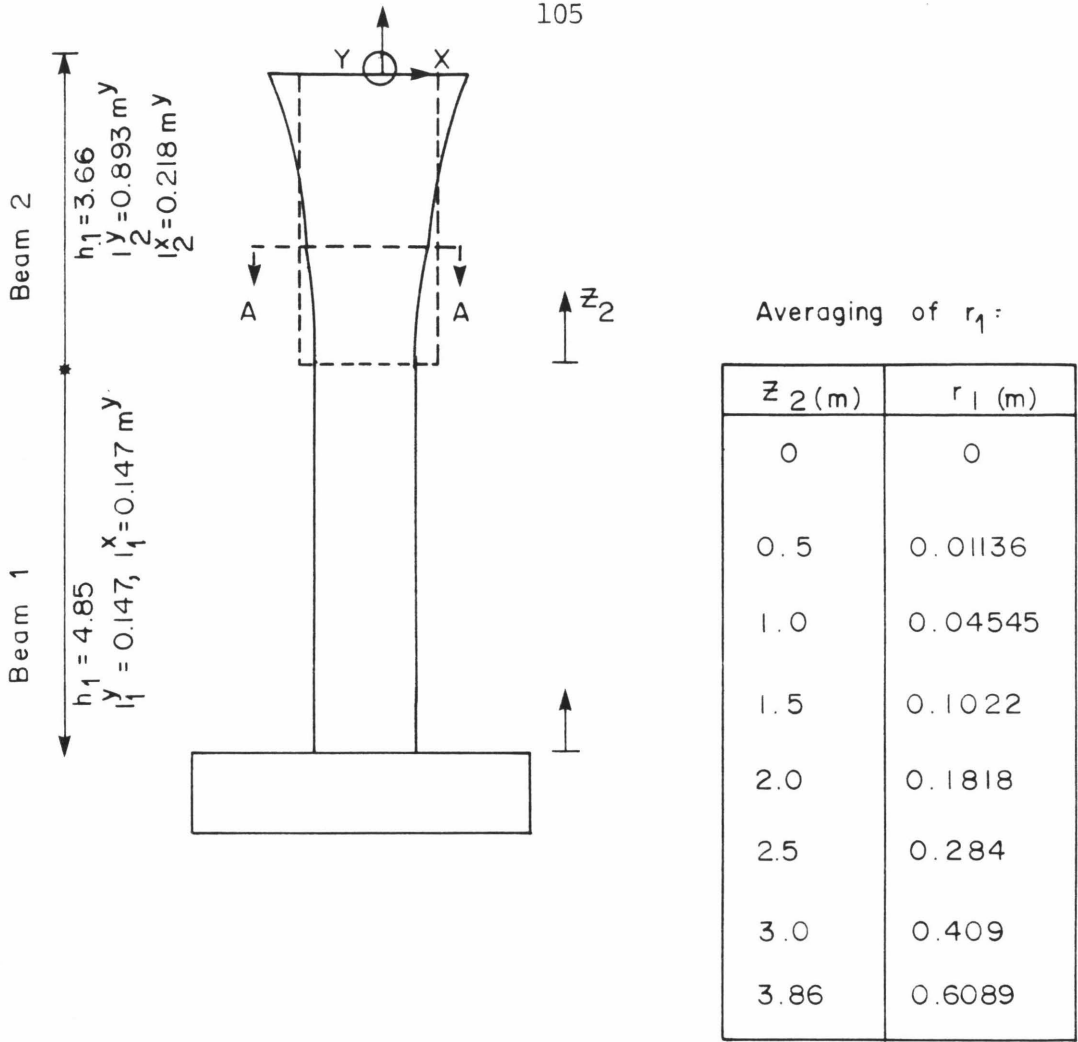


FIG. 3.6 REPRESENTATION OF THE COLUMN BY TWO BENDING BEAMS OF UNIFORM CROSS SECTION

Solution of the above system gives:

$$\begin{array}{ll}
 A_1^Y = 0.023 & A_2^Y = 0.687 \\
 B_1^Y = 0.006 & B_2^Y = 0.1447 \\
 C_1^Y = 0.052 & C_2^Y = -0.009 \\
 D_1^Y = -0.00524 & D_2^Y = -0.002
 \end{array}$$

From equation (3.65), it is seen that the stiffness for bending about the Y-axis is:

$$k^Y = 6EI_2^Y \left| D_2^Y \right| = 11124 \text{ t/m} \quad (3.79)$$

Bending about X-axis

In this case the system to be solved is given by system (3.77b)

which has the solution:

$$\begin{array}{ll}
 A_1^X = 0.0167 & A_2^X = 0.64 \\
 B_1^X = 0.005 & B_2^X = 0.1620 \\
 C_1^X = 0.044 & C_2^X = -0.008 \\
 D_1^X = -0.0038 & D_2^X = -0.0026
 \end{array}$$

The stiffness of the column for bending about the X-axis is:

$$k^X = 6EI_2^X \left| D_2^X \right| = 8124 \text{ t/m} \quad (3.80)$$

Comparison of the results obtained from the analytical method with those found from the approximate analysis shows very good agreement. This is despite the fact that in the approximate method the flare was represented by just one uniform beam. This close agreement is encouraging for applications of the more general approximate method. It is realized, of course, that in other cases more individual beams may be required to approximate the flare satisfactorily.

3.5.3 Yielding of the Column along the Two Directions of Bending

In order to characterize the force-deflection relations of the columns for the nonlinear analysis, it is necessary to approximate the

$$\begin{bmatrix}
 4.85 \times 10^5 & 0 & 0 & 21.19 \times 10^5 & 0 & 0 & 0 & 0 \\
 0 & -5.87 \times 10^6 & 7.05 \times 10^5 & 0 & 0 & 0 & 0 & 0 \\
 0 & 0 & 0 & 0 & 1 & 3.66 & 13.4 & 49.001 \\
 0 & 0 & 0 & 0 & 0 & 1 & 7.32 & 40.18 \\
 1 & 4.85 & 23.52 & 114.084 & -1 & 0 & 0 & 0 \\
 0 & 1 & 9.7 & 70.5675 & 0 & -1 & 0 & 0 \\
 0 & 0 & 7.05 \times 10^5 & 102.7 \times 10^5 & 0 & 0 & -10.47 \times 10^5 & 0 \\
 0 & 0 & 0 & 3.53 \times 10^5 & 0 & 0 & 0 & -5.23 \times 10^5
 \end{bmatrix}
 \begin{bmatrix}
 A_1^X \\
 B_1^X \\
 C_1^X \\
 D_1^X \\
 A_2^X \\
 B_2^X \\
 C_2^X \\
 D_2^X
 \end{bmatrix}
 =
 \begin{bmatrix}
 0 \\
 0 \\
 1 \\
 0 \\
 0 \\
 0 \\
 0 \\
 0
 \end{bmatrix}$$

(3.77b)

yielding and failure of the columns in both the X and Y directions. To make the analysis of the yielding as simple as possible, the following assumptions are adopted:

(1) The ultimate shear strength and the ultimate torsional strength are so large that they can be considered infinite;

(2) The column is under a constant axial force from the weight of the bridge deck; and

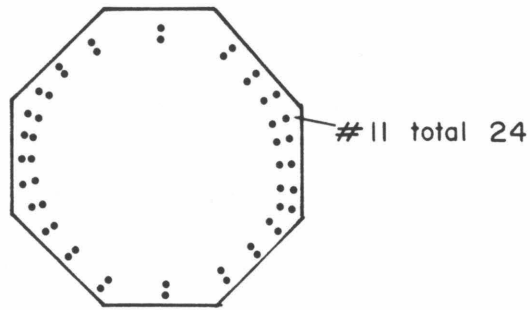
(3) The ultimate bending moments of a cross section are determined from the axial stress distribution present on the cross section under ultimate conditions and are independent of the shear stresses.

The method by which the ultimate bending moments are determined is outlined in Appendix A.

The steel reinforcement and the axial load acting on the column are shown in Fig. 3.7. The properties of steel and concrete used are shown in Table 3.3.

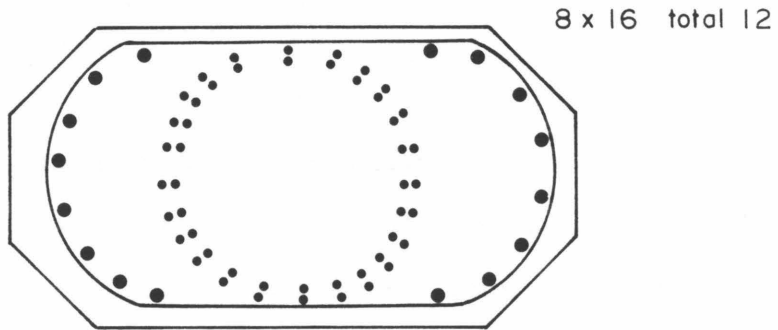
TABLE 3.3: PROPERTIES OF CONCRETE & STEEL REINFORCEMENT

Description	Value
Concrete Modulus of Elasticity	$E_C = 3,390,000 \text{ psi} = 2.4 \times 10^6 \text{ t/m}^2$
Concrete Yielding Stress	$f'_C = 3,500 \text{ psi} = 2460 \text{ t/m}^2$
Concrete Yielding Deformation	$E_C = 0.003$
Steel Modulus of Elasticity	$E_S = 29 \times 10^6 \text{ psi} = 20 \times 10^6 \text{ t/m}^2$
Steel Yielding Stress	$f_S = 50,000 \text{ psi} = 3.5153.5 \text{ t/m}^2$
Steel Yielding Deformation	$E_S = 0.00172$

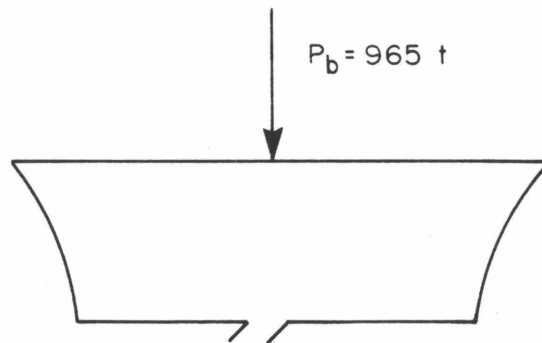


a. Bottom cross - section

8 x 11 - total 4



b. Top cross - section



c. Compressive force due to the weight of the deck

FIG. 3.7 CROSS SECTIONS OF THE REINFORCED COLUMN

3.5.3.1 Estimation of the ultimate bending moments

The ultimate bending moments in the two directions of bending for the bottom and the top cross section are given in Table 3.4. The method by which they were found is briefly described in Appendix A.

TABLE 3.4: ULTIMATE MOMENT CAPACITY

Cross Section	Bending about Y-axis	Bending about X-axis
Bottom	1315 tm	1315 tm
Top	1699 tm	3029 tm

3.5.3.2 Construction of the force-deflection diagrams for bending

From equations (3.6) and (3.11) and the analogous ones governing bending about the X direction, the solutions of the systems (3.30) and (3.32) and the values of the ultimate moment capacities, the force-deflection relations for loading at the top of the columns can be constructed. The force-deflection relations include an elastic portion and changes in slope corresponding to yielding at the bottom and at the top cross sections. An analysis of the deflection needed to cause yielding at the top and the bottom cross section indicates that the column first yields at the bottom. Furthermore, considering the fact that after yielding at the bottom no extra moments can be assumed by the bottom cross section, the stiffness of the columns after the yielding at the bottom was found to be: $k^X = 2269.65 \text{ t/m}$. This stiffness remains in effect until the top of the column yields producing a mechanism.

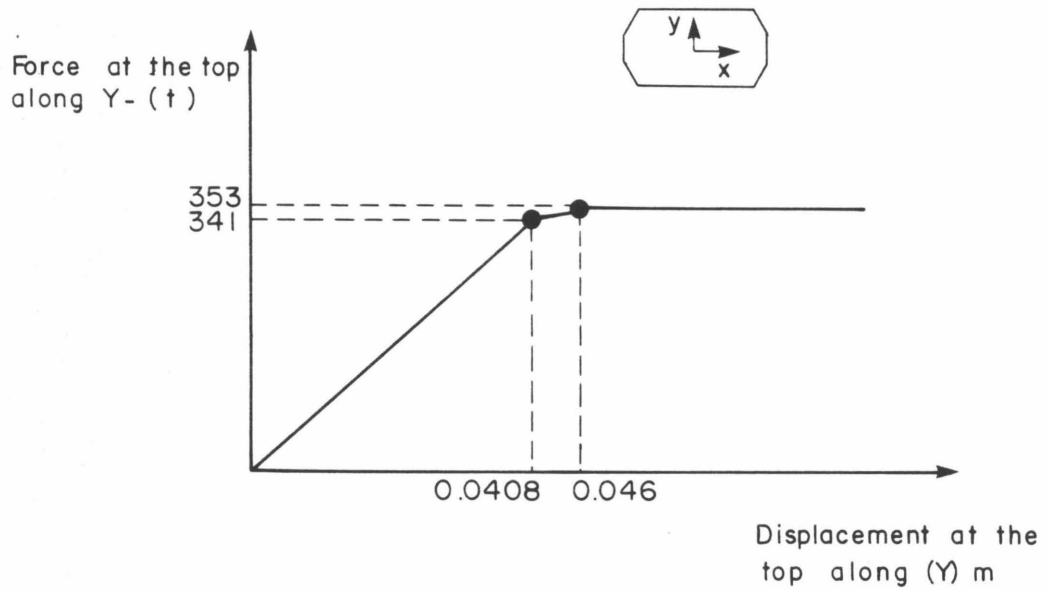
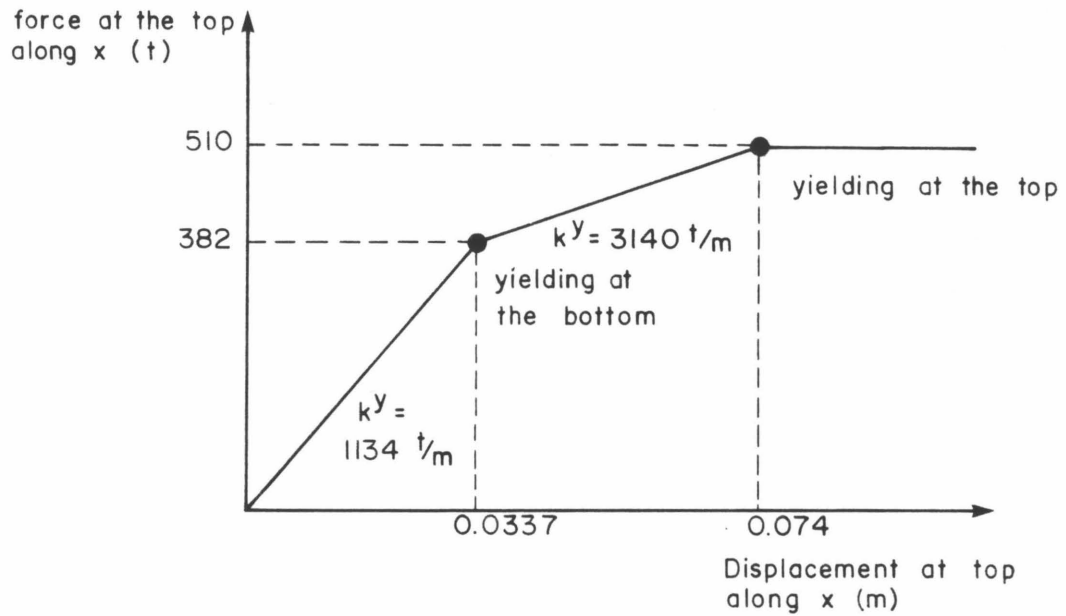


FIG. 3.8 FORCE-DEFLECTION DIAGRAMS FOR LOADING AT THE TOP OF THE COLUMN
 a. Bending about Y-axis
 b. Bending about X-axis

Based on this analysis, the force-deflection diagram for bending about the X and Y axes were found to be as shown in Figs. 3.9a and 3.9b, respectively.

ESTIMATION OF THE EQUIVALENT ABUTMENT STIFFNESS

4.1 INTRODUCTION

As was shown in chapter 2, one of the most important parameters for the development of a model which will capture the basic features of the rigid body motions of a skew bridge is the abutment stiffness, k_{ab} . The calculation of a precise value of the abutment stiffness would involve very difficult calculations since an accurate representation of the abutment-soil system would be very complicated involving complex three-dimensional geometry, many degrees of freedom, and the nonlinear constitutive relations for the properties of the soil. But, as was discussed in chapter 2, a reasonable estimate of the abutment stiffness is sufficient for constructing a simple model for the rigid body motions of a skew bridge. Thus, the purpose of this chapter is the development of a simplified method by which one can find an approximate value of the abutment stiffness, k_{ab} .

The presentation is divided into three sections. In the first section, some fundamental concepts of soil mechanics and abutment design are presented briefly; in the second, the simplifying assumptions are given; and, in the third, the statement of the simplified problem and its solution are provided.

The solution is divided into two parts. In the first part, the soil is modelled as a Winkler foundation with springs that are either constant or which vary linearly with depth. In the second part, the soil is represented by n discrete springs with independently determined constants. The soil springs are considered to be linearly elastic, but the soils on the left and right sides of the abutment are allowed to

yield. The yielding criterion used for the soils is given in the section containing the basic assumptions of the analysis. The final result for each case treated is an approximate elasto-plastic force-deflection relation for the abutment-soil system.

4.2 PRELIMINARY CONCEPTS

4.2.1 Abutments

The abutments of a bridge support the ends of the span and retain the earth behind them. For highway bridges, there are several types of abutments depending on the material of construction (plain concrete, reinforced concrete, stone) and on their function (full height abutment, stub or semi-stub abutment, open abutment). The method which follows deals with abutments whose profile can be approximated by the two-dimensional configuration shown in Fig. 4.1.

4.2.2 Geostatic Stresses in the Soil

Generally, the pattern of stresses in soil, even those caused by its own weight, is very complicated. However, there is a common situation in which the weight of the soil gives rise to a simple state of stress: when the ground surface is horizontal and the soil is laterally homogeneous. In this case, the stresses are called geostatic stresses; and the vertical and horizontal planes are principal planes since no shear stresses act on them. The vertical geostatic stresses at any depth are given by:

$$\sigma_v(Z) = \gamma Z \quad (4.1)$$

where γ is the unit weight of the soil (assumed to be constant with depth and Z is the depth. The ratio of horizontal to vertical stress is expressed by a factor, called the coefficient of lateral stress and

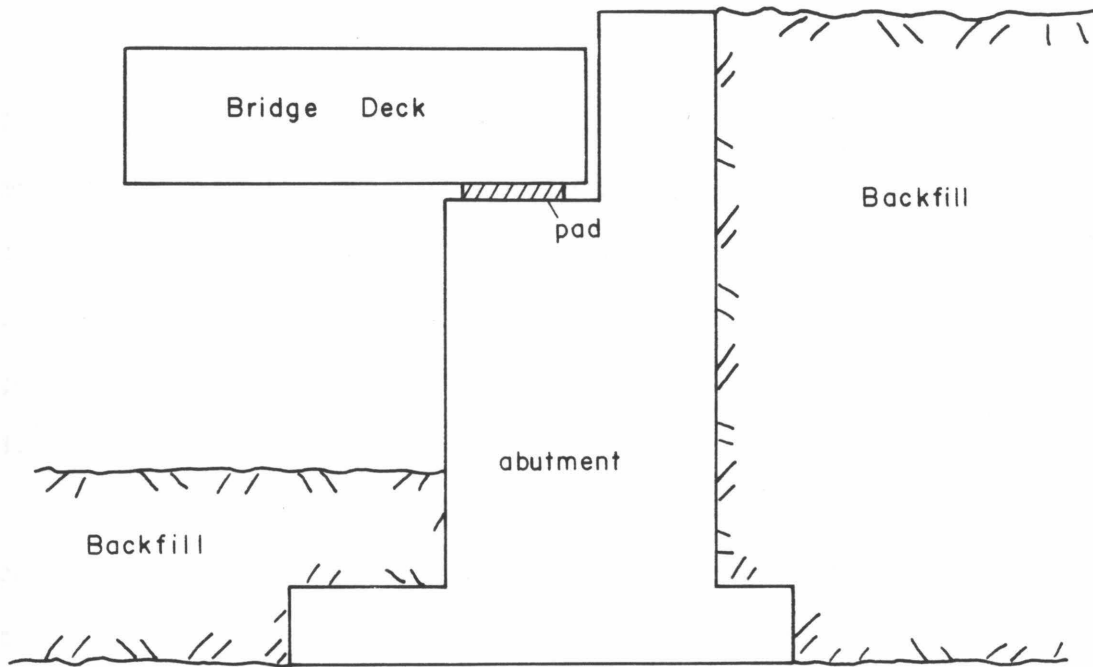


FIG. 4.1 ABUTMENT PROFILE

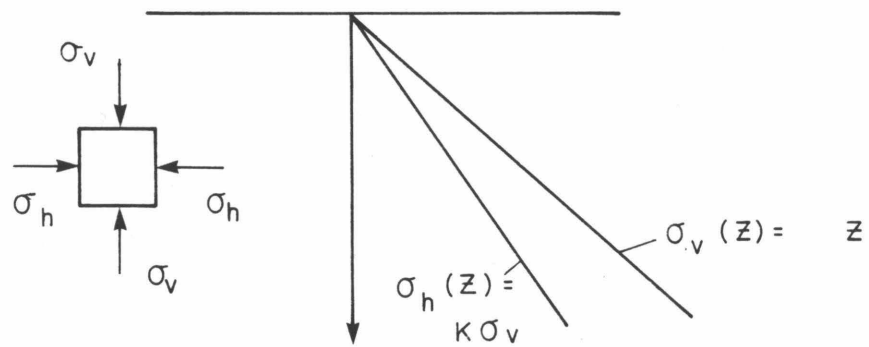


FIG. 4.2 GEOSTATIC STRESSES

denoted by K :

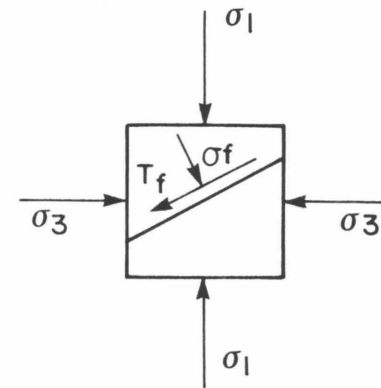
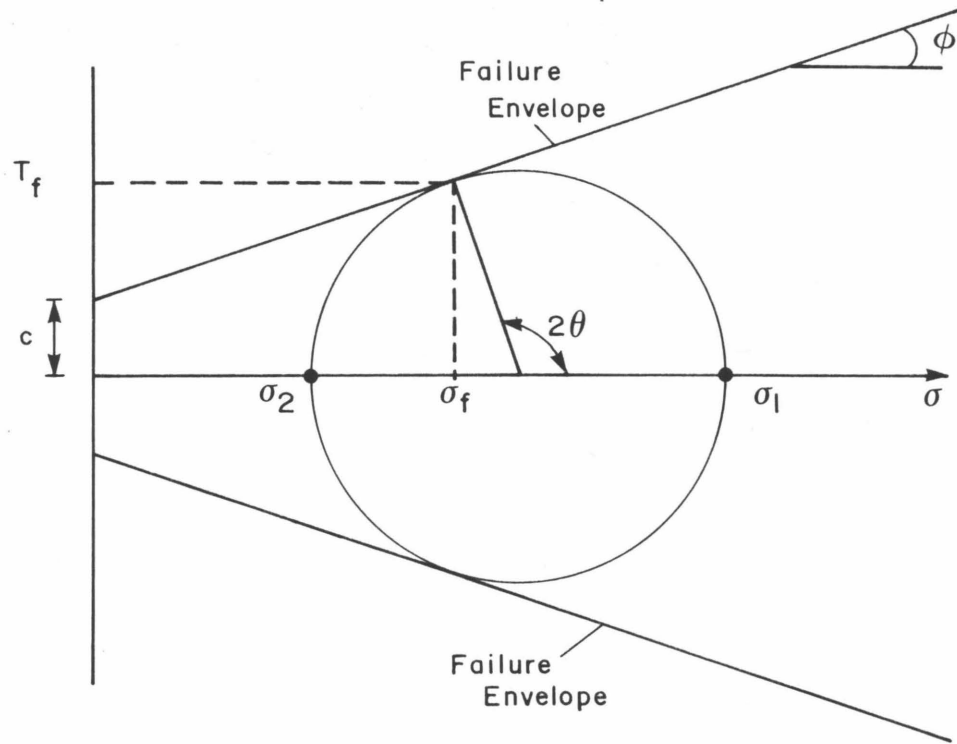
$$K = \frac{\sigma_h}{\sigma_v} \quad (4.2)$$

In the special case where there is no lateral strain in the ground, soil mechanics employ the term coefficient of lateral stress at rest and use the symbol K_0 . Depending on the soil, K_0 can be greater or less than one. For typical sand deposits K_0 varies between 0.4 and 0.5. The geostatic stresses are shown in Fig. 4.2.

4.2.3 Rankine Theory

The Rankine theory is one of two classical theories of earth pressure (the other one is due to Coulomb). Rankine theory is based on the Mohr-Coulomb yielding criterion which is summarized in Fig. 4.3. In this figure, σ_1 and $\sigma_2 = \sigma_3$ are the principal stresses; and the cohesion of the soil is denoted by c .

Consider a semi-infinite mass of soil with a horizontal surface and having a vertical boundary formed by a frictionless wall extending to a semi-infinite depth (see Fig. 4.4a). The soil is assumed to be isotropic and homogeneous. Let σ_v and σ_h be vertical and horizontal stresses, respectively, upon a soil element at depth Z . If there is now a movement of the wall away from the soil, the value of σ_h decreases as the soil expands outwards. If the expansion is large enough, σ_h decreases to a minimum value σ_a such that a state of plastic equilibrium develops. The stress σ_a is called the active stress and is the minor principal stress in the Mohr's circle. The state of the soil when $\sigma_h = \sigma_a$ is called the Active Rankine State (see Fig. 4.4). If, on the other hand, the wall is moved against the soil, there will be a lateral



$$\tau_f = c + \sigma_f \tan \phi$$

$$\theta = 45^\circ + \frac{\phi}{2}$$

FIG. 4.3 MOHR-COULOMB YIELDING CRITERION

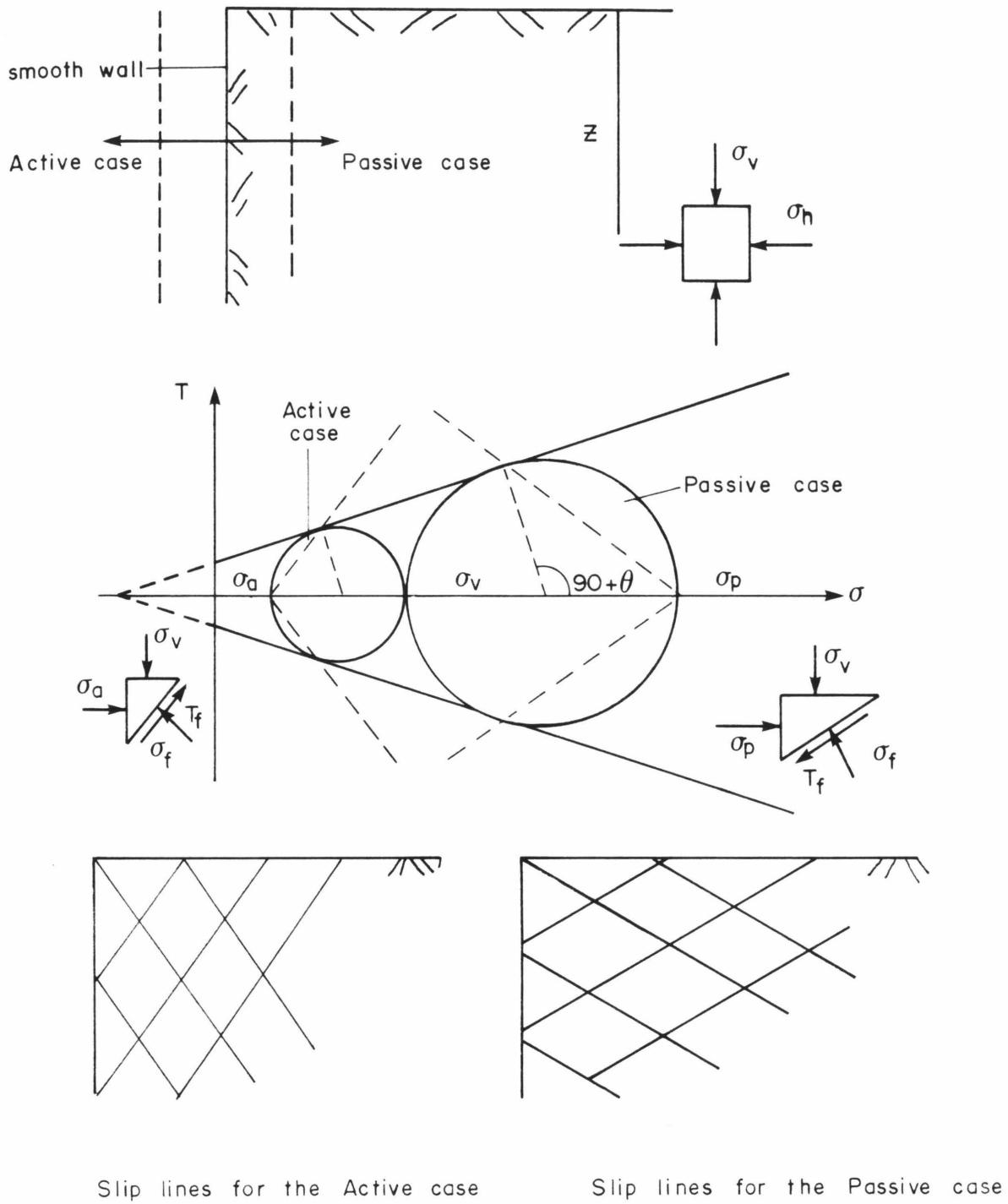


FIG. 4.4 ACTIVE AND PASSIVE RANKINE STATES

compression of the soil and the value of σ_h will increase until another state of plastic equilibrium is reached. The maximum value of σ_h , in this case, denoted by σ_p , is called passive stress and is the maximum principal stress in the Mohr's circle. The corresponding state is called the Passive Rankine State. Relative to the Rankine states in Fig. 4.4, the following relations can be derived:

$$\sigma_a = K_A \gamma Z - 2c\sqrt{K_A} \quad (4.3)$$

$$\sigma_p = K_p \gamma Z + 2c\sqrt{K_p} \quad (4.4)$$

where K_A and K_p , the active and passive pressure coefficients, respectively, are

$$K_A = \frac{1 - \sin \phi}{1 + \sin \phi} \quad (4.5)$$

$$K_p = \frac{1 + \sin \phi}{1 - \sin \phi} \quad (4.6)$$

4.2.4 Active Thrust and Passive Resistance

Equations (4.3) and (4.4) show that the active and passive stresses increase linearly with depth as indicated in Fig. 4.4b. When the cohesion c is zero, triangular distributions are obtained in each case. When c is greater than zero, the value of σ_a is zero at a particular depth Z_0 . From equation (4.3) with $\sigma_a = 0$:

$$Z_0 = \frac{2c}{\gamma\sqrt{K_A}} \quad (4.7)$$

This implies that, in the active case, the soil is in a state of tension

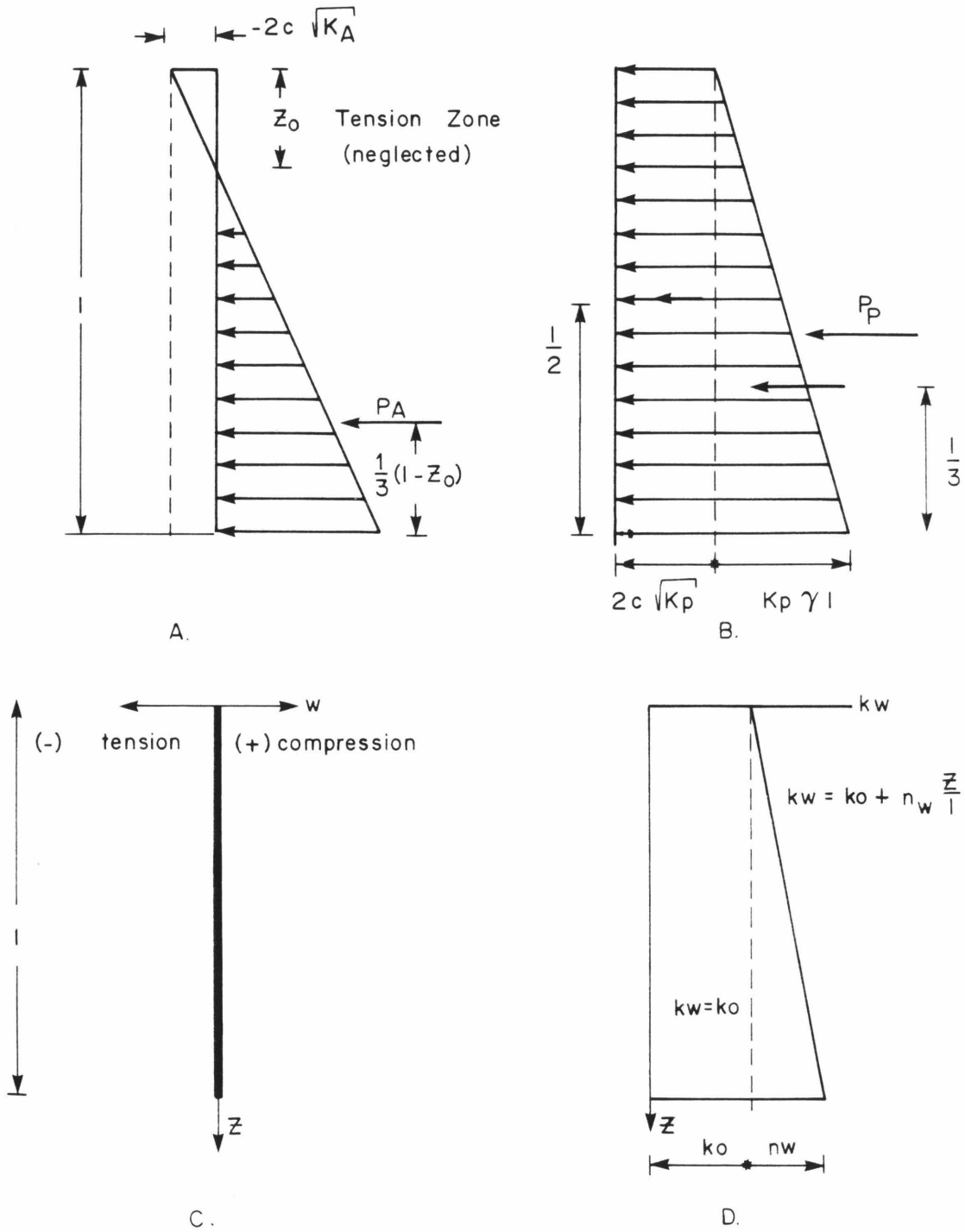


FIG. 4.5 a. Active and Passive Stress Distributions
 b. Sign Conversion
 c. Variation of k_w with depth

between the surface and depth z_0 . But, in soils, cracks are likely to develop within the tension zones; and the tensile stresses acting on the wall are commonly neglected. The force per unit width of the wall due to the active stress distribution is referred to as total active thrust (P_A). For a vertical wall of height :

$$P_A = \int_{z_0}^1 \sigma_a dz = 1/2 K_A \gamma (1^2 - z_0^2) - 2c\sqrt{K_A} (1 - z_0) \quad (4.8)$$

The force due to the passive stress distribution is called the total passive resistance (P_p). For a vertical wall of height l , the passive resistance per unit width is:

$$P_p = \int_0^l \sigma_p dz = 1/2 K_p \gamma l^2 + 2c\sqrt{K_p} l \quad (4.9)$$

The active and passive stress distributions are shown in Fig. 4.5a.

4.3 BASIC ASSUMPTIONS

The approach presented below is based on the following simplifying assumptions:

(a) The problems to be solved are static; consequently, no inertia forces are included in the analysis;

(b) The abutment is assumed to behave as a uniform, rigid plate, i.e., deformations due to bending and shear are neglected;

(c) When elastic, the soil is assumed to behave as a Winkler foundation.

Thus, the pressure, p , exerted by the ground at a point, is assumed to depend only on the displacement, W , of that point through a proportion-

ality factor k_w .

$$p = k_w W \quad (4.10)$$

The factor k_w is called the horizontal subgrade reaction coefficient. In the first part of the analysis, k_w is assumed to vary linearly with depth according to the relation:

$$k_w = n_w \frac{z}{l} + k_o \quad (4.11)$$

where l is the total height of the soil deposit (which for the deposit on the right of the abutment is equal to the height of the abutment), z is the depth and n_w and k_o are constants. Equation (4.11) includes both a uniform subgrade coefficient ($n_w = 0$) and triangular distribution of resistance with depth ($k_o = 0$), which are the two most frequently used expressions for the factor k_w . The resistance of the soil at the bottom of the abutment is modelled by a torsional spring which resists the rigid body rotation of the abutment.

The contact between the abutment and the soil is assumed to be frictionless.

(d) When no force or displacement is imposed on the soil by the bridge, the system of the soil and the abutment is in equilibrium under the initially applied forces (weight and geostatic forces). Thus, in the analysis, only the equilibrium of the forces applied beyond the initial equilibrium state will be examined.

(e) A soil deposit is considered to yield if the total compressive force imposed on that deposit equals either its active thrust or its passive resistance. It will be assumed that when the total compressive force is between these two values, the soil deposit will behave

elastically. The above "yielding criterion" is global in nature and does not take into account that the state of stress at yielding of each soil element will, in actuality, depend on its depth. But, for the purpose of the analysis, it is considered to be an acceptable assumption.

(f) A soil deposit cannot assume tensile stresses. The deposit is said to be "tensioned" only in the sense that its initial compressive stresses are decreased. The maximum level of the decrease is specified by (e).

4.4 ESTIMATION OF THE EQUIVALENT ABUTMENT STIFFNESS

4.4.1 Statement of the Problem

The problem to be solved can be briefly summarized as follows: Let W_a be the deflection imposed by the bridge deck on the soil through the abutment and let P_t equal the reaction of the soil on the bridge. The problem is to find an equivalent nonlinear stiffness k_{ab} such that

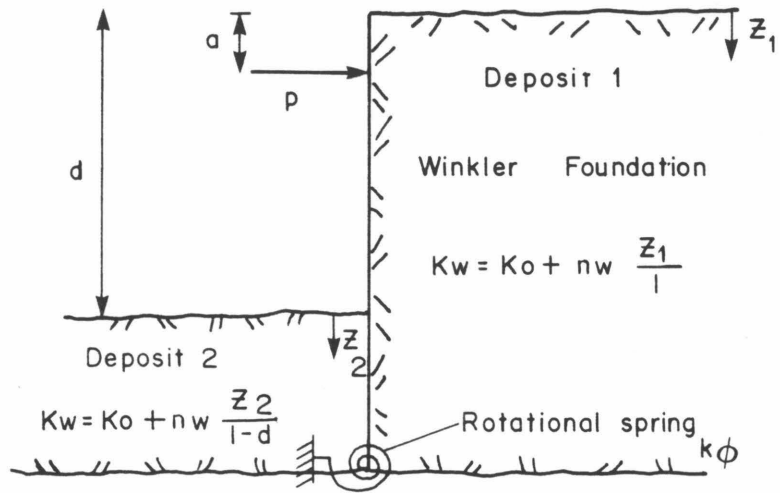
$$P_t = k_{ab} a$$

4.4.2 Solution of the Problem in the Case of Winkler Foundation

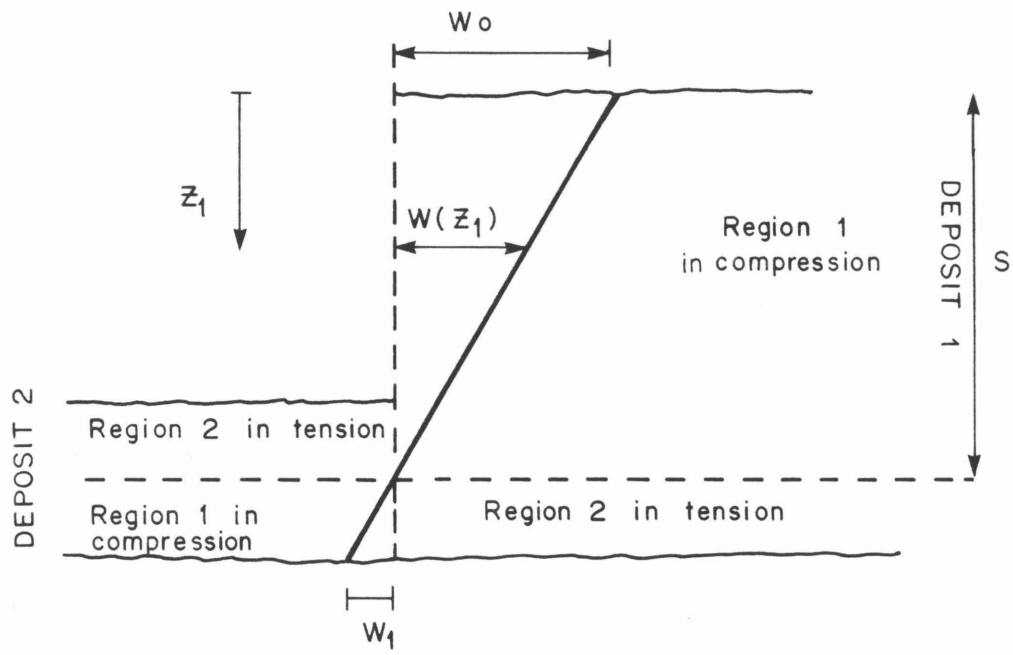
Consider a strip of the abutment of unit width loaded by load P per unit width applied at a distance a from the top (see Fig. 4.6a). Let the displaced position of the abutment be that shown in Fig. 4.6b, and let W_0 and W_1 be the displacements of the top and bottom of the abutment, respectively. If $W(z_1)$ is the displacement at a depth z_1 , then:

$$W(z_1) = W_0 - \frac{W_0 - W_1}{1} z_1 \quad (4.13)$$

$$\phi = \frac{W_0 - W_1}{1}$$



A.



B.

FIG. 4.6 a. Initial Position of the Abutment with the Soil Deposits and the Load Applied by the Bridge Deck
 b. Displaced Position of the Abutment

The stress between the soil and the abutment can be expressed as a function of depth as follows:

$$\left. \begin{aligned} p_R(z_1) &= W(z_1)k(z_1) & 0 \leq z_1 \leq 1 & \text{(on the right side} \\ & & & \text{of the abutment)} \\ p_L(z_1) &= W(z_1)k_w(z_1) & d \leq z_1 \leq 1 & \text{(on the left side} \\ & & & \text{of the abutment)} \end{aligned} \right\} (4.14)$$

By substituting $W(z_1)$ from (4.13) and $k_w(z)$ from Fig. 4.6a, one gets from equation (4.14):

$$\left. \begin{aligned} p_R(z_1) &= (W_1 - W_0) \frac{n_w}{12} z_1^2 + [W_0(n_w - k_0) \\ &+ W_1 k_0] \frac{z_1}{1} + k_0 W_0 & 0 \leq z_1 \leq 1 \\ p_L(z_1) &= (W_1 - W_0) \frac{n_w}{1(1-d)} z_1^2 + \\ &[W_0 \left(-\frac{k_0}{1} + \frac{n_w}{1-d} + \frac{n_w d}{1(1-d)} \right) + \\ &W_1 \left(\frac{k_0}{1} - \frac{n_w d}{1(1-d)} \right)] z_1 + W_0 \left(k_0 - \frac{n_w d}{1-d} \right) & d \leq z_1 \leq 1 \end{aligned} \right\} (4.15)$$

The equation of force equilibrium requires that:

$$P = \int_0^1 p_R(z_1) dz_1 + \int_d^1 p_L(z_1) dz_1 \quad (4.16)$$

From the equation of moments about $z_1 = 1$:

$$P(1-a) = \int_0^1 p_R(z_1) (1-z_1) dz_1 + \int_d^1 p_L(z_1) (1-z_1) dz_1 + k_\phi \phi \quad (4.17)$$

From (4.16), (4.17) and (4.15), one gets:

$$\left. \begin{aligned} P &= R_0 W_0 + R_1 W_1 \\ P(1-a) &= T_0 W_0 + T_1 W_1 \end{aligned} \right\} (4.18)$$

where:

$$\left. \begin{aligned} R_0 &= -\frac{n_w l}{3} + \frac{(n_w - k_0)l}{2} + k_0 l - \frac{n_w(l^3 - d^3)}{3l(1-d)} + \\ &+ \frac{l^2 - d^2}{2} \left(-\frac{k_0}{1} + \frac{n_w}{1-d} + \frac{n_w d}{l(1-d)} \right) + \\ &\left(k_0 - \frac{n_w d}{1-d} \right) (1-d) \\ R_1 &= \frac{n_w l}{3} + k_0 \frac{l}{2} + \frac{n_w(l^3 - d^3)}{3l(1-d)} + \\ &\left(\frac{k_0}{1} - \frac{n_w d}{l(1-d)} \right) \frac{l^2 - d^2}{2} \\ T_0 &= -\frac{n_w l^2}{12} + (n_w - k_0) \frac{l^2}{6} + \frac{k_0 l^2}{2} + \\ &\frac{n_w}{1-d} \left(\frac{l^4 - d^4}{4} - \frac{l^3 - d^3}{3} \right) + \\ &\left(-\frac{k_0}{1} + \frac{n_w}{1-d} + \frac{n_w d}{l(1-d)} \right) \left(l \frac{l^2 - d^2}{2} - \frac{l^3 - d^3}{3} \right) + \\ &\left(k_0 - \frac{n_w d}{1-d} \right) \left(l(1-d) - \frac{l^2 - d^2}{2} \right) + \frac{k_\phi}{1} \\ T_1 &= \frac{n_w l^2}{12} + \frac{k_0 l^2}{6} + \frac{n_w}{1-d} \left(\frac{l^3 - d^3}{3} - \frac{l^4 - d^4}{4} \right) + \\ &+ \left(\frac{k_0}{1} - \frac{n_w d}{l(1-d)} \right) \left(\frac{l^2 - d^2}{2} - \frac{l^3 - d^3}{3} \right) - \frac{k_\phi}{1} \end{aligned} \right\} (4.19)$$

Solving equation (4.18) for the displacements gives:

$$\left. \begin{aligned} W_0 &= PA_0 \\ W_1 &= PA_1 \\ \text{where: } A_0 &= \frac{R_1(1-a) - T_1}{R_1T_0 - R_0T_1} \\ A_1 &= \frac{R_0(1-a) - T_0}{R_0T_1 - R_1T_0} \end{aligned} \right\} (4.20)$$

From equations (4.20) and (4.13)

$$W(Z_1) = P \left(A_0 - \frac{A_0 - A_1}{l} Z_1 \right) \quad (4.21)$$

For $Z_1 = a$, equation 4.21 gives:

$$P = \frac{W_a}{A_0 - \frac{A_0 - A_1}{l} a} \quad (4.22)$$

The total force P_t is found by multiplying by the foundation width, b .

$$P_t = \frac{b}{A_0 - \frac{A_0 - A_1}{l} a} W_a$$

So, the desired stiffness coefficient is

$$k_{ab} = \frac{b}{A_0 - \frac{A_0 - A_1}{l} a} \quad (4.23)$$

Equation (4.23) provides an expression for the equivalent abutment stiffness when the soil behaves elastically. It should be noted that the expression for k_{ab} also applies for the special cases when $k_w = n_w Z/l$ or $k_w = k$, by setting $k_0 = 0$ or $n_w = 0$, respectively.

4.4.3 Yielding of regions of the two soil deposits

As shown in Fig. 4.6, in the general case each soil deposit is divided into two regions: region 1, which in both deposits is compressed by the abutment, and region 2, which in both deposits is in tension as defined earlier. The distance s , which defines the point of zero displacement, can be found from equations 4.13 and 4.20:

$$s = l \frac{A_0}{A_0 - A_1} \quad (4.24)$$

Based on the yielding criterion (e) which was stated in section 4.3, the displacement W_a , which causes yielding of each of the four regions, can be estimated as follows.

4.4.3.1 Yielding of the regions of deposit 1

(i) Region 1 (in compression)

a. Initial force (due to geostatic stresses only):

$$P_{O,11} = K_0 \int_0^s \sigma_v(z_1) dz_1 = 1/2 K_0 \gamma s^2$$

or from equation (4.24)

$$P_{O,11} = 1/2 K_0 \gamma l^2 \frac{A_0^2}{(A_0 - A_1)^2} \quad (4.25)$$

b. Force imposed by the motion of the abutment:

$$P_{r,11} = \int_0^s p_r(z_1) dz_1$$

and from equations 4.15 and 4.17

$$P_{,11} = (W_1 - W_0) \frac{n_w}{1} \frac{s^3}{2} + [W_0(n_w - k_0) + W_1 k_0] \frac{s^2}{21}$$

$$+ k_0 W_0 s = W_a \alpha_1$$

where:

$$\alpha_1 = \frac{k_{ab}}{b} \frac{A_0}{A_0 - A_1} \left[1 + \left\{ n_w \frac{A^2}{3(A_1 - A_0)} \right. \right.$$

$$\left. \left. + [A_0(n_w - k_0) + A_1 k_0] \frac{A_0}{2(A_0 - A_1)} + k_0 A_0 \right\} \right] \quad (4.26)$$

c. Total Passive Resistance:

$$P_{p,11} = 1/2 K_p \gamma s^2 + 2c K_p s =$$

$$1 \frac{A_0}{A_0 - A_1} \left(1/2 K_p \gamma \left[1 + \frac{A_0}{A_0 - A_1} + 2c \sqrt{K_p} \right] \right) \quad (4.27)$$

According to the yielding criterion followed in this analysis, this region will yield when:

$$P_{0,11} + P_{,11} = P_{p,11} \quad (4.28)$$

From (4.28), the displacement W_a , required to cause yielding of this region, is found to be:

$$W_{a,11}^Y = \frac{1}{\alpha_1} \left[1 + \frac{A_0}{A_0 - A_1} \left(1/2 K_p \gamma \left[1 + \frac{A_0}{A_0 - A_1} + 2c \sqrt{K_p} \right] - \right. \right.$$

$$\left. \left. 1/2 K_0 \gamma \left[1 + \frac{A_0^2}{(A_0 - A_1)^2} \right] \right) \right] \quad (4.29)$$

(ii) Region 2 (in tension)

a. Initial force (due to geostatic stresses only)

$$P_{O,12} = K_O \int_s^1 \sigma_v(z_1) dz_1 = 1/2 K_O (l^2 - s^2)$$

and from equation 4.24

$$P_{O,12} = 1/2 K_O \gamma l^2 \left(1 - \frac{A_O^2}{(A_O - A_1)^2}\right) \quad (4.30)$$

b. Force imposed by the motion of the abutment:

$$P_{,12} = \int_s^1 P_r(z_1) dz_1 \quad \text{or}$$

$$P_{,12} = (W_1 - W_O) \frac{n_w}{l^2} \frac{l^3 - s^3}{3} + [W_O(n_w - k_O) + W_1 k_O] \frac{l^2 - s^2}{2}$$

$$+ k_O W_O (1 - s) = W_a \alpha_2$$

where:

$$\alpha_2 = \frac{k_{ab}}{b} \left\{ (A_1 - A_O) n_w \frac{1 - \frac{A_O^3}{(A_O - A_1)^3}}{3} + [A_O(n_w - k_O) + A_1 k_O] \frac{1 - \frac{A_O^2}{(A_O - A_1)^2}}{2} + k_O A_O \left(1 - \frac{A_O}{A_O - A_1}\right) \right\}$$

c. Active Thrust:

From equation (4.7):

$$z_1^0 = \frac{2c}{\gamma \sqrt{K_A}} \quad (4.31)$$

Depending on the value of z_1^0 , the active thrust can be estimated as

follows:

$$1. \text{ If } z_1^0 > 1 : \quad P_{A,12} = 0 \quad (4.32)$$

$$2. \text{ If } s < z_1^0 < 1 : \quad P_{A,12} = \int_{z_1^0}^1 \sigma_a(z_1) dz_1 \text{ or}$$

$$P_{A,12} = 1/2 K_A (1^2 - z_1^0{}^2) - 2c\sqrt{K_A} (1 - z_1^0) \quad (4.33)$$

$$3. \text{ If } z_1^0 < s : \quad P_{A,12} = \int_s^1 \sigma_a(z_1) dz_1 \quad \text{or}$$

$$P_{A,12} = 1/2 K_A \gamma^2 \left(1 - \frac{A^2}{(A_0 - A_1)^2}\right) - 2c\sqrt{K_A} \left[1 - \frac{A_0}{A_0 - A_1}\right] \quad (4.34)$$

This region will yield when:

$$P_{O,12} + P_{,12} = P_{A,12} \quad (4.35)$$

From (4.35), the displacement W_a required to cause yielding of this region is found to be:

$$\text{If } z_1^0 > 1 : \quad W_{a,12}^Y = - \frac{1}{\alpha_2} \left[1/2 K_O \gamma^2 \left(1 - \frac{A_0^2}{(A_0 - A_1)^2}\right) \right]$$

$$\text{If } s < z_1^0 < 1 : \quad W_{a,12}^Y = - \frac{1}{\alpha_2} \left[1/2 K_A (1^2 - z_1^0{}^2) - \right.$$

$$\left. 2c\sqrt{K_A} (1 - z_1^0) - 1/2 K_O \gamma^2 \left(1 - \frac{A_0^2}{(A_0 - A_1)^2}\right) \right] \quad (4.36)$$

$$\text{If } z_1^0 < s : \quad W_{a,12}^Y = \frac{1}{\alpha_2} \left[1/2 K_A \gamma^2 \left(1 - \frac{A_0^2}{(A_0 - A_1)^2} - \right. \right.$$

$$\left. \left. 2c\sqrt{K_A} \left[1 - \frac{A_0}{A_0 - A_1} - 1/2 K_O \gamma^2 \left(1 - \frac{A_0^2}{(A_0 - A_1)^2}\right) \right] \right] \right]$$

4.3.3.2 Yielding of the regions of deposit 2

(i) Region 1 (in compression)

a. Initial force (due to geostatic stresses only):

$$\begin{aligned}
 P_{0,21} &= K_0 \int_s^1 \gamma (z_1 - d) dz_1 \\
 &= 1/2 K_0 \gamma [(1-d)^2 - (s-d)^2] = \\
 &1/2 K_0 \gamma [(1-d)^2 - (1 - \frac{A_0}{A_0 - A_1} - d)^2] \quad (4.37)
 \end{aligned}$$

b. Force imposed by the motion of the abutment:

$$\begin{aligned}
 P_{,21} &= - \int_s^1 p_1(z_1) dz_1 \\
 &= - \{ (W_1 - W_0) \frac{n_w}{1(1-d)} \frac{l^3 - s^3}{3} + [W_0 (-\frac{k_0}{1} + \frac{n_w}{1-d} + \frac{n_w d}{1(1-d)} \\
 &+ W_1 (\frac{k_0}{1} - \frac{n_w d}{1(1-d)})] \frac{l^2 - s^2}{2} + W_0 (k_0 - \frac{n_w d}{1-d}) (1-s) \} \quad \text{or}
 \end{aligned}$$

$$P_{2,1} = \beta_1 W_a$$

where:

$$\begin{aligned}
 \beta_1 &= - \frac{k_{ab}}{b} \left\{ (A_1 - A_0) \frac{n_w l}{3(1-d)} \left(1 - \frac{A_0^3}{(A_0 - A_1)^3} \right) \right. \\
 &+ [A_0 (-\frac{k_0}{1} - \frac{n_w}{1-d} + \frac{n_w d}{1(1-d)}) + \\
 &+ A_1 (\frac{k_0}{1} - \frac{n_w d}{1(1-d)})] \frac{1}{2} \left(1 - \frac{A_0^2}{(A_0 - A_1)^2} \right) \\
 &+ A_0 (k_0 - \frac{n_w d}{1-d}) \left(1 - \frac{A_0}{A_0 - A_1} \right) \left. \right\} \quad (4.38)
 \end{aligned}$$

c. Total Passive Resistance:

$$P_{p,21} = 1/2 K_p \gamma [(1-d)^2 - (s-d)^2] + 2c\sqrt{K_p} (1-s) =$$

$$1/2 K_p \gamma [(1-d)^2 - (1 - \frac{A_0}{A_0 - A_1} - d)^2] + 2c\sqrt{K_p} (1 - \frac{A_0}{A_0 - A_1}) \quad (4.39)$$

This region will yield when:

$$P_{o,21} + P_{,21} = P_{p,21} \quad (4.40)$$

From (4.40), one can find the displacement W_a required to cause yielding of this region:

$$W_{a,21}^Y = \frac{1}{\beta_1} \{ 1/2 \gamma [(1-d)^2 - (1 - \frac{A_0}{A_0 - A_1} - d)^2] (K_p - K_o)$$

$$+ 2c\sqrt{K_p} (1 - \frac{A_0}{A_0 - A_1}) \} \quad (4.41)$$

Region 2 (in tension)

a. Initial force (due to geostatic stresses only)

$$P_{o,22} = K_o \int_d^s \gamma (z_1 - d) dz_1 =$$

$$1/2 K_o (1 - \frac{A_0}{A_0 - A_1} - d)^2 \quad (4.42)$$

b. Force imposed by the motion of the abutment:

$$P_{,22} = - \int_d^s P_1(z_1) dz_1 =$$

$$- \left\{ (W_1 - W_0) \frac{n_w}{1(1-d)} \frac{s^3 - d^3}{3} + \left[W_0 \left(-\frac{k_0}{1} + \frac{n_w}{1-d} + \frac{n_w d}{1(1-d)} \right) + \right. \right.$$

$$\left. W_1 \left(\frac{k_0}{1} - \frac{n_w d}{1(1-d)} \right) \right] \frac{s^2 - d^2}{2} + W_0 \left(k_0 - \frac{n_w d}{1-d} \right) (s - d) \right\} \quad \text{or}$$

$$P_{,22} = \beta_2 W_a$$

where:

$$\beta_2 = - \frac{k_{ab}}{b} \left\{ (A_1 - A_0) \frac{n_w}{1(1-d)} \frac{1^3 \frac{A_0^3}{(A_0 - A_1)^3} - d^3}{3} \right.$$

$$+ \left[A_0 \left(-\frac{k_0}{1} + \frac{n_w}{1-d} + \frac{n_w d}{1(1-d)} \right) + \right.$$

$$\left. A_1 \left(\frac{k_0}{1} - \frac{n_w d}{1(1-d)} \right) \right] \frac{1^2 \frac{A_0^2}{(A_0 - A_1)^2} - d^2}{2} +$$

$$\left. A_0 \left(k_0 - \frac{n_w d}{1-d} \right) \left(1 - \frac{A_0}{A_0 - A_1} - d \right) \right\} \quad (4.43)$$

c. Active Thrust

Following the same procedure as followed for the estimation of the active thrust of region 2 of deposit 1, one finds:

$$z_1^0 = \frac{2c}{\sqrt{\gamma K_A}} + d \quad (4.44)$$

$$\text{If } z_1^0 > s : \quad P_{A,22} = 0 \quad (4.45)$$

$$\begin{aligned} \text{If } d < z_1^0 < s : \quad P_{A,22} &= \int_{z_1^0}^s \sigma_a(z_1) dz_1 \\ &= 1/2 K_A \gamma \left[\left(1 - \frac{A_0}{A_0 - A_1} - d \right)^2 - (z_1^0 - d)^2 \right] - \\ &\quad 2c\sqrt{K_A} \left(1 - \frac{A_0}{A_0 - A_1} - z_1^0 \right) \end{aligned} \quad (4.46)$$

Region 2 of deposit 2 will yield when:

$$P_{O,22} + P_{,22} = P_{A,22} \quad (4.47)$$

From (4.47) the displacement required to cause yielding of this region is found to be:

$$\text{If } z_1^0 > s : \quad w_{a,22}^Y = - \frac{1}{\beta_2} 1/2 K_O \left(1 - \frac{A_0}{A_0 - A_1} - d \right)^2$$

$$\text{If } d < z_1^0 < s : \quad w_{a,22}^Y =$$

$$\begin{aligned} &\frac{1}{\beta_2} \left\{ 1/2 K_A \left[\left(1 - \frac{A_0}{A_0 - A_1} - d \right)^2 - (z_1^0 - d)^2 \right] \right. \\ &\quad \left. - 2c\sqrt{K_A} \left(1 - \frac{A_0}{A_0 - A_1} - z_1^0 \right) - 1/2 K_O \left(1 - \frac{A_0}{A_0 - A_1} - d \right)^2 \right\} \end{aligned} \quad (4.48)$$

It is obvious that the region which requires the smallest displacement w_a in order to yield will yield first. After a region has yielded, it stops contributing additional force to the resistance to the

abutment motion. Consequently, after the yielding of a region, a redistribution of stresses and displacements will take place and a new problem has to be solved in order to find the new expression for the equivalent abutment stiffness. Therefore, the whole problem can be divided into phases. The end of one phase and the beginning of the next one are marked by the yielding of a soil region. The stress and displacement conditions at the beginning of a phase can be found from the stress and displacement conditions at the end of the previous phase.

The general picture of the problem during any phase is shown in Fig. 4.7. By varying the lengths l_1, l_2, l_3, l_4 , one can achieve the situation in any phase (e.g., the combination $l_1 = 0, l_2 = 0, l_3 = d, l_4 = l$ results in phase 1, which has been already examined). So by finding the expression for the abutment stiffness in this general case, one can estimate the abutment stiffness during any phase.

4.4.4 Estimation of the Equivalent Abutment Stiffness in the General Case

a. Displacement equation:

$$W(Z) = W_0 - \frac{W_0 - W_1}{l} Z, \quad \phi = \frac{W_0 - W_1}{l} \quad (4.49)$$

where W_0 and W_1 are the displacements at the top and the bottom of the abutment, respectively.

b. Distribution of pressure

$$p_r(Z) = W(Z)k_w^r(Z) \quad l_1 \leq Z \leq l_2 \quad (\text{on the right side of the abutment})$$

$$p_l(Z) = W(Z)k_w^l(Z) \quad l_3 \leq Z \leq l_4 \quad (\text{on the left side of the abutment})$$

or

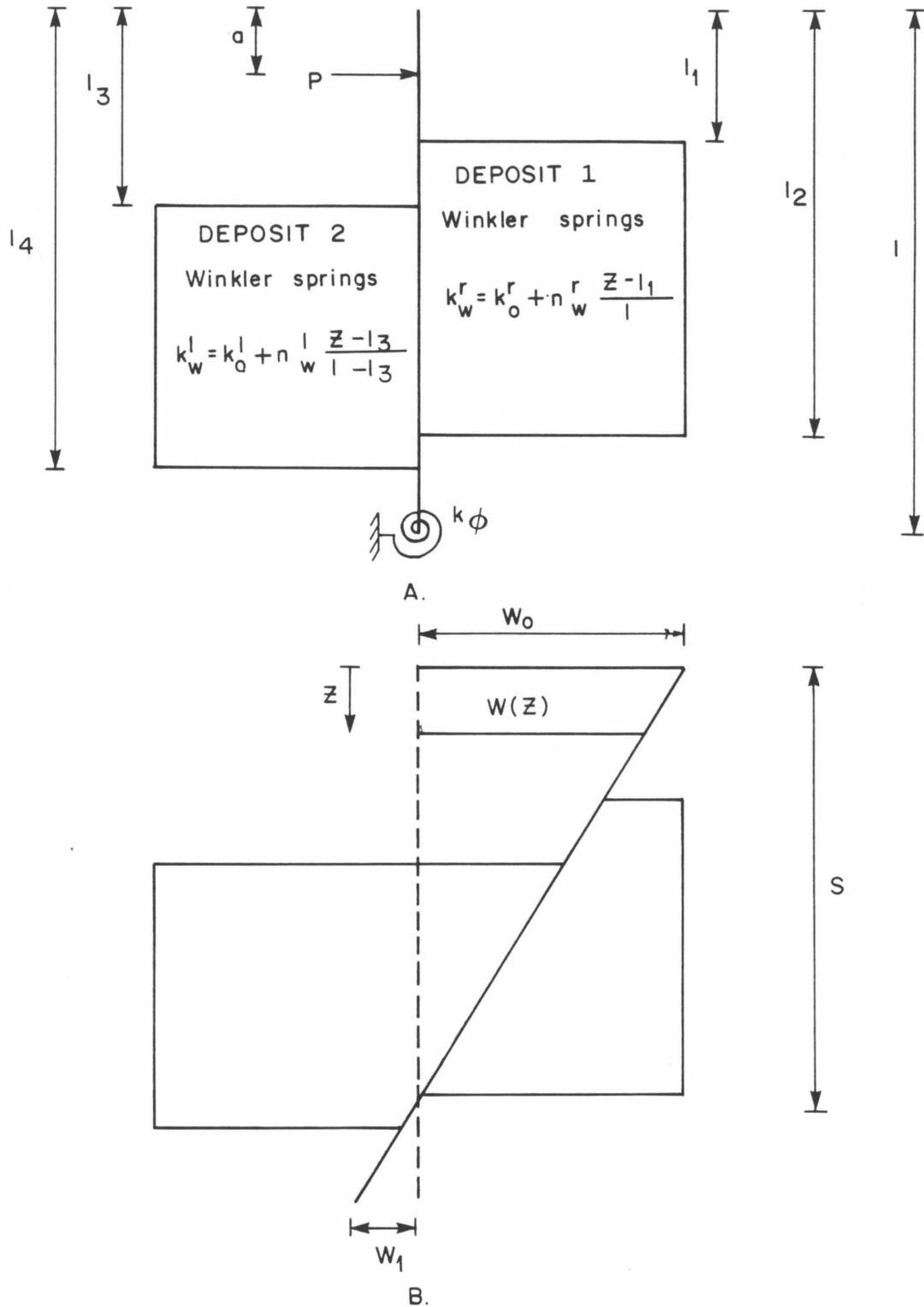


FIG. 4.7 GENERAL CASE

- a. Initial Position of the Abutment with the Soil Deposits and the Load Applied by the Bridge Deck
- b. Displaced Position of the Abutment

$$\begin{aligned}
p_r(z) &= (W_1 - W_0) \frac{n_w^r}{2} z^2 + \\
& [W_0 \left(-\frac{k_0^r}{1} + \frac{n_w^r}{1} + \frac{n_w^r l_1}{l_2} \right) + W_1 \left(-\frac{k_0^r}{1} - \frac{n_w^r l_1}{l_2} \right)] z + \\
& W_0 \left(k_0^r - \frac{n_w^r l_1}{1} \right) \quad l_1 \leq z \leq l_2 \text{ (on the right side)} \\
p_l(z) &= (W_1 - W_0) \frac{n_w^l}{1(1-l_3)} z^2 + \\
& [W_0 \left(-\frac{k_0^l}{1} + \frac{n_w^l}{1-l_3} + \frac{n_w^l l_3}{1(1-l_3)} \right) + W_1 \left(-\frac{k_0^l}{1} - \frac{n_w^l l_3}{1(1-l_3)} \right)] z \\
& + W_0 \left(k_0^l - \frac{n_w^l l_3}{1-l_3} \right) \quad l_3 \leq z \leq l_4 \text{ (on the left side)}
\end{aligned} \tag{4.50}$$

c. Equation of force equilibrium

$$\begin{aligned}
P &= \int_{l_1}^{l_2} p_r(z) dz + \int_{l_3}^{l_4} p_l(z) dz = \\
& (W_1 - W_0) \frac{n_w^r}{l_2} \frac{l_2^3 - l_1^3}{3} + \\
& [W_0 \left(-\frac{k_0^r}{1} + \frac{n_w^r}{1} + \frac{n_w^r l_1}{l_2} \right) + W_1 \left(-\frac{k_0^r}{1} - \frac{n_w^r l_1}{l_2} \right)] \frac{l_2^2 - l_1^2}{2} + \\
& W_0 \left(k_0^r - \frac{n_w^r l_1}{1} \right) (l_2 - l_1) + (W_1 - W_0) \frac{n_w^l}{1(1-l_3)} \frac{l_4^3 - l_3^3}{3} \\
& + W_0 \left(-\frac{k_0^l}{1} + \frac{n_w^l}{1-l_3} + \frac{n_w^l l_3}{1(1-l_3)} \right) + \\
& W_1 \left(-\frac{k_0^l}{1} - \frac{n_w^l l_3}{1(1-l_3)} \right) \frac{l_4^2 - l_3^2}{2} +
\end{aligned}$$

$$+ W_0 \left(k_0^1 - \frac{n_w^1 l_3}{1 - l_3} \right) (l_4 - l_3)$$

or

$$\begin{aligned}
 P = & \left[- \frac{n_w^r}{l^2} \frac{l_2^3 - l_1^3}{3} - \frac{n_w^1}{1(1-l_3)} \frac{l_4^3 - l_3^3}{3} + \right. \\
 & \left. \left(- \frac{k_0^r}{1} + \frac{n_w^r}{1} + \frac{n_w^r l_1}{l^2} \right) \frac{l_2^2 - l_1^2}{2} + \right. \\
 & \left. \left(- \frac{k_0^1}{1} + \frac{n_w^1}{1-l_3} + \frac{n_w^1 l_3}{1(1-l_3)} \right) \frac{l_4^2 - l_3^2}{2} + \right. \\
 & \left. \left(k_0^r - \frac{n_w^r l_1}{1} \right) (l_2 - l_1) + \left(k_0^1 - \frac{n_w^1 l_3}{1-l_3} \right) (l_4 - l_3) \right] W_0 + \\
 & \left[\frac{n_w^r}{l^2} \frac{l_2^3 - l_1^3}{3} + \frac{n_w^1}{1(1-l_3)} \frac{l_4^3 - l_3^3}{3} + \right. \\
 & \left. \left(\frac{k_0^r}{1} - \frac{n_w^r l_1}{l^2} \right) \frac{l_2^2 - l_1^2}{2} + \left(\frac{k_0^1}{1} - \frac{n_w^1 l_3}{1(1-l_3)} \right) \right] W_1
 \end{aligned} \tag{4.51}$$

d. Equation of moment equilibrium:

$$\begin{aligned}
 P(1-a) &= \int_{l_1}^{l_2} p_r(z) (1-z) dz + \int_{l_3}^{l_4} p_l(z) (1-z) dz + k_\phi \phi \\
 &= (W_1 - W_0) \frac{n_w^r}{1} \frac{l_2^3 - l_1^3}{3} + \\
 & \left[W_0 \left(- \frac{k_0^r}{1} + \frac{n_w^r}{1} + \frac{n_w^r l_1}{l^2} \right) + W_1 \left(\frac{k_0^r}{1} - \frac{n_w^r l_1}{l^2} \right) \right] \frac{l_2^2 - l_1^2}{2} \\
 & + W_0 \left(k_0^r - \frac{n_w^r l_1}{1} \right) (l_2 - l_1) - (W_1 - W_0) \frac{n_w^r}{l^2} \frac{l_2^4 - l_1^4}{4} -
 \end{aligned}$$

$$\begin{aligned}
& [W_0 \left(-\frac{k_0^r}{1} + \frac{n_w^r}{1} + \frac{n_w^r l_1}{l^2} \right) + W_1 \left(\frac{k_0^r}{1} - \frac{n_w^r l_1}{l^2} \right)] \frac{l_2^3 - l_1^3}{3} - \\
& W_0 \left(k_0^r - \frac{n_w l_1}{1} \right) \frac{l_2^2 - l_1^2}{2} + (W_1 - W_0) \frac{n_w^l}{1 - l_3} \frac{l_4^3 - l_3^3}{3} + \\
& [W_0 \left(-\frac{k_0^l}{1} + \frac{n_w^l}{1 - l_3} + \frac{n_w^l l_3}{1(1 - l_3)} \right) + \\
& W_1 \left(\frac{k_0^l}{1} - \frac{n_w^l l_3}{1(1 - l_3)} \right)] \frac{l_4^2 - l_3^2}{2} + \\
& W_0^l \left(k_0^l - \frac{n_w^l l_3}{1 - l_3} \right) (l_4 - l_3) \\
& - (W_1 - W_0) \frac{n_w^l}{1(1 - l_3)} \frac{l_4^4 - l_3^4}{4} - \\
& [W_0 \left(-\frac{k_0^l}{1} + \frac{n_w^l}{1 - l_3} + \frac{n_w^l l_3}{1(1 - l_3)} \right) + \\
& W_1 \left(\frac{k_0^l}{1} - \frac{n_w^l l_3}{1(1 - l_3)} \right)] \frac{l_4^3 - l_3^3}{3} - \\
& W_0 \left(k_0 - \frac{n_w^l l_3}{1 - l_3} \right) \frac{l_4^2 - l_3^2}{2}
\end{aligned}$$

or

$$P(1 - a) = \left[-\frac{n_w^r}{1} \left(-\frac{l_2^3 - l_1^3}{3} + \frac{l_2^4 - l_1^4}{4l} \right) + \right.$$

$$\left. \dots \right]$$

$$\begin{aligned}
& \left(-\frac{k_O^r}{1} + \frac{n_w^r}{1} + \frac{n_w^r l_1}{1^2} \right) \left(\frac{l_2^2 - l_1^2}{2} - \frac{l_2^3 - l_1^3}{3} \right) + \\
& \left(k_O^r - \frac{n_w^r l_1}{1} \right) \left(l(l_2 - l_1) - \frac{l_2^2 - l_1^2}{2} \right) + \\
& \frac{n_w^l}{1 - l_3} \left(-\frac{l_4^3 - l_3^3}{3} + \frac{l_4^4 - l_3^4}{4} \right) + \\
& \left(-\frac{k_O^l}{1} + \frac{n_w^l}{1 - l_3} + \frac{n_w^l l_3}{1(1 - l_3)} \right) \left(\frac{l_4^2 - l_3^2}{2} - \frac{l_4^3 - l_3^3}{3} \right) + \\
& \left(k_O^l - \frac{n_w^l l_3}{1 - l_3} \right) \left(l(l_4 - l_3) - \frac{l_4^2 - l_3^2}{2} \right) + \frac{k_\phi}{1} W_O + \\
& \left[\frac{n_w^r}{1} \left(\frac{l_2^3 - l_1^3}{3} - \frac{l_2^4 - l_1^4}{4l} \right) + \right. \\
& \left. \left(\frac{k_O^r}{1} - \frac{n_w^r l_1}{1^2} \right) \left(\frac{l_2^2 - l_1^2}{2} - \frac{l_2^3 - l_1^3}{3} \right) + \right. \\
& \left. \frac{n_w^l}{1 - l_3} \left(\frac{l_4^3 - l_3^3}{3} - \frac{l_4^4 - l_3^4}{4} \right) + \right. \\
& \left. \left(\frac{k_O^l}{1} - \frac{n_w^l l_3}{1(1 - l_3)} \right) \left(l \frac{l_4^2 - l_3^2}{2} - \frac{l_4^3 - l_3^3}{3} \right) - \frac{k_\phi}{1} W_1 \right]
\end{aligned} \tag{4.52}$$

e. Expressions for W_0, W_1

$$W_0 = PA_0$$

$$W_1 = PA_1$$

$$A_0 = \frac{R_1(1 - a) - T_1}{R_1 T_0 - R_0 T_1}, \quad A_1 = \frac{R_0(1 - a) - T_0}{R_0 T_1 - R_1 T_0} \tag{4.53}$$

$$R_0 = -\frac{n_w^r}{1^2} \frac{l_2^3 - l_1^3}{3} - \frac{n_w^l}{1(1 - l_3)} \frac{l_4^3 - l_3^3}{3} - \frac{k_O^r}{1} + \frac{n_w^r}{1}$$

$$+ \frac{n_w^r l_1}{l^2} - \frac{k_O^l}{1} + \frac{n_w^l}{1 - l_3} + \frac{n_w^l l_3}{1(1 - l_3)} +$$

$$(k_O^r - \frac{n_w^r l_1}{1})(l_2 - l_1) + (k_O - \frac{n_w l_3}{1 - l_3})(l_4 - l_3)$$

$$R_1 = \frac{n_w^r}{2} \frac{l_2^3 - l_1^3}{3} + \frac{n_w^l}{1(1 - l_3)} \frac{l_4^3 - l_3^3}{3} + \frac{k_O^r}{1} - \frac{n_w^r l_1}{l^2}$$

$$+ \frac{k_O^l}{1} - \frac{n_w^l l_3}{1(1 - l_3)}$$

$$T_O = \frac{n_w^r}{1} \left(-\frac{l_2^3 - l_1^3}{3} + \frac{l_2^4 - l_1^4}{4l} \right) +$$

$$\left(-\frac{k_O^r}{1} + \frac{n_w^r}{1} + \frac{n_w^r l_1}{l^2} \right) \left(\frac{l_2^2 - l_1^2}{2} - \frac{l_2^3 - l_1^3}{3} \right) +$$

$$\left(k_O^r - \frac{n_w l_1}{1} \right) (l(l_2 - l_1) - \frac{l_2^2 - l_1^2}{2})$$

$$+ \frac{n_w^l}{1 - l_3} \left(-\frac{l_4^3 - l_3^3}{3} + \frac{l_4^4 - l_3^4}{4l} \right) +$$

$$\left(-\frac{k_O^l}{1} + \frac{n_w^l}{1 - l_3} + \frac{n_w^l l_3}{1(1 - l_3)} \right) \left(l \frac{l_4^2 - l_3^2}{2} - \frac{l_4^3 - l_3^3}{3} \right)$$

$$+ \left(k_O^l - \frac{n_w^l l_3}{1 - l_3} \right) (l(l_4 - l_3) - \frac{l_4^2 - l_3^2}{2}) + \frac{k_\phi}{1}$$

$$T_1 = \frac{n_w^r}{1} \left(\frac{l_2^3 - l_1^3}{3} - \frac{l_2^4 - l_1^4}{4l} \right) +$$

$$\left(\frac{k_O^r}{1} - \frac{n_w^r l_1}{l^2} \right) \left(l \frac{l_2^2 - l_1^2}{2} - \frac{l_2^3 - l_1^3}{3} \right) +$$

$$\frac{n_w^l}{1 - l_3} \left(\frac{l_4^3 - l_3^3}{3} - \frac{l_4^4 - l_3^4}{4} \right) +$$

(4.53)
cont.

$$\left(\frac{k_0^1}{1} - \frac{n_w^1 l_3}{1(1 - l_3)} \right) \left(1 - \frac{l_4^2 - l_3^2}{2} - \frac{l_4^3 - l_3^3}{3} \right) - \frac{k_\phi}{1} \quad \left. \vphantom{\left(\frac{k_0^1}{1} - \frac{n_w^1 l_3}{1(1 - l_3)} \right)} \right\} \begin{array}{l} \vdots \\ (4.53) \\ \text{cont.} \end{array}$$

f. Expression for the equivalent abutment stiffness:

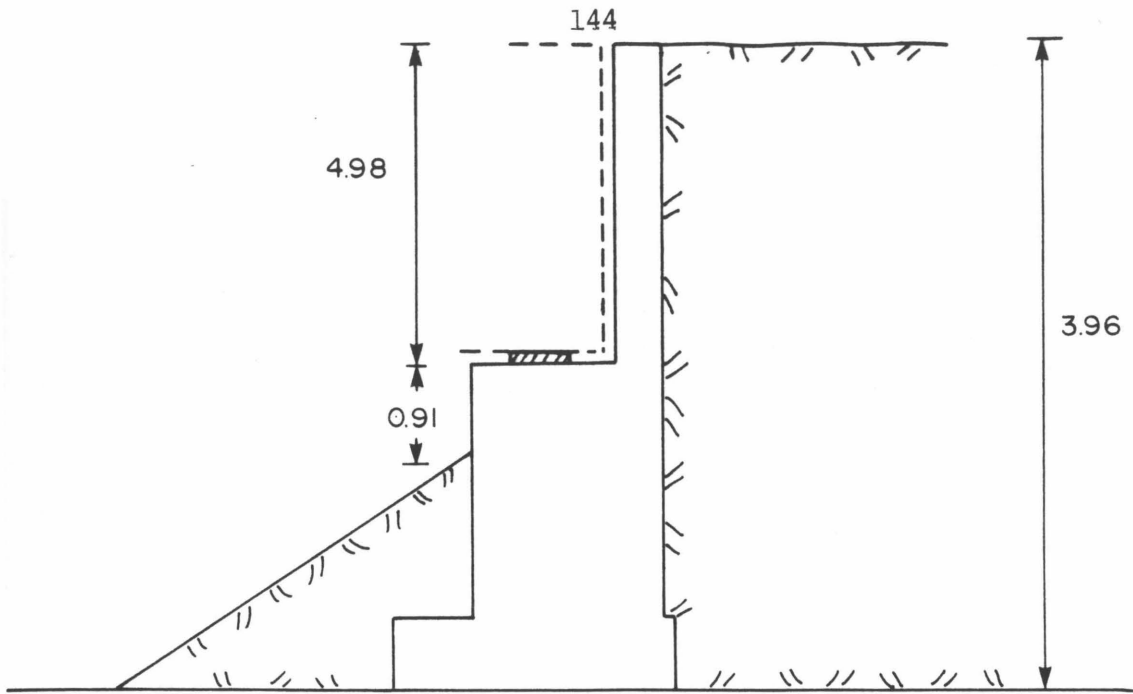
$$k_{ab} = \frac{b}{A_0 - \frac{A_0 - A_1}{1} a} \quad (4.54)$$

Equations (4.54) and 4.53) provide expressions for the equivalent abutment stiffness in the general case. In order to estimate the progressive yielding of the soil, one should follow a procedure similar to that followed in the case of phase 1 paying special attention to the identification of the proper initial conditions at each phase change. Since the initial conditions change from phase to phase, no general formulas can be provided as far as the general case is concerned.

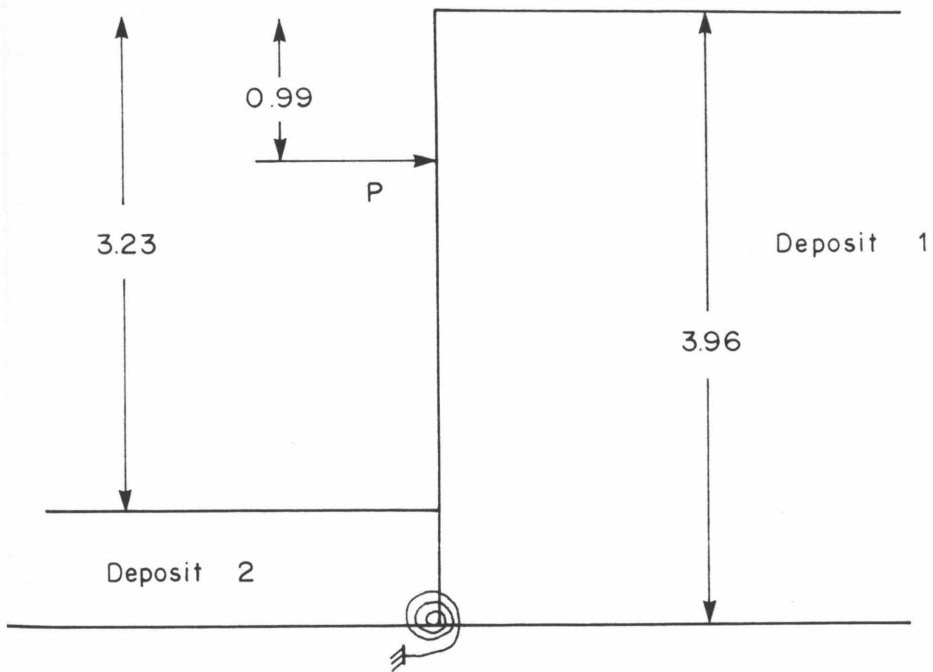
4.5 EXAMPLE

Consider the abutment shown in Fig. 3.8a. This is a section of one of the abutments of the Nichols Road Overcrossing. The model to find the stiffness of this abutment is shown in Fig. 3.8b. The height of deposit 2 in the model is the average height of the deposit on the left hand side of the abutment. The values of the soil springs were estimated based on the properties of stiff soil (Appendix B).

The solution of the problem can be divided into five phases. The intermediate and final results required for the estimation of the abutment stiffness in each phase are shown in Table 4.7. This table also shows the soil region that yields at the end of each phase and the displacement which is required for its yielding. More specifically, examination of the yielding in the first phase produced the following values of yielding displacements.



A.



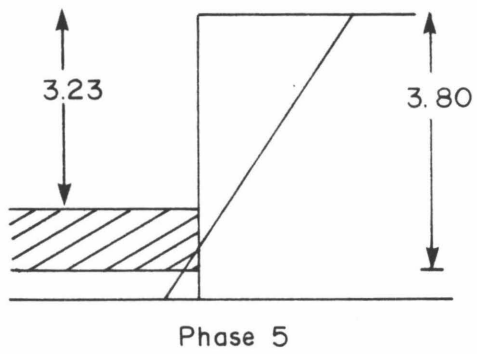
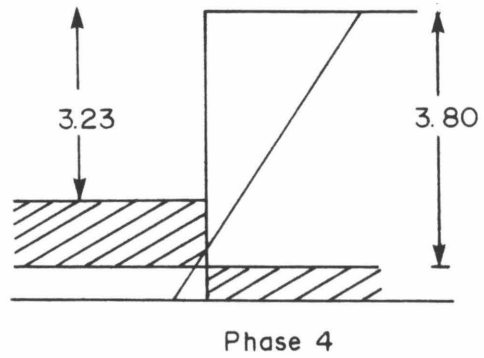
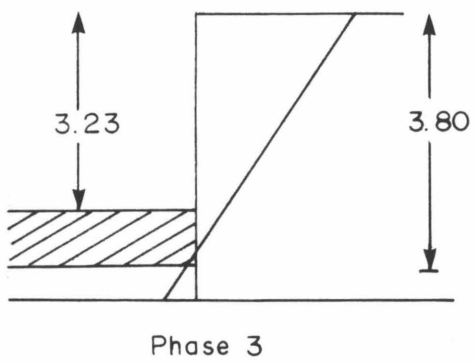
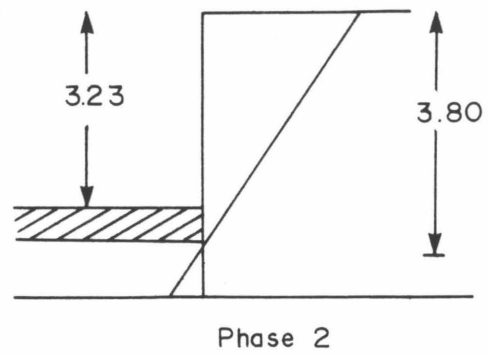
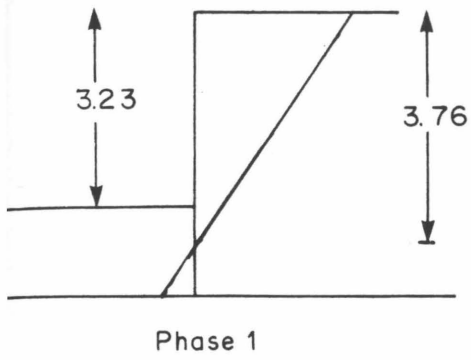
B.

FIG. 4.8 NUMERICAL EXAMPLE OF MODELING OF ABUTMENT STIFFNESS
 a. Abutment of Nichols Road Overcrossing
 b. Model

TABLE 4.7: RESULTS OF EXAMPLE 4.5

Phase	Soil Properties					Height of Deposits				Estimation of Abutment Stiffness				Examination of Yielding		
	k_O^r (t/m ²)	k_O^l (t/m ²)	n_w^r (t/m ²)	n_w^l (t/m ²)	k_ϕ	1 (m)	2 (m)	3 (m)	4 (m)	A_O	A_1	k_{ab} (t/m)	S (m)	Required Yielding Displacement W_a (m)	Critical Region R* D*	
1	135	135	1412.5	1412.5	3110	0	3.96	3.23	3.96	9.1×10^{-4}	4.6×10^{-5}	21676	3.76	0.005	2	2
2	135	1175	1412.5	1412.5	3110	0	3.96	3.76	3.96	9×10^{-4}	-3.7×10^{-5}	21636	3.8	0.0052	2	2
3	135	1240.7	1412.5	1412.5	3110	0	3.96	3.80	3.96	9×10^{-4}	3.77×10^{-5}	21636	3.8	0.073	2	1
4	135	1240.7	1412.5	1412.5	3110	0	3.80	3.8	3.96	9×10^{-4}	4×10^{-5}	21632	3.8	0.013	1	1
5	0	1240.7	0	1412.5	3110	---	---	3.8	3.96	6.66×10^{-3}	3×10^{-3}	2526.4	---	0.52		

R* Region
D* Deposit



: Denotes inactive soil

FIG. 4.9 THE FIVE PHASES OF THE EXAMPLE

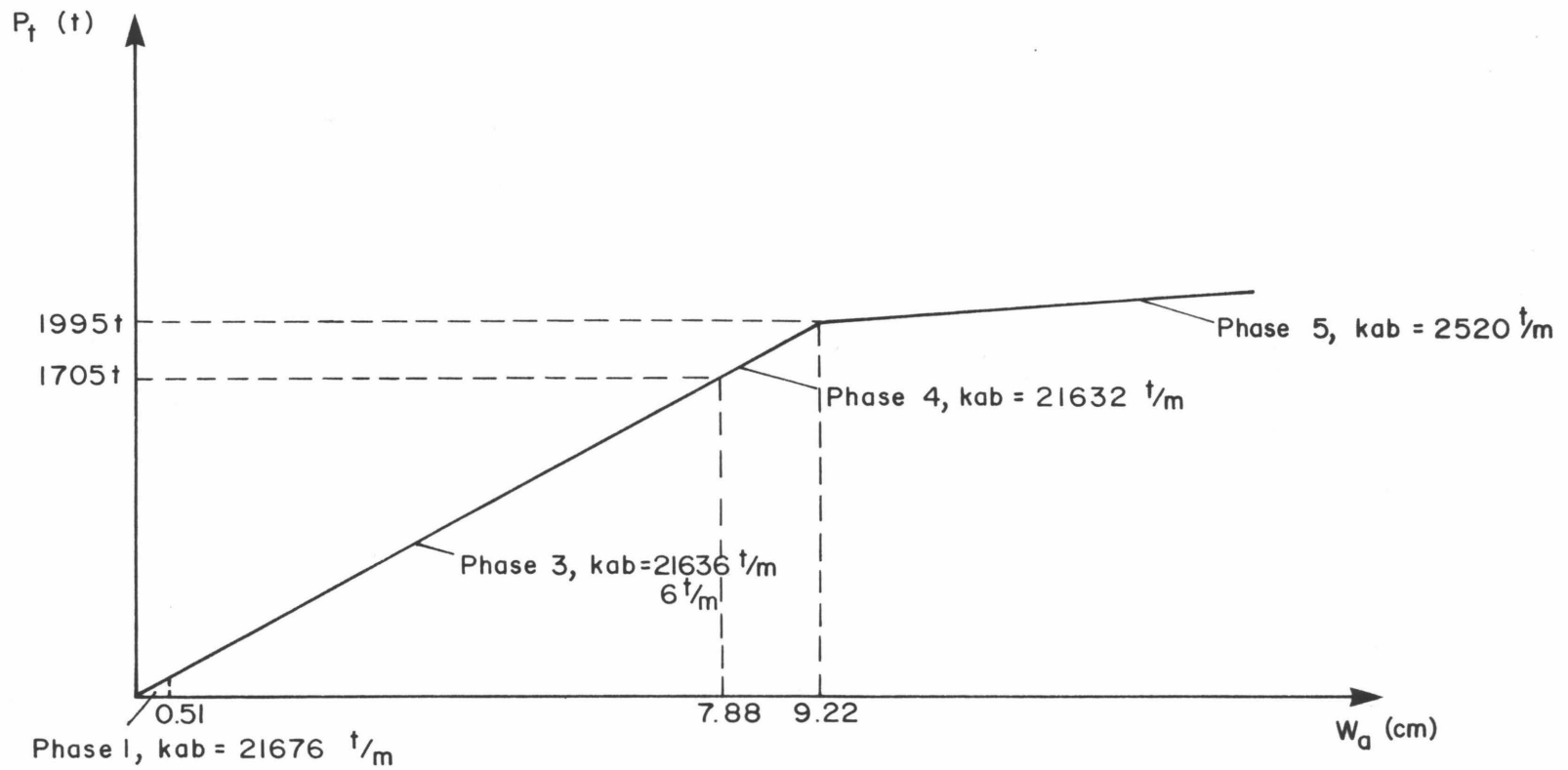


FIG. 4.10 FORCE DISPLACEMENT DIAGRAM OF THE ABUTMENT SHOWN IN FIG. 4.8

Region 1, Deposit 1:	$W_{a,11} = 0.092\text{m}$
Region 2, Deposit 1:	$W_{2,12} = 0.0658\text{m}$
Region 1, Deposit 2:	$W_{2,21} = 0.53\text{m}$
Region 2, Deposit 2:	$W_{2,22} = 0.0051\text{m}$

From these values, it is clear that Region 2 of Deposit 2 will yield first. The examination of yielding in the other phases is similar.

From the results shown in Table 4.1, it is obvious that, during Phase 5, there is active soil only on the left side of the abutment (Region 1 - Deposit 2). The yielding of the soil in this phase is of no practical importance since a total displacement of about 0.53m is required to cause yielding. The pictures of the soil deposits during the five phases are shown in Fig. 4.9.

The force deflection diagram is shown in Fig. 4.10. It is this diagram that would be used in calculating the earthquake response of the bridge.

4.6 SOLUTION OF THE PROBLEM IN THE CASE OF DISCRETE SPRINGS

Assume that the deposit on the right side of the abutment is divided in n_r segments, while the deposit on the left side is divided in n_l segments. The depths of the segments on either side can be arbitrary and unequal. In the analysis, a soil spring is placed at the middle of each segment of every deposit; the springs represent the resistance of the segments to lateral movement of the abutment. The values of the spring stiffnesses can be assigned arbitrarily or estimated from soil properties.

Consider now the i^{th} segment of the right deposit. Let the middle point of this segment be located at a distance Z_r^i from the top of the

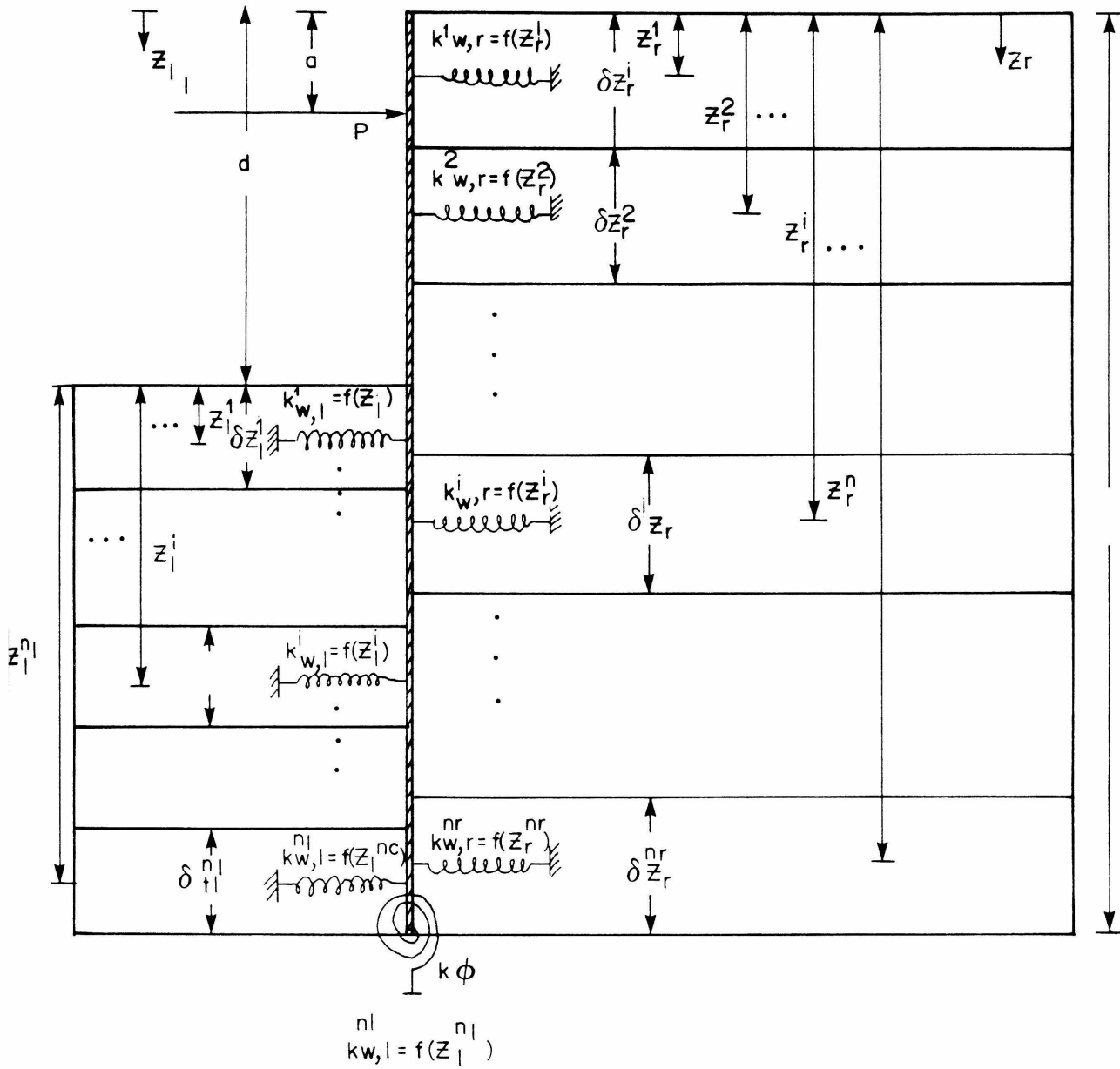


FIG. 4.11 MODELING OF THE ABUTMENT SOIL WITH DISCRETE SPRINGS

abutment, and let the length of the segment be δz_r^i (see Fig. 4.11). Suppose that the spring constant of this segment is $k_{w,r}^i$, then the resisting force of the segment will be:

$$f_r^i = k_{w,r}^i \delta z_r^i w_r^i \quad (4.55)$$

The moment of the force f_r^i about the bottom of the abutment will be:

$$m_r^i = k_{w,r}^i \delta z_r^i w_r^i (1 - z_r^i) \quad (4.56)$$

In the above relations, w_r^i is the displacement of the abutment at depth z_r^i ; it can be expressed as a function of the displacements w_0 and w_1 from the relation (4.49). Thus:

$$w_r^i = w_0 - \frac{w_0 - w_1}{1} z_r^i \quad (4.57)$$

Similarly, for the j^{th} segment of the left deposit, one gets:

$$f_l^j = k_{w,l}^j \delta z_l^j w_l^j \quad (4.58)$$

$$m_l^j = k_{w,l}^j \delta z_l^j w_l^j (1 - z_l^j) \quad (4.59)$$

$$w_l^j = w_0 - \frac{w_0 - w_1}{1} z_l^j \quad (4.60)$$

Next, application of the force equilibrium gives:

$$P = \sum_{i=1}^{n_r} f_r^i + \sum_{j=1}^{n_l} f_l^j \quad (4.61)$$

Combination of (4.55), (4.57), (4.58), (4.60), and (4.61) produces

$$P = \sum_{i=1}^{n_r} k_{w,r}^i \delta z_r^i \left(w_0 - \frac{w_0 - w_1}{1} z_r^i \right) + \sum_{j=1}^{n_l} k_{w,l}^j \delta z_l^j \left(w_0 - \frac{w_0 - w_1}{1} z_l^j \right)$$

or

$$\begin{aligned}
P = & \left(\sum_{i=1}^{n_r} k_{w,r}^i \delta z_r^i - \frac{1}{l} \sum_{i=1}^{n_r} k_{w,r}^i \delta z_r^i z_r^i + \sum_{j=1}^{n_l} k_{w,l}^j \delta z_l^j \right. \\
& \left. - \frac{1}{l} \sum_{j=1}^{n_l} k_{w,l}^j \delta z_l^j z_l^j \right) W_0 + \frac{1}{l} \left(\sum_{i=1}^{n_r} k_{w,r}^i z_r^i \delta z_r^i + \sum_{j=1}^{n_l} k_{w,l}^j z_l^j \delta z_l^j \right) W_1
\end{aligned} \tag{4.62}$$

Similarly, the equation of moment equilibrium gives:

$$P(1-a) = \sum_{i=1}^{n_r} m_r^i + \sum_{j=1}^{n_l} m_l^j \tag{4.63}$$

From (4.58), one gets:

$$\begin{aligned}
P(1-a) = & \left[\sum_{i=1}^{n_r} k_{w,r}^i \left[1 - 2z_r^i + \frac{(z_r^i)^2}{l} \right] \delta z_r^i \right. \\
& + \sum_{j=1}^{n_l} k_{w,l}^j \left[1 - 2z_l^j + \frac{(z_l^j)^2}{l} \right] \delta z_l^j + \frac{k_\phi}{l} \left. \right] W_0 + \\
& \left[\sum_{i=1}^{n_r} \delta z_r^i k_{w,r}^i z_r^i \left(1 - \frac{z_r^i}{l} \right) + \sum_{j=1}^{n_l} \delta z_l^j k_{w,l}^j z_l^j \left(1 - \frac{z_l^j}{l} \right) - \frac{k_\phi}{l} \right] W_1
\end{aligned} \tag{4.64}$$

Solution of the system of equations (4.57) and (4.59) provides the following expressions for W_0, W_1 :

$$\begin{aligned}
W_0 &= PA_0 \\
W_1 &= PA_1 \\
A_0 &= \frac{R_1(1-a) - T_1}{R_1 T_0 - R_0 T_1} & A_1 &= \frac{R_0(1-a) - T_0}{R_0 T_1 - R_1 T_0} \\
R_0 &= \sum_{i=1}^{n_r} k_{w,r}^i \delta z_r^i + \sum_{j=1}^{n_l} k_{w,l}^j \delta z_l^j - \\
& \frac{1}{l} \left[\sum_{i=1}^{n_r} k_{w,r}^i \delta z_r^i z_r^i + \sum_{j=1}^{n_l} k_{w,l}^j \delta z_l^j z_l^j \right]
\end{aligned} \tag{4.65}$$

$$\begin{aligned}
 R_1 &= \frac{1}{1} \left[\sum_{i=1}^{n_r} k_{w,r}^i z_r^i \delta z_r^i + \sum_{j=1}^{n_l} k_{w,l}^j z_l^j \delta z_l^j \right] \\
 T_0 &= \sum_{i=1}^{n_r} k_{w,r}^i \left[1 - 2z_r^i + \frac{(z_r^i)^2}{1} \right] \delta z_r^i + \\
 &\sum_{j=1}^{n_l} k_{w,l}^j \left[1 - 2z_l^j + \frac{(z_l^j)^2}{1} \right] \delta z_l^j + \frac{k_\phi}{1} \\
 T_1 &= \sum_{i=1}^{n_r} \delta z_r^i k_{w,r}^i z_r^i \left(1 - \frac{z_r^i}{1} \right) + \\
 &\sum_{j=1}^{n_l} \delta z_l^j k_{w,l}^j z_l^j \left(1 - \frac{z_l^j}{1} \right) - \frac{k_\phi}{1}
 \end{aligned}
 \tag{4.65} \text{ cont.}$$

Finally, the equivalent abutment stiffness is given by the relation (4.54).

The discrete formulation is particularly convenient for evaluation by small computers and programmable calculations.

CHAPTER 5

A DETAILED MODEL FOR THE INVESTIGATION OF THE RIGID BODY MOTIONS OF SKEW BRIDGES

5.1 INTRODUCTION

In chapter 2, a model was proposed to illustrate some of the dynamic features shown by skew bridges. The model was kept as simple as possible consistent with its purpose to explain the kinematic mechanisms, which induce planar vibrations of skew bridges subjected to strong earthquake shaking. The model was used also to investigate the effects of some parameters on the rigid body motions of a skew bridge. The model was successful for these purposes, but the approximations which were made did not allow a clear representation of the rigid body motions of skew bridges. For this purpose, a more accurate and complex model is required.

In this chapter, a more detailed model for the representation of skew bridges is presented and examined. The principles on which the model is based are similar to the ones for the model of chapter 2. However, in the new model the resistance of the pads is taken into consideration along with translational and rotational damping. Also, the restoring elements of the bridge are allowed to yield and the model is not restricted to the symmetric case. Finally, the new model has three degrees of freedom which permits excitation along the Y direction to be considered. Lateral excitation is not of major concern if the bridge is symmetric or nearly so, but it may be important in other applications of the model.

In the first part of the chapter, the model is presented and explained and the equations of motions are derived. In the second part,

a particular bridge is modeled to illustrate the use of the procedure. The parameters of the model are estimated and several cases of input excitation are examined. Earthquake motions of different strengths are used to illustrate different features of the model.

5.2 THE MODEL

Since the purpose of the model is to capture the most important features of the rigid body motion of a skew bridge, the deck of the bridge is represented as a one dimensional rigid bar having the inertial and geometric properties of the real bridge deck. The resisting mechanisms of the model are the following (see Fig. 5.1).

a. The bridge piers, located at points 1, 2, at distances l_1 and l_2 , respectively, from the center of mass of the deck

Each pier is represented by:

(i) Two elastic bilinear hysteretic springs oriented along the X and Y directions,

(ii) Two viscous dampers oriented along the X and Y direction, and

(iii) One rotational spring resisting the planar rigid body rotations of the bridge deck.

b. The elastomeric pads, located at the two ends of the bridge deck (points 3,4)

Similar to the modeling of the bridge piers, each pad is represented by translational elastic-linearly plastic springs, viscous dampers and one rotational spring.

c. The bridge abutments located at the two ends of the deck (points 3,4)

Each abutment is represented by:

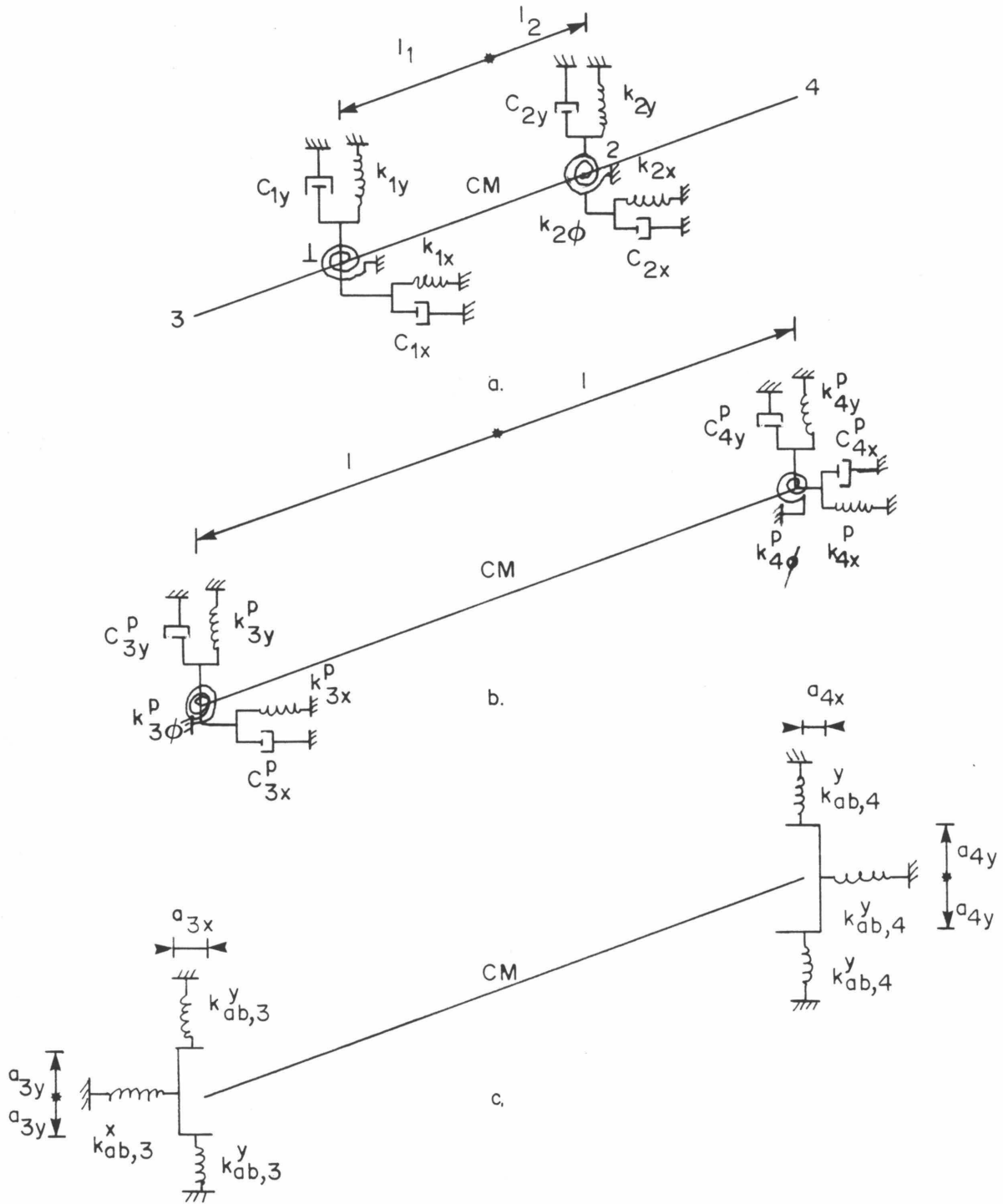
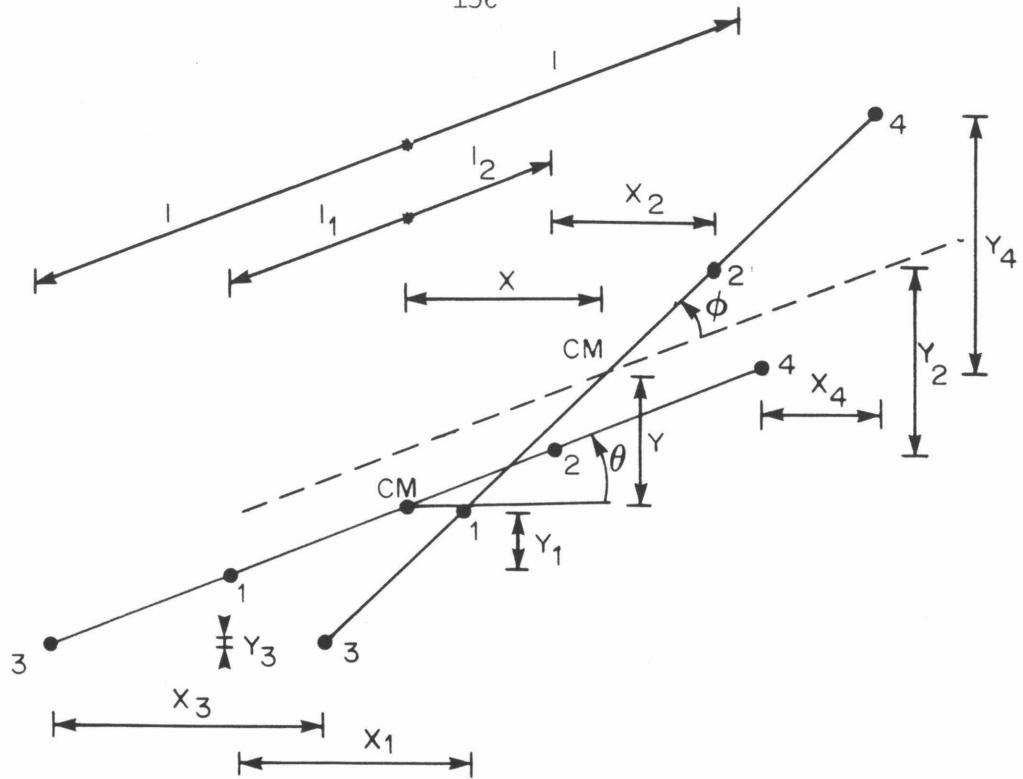


FIG. 5.1 RESISTING MECHANISMS OF THE MODEL
 a. Piers
 b. Elastomeric Pads
 c. Abutments



$$X_1 = X + l_1 \sin \theta \phi$$

$$Y_1 = Y - l_1 \cos \theta \phi$$

$$X_2 = X - l_2 \sin \theta \phi$$

$$Y_2 = p + l_2 \cos \theta \phi$$

$$X_3 = X + l \sin \theta \phi$$

$$Y_3 = p - l \cos \theta \phi$$

$$X_4 = X - l \sin \theta \phi$$

$$Y_4 = Y + l \cos \theta \phi$$

FIG. 5.2 GEOMETRY OF THE MODEL UNDER DISPLACEMENTS X, Y, AND

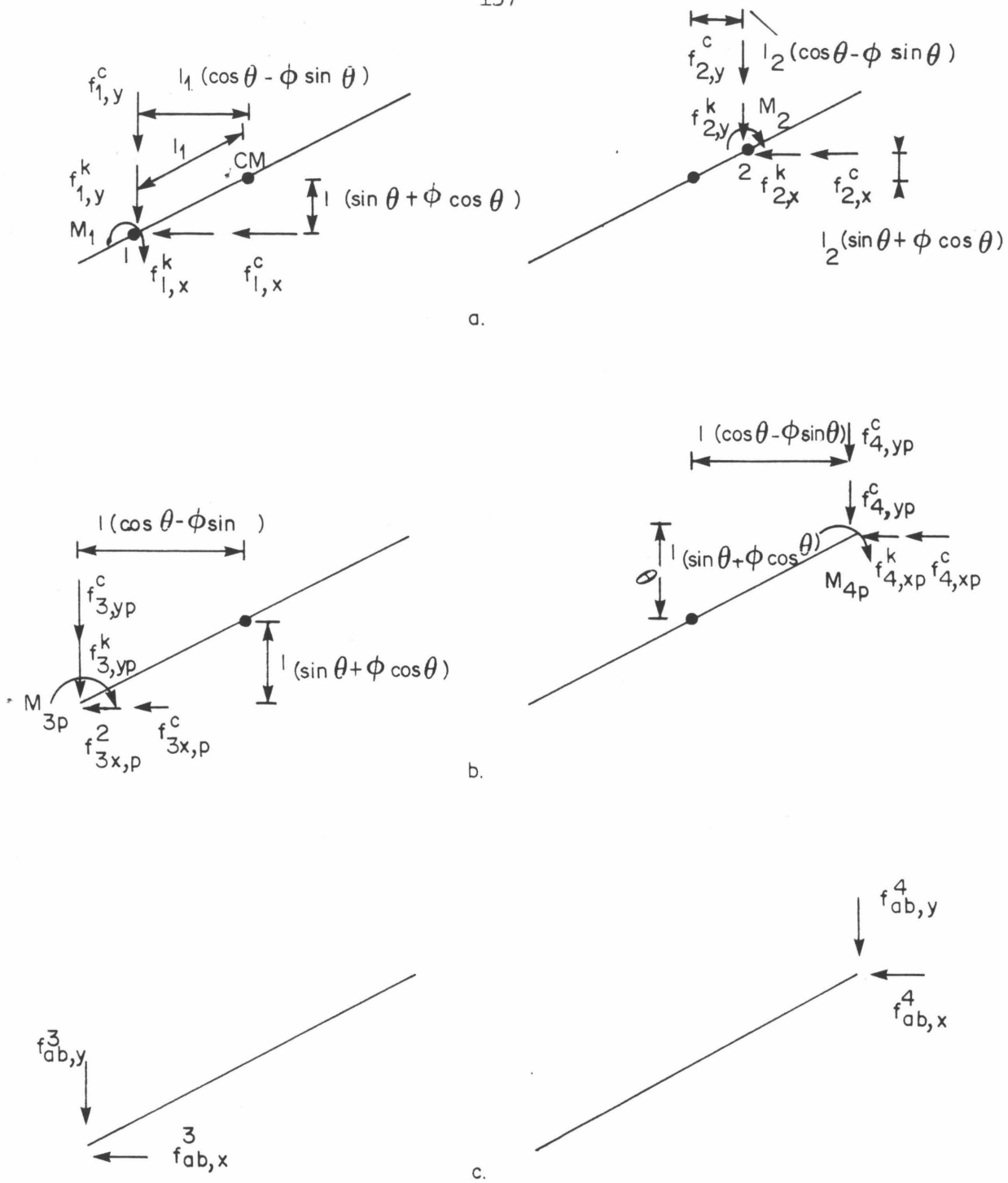


FIG. 5.3 FORCES ACTING ON THE MODEL
 a. Pier Forces
 b. Pad Forces
 c. Abutment Forces

(i) Three elastic-bilinear hysteretic springs (One of these is directed along the X direction and is used to model the resistance of the abutment itself and two are directed along the Y direction to model the resistance of the wing walls.) and

(ii) Three gaps, each one corresponding to an abutment spring. (Therefore, each spring gets activated when the corresponding gap closes, i.e., when impact occurs between the bridge deck and the spring).

The resisting mechanisms of the model are shown in Fig. 5.1. The geometry of the model (which is similar to the geometry of the model developed in chapter 2) and the forces which act on it, are shown in Figs. 5.2 and 5.3, respectively. One can easily see that the model has three degrees of freedom: X, Y, and ϕ . The displacements of all the points of the deck are expressible as functions of these degrees of freedom (see Fig. 5.2).

5.3 FORCES

The forces acting on the model and their moments about the center of mass of the deck are given by the following expressions.

5.3.1 Column Forces

(i) Column at point 1

$$1. \quad f_{1,X}^k = k_{1X} X_1 = k_{1X} X + k_{1X} l_1 \sin \theta \phi \quad (5.1)$$

$$\text{Moment: } m_{1,X}^k = (k_{1X} X + k_{1X} l_1 \sin \theta \phi) l_1 (\sin \theta + \phi \cos \theta) = k_{1X} l_1 \sin \theta X + k_{1X} l_1^2 \sin^2 \theta \phi^* \quad (5.2)$$

$$2. \quad f_{1,X}^c = c_{1X} \dot{X}_1 = c_{1X} \dot{X} + c_{1X} l_1 \sin \theta \dot{\phi} \quad (5.3)$$

$$\text{Moment: } m_{1,X}^c = c_{1X} l_1 \sin \theta \dot{X} + c_{1X} l_1^2 \sin^2 \theta \dot{\phi} \quad (5.4)$$

* In the final expressions of the moments the second order terms are neglected.

$$3. f_{1,Y}^k = k_{1Y}Y_1 = k_{1Y}Y - k_{1Y}l_1\cos\theta\dot{\phi} \quad (5.5)$$

$$\text{Moment: } m_{1,Y}^k = k_{1Y}l_1\cos\theta\dot{Y} - k_{1Y}l_1^2\cos^2\theta\ddot{\phi} \quad (5.6)$$

$$4. f_{1,Y}^c = c_{1Y}\dot{Y}_1 = c_{1Y}\dot{Y} - c_{1Y}l_1\cos\theta\dot{\phi} \quad (5.7)$$

$$\text{Moment: } m_{1,Y}^c = c_{1Y}l_1\cos\theta\dot{Y} - c_{1Y}l_1^2\cos^2\theta\ddot{\phi} \quad (5.8)$$

(ii) Column at point 2

$$1. f_{2,X}^k = k_{2X}X_2 = k_{2X}X - k_{2X}l_2\sin\theta\dot{\phi} \quad (5.9)$$

$$\text{Moment: } m_{2,X}^k = k_{2X}l_2\sin\theta\dot{X} - k_{2X}l_2^2\sin^2\theta\ddot{\phi} \quad (5.10)$$

$$2. f_{2,X}^c = c_{2X}\dot{X}_2 = c_{2X}\dot{X} - c_{2X}l_2\sin\theta\dot{\phi} \quad (5.11)$$

$$\text{Moment: } m_{2,X}^c = c_{2X}l_2\sin\theta\dot{X} - c_{2X}l_2^2\sin^2\theta\ddot{\phi} \quad (5.12)$$

$$3. f_{2,Y}^k = k_{2Y}Y_2 = k_{2Y}Y + k_{2Y}l_2\cos\theta\dot{\phi} \quad (5.13)$$

$$\text{Moment: } m_{2,Y}^k = k_{2,Y}l_2\cos\theta\dot{Y} + k_{2,Y}l_2^2\cos^2\theta\ddot{\phi} \quad (5.14)$$

$$4. f_{2,Y}^c = c_{2Y}\dot{Y}_2 = c_{2Y}\dot{Y} + c_{2Y}l_2\cos\theta\dot{\phi} \quad (5.15)$$

$$\text{Moment: } m_{2,Y}^c = c_{2Y}l_2\cos\theta\dot{Y} + c_{2Y}l_2^2\cos^2\theta\ddot{\phi} \quad (5.16)$$

5.3.2 Pad Forces

(i) Pads at point 3

$$1. f_{3,pX}^k = k_{3X}^p X + k_{3X}^p \sin\theta\dot{\phi} \quad (5.17)$$

$$\text{Moment: } m_{3,pX}^k = k_{3X}^p l \sin\theta\dot{X} + k_{3X}^p l^2 \sin^2\theta\ddot{\phi} \quad (5.18)$$

$$2. f_{3,pX}^c = c_{3X}^p \dot{X} + c_{3X}^p l \sin\theta\dot{\phi} \quad (5.19)$$

$$\text{Moment: } m_{3,pX}^c = c_{3X}^p l \sin\theta\dot{X} + c_{3X}^p l^2 \sin^2\theta\ddot{\phi} \quad (5.20)$$

$$3. f_{3,pY}^k = k_{3Y}^p Y - k_{3Y}^p l \cos\theta\dot{\phi} \quad (5.21)$$

$$\text{Moment: } m_{3,pY}^k = k_{3Y}^p l \cos\theta\dot{Y} - k_{3Y}^p l^2 \cos^2\theta\ddot{\phi} \quad (5.22)$$

$$4. f_{3,pY}^c = c_{3Y}^p \dot{Y} - c_{3Y}^p l \cos\theta\dot{\phi} \quad (5.23)$$

$$\text{Moment: } m_{3,pY}^c = c_{3Y}^p l \cos\theta\dot{Y} - c_{3Y}^p l^2 \cos^2\theta\ddot{\phi} \quad (5.24)$$

(ii) Pads at point 4

$$1. f_{4,pX}^k = k_{4X}^p X - k_{4X}^p \sin\theta\dot{\phi} \quad (5.25)$$

$$\text{Moment: } m_{4,pX}^k = k_{4X}^p l \sin\theta\dot{X} - k_{4X}^p l^2 \sin^2\theta\ddot{\phi} \quad (5.26)$$

$$2. f_{4,pX}^C = c_{4X}^D \dot{X} - c_{4X}^D l \sin \theta \dot{\phi} \quad (5.27)$$

$$\text{Moment: } m_{4,pX}^C = c_{4X}^D l \sin \theta \dot{X} - c_{4X}^D l^2 \sin^2 \theta \dot{\phi} \quad (5.28)$$

$$3. f_{4,pY}^k = k_{4Y}^D Y + k_{4Y}^D l \cos \theta \phi \quad (5.29)$$

$$\text{Moment: } m_{4,pY}^k = k_{4Y}^D l \cos \theta Y + k_{4Y}^D l^2 \cos^2 \theta \phi \quad (5.30)$$

$$4. f_{4,pY}^C = c_{4Y}^D \dot{Y} + c_{4Y}^D l \cos \theta \dot{\phi} \quad (5.31)$$

$$\text{Moment: } m_{4,pY}^C = c_{4Y}^D l \cos \theta \dot{Y} + c_{4Y}^D l^2 \cos^2 \theta \dot{\phi} \quad (5.32)$$

5.3.3 Abutment Forces

(i) Abutment at 4

$$1. f_{ab,X}^4 = b_X^4 k_{ab,4}^X X - b_X^4 k_{ab,4}^X l \sin \theta \phi - b_X^4 k_{ab,4}^X a_X^4 \quad (5.33)$$

where:

$$b_X^4 = \begin{cases} 0 & \text{if } X_4 < a_X^4 \\ 1 & \text{if } X_4 > a_X^4 \end{cases} \quad (5.33)$$

$$\text{Moment: } m_{ab,X}^4 = b_X^4 k_{ab,4}^X l \sin \theta X - b_X^4 k_{ab,4}^X l^2 \sin^2 \theta \phi - b_X^4 k_{ab,4}^X a_X^4 l \sin \theta - b_X^4 k_{ab,4}^X a_X^4 l \cos \theta \phi \quad (5.34)$$

$$2. f_{ab,Y}^4 = b_Y^4 k_{ab,4}^Y Y + b_Y^4 k_{ab,4}^Y l \cos \theta \phi - \text{sign}_4 b_Y^4 k_{ab,4}^Y a_Y \quad (5.35)$$

where:

$$b_Y^4 = \begin{cases} 1 & \text{if } Y_4 > a_Y \text{ or } Y_4 < 0 \text{ and } |Y_4| > a_Y \\ 0 & \text{in all other cases} \end{cases} \quad (5.35)$$

$$\text{sign}_4 = \begin{cases} 1 & \text{if } Y_4 > a_Y \\ -1 & \text{if } Y_4 < 0 \text{ and } |Y_4| > a_Y \end{cases}$$

$$\text{Moment: } m_{ab,Y}^4 = b_Y^4 k_{ab,4}^Y l \cos \theta Y + b_Y^4 k_{ab,4}^Y l^2 \cos^2 \theta \phi - \text{sign}_4 b_Y^4 k_{ab,4}^Y a_Y l \cos \theta + \text{sign}_4 l \sin \theta b_Y^4 k_{ab,4}^Y a_Y \phi \quad (5.36)$$

(ii) Abutment at 3

$$1. f_{ab,X}^3 = b_X^3 k_{ab,3}^X X + b_X^3 k_{ab,3}^X l \sin \theta \phi + b_X^3 k_{ab,3}^X a_X^3 \quad (5.37)$$

where:

$$b_X^3 = \begin{cases} 1 & \text{if } X_3 < 0 \text{ and } |X_3| > a_X^3 \\ 0 & \text{in all other cases} \end{cases} \quad (5.37)$$

$$\text{Moment: } m_{ab,X}^3 = b_X^3 k_{ab,3}^X l \sin \theta + b_X^3 k_{ab,3}^X l^2 \sin^2 \theta + b_X^3 k_{ab,3}^X a_X^3 l \sin \theta + b_X^3 k_{ab,3}^X a_X^3 l \cos \theta \quad (5.38)$$

$$2. \quad f_{ab,Y}^3 = b_Y^3 k_{ab,3}^Y Y - b_Y^3 k_{ab,3}^Y l \cos \theta \phi - \text{sign}^3 b_Y^3 k_{ab,3}^Y a_Y$$

where:

$$b_Y^3 = \begin{cases} 1 & \text{if } Y_3 > a_Y \text{ or } Y_3 < 0 \text{ and } |Y_3| > a_Y \\ 0 & \text{in all other cases} \end{cases} \quad (5.39)$$

$$\text{sign } 3 = \begin{cases} 1 & \text{if } Y_3 > a_Y \\ -1 & \text{if } Y_3 < 0 \text{ and } |Y_3| > a_Y \end{cases}$$

$$\text{Moment: } m_{ab,Y}^3 = b_Y^3 k_{ab,3}^Y l \cos \theta Y - b_Y^3 k_{ab,3}^Y l^2 \cos^2 \theta \phi - \text{sign}^3 b_Y^3 k_{ab,3}^Y a_Y l \cos \theta + \text{sign}^3 b_Y^3 k_{ab,3}^Y a_Y l \sin \theta \phi \quad (5.40)$$

5.4 EQUATIONS OF MOTION

Writing Newton's second law for each one of the three degrees of freedom, one gets:

$$\Sigma F_X = m\ddot{X} \quad (5.41)$$

$$\Sigma F_Y = m\ddot{Y} \quad (5.42)$$

$$\Sigma M = I\ddot{\phi} \quad (5.43)$$

where: ΣF_X is the sum of all the forces along the X direction; ΣF_Y is the sum of all the forces along the Y direction; and ΣM is the sum of all the moments about the center of mass of the bridge deck. Combining the above relations with the expressions for the forces of the model (Equations 5.1 through 5.40), the following expressions for the

equations of motion are obtained:

$$\begin{aligned}
 \ddot{X} + A_1\dot{X} + A_2X + A_3\dot{Y} + A_4Y + A_5\dot{\phi} + A_6\phi + A_7 &= -\ddot{X}_G \\
 Y + B_1\dot{Y} + B_2Y + B_3\dot{X} + B_4X + B_5\dot{\phi} + B_6\phi + B_7 &= -\ddot{Y}_G \\
 \dot{\phi} + C_1\dot{\phi} + C_2\phi + C_3\dot{X} + C_4X + C_5\dot{Y} + C_6Y + C_7 &= 0
 \end{aligned} \tag{5.44}$$

where X_G , Y_G are the translational components of ground accelerations (rotational accelerations are not considered in the analysis). The coefficients in the above equations are defined by the following relations:

$$A_1 = \frac{c_{1X} + c_{2X} + c_{3X}^p + c_{4X}^p}{m} \tag{5.45}$$

$$A_2 = \frac{k_{1X} + k_{2X} + k_{3X}^p + k_{4X}^p + b_X^4 k_{ab,4}^X + b_X^3 k_{ab,3}^X}{m} \tag{5.46}$$

$$A_3 = 0 \tag{5.47}$$

$$A_4 = 0 \tag{5.48}$$

$$A_5 = \frac{c_{1X} l_1 \sin\theta - c_{2X} l_2 \sin\theta + c_3^p X l \sin\theta - c_4^p X l \sin\theta}{m} \tag{5.49}$$

$$A_6 = \frac{(k_{1X} l_1 - k_{2X} l_2) \sin\theta}{m} + \tag{5.50}$$

$$\frac{(k_{3X}^p - k_{4X}^p - b_X^4 k_{ab,4}^X + b_X^3 k_{ab,3}^X) l \sin\theta}{m}$$

$$A_7 = \frac{-b_X^4 k_{ab,4}^X a_X^4 + b_X^3 k_{ab,3}^X a_X^3}{m} \tag{5.51}$$

$$B_1 = \frac{c_{1Y} + c_{2Y} + c_{3Y}^p + c_{4Y}^p}{m} \tag{5.52}$$

$$B_2 = \frac{k_{1Y} + k_{2Y} + k_{3Y}^p + k_{4Y}^p + b_Y^4 k_{ab,4}^Y + b_Y^3 k_{ab,3}^Y}{m} \quad (5.53)$$

$$B_3 = 0 \quad (5.54)$$

$$B_4 = 0 \quad (5.55)$$

$$B_5 = \frac{(c_{2Y}l_2 - c_{1Y}l_1)\cos\theta + (c_{4Y}^p - c_{3Y}^p)l\cos\theta}{m} \quad (5.56)$$

$$B_6 = \frac{(k_{2Y}l_2 - k_{1Y}l_1)\cos\theta}{m} + \quad (5.57)$$

$$\frac{(k_{4Y}^p - k_{3Y}^p + b_Y^4 k_{ab,4}^Y - b_Y^3 k_{ab,3}^Y)l\cos\theta}{m}$$

$$B_7 = \frac{\text{sign}_4 b_Y^4 k_{ab,4}^Y a_Y + \text{sign}_3 b_Y^3 k_{ab,3}^Y a_Y}{m} \quad (5.58)$$

$$C_1 = \frac{(c_{1X}l_1^2 + c_{2X}l_2^2)\sin^2\theta + (c_{1p}l_1^2 + c_{2Y}l_2^2)\cos^2\theta}{I} + \frac{(c_{3X}^p + c_{4X}^p)l^2\sin^2\theta + (c_{3Y}^p + c_{4Y}^p)l^2\cos^2\theta}{I} + \frac{c_\phi}{I} \quad (5.59)$$

$$C_2 = \frac{(k_{1X}l_1^2 + k_{2X}l_2^2)\sin^2\theta + (k_{1Y}l_1^2 + k_{2Y}l_2^2)\cos^2\theta}{I} + \frac{(k_{3X}^p + k_{4X}^p)l^2\sin^2\theta + (k_{3Y}^p + k_{4Y}^p)l^2\cos^2\theta}{I} + \frac{(b_X^4 k_{ab,4}^X + b_X^3 k_{ab,3}^X)l^2\sin^2\theta}{I} + \frac{(b_X^4 k_{ab,4}^X a_X^4 + b_X^3 k_{ab,3}^X a_X^3)l\cos\theta}{I} + \quad (5.60)$$

$$\frac{(b_Y^4 k_{ab,4}^Y + b_Y^3 k_{ab,3}^Y) l^2 \cos^2 \theta}{I} +$$

$$\frac{(\text{sign}4 b_Y^4 k_{ab,4}^Y - \text{sign}3 b_Y^3 k_{ab,3}^Y) a_Y l \sin \theta}{I} \quad (5.60)$$

cont.

$$C_3 = \frac{(c_{1X} l_1 - c_{2X} l_2) \sin \theta + (c_{3X}^D - c_{4X}^D) l \sin \theta}{I} \quad (5.61)$$

$$C_4 = \frac{(k_{1X} l_1 - k_{2X} l_2) \sin \theta}{I} +$$

$$\frac{(k_{3X}^D - k_{4X}^D - b_X^4 k_{ab,4}^X + b_X^3 k_{ab,3}^X) l \sin \theta}{I} \quad (5.62)$$

$$C_5 = \frac{(c_{2Y} l_2 - c_{1Y} l_1) \cos \theta + (c_{4Y}^D - c_{3Y}^D) l \cos \theta}{I} \quad (5.63)$$

$$C_6 = \frac{(k_{2Y} l_2 - k_{1Y} l_1) \cos \theta}{I} +$$

$$\frac{(k_{4Y}^D - k_{3Y}^D + b_Y^4 k_{ab,4}^Y - b_Y^3 k_{ab,3}^Y) l \cos \theta}{I} \quad (5.64)$$

$$C_7 = \frac{(b_X^4 k_{ab,4}^X a_X^4 + b_X^3 k_{ab,3}^X a_X^3) l \sin \theta}{I} +$$

$$\frac{(\text{sign}4 b_Y^4 k_{ab,4}^Y - \text{sign}3 b_Y^3 k_{ab,3}^Y) a_Y l \cos \theta}{I} \quad (5.65)$$

5.5 EXAMPLE OF REPSONSE

The model presented in the preceding section is used to investigate the rigid body motions of Nichols Road Overcrossing, Bridge #56-725, located at Riverside, California. In Fig. 5.4, simplified drawings of the bridge deck and its cross section are shown. The bridge has a total

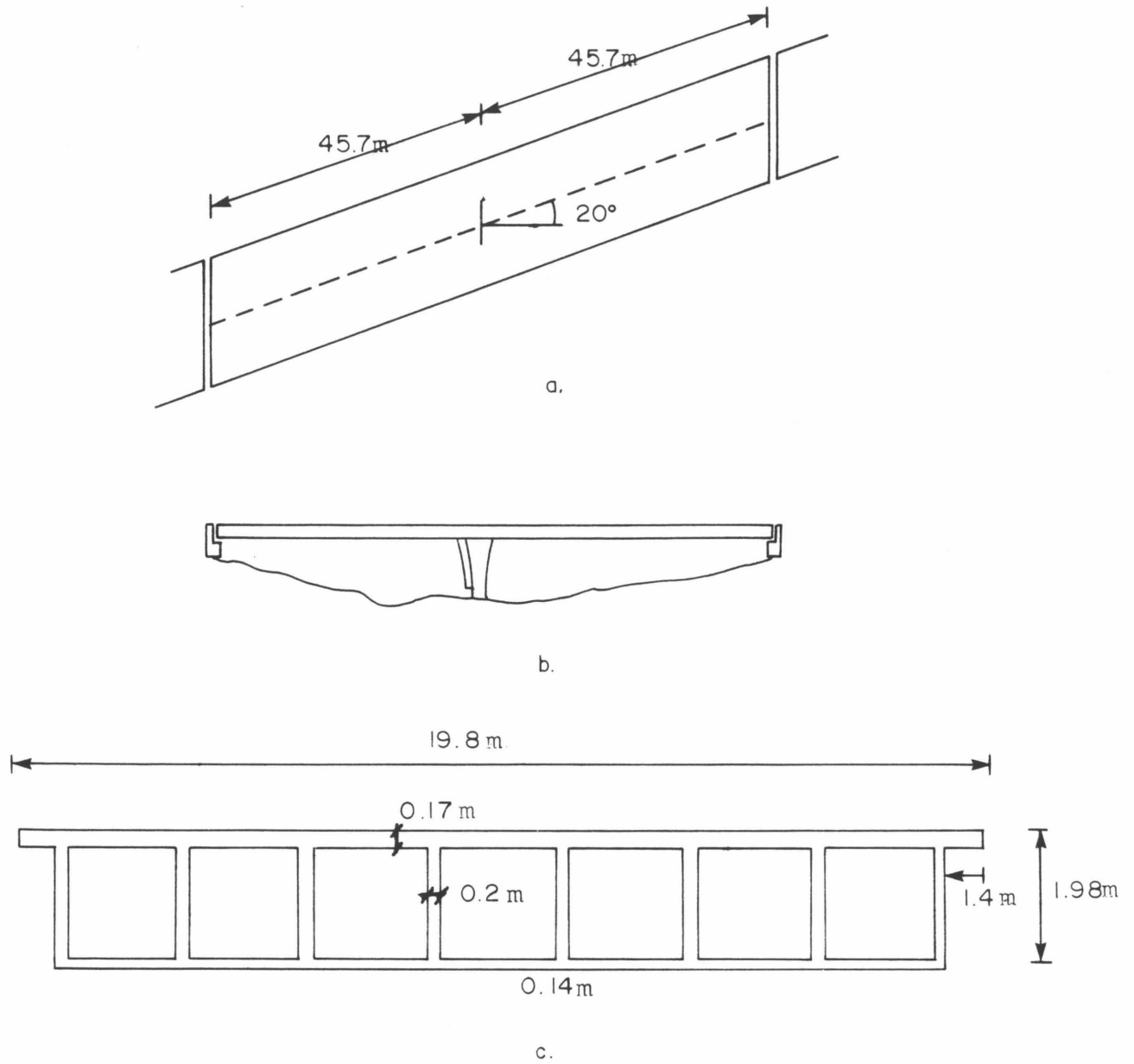


FIG. 5.4 SIMPLIFIED DRAWINGS OF NICHOLS ROAD OVERCROSSING
 a. Top View
 b. Side View
 c. Deck Section

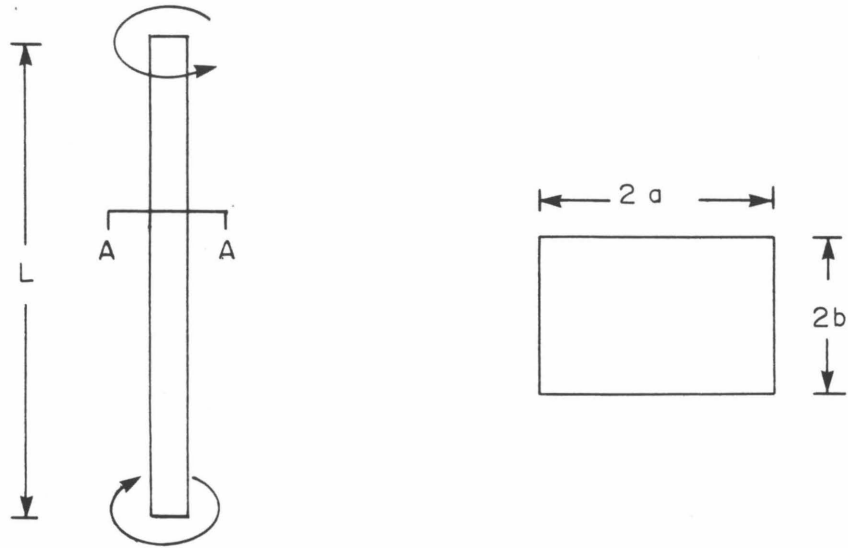
length of 91.4m, is skew at an angle of 20° , and has a set of two columns located 0.63m left of the center of mass of the deck. Simplified drawings of the bridge columns and abutments are shown in Figs.3.5 and 4.8, respectively.

5.5.1 Estimation of the Parameters

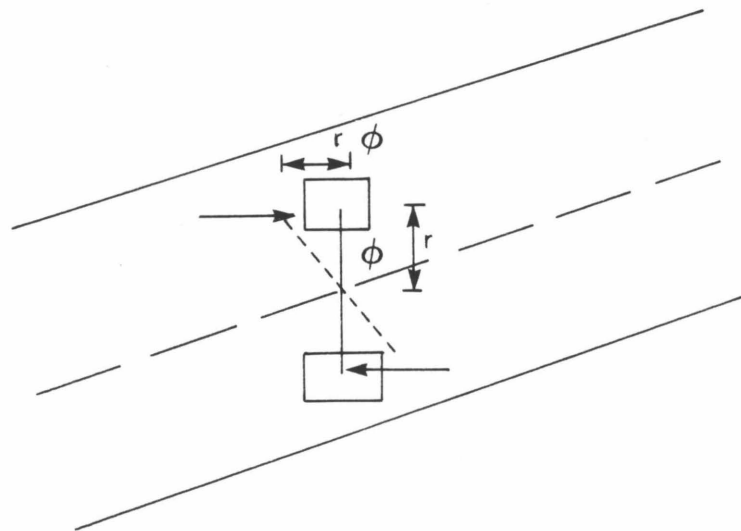
The values of the parameters of the model used in this example were estimated as follows.

a. Translational stiffness of the columns The method for estimating the elastic stiffness of the columns was presented in detail in chapter 2. In that chapter, the method was applied to the columns of the Nichols Road Overcrossing and the results, including the complete force-deflection diagrams for bending of each column in the X and Y directions, were presented in Fig. 3.8. It should be mentioned that in the construction of the force-deflection diagrams of each column it was assumed that bending in the X and Y direction was independent. This assumption is acceptable for the longitudinal excitation of bridges with columns located closely to the center of mass of the bridge since, in this case, there is no significant movement of the columns in the Y direction. Consequently, the bending of the columns is dominated by their movement in the X direction.

b. Torsional stiffness of each column In view of the complicated cross section of the columns, the exact estimation of the torsional stiffness of each column (which is small compared to the torsional resistance arising from the bending of the columns during the rotation of the deck) would involve the solution of a very difficult elasticity problem. So, the torsional stiffness of each column was estimated approximately. For this purpose, the column was first approximated by a



a.



b.

FIG. 5.5 TORSIONAL STIFFNESS OF THE COLUMNS
 a. Stiffness of an Individual Column (of equivalent rectangular cross section)
 b. Stiffness of the System of Two Columns

column of a uniform, rectangular cross section. To do this, first the average octagonal cross section was found by averaging each dimension of the cross section over the column height; then an equivalent cross section was estimated based on equivalency of areas and in equivalency of the depth to width ratio. The equivalent rectangular cross section was found to have dimensions $2a \times 2b$ where $a = 0.65\text{m}$ and $b = 0.56\text{m}$.

The torsional stiffness of each column was then found by applying the well-known formulas (Ref. 44)

$$k = \frac{KG}{L} \quad (5.66)$$

$$K = ab^3 \left[\frac{16}{3} - 3.36 \frac{b}{a} \left(1 - \frac{b^4}{12a^4} \right) \right]$$

These two equations describe the torsional stiffness of a beam of length L , rectangular cross section $2a \times 2b$ and shear modulus G (see Fig. 5.5a). The torsional stiffness of each column was found to be:

$$k = 3.525 \times 10^6 \text{ tm/rad} \quad (5.67)$$

c. Torsional stiffness of the pair of column Consider the system of two bridge columns shown in Fig. 5.5b. Suppose that the bridge deck rotates rigidly by a small angle ϕ . Then, the total restoring moment of the system of the two columns is:

$$M_\phi = 2(k_\phi + r^2 k_x) \phi \quad (5.68)$$

Hence, the total torsional stiffness of the system of two columns is:

$$k_\phi^t = 2(k_\phi + r^2 k_x) \quad (5.69)$$

For this particular bridge, the distance r is equal to 3.2m.

d. Abutment stiffness-gap The method for the estimation of the force-deflection diagram for the abutments was presented in detail in

Chapter 4. In the example presented in that chapter, the abutments of the bridge under consideration were used. The nonlinear force-deflection diagram (after closure of the gap) is shown in Fig. 4.10. The value of the abutment gap for this particular bridge is 0.025m.

e. Viscous damping coefficients and inertial properties Since the columns are located very near the middle of the bridge deck, it was assumed that, before impact between the deck and the abutments occurs, the vibrations of the bridge in the X, Y and ϕ directions are uncoupled. Damping coefficients were determined by estimates of the modal damping in the three uncoupled modes and were then used throughout the seismic excitation of the model. For most of the numerical examples, values of five percent were used for the modal damping (Refs. 15 and 17). The formulas used for the estimation of the translational and rotational damping coefficients are:

$$\begin{aligned} c_X &= 2\zeta_X \sqrt{k_X^t M} \\ c_Y &= 2\zeta_Y \sqrt{k_Y^t M} \\ c_\phi &= 2\zeta_\phi \sqrt{k_\phi^t I} \end{aligned} \quad (5.70)$$

where ζ_X , ζ_Y and ζ_ϕ are the damping ratios in the three directions of motions, k_X^t , k_Y^t , k_ϕ^t are the values of the total stiffness in the direction of motion, and M and I are the mass and the moment of inertia of the bridge deck, respectively. Using $\gamma c = 2.4 \text{ t/m}^3$ for the unit weight of reinforced concrete and the basic geometry of the bridge (see Fig. 5.4) the mass and the moment of inertia were found to be:

$$M = 157.7 \frac{\text{tsec}^2}{\text{m}}, \quad I = 110,000 \frac{\text{tsec}^2 \text{m}}{\text{rad}}$$

Finally, the translational damping coefficients were distributed to the columns and the pads according to their relative stiffnesses. The values

of the damping coefficients are given in Table 5.1.

Direction	Columns	Pads
X	165.1	25.8 per pad
Y	136.07	28.8 per pad

The total rotational damping coefficient was found to be = 128100 tmsec/rad.

f. Pad stiffness For the estimation of the pad stiffness, each pad was assumed to be under a condition of pure shear (Ref.19). The model of each pad, on which the estimation of its stiffness was based, is shown in Fig. 5.6a. From this figure one can see that

$$\tau = G\gamma = G \frac{u}{h}$$

$$\text{from which } k = G \frac{ab}{h} \quad (5.71)$$

where u is the displacement of the pad in a given direction and k is the pad stiffness in this direction. The bridge under consideration has five elastomeric pads at each end. Each pad measures 0.71m x 0.36m. The shear modulus G was given a representative value of $G = 150 \text{ psi} = 105.4 \text{ t/m}$. From this value and equation 5.71, the elastic stiffness of each pad was found to be equal to 708.9 t/m. So, the total elastic pad stiffness in both directions X and Y is:

$$K_P^t = 3545 \text{ t/m} \quad (5.72)$$

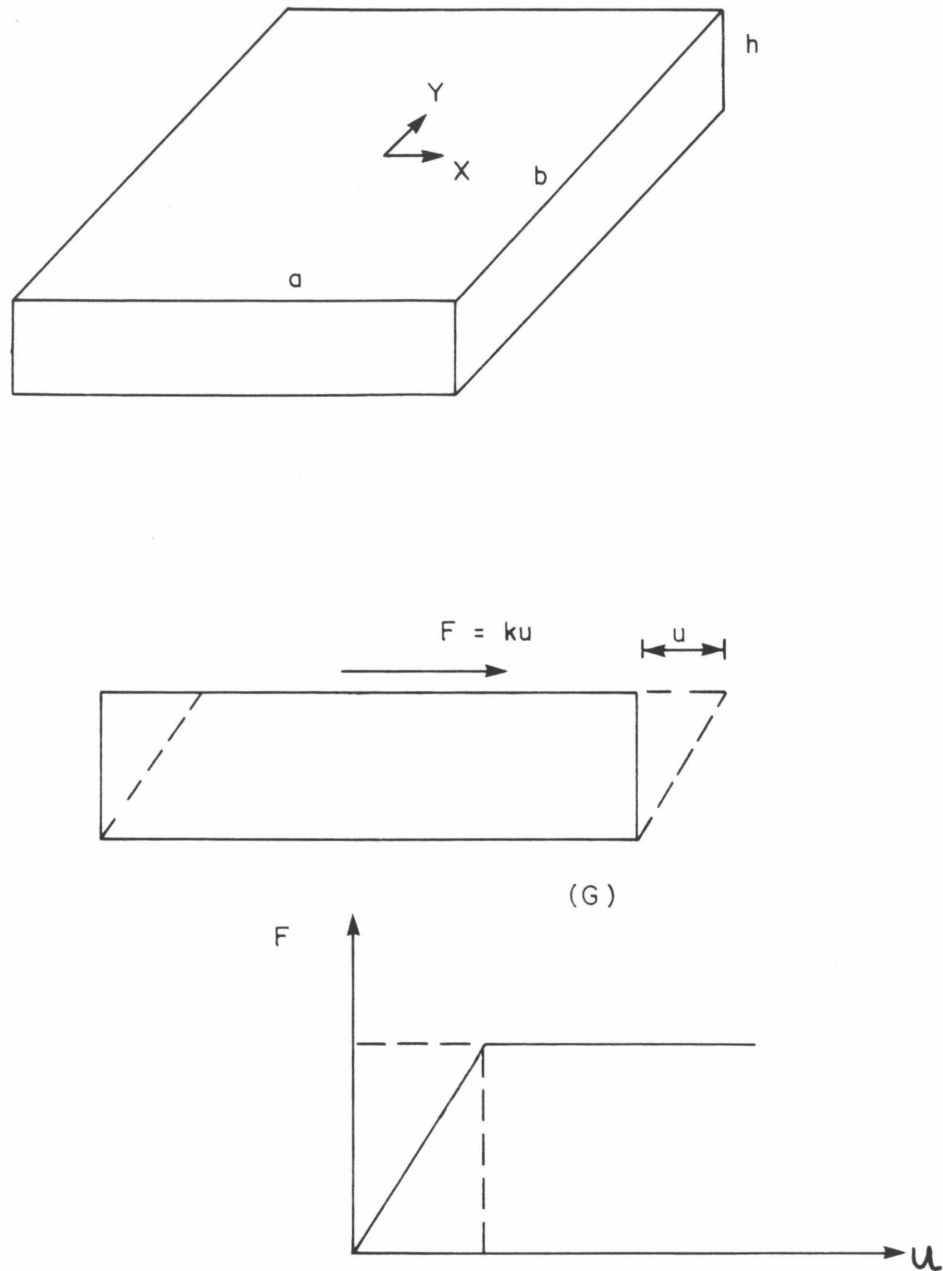


FIG. 5.6 ELASTOMERIC PAD STIFFNESS
 a. Geometry of a Single Pad
 b. Shearing Deformation of a Pad
 c. Elasto-Plastic Spring Representing Each Pad System

Each pad was assumed to behave as an elastic-perfectly plastic element. The yielding levels were approximated by assuming a friction coefficient of 0.3 (values between 0.3 - 0.5 are usually used) (Ref. 19). The dead load of the bridge deck exerted on the five pads at each end was found to be equal to 472.6t. (To find this the deck was assumed to be a continuous two span beam with supports at the end and the middle.) Thus, the force-deflection diagram for the pad system at each end in both the X and Y directions is that shown in Fig. 5.6c. When the force exerted by the bridge deck on the pads in either the X or Y directions becomes greater than 141.8t, the deck is assumed to start sliding on the pads.

5.5.2 Cases Examined

The response of the model was examined for several different input excitations and for different values of key parameters in order to illustrate the features of the model and to obtain a picture of how the response is affected by these changes. There were three principal goals of this part of the study:

(i) To examine cases in which the response of the bridge was elastic,

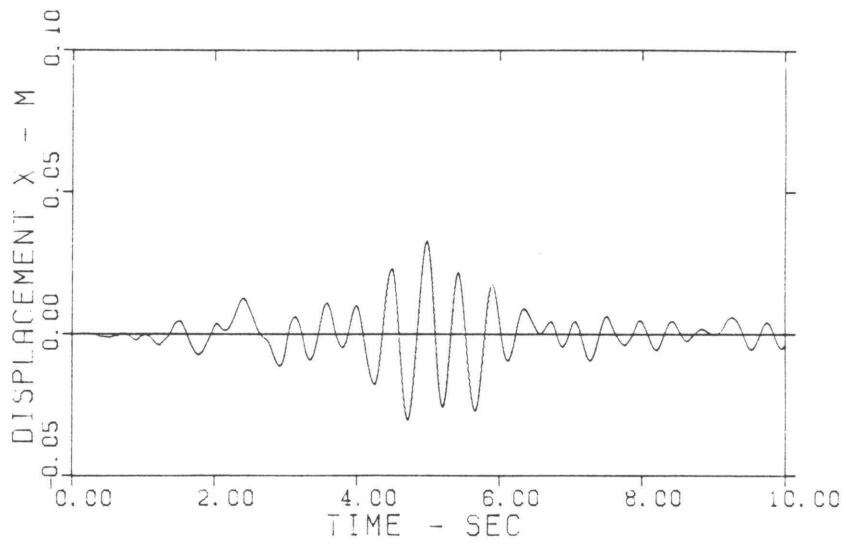
(ii) To show the ability of the model to handle cases in which structural elements of the bridge (columns, pads, abutments) yield, and

(iii) To explore the conditions under which the abutments may show significant yielding, under the yielding criterion which were adopted in chapter 4 (Section 4.3e).

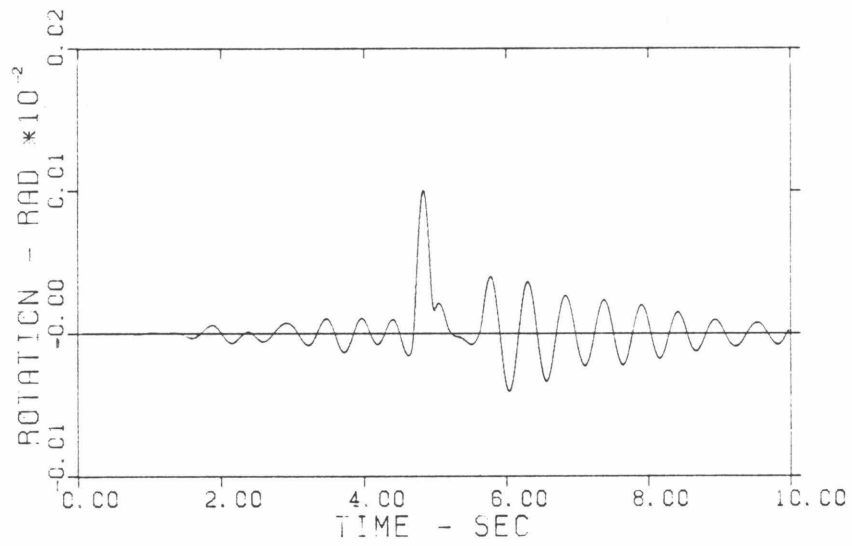
In what follows in this section, some representative cases are shown. For each case, the input excitation and the structural parameters used (if different from the ones estimated in 5.5.1) are described; and the response is presented with figures and a brief description. Only a few

calculations were performed, and the limited conclusions that can be made are included in the general conclusions and remarks presented in chapter 6.

Case 1: The model was excited along the X direction by the ten most important seconds of the record from the Imperial Valley Earthquake of October 15, 1979 (Imperial County Services Building, Free-Field Site N 02° E). The accelerogram is shown in Fig. 2.5. In the rest of this chapter, it is called Excitation 1. The parameters of the bridge are those presented in 5.5.1. As it can be seen in Figs. 5.7-5.11, the bridge responds completely in the elastic range. The weak rotational vibrations which are triggered before the impact between the deck and the abutment are a result of the slight asymmetry of the bridge. The columns are located slightly to the left of the center of mass of the deck. From Fig. 5.8a, one can see that the first impact between the deck and the abutment takes place at the left end (point 3) at about 4.7 seconds from the beginning of the excitation. The moment of the reaction force of the abutment about the center of mass of the rod induces strong rotational vibrations, the magnitude of which is substantially stronger than the magnitude of the rotational vibrations induced by the asymmetry of the bridge (see Fig. 5.7b). In Fig. 5.9 the movements of the ends of the deck in the Y direction are shown. These movements are a direct effect of the rotational vibration of the deck since no excitation in the Y direction is considered. In Figs. 5.10a and 5.10b, respectively, the force-deflection responses of the bridge columns and the elastomeric pads at the left end of the bridge are shown; while Figs. 5.11a and 5.11b show the force-deflection responses of the two abutments. These figures reveal that all the structural components of the bridge respond

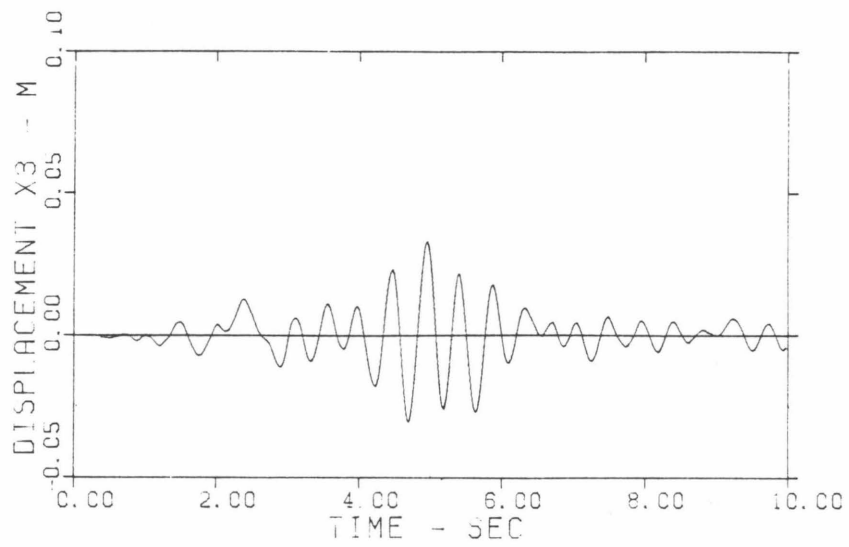


a

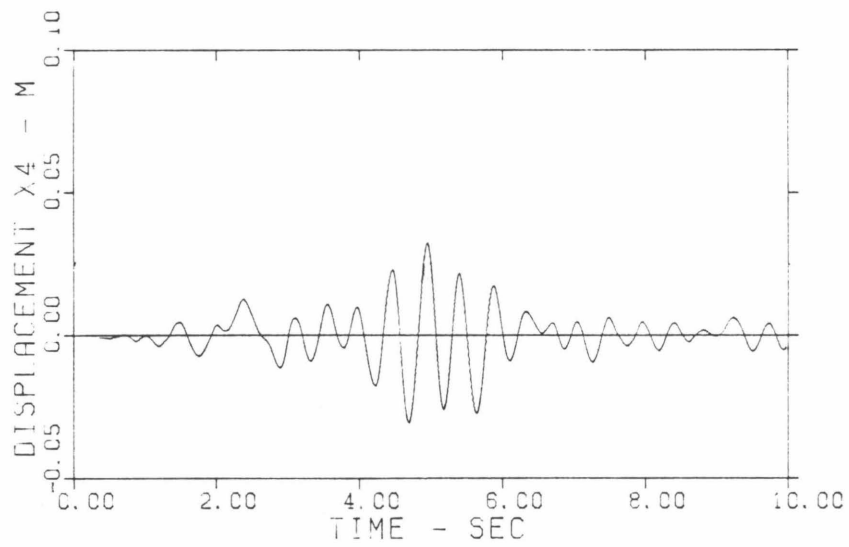


b

FIG. 5.7 CASE 1
a. Displacement in X Direction
b. Rotation



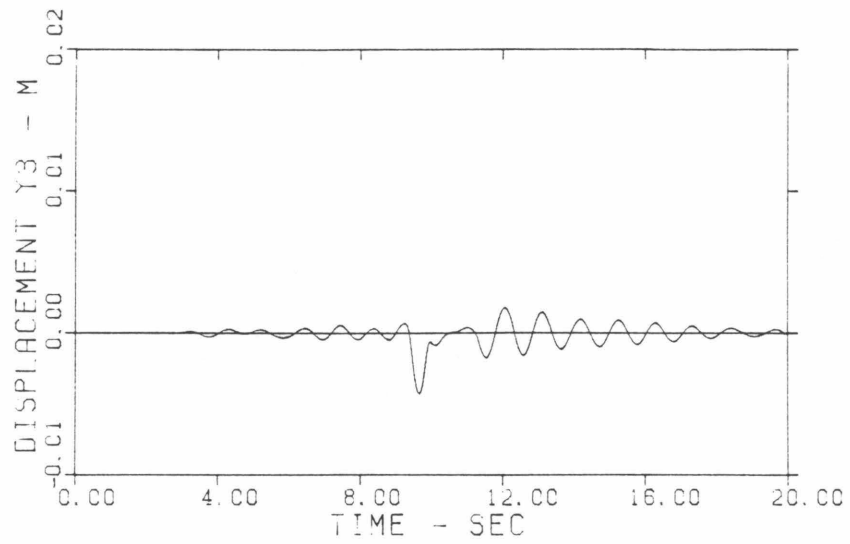
a



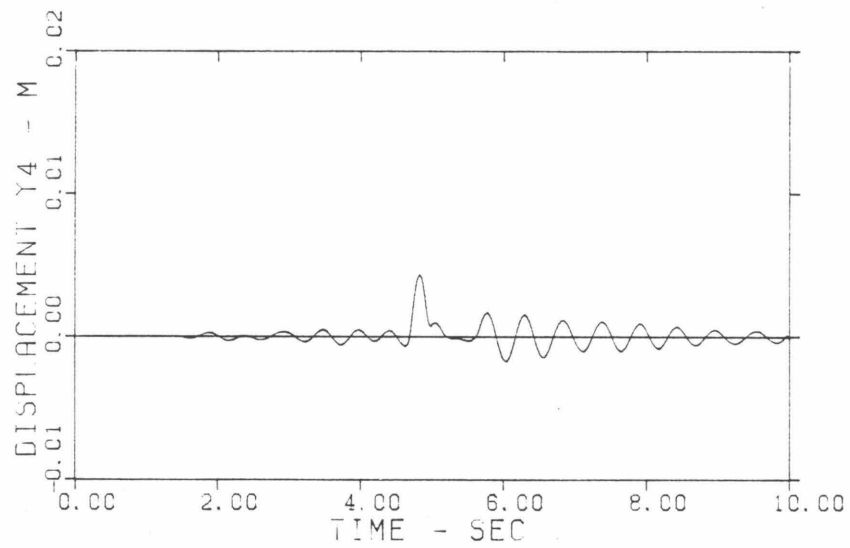
b

FIG. 5.8 CASE 1

- a. Response of Point 3 in X Direction
- b. Response of Point 4 in X Direction



a



b

FIG. 5.9 CASE 1

- a. Response of Point 3 in Y Direction
- b. Response of Point 4 in Y Direction

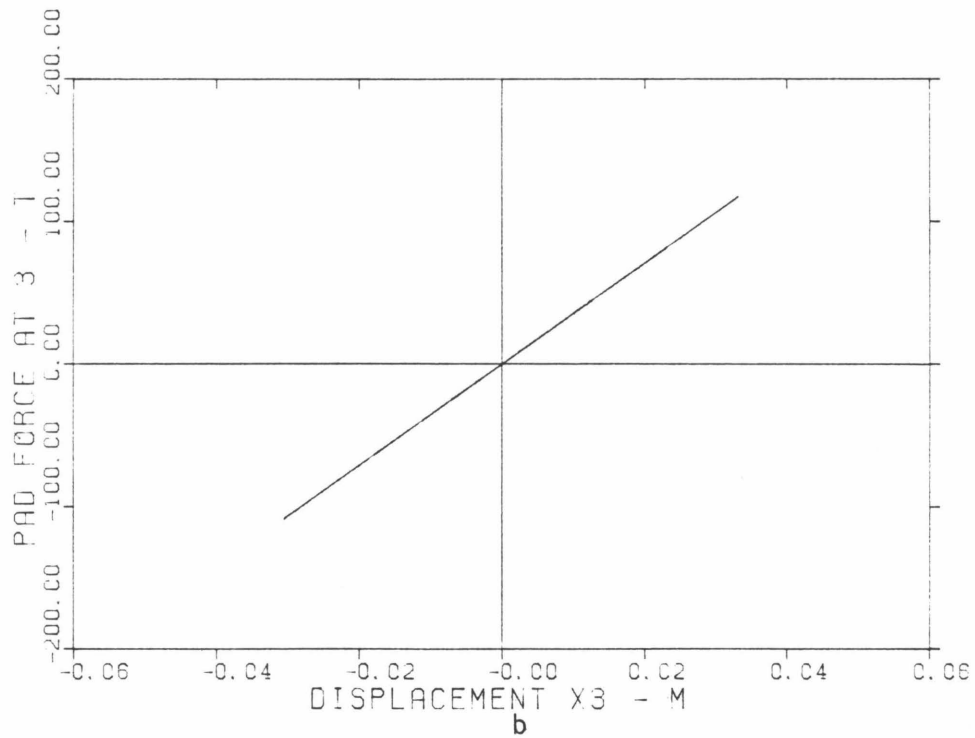
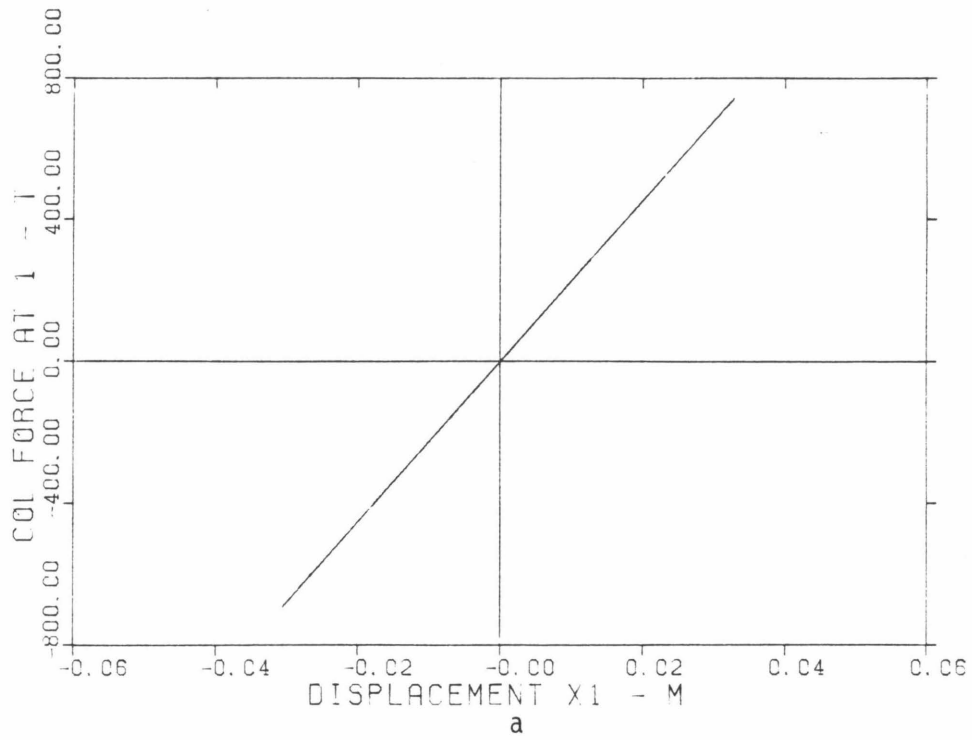


FIG. 5.10 CASE 1

- a. Column Force-Deflection Response
- b. Pad Force-Deflection Response

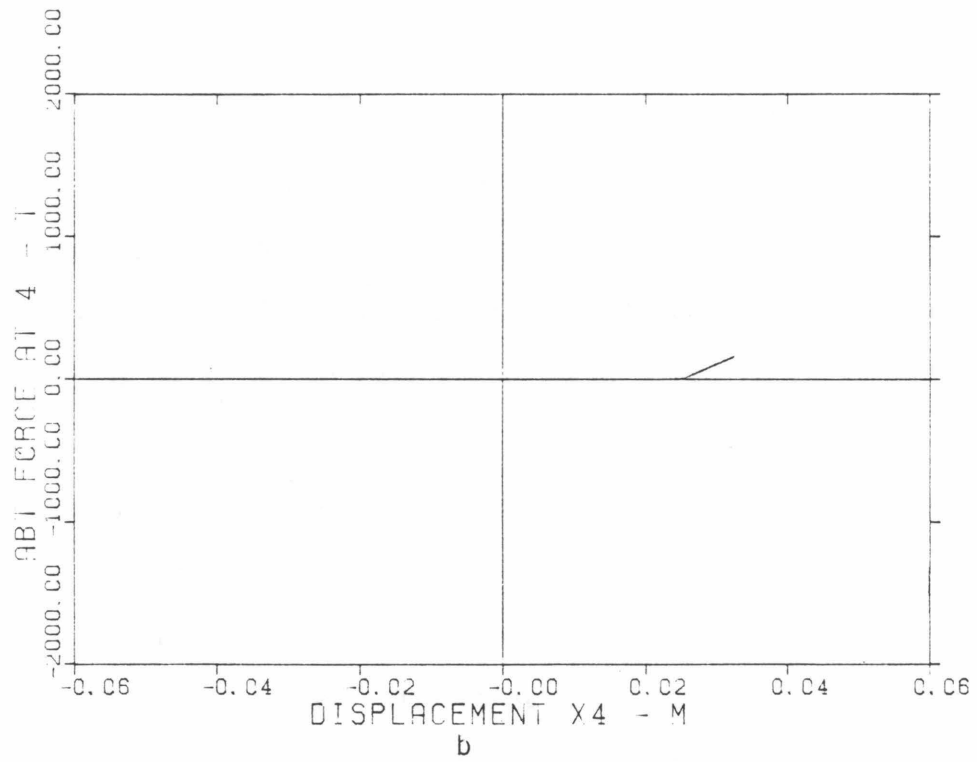
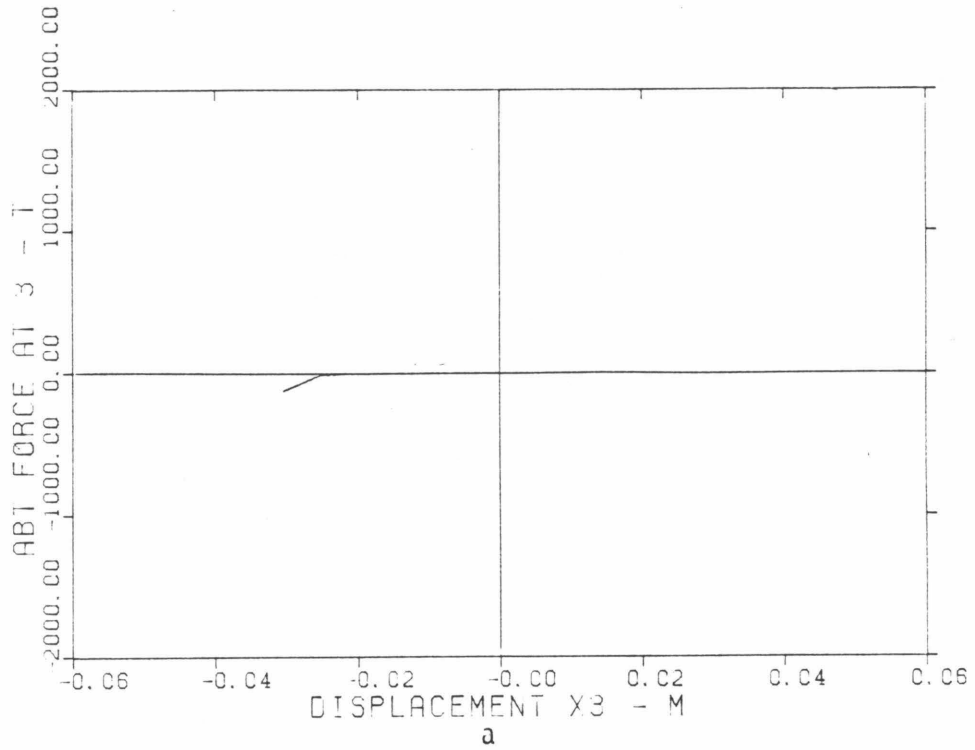


FIG. 5.11 CASE 1
 a. Force-Deflection Diagram of Abutment at Point 3
 b. Force-Deflection Diagram of Abutment at Point 3

within the elastic range and that the level of the magnitude of the abutment reaction forces is very low due to the fact that the contact between the deck and the abutments is weak.

Case 2: In this second example, the model was excited along the X direction by the twenty most important seconds of the E - W component of the Imperial Valley earthquake of May 18, 1940. The accelerogram of this motion (Excitation 2) is shown in Fig. 5.12. The response of the model is shown in Figs. 5.13-5.17. From Figs. 5.14a and 5.14b, one can see that, in this case, the first impact between the deck and the abutments occurs at the right abutment about 2.0 seconds after the beginning of the excitation. At that point, significant rotational vibrations are induced. Although the gaps are closed more often than in Case 1, the results shown in Figs. 5.13-5.17 are similar to those of Case 1. In particular, the response of the bridge remains elastic.

Case 3: Next, the model was excited along the X direction by the accelerogram of Excitation 1 scaled by a factor of 4. Scaling the record by this amount produces an extremely strong motion with peak accelerations of over 2g. Such intense shaking is not necessarily realistic but is required to excite the model into the fully nonlinear yielding range of response. The parameters of the model are those presented in 5.5.1. The response is shown in Figs. 5.18-5.21. One can see that, as expected, the vibrations of the bridge were much stronger than in Cases 1 and 2. The bridge columns significantly exceed their yield level, while significant sliding at the pads also occurs (see Fig. 5.21). Actually, yielding of the columns and the pads occurred in the cases of Excitation 1 scaled by factors of 2 and 3; but the case of scaling by 4 is presented since the yielding was more intense. The

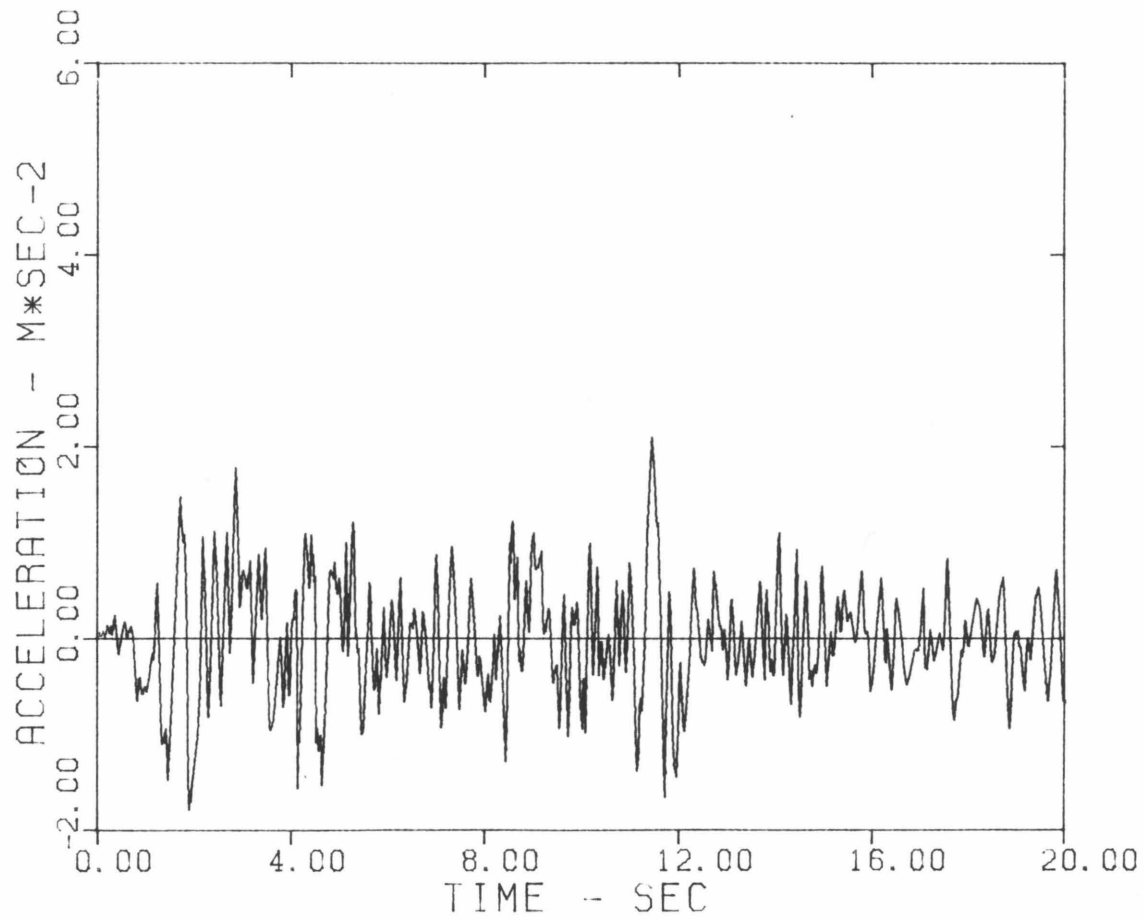
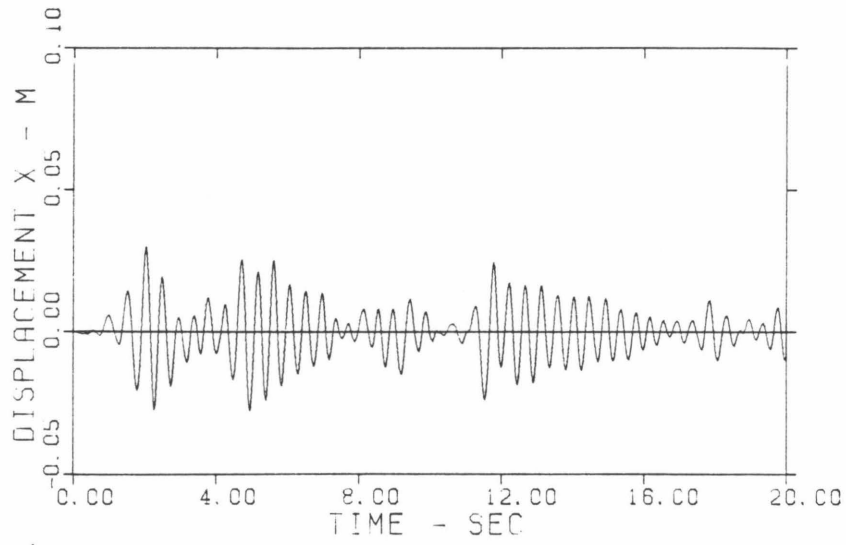
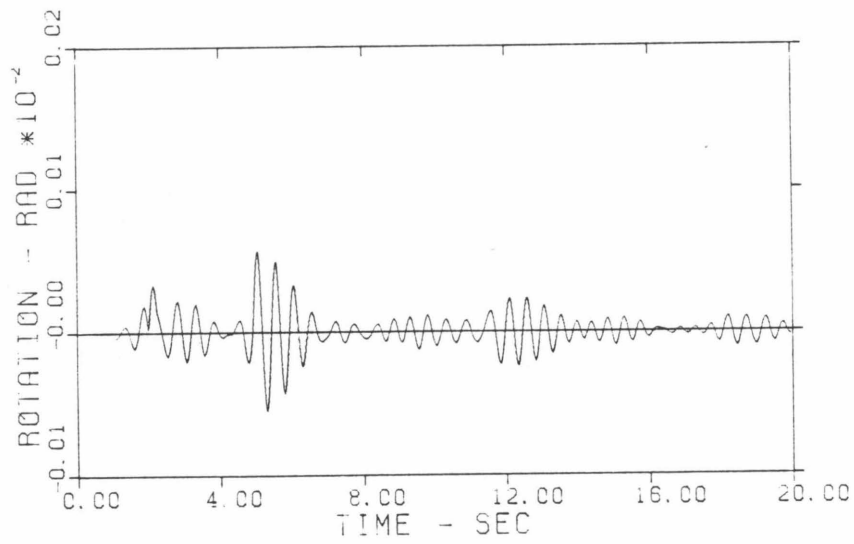


FIG. 5.12 THE TWENTY MOST IMPORTANT SECONDS OF THE IMPERIAL VALLEY EARTHQUAKE, MAY 18, 1940 (EL CENTRO SITE, S 90 W)

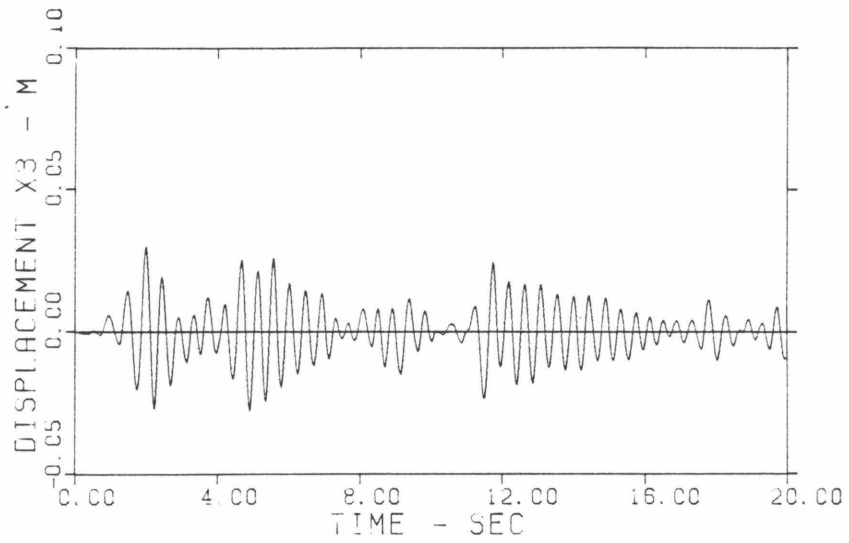


a

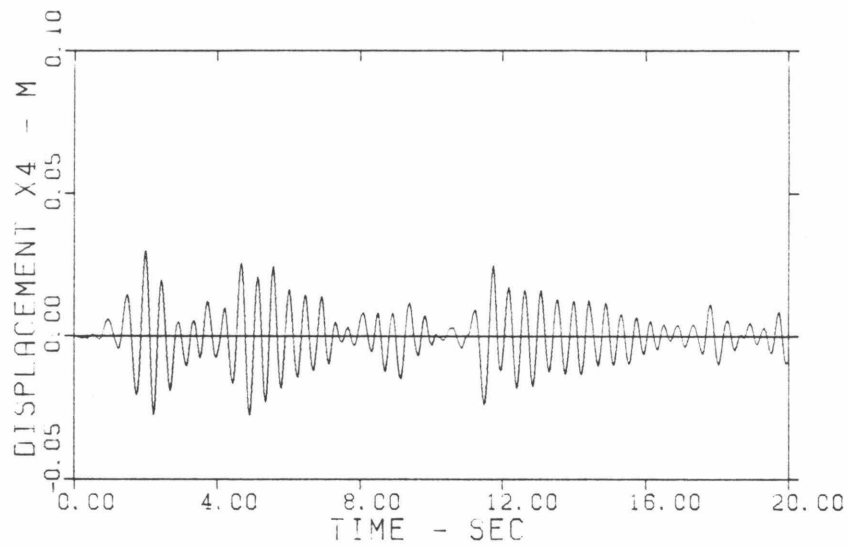


b

FIG. 5.13 CASE 2
a. Displacement in X Direction
b. Rotation



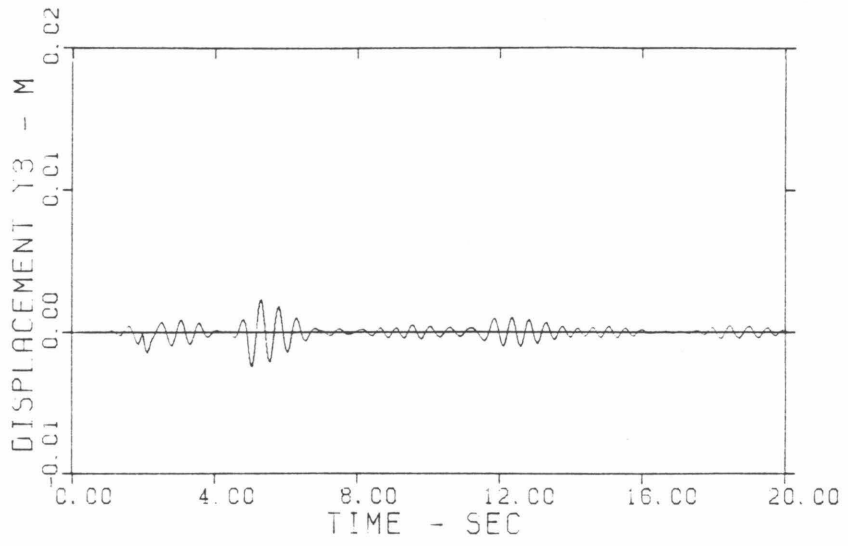
a



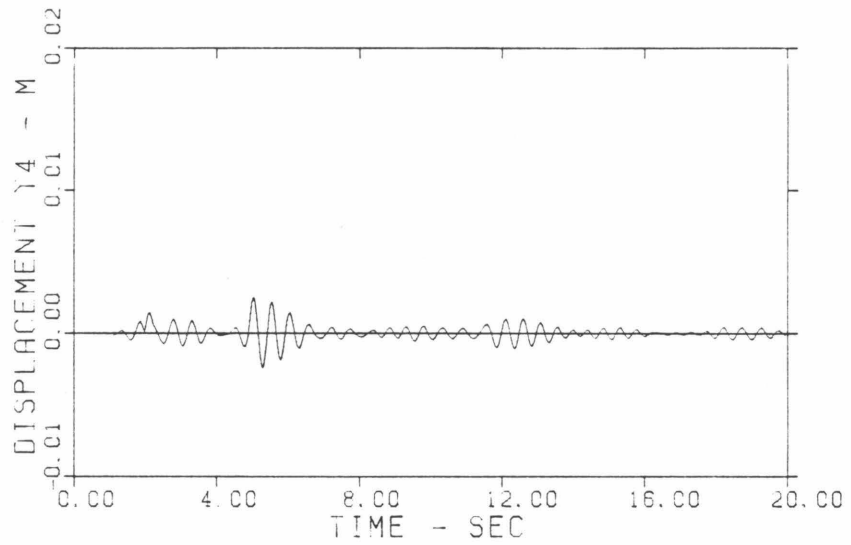
b

FIG. 5.14 CASE 2

- a. Response of Point 3 in X Direction
- b. Response of Point 4 in X Direction



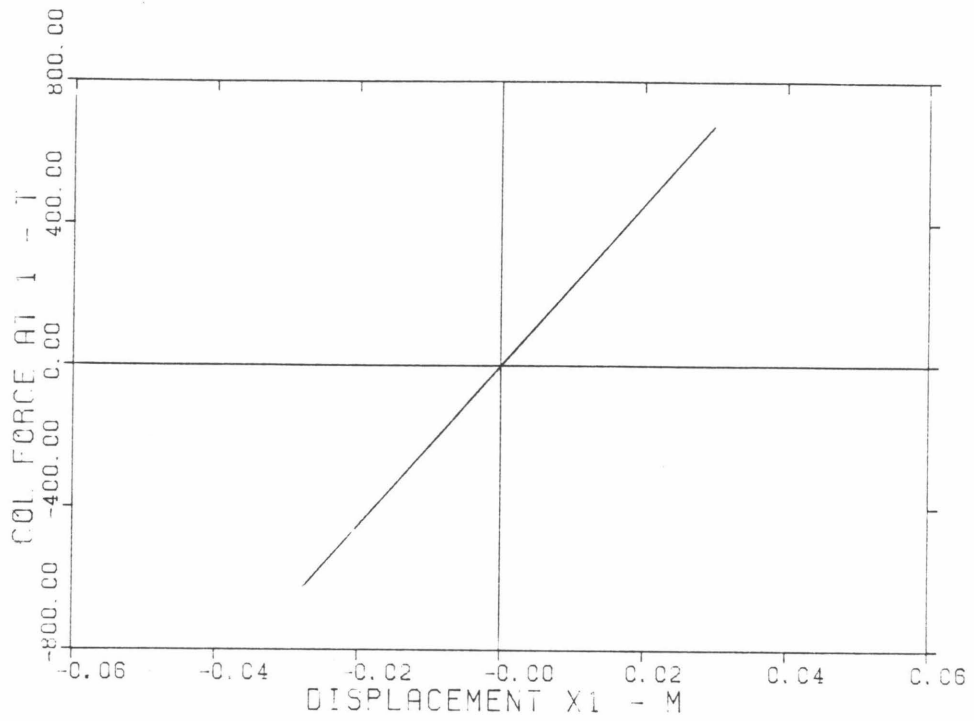
a



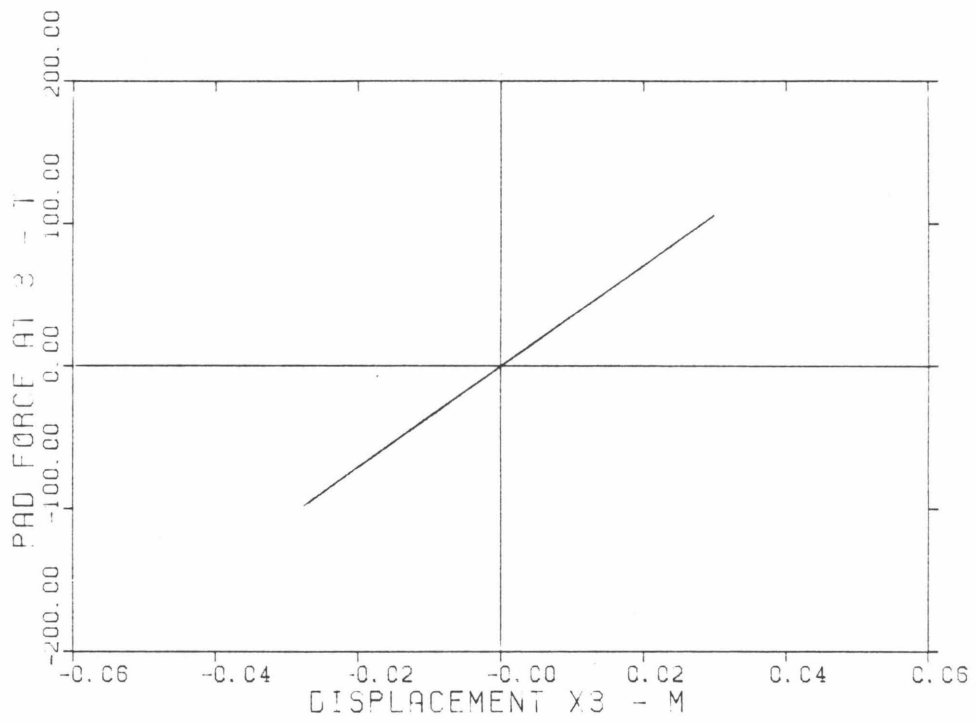
b

FIG. 5.15 CASE 2

- a. Response of Point 3 in Y Direction
- b. Response of Point 4 in Y Direction



a



b

FIG. 5.16 CASE 2

a. Column Force-Deflection Response

b. Pad Force-Deflection Response

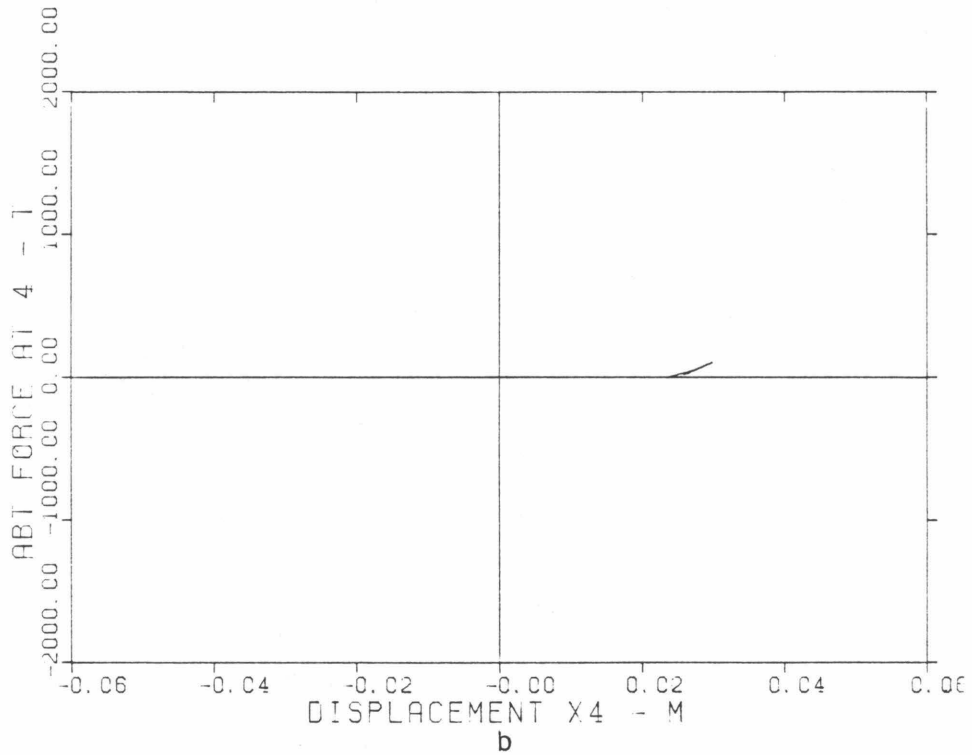
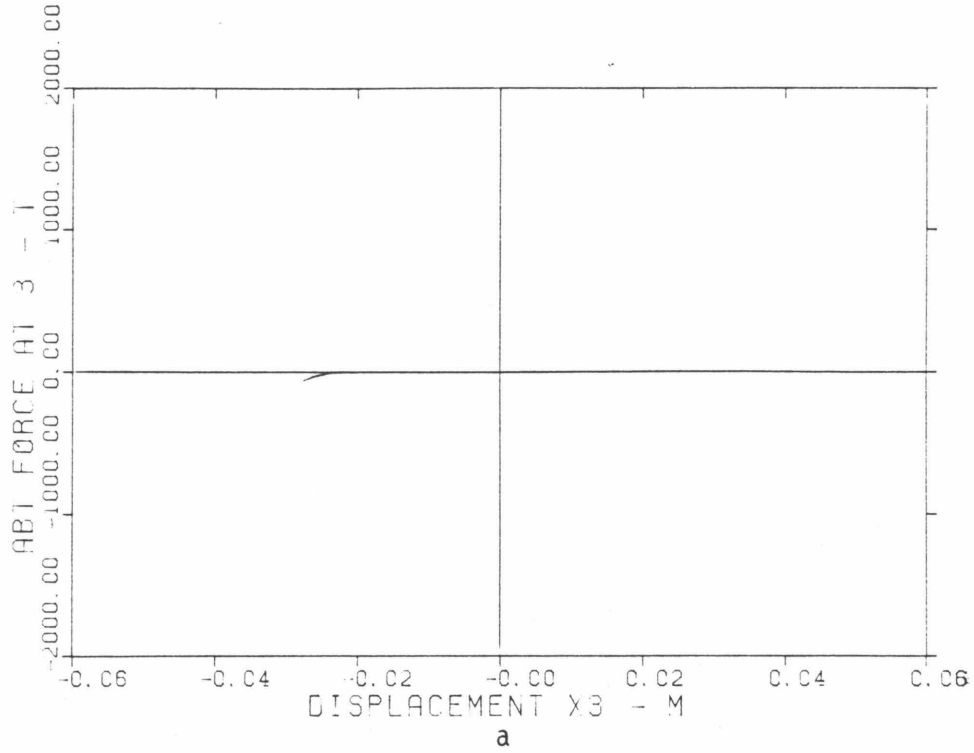
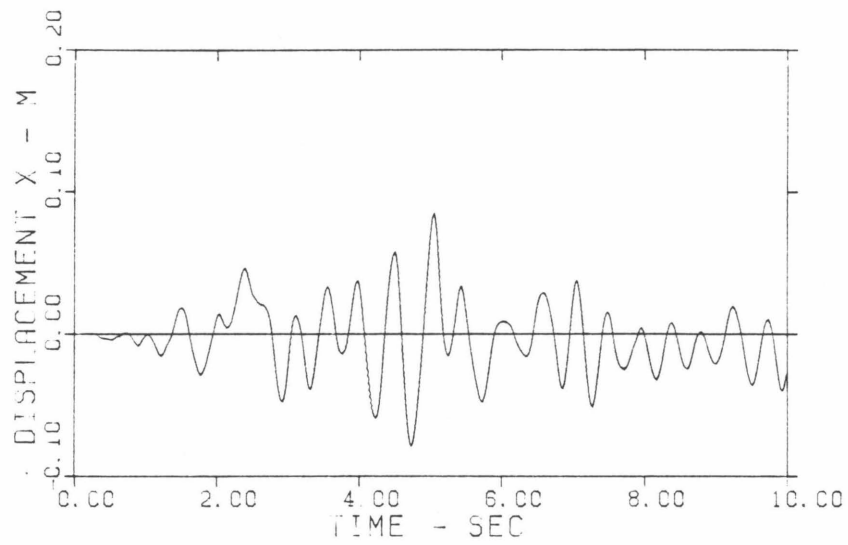
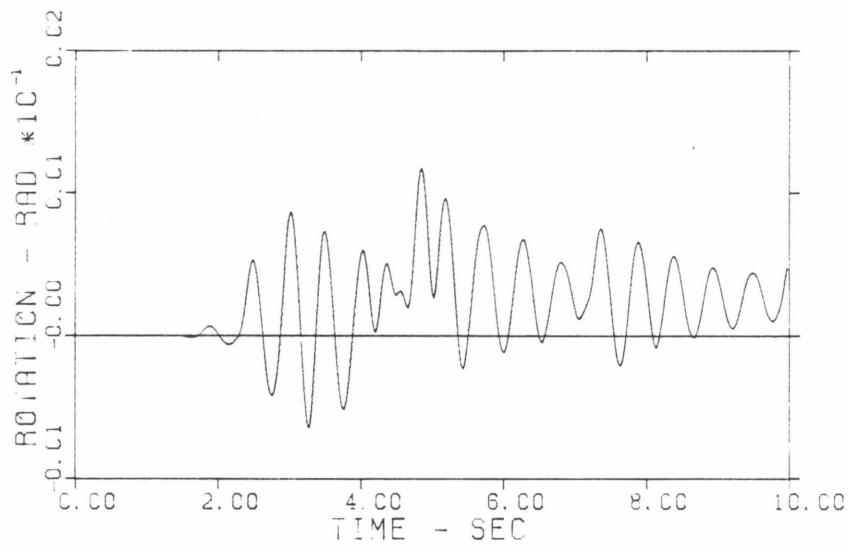


FIG. 5.17 CASE 2

- a. Force-Deflection Diagram of Abutment at Point 3
- b. Force-Deflection Diagram of Abutment at Point 3

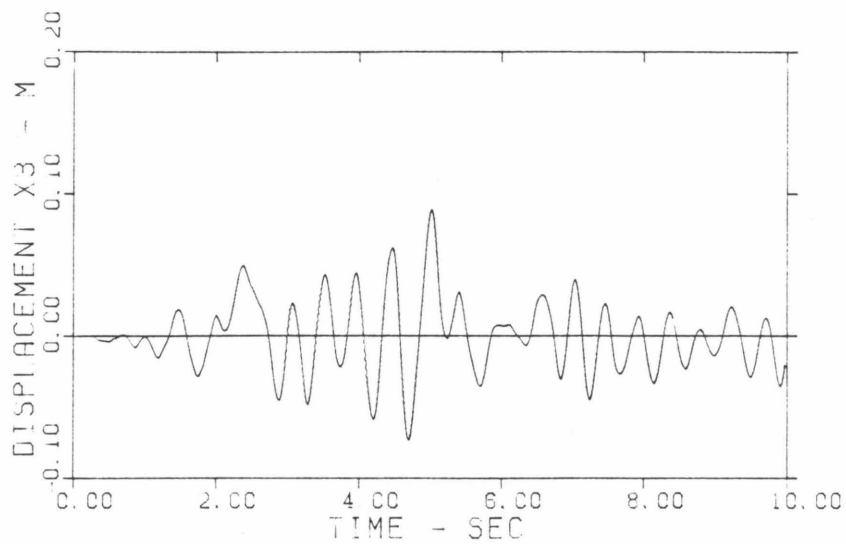


a

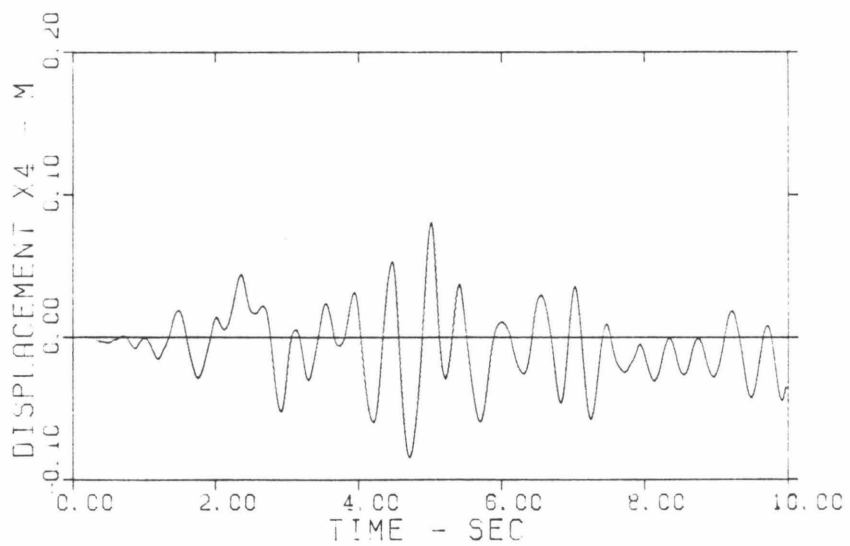


b

FIG. 5.18 CASE 3
a. Displacement in X Direction
b. Rotation



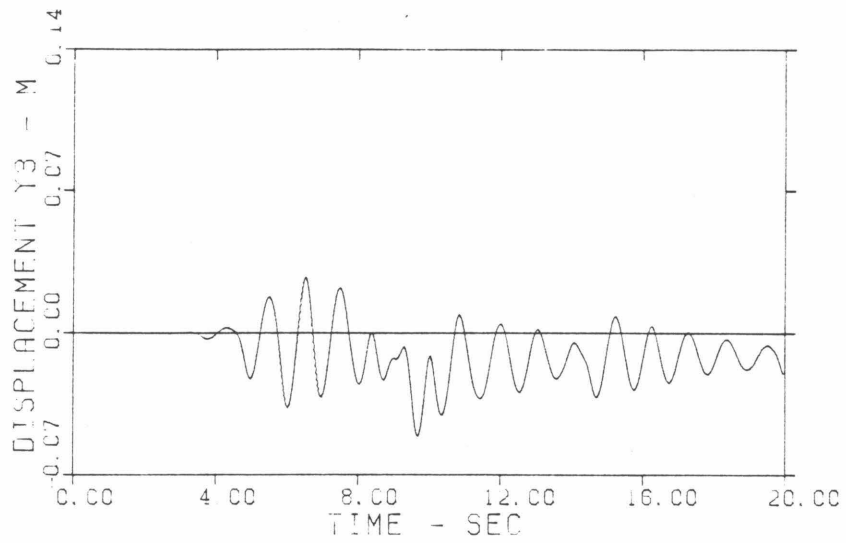
a



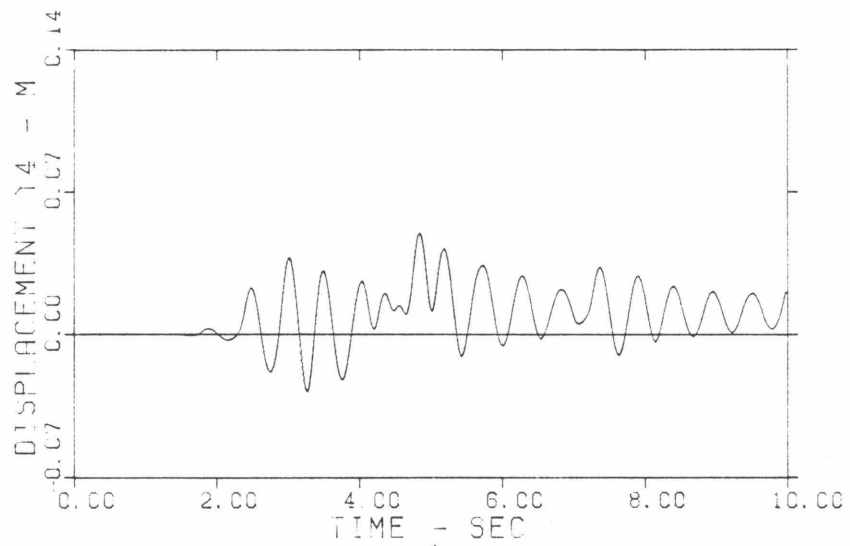
b

FIG. 5.19 CASE 3

- a. Response of Point 3 in X Direction
- b. Response of Point 4 in X Direction



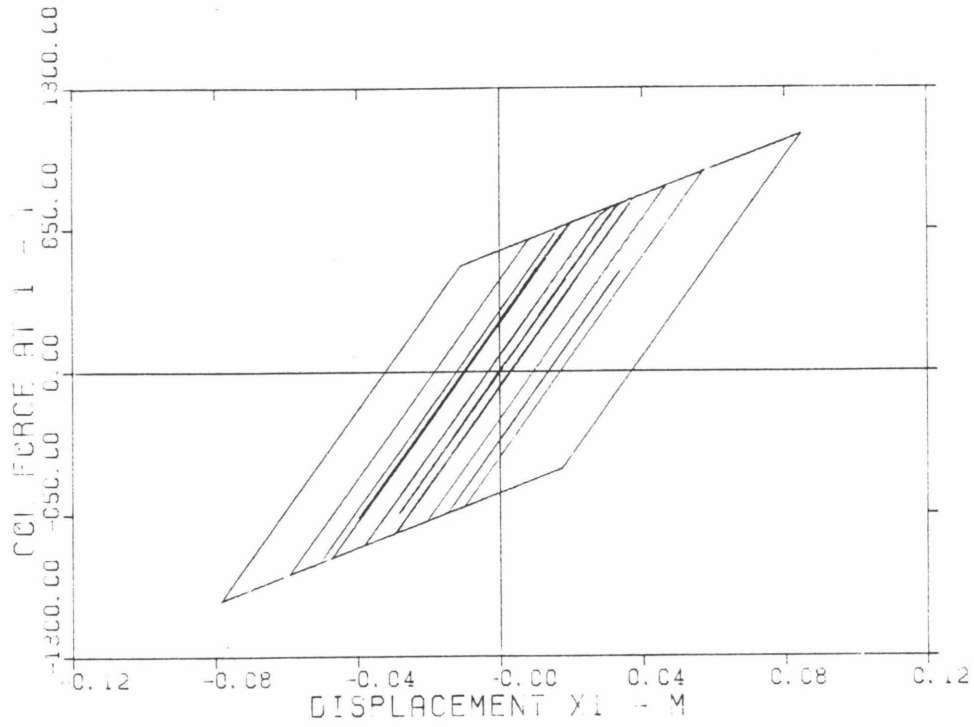
a



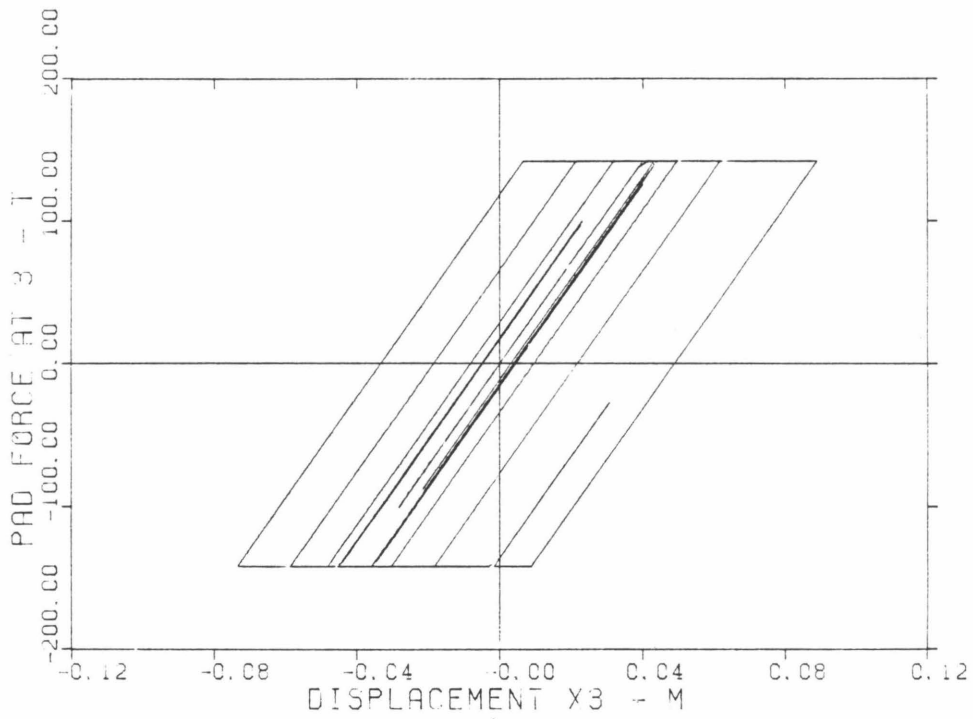
b

FIG. 5.20 CASE 3

- a. Response of Point 3 in Y Direction
- b. Response of Point 4 in Y Direction

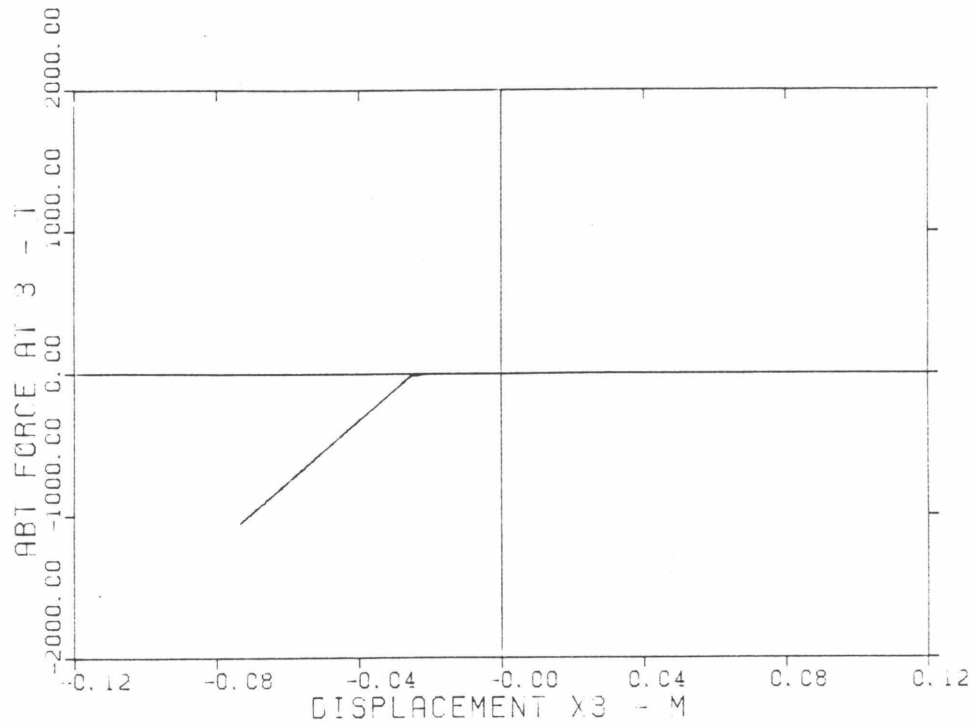


a

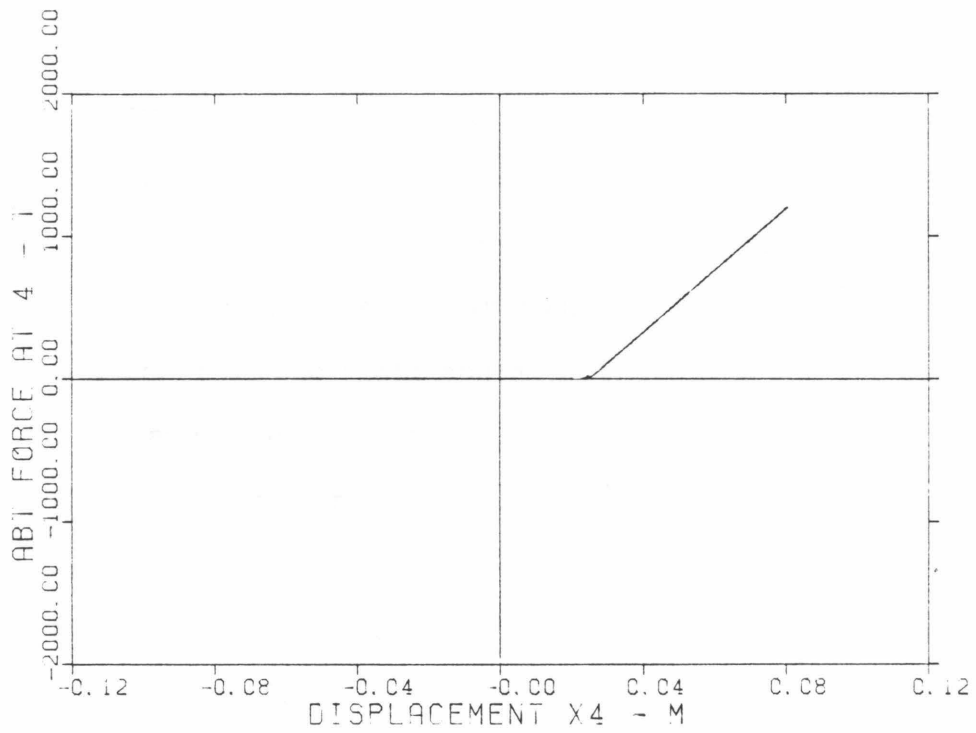


b

FIG. 5.21 CASE 3
 a. Column Force-Deflection Response
 b. Pad Force-Deflection Response



a



b

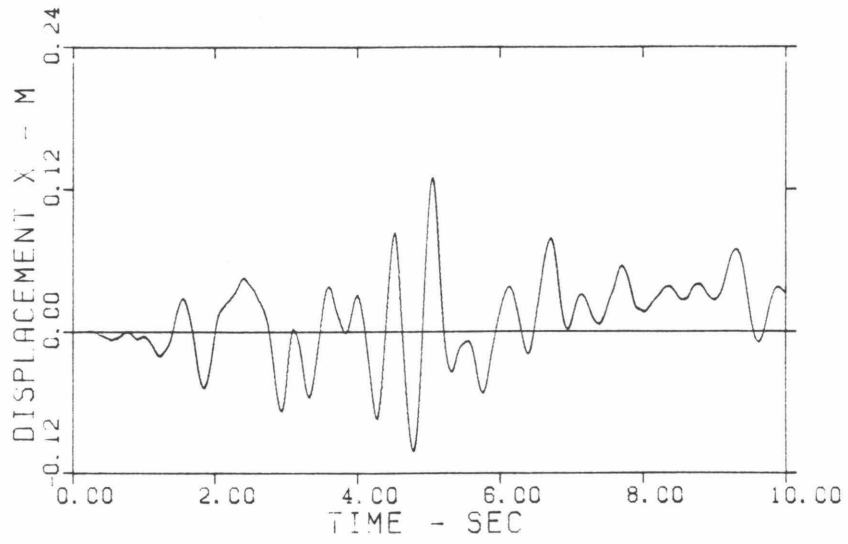
FIG. 5.22 CASE 3

- a. Force-Deflection Diagram of Abutment at Point 3
- b. Force-Deflection Diagram of Abutment at Point 3

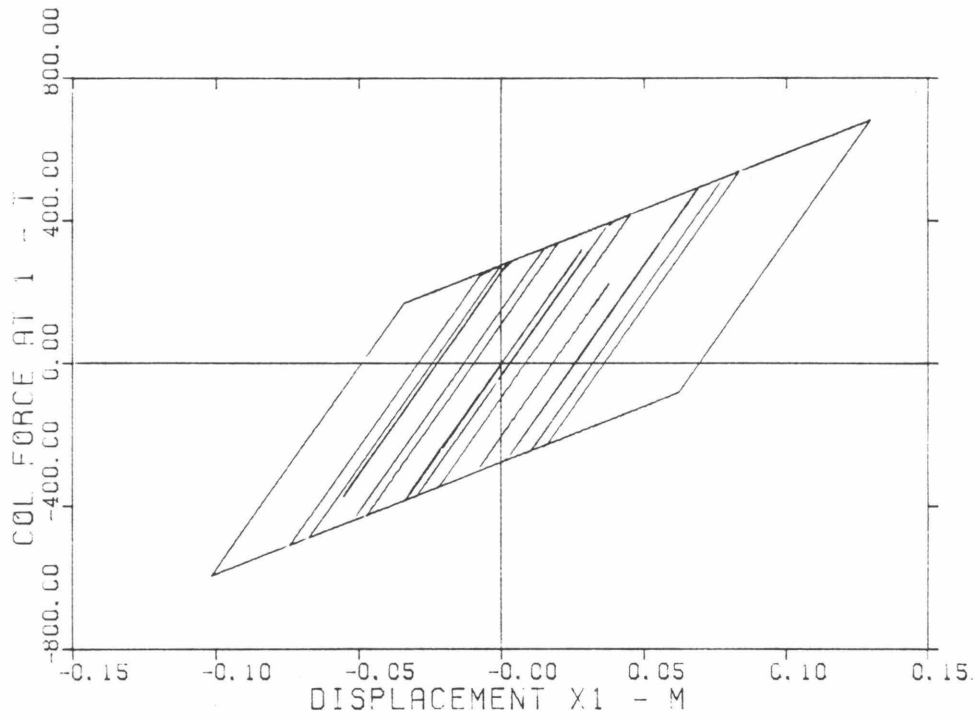
abutment force has increased significantly but still remains in the elastic range (see Fig. 5.22).

Case 4: The model was excited along the X direction by the same excitation as in Case 3. However, in this case, it was assumed that the bridge was not skew ($\theta = 0$) and that the stiffness of the columns was equal to half of the stiffness estimated in 5.5.1. The primary reason for these assumptions was to create conditions which would favor the occurrence of yielding in the soil deposits behind the abutments. By reducing the stiffness of the deck by half, its longitudinal vibrations under the same earthquake excitation become significantly larger. Also, making the initial angle of skewness equal to zero eliminates rotational vibrations which tend to reduce the movements in the longitudinal direction. Under these conditions, the impacts between the deck and the abutments will be much more intense. The response of the bridge in this case is shown in Figs. 5.23 and 5.24. The displacements along the X direction and the yielding of the columns are larger than in the previous cases, and it can be observed that the soil deposit behind the right abutment yields slightly. It should be noted that the yielding of the soil deposit at the right abutment increases the gap between the deck and the abutment. The new gap will be equal to the original gap plus the permanent set of the soil deposit.

Case 5: The only difference between Cases 4 and 5 is that in Case 5 the bridge is assumed to be without pads. (It is possible that at such a high excitation level the pads will not play a significant role.) The response is shown in Figs. 5.25 and 5.26. One can see that both abutments yield, while the displacement in the X direction becomes even greater. Yielding of the abutments also occurred at a lower



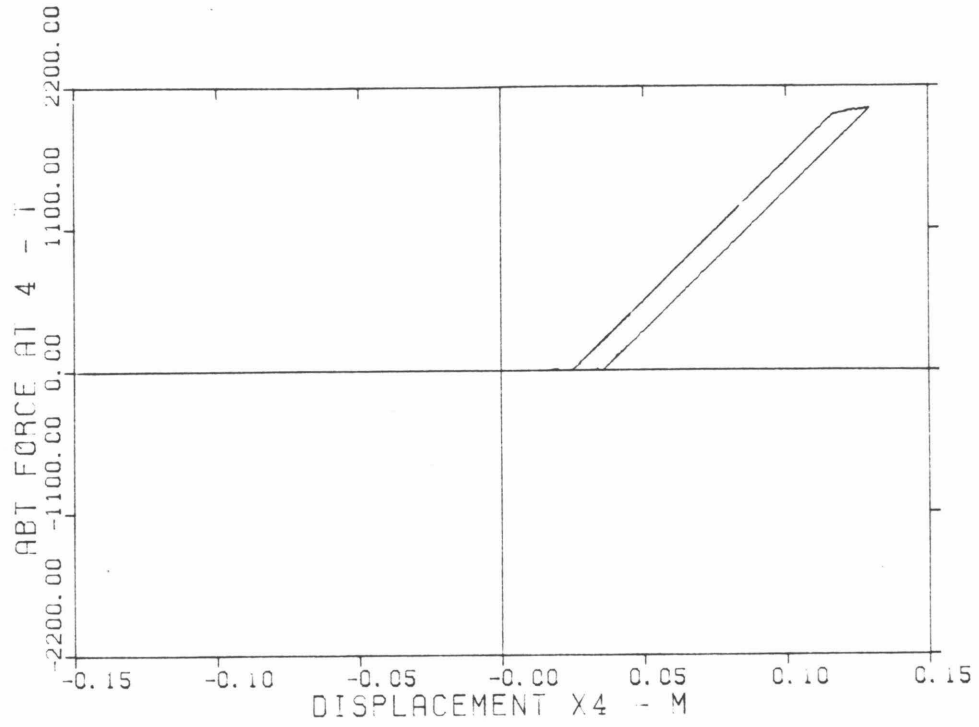
a



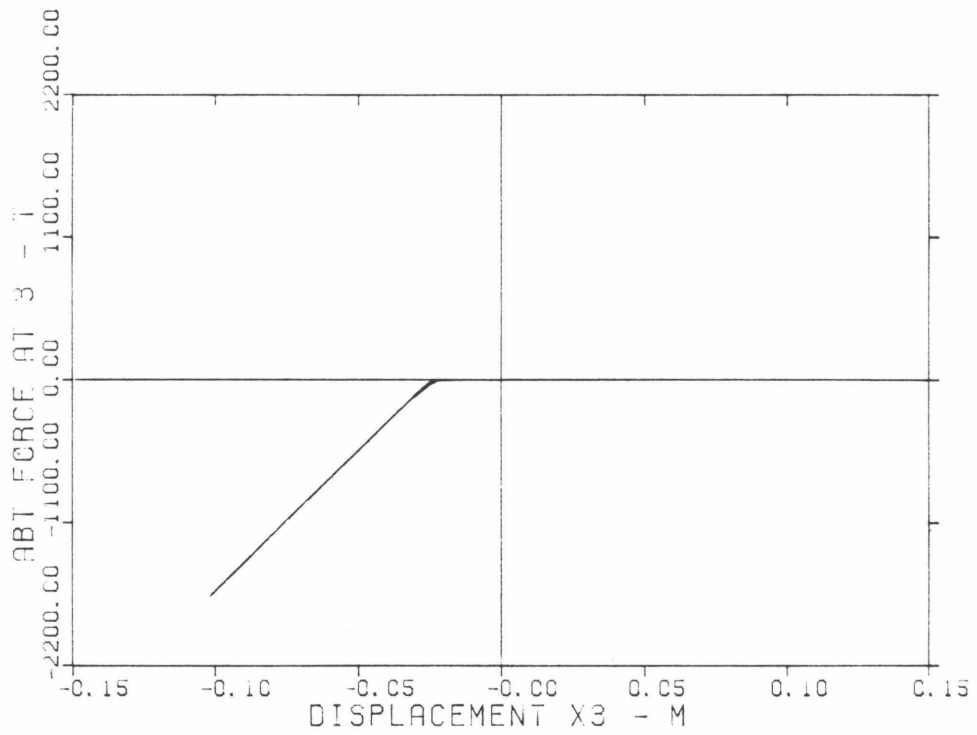
b

FIG. 5.23 CASE 4

- a. Displacement Response in X Direction
- b. Force-Deflection Diagram of the Columns

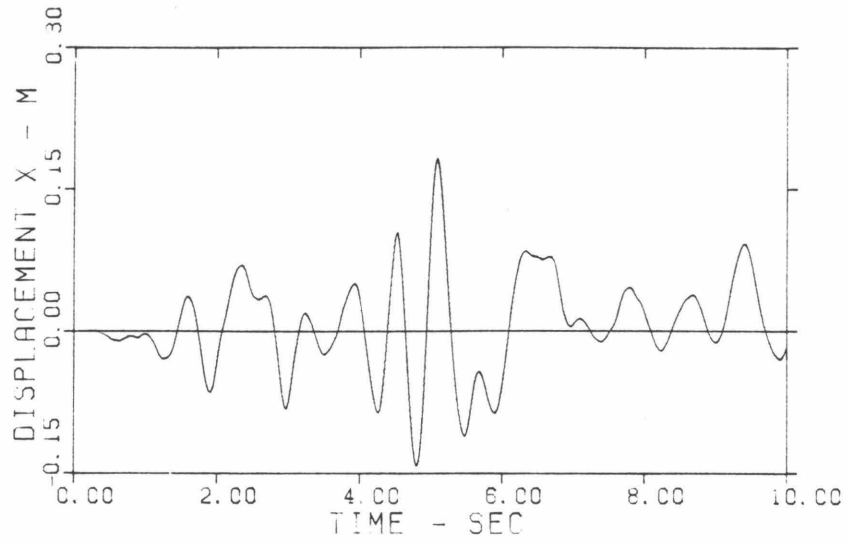


a

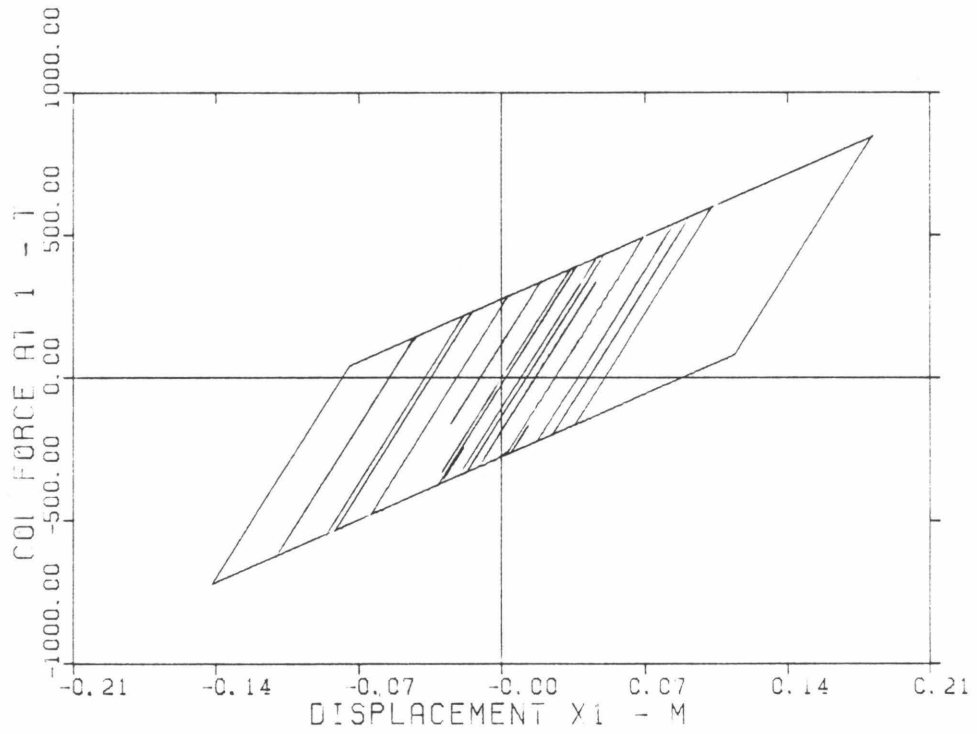


b

FIG. 5.24 CASE 4
Force-Deflection Diagrams of the Abutments



a



b

FIG. 5.25 CASE 5

- a. Displacement Response in X Direction
- b. Force-Deflection Diagram of the Columns

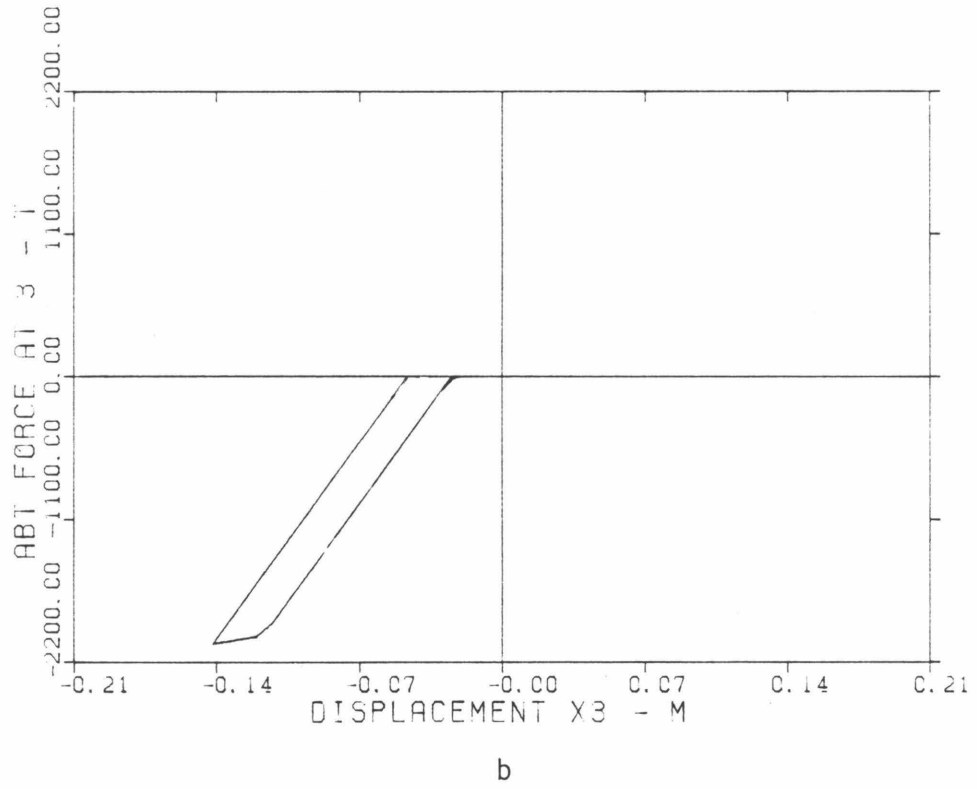
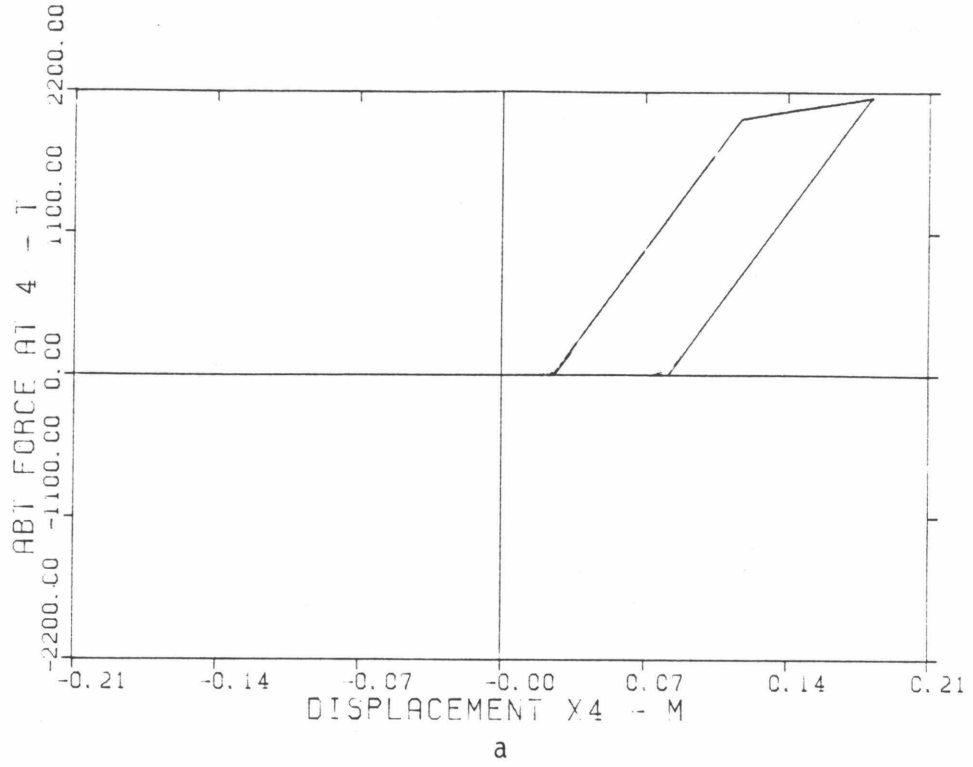


FIG. 5.26 CASE 5
Force-Deflection Diagrams of the Abutments

excitation level (Excitation 1 scaled by 3) when the bridge was assumed straight and the pads were not present.

Finally, to check the capability of the model to handle simultaneous excitations along the X and Y directions, cases of concurrent earthquake excitations were examined. From the results, it was concluded that the computer programs were found to be working effectively in this case. However, the response is not presented and discussed because excitation along the Y direction induces significant displacements of the bridge columns in the Y direction making the assumption of independence between the bending of the columns about the X and Y-axes unrealistic.

CHAPTER 6

SUMMARY AND CONCLUSIONS

This study investigates the effects of the rigid body motions of the deck of short-span skew bridges focusing on the mechanism that causes in-plane rotational vibrations of the deck during strong earthquake motion. A study of the damage to bridges during earthquakes, particularly the San Fernando event of February 9, 1971, reveals the triggering of rigid body rotations of the bridge deck as a result of the interaction between the deck and the abutments. In many cases, this kind of behavior caused permanent rotation with attendant damage to the bridge columns and abutments. Some examples of bridges which experienced this type of damage are described in Chapter 1 following a brief description of the history of the seismic response of highway bridges.

As a first approach to the problem, a simple bridge model is proposed in Chapter 2. In this model, the deck is represented as a rigid rod skewed at an angle θ with respect to the horizontal direction and restricted by linearly elastic columns and abutment springs. The abutments are located at a distance a from the ends of the rod, which represents the gap usually present for thermal expansion of the deck. The basic conclusion of Chapter 2 is that the simple model examined is capable of illustrating the basic features of the kinematics of planar rigid body rotation of the decks of skew bridges, including the interaction between the deck and the abutment, and can, therefore, be used as a basis for more detailed modeling of the response of skew bridges. The examination of the effects of the parameters on the response of the simple model presented in Chapter 2 reveals that a

reasonably accurate estimation of the abutment and the column stiffnesses will be important for a more realistic, and necessarily more complicated, model.

Chapter 3 presents methods for the estimation of the elastic stiffness of a bridge column with a parabolic flare including the effects of translational and rotational compliance of the base. This type of column is frequently used in the design of bridges. Although such accuracy is not required for the principal purposes of the present study, an exact method (according to the Euler-Bernoulli beam theory) is presented for the determination of the column stiffness. This result could be useful in other problems in which a more accurate estimation of the stiffness of this type of column is necessary. Additionally, an approximate method for the estimation of the stiffness is presented; it can be used with columns of any type of geometry. The chapter concludes with an example in which the stiffnesses of the columns of the Nichols Road Overcrossing (Bridge No. 56-725 near Riverside, California) in the two directions of bending is estimated by both methods. Also, the complete force-deflection diagram is constructed for each direction.

In Chapter 4, a method for the estimation of the force-deflection relation of the abutments is presented. The abutments are represented as rigid blocks bearing against linearly elastic, Winkler-type soil springs with moduli varying linearly with depth. For the examination of the yielding of the soil, a global yielding criterion based on the Rankine Theory of active thrust and passive resistance is adopted. The problem is also solved for the case of discrete foundation springs; this approach is more general in the sense that it can handle arbitrary variations of the effective modulus of the soil. Finally, at the end of

the chapter, an example is solved in which the abutments of the Nichols Road Overcrossing are examined.

In Chapter 5, a more detailed model for the rigid body motions of the deck of skew bridges is proposed. This model has three degrees of freedom (displacements in the X and Y directions, rigid body in-plane rotation, and other resisting mechanisms are taken into account) in addition to the translational resistance of the columns and abutments. These mechanisms include the rotational resistance of columns, the effects of the elastomeric pads, and viscous damping. Furthermore, the model is capable of approximating the nonlinear yielding behavior of the columns, pads, and abutments. It should be noted that the model itself and the computer program which solves the three second order coupled differential equations of motion are presented in a general form so that they can accommodate any form of the force-deflection relationship of the columns, pads, and abutments. To achieve this, the resisting force of each of the above mechanisms in the direction of a displacement r is represented by the general formula:

$$F(r) = k(r)r$$

where $k(r)$ is the generalized stiffness. In this particular study, simple bilinear hysteretic or elasto-plastic force-deflection relations are employed for the columns, pads, and abutments.

At the end of Chapter 5, an example of response is given in which the values of the model parameters are assigned based on the properties of the Nichols Road Overcrossing. Different input excitations and different values of key parameters are examined in order to show the capabilities of the model and gain insight into the response of this particular bridge. From the response of the model in these cases,

presented in section 5.5.2, one can draw the following conclusions and general remarks.

a. As expected, the planar rigid body rotations of the deck are induced primarily as a result of the skewness of the deck and the impact between the deck and the abutment. Thus, after the closure of either of the gaps between the ends of the deck and the abutments, impact forces are created; the moment of these forces about the center of mass of the deck induces rotational vibrations and couples the equations of motion. Minor rotational vibrations can also be induced by the non-symmetric position of the columns with respect to the center of mass of the deck.

b. The impact between the deck and the abutments is dominated by the excitations and response in the X direction. The model, though, can handle the general case in which each abutment is represented by gaps and springs in two directions (see Fig. 5.1.c) so that the impact between the deck and the wing walls resulting from the motion of the ends in the Y direction could also be investigated. However, it is believed that this type of interaction between the deck and the wing walls will not be very important for the rotational motion of the bridge deck for two reasons.

(i) The gap in the Y direction is usually large and so it is less likely to close.

(ii) Even if it does close, the reaction of the wing wall appears, from in-field observations, to be small compared to rotational forces in the X direction. So, although the impact can result in wing wall damage (see below), it will not contribute significantly to restraining the deck motion.

c. Due to the rotation of the deck, significant displacements of

its ends in the Y direction occur, which explains some of the damage to skew bridges after the San Fernando earthquake (displacement of superstructures at the abutments in the transverse direction, falling of superstructure from elastomeric pads, and damaged wing walls). These displacements are, of course, magnified by excitation in the transverse direction, which indicates that mechanisms resisting the movement of the deck in the transverse direction are necessary.

d. All the structural components of the bridge examined seem to behave in the elastic range in cases 1 and 2 (see section 5.5.2). However, under the intense ground motions of case 3, the columns and the pads show significant yielding caused primarily by the longitudinal motion. It should also be mentioned that, although in this study the torsional resistance of the columns was assumed to be elastic, extensive rotation of the deck could cause significant shear failures to the columns. This problem needs further investigation.

e. The contribution of the abutments to the response of the deck seems to be very important for the following reasons.

(i) It is the impact between the deck and the abutments that causes the rotation of the deck.

(ii) The approximate method of the estimation of the abutment stiffness presented in Chapter 4 reveals that the abutments contribute significantly to resisting the longitudinal motions of the bridge. For the example studied, the comparatively stiff soil produced estimated abutment stiffness twice that of the individual columns. So, one can easily see that the abutment restraint is predominant for the longitudinal vibrations of the deck especially in the case of stiff soils. This point deserves special attention because a more detailed

investigation could lead to an appropriate lowering of the seismic design loading for small bridges where structural restraint is dominated by the abutments.

As items of further research on this topic, it is recommended that the contribution of the abutment mass, which is neglected in this investigation, be considered along with more detailed examination of the resistance of abutments. Specifically, it is suggested that research be undertaken to determine accurate force-deflection and energy dissipation characteristics under cyclic loading for various representative abutment types. An understanding of this complicated problem will contribute significantly to the general understanding of the seismic response of bridges.

It is also suggested that further investigation be made to model more accurately the impact between the bridge deck and the abutments. In this thesis, it was assumed that the contact is concentrated at one point (the middle of the bridge deck); however, this approximation might not be sufficient for a detailed modeling of skew bridges since, in actuality, the point of contact between the deck and the abutment is changing, which indicates that the width of the deck might be a factor for its in-plane rotational vibration.

f. Yielding of the abutments, as examined in this study, is based on a global yielding criterion and only occurred when the deck pushed sufficiently hard against the abutment. In the example, yielding of the abutments required not only a very strong excitation in the X direction but also simultaneous reduction of the values of the column or pad stiffness. Only then, did the deck move enough to push the abutment to the yielding point (see cases 4 and 5 in section 5.5.2).

Therefore, under realistic assumptions about the strength of shaking and the strength of the various elements, it is not expected that the abutment soils will yield for this type of bridge. It should also be noted that the yielding criterion used prevents this model from explaining the local yielding (cracks at the soil) which is commonly observed after earthquakes. It is believed that modeling this phenomenon would require a more detailed model of the soil-abutment system.

Finally, based on the conclusions and remarks of this investigation, a detailed instrumentation of small skew bridges is suggested in order to acquire the experimental data required for a more detailed investigation of the rigid body rotational vibrations which are induced by the impact of the deck with the abutments. Bridges with simple geometry, like the one examined in Chapter 5, are particularly recommended for an appropriate instrumentation. For this particular bridge, such an instrumentation should include the installation of at least three pairs of accelerometers: one at the middle of the bridge and one at each end. This location of accelerometers could provide recordings of the motions of the bridge deck at the middle and the two ends along the two directions, X and Y. Based on these recordings, the rotation of the bridge deck would be confirmed and investigated experimentally.

REFERENCES

1. Penzien, J., Iwasaki, T. and Clough, R., "Literature Survey-Seismic Effects on Highway Bridges" Report EERC 72-11, Earthquake Engineering Research Center, University of California, Berkeley, CA, November 1972.
2. Imbsen, R.A., Nutt, R.V., and Penzien, J., "Seismic Response of Bridges-Case Studies," Report No. UCB/EERC-78/14, Earthquake Engineering Research Center, University of California, Berkeley, CA, June 1978.
3. Gates, J.H., "Factors Considered in the Development of the California Seismic Design Criteria for Bridges," Applied Technology Council Workshop on the Research Needs of Seismic Problems Related to Bridges, January 1979.
4. Sharpe, R.L., Mayes, R.L., "Development of Highway Bridge Seismic Design Criteria for the United States," Applied Technology Council Workshop on the Research Needs of Seismic Problems Related to Bridges, January 1979.
5. Jennings, P.C., (Ed.) "Engineering Features of the San Fernando Earthquake," EERL 71-02, Caltech, Pasadena, CA, June 1971.
6. Wood, J.H., and Jennings, P.C., "Damage to Freeway Structures in the San Fernando Earthquake," Bulletin of the New Zealand Society for Earthquake Engineering, Vol. 4, No. 3, December 1971, pp. 347-376.
7. Lew, H.S., Leyendecker, E.V., and Dijkers, R.D., "Engineering Aspects of the 1971 San Fernando Earthquake," U.S. Department of Commerce, Building Science Series 40, December 1971.
8. Ghobarah, A.A. and Tso, W.K., "Seismic Analysis of Skewed Highway Bridges with Intermediate Supports," Earthquake Engineering and Structural Dynamics, Vol. 2, , 1974, pp. 235-248.
9. Elliott, A.L. and Nagai, I., "Earthquake Damage to Freeway Bridges" U.S. Department of Commerce, 1973 Report on the San Fernando, California Earthquake of February 9, 1971, Vol. II, 1973.
10. Fung, G. et al., "Field Investigation of Bridge Damage in San Fernando Earthquake," Bridge Department, Division of Highways, California Department of Transportation, Sacramento, CA, 1971.
11. Cooper, J.D., "Bridge and Highway Damage Resulting from the 1976 Guatemala Earthquake."
12. Elms, D.G. and Martin, G.R., "Factors Involved in the Seismic Design of Abutments," Applied Technology Council Workshop on the Research Needs of Seismic Problems Related to Bridges, January 1979.

13. Evans, G.L., "The Behavior of Bridges Under Earthquakes," Proceedings of the New Zealand Roading Symposium, Victoria University, Vol. 2, (1971), pp. 664-684.
14. Libby, J.R. et al., "Typical Configuration of Bridges in the United States," Applied Technology Council Workshop on the Research Needs of Seismic Problems Related to Bridges, January 1979.
15. Priestly, M.J.N. and Park, R., "Seismic Resistance of Reinforced Concrete Columns," Applied Technology Council Workshop on the Research Needs of Seismic Problems Related to Bridges, January 1979.
16. Munro, I.R.M., "Seismic Behavior of Reinforced Concrete Bridge Piers," M.E. Report, Department of Civil Engineering, University of Canterbury, New Zealand, Research Report 76-9, February 1976, 106 pp.
17. Priestly, J.J.N., Park, R., Davey, B.E., and Murno, I.R.M., "Ductility of Reinforced Concrete Bridge Piers," Proceedings of the 6th World Conference on Earthquake Engineering, New Delhi, January 1977, 6 pp.
18. Davey, B.E., "Reinforced Concrete Bridge Piers Under Seismic Loading," M.E. Report, Department of Civil Engineering, University of Canterbury, New Zealand, Research Report 75-3, 1975.
19. Imbsen, R.A. and Schamber, R.A., "Increased Seismic Resistance of Highway Bridges Using Improved Bearing Design Concepts," Vol. I, ECC, December, 1981.
20. Tseng, W.C. and Penzien, J., "Analytical Investigation of the Seismic Response of Long Multiple Span Highway Bridges," EERC-73/12, Earthquake Engineering Research Center, University of California, Berkeley, CA, 1973.
21. Chen, M.C. and Penzien, J., "Analytical Investigation of Seismic Response of Short, Single or Multiple Span Highway Bridges," EERC 75-4, Earthquake Engineering Research Center, University of California, Berkeley, CA, 1975.
22. Chen, M.C. and Penzien, J., "Nonlinear Soil-Structure Interaction of Skew Highway Bridges," EERC-77/24, Earthquake Engineering Research Center, University of California, Berkeley, CA, 1977.
23. Douglas, B.M., Saiddi, M., and Richardson, J., "Dynamic Response of Highway Bridges," Proceedings U.S. - P.R.C. Bilateral Workshop on Earthquake Engineering, Harbin, China, August 30, 1982, pp. B-7-1 to B-7-15.
24. Nandakumarau, P. and Joshi, V.H., "Static and Dynamic Active Earth Pressures Behind Retaining Walls," Bulletin, The Indian Society of Earthquake Technology, 10, 3 Paper No. 136, September 1973.

25. Yeh, C.S., "Dynamic Response of Retaining Walls During Earthquake," Proceedings, International Symposium on Earthquake Structural Engineering, Vol. I.
26. Gilles, A.G. and Shepherd, R., "Dynamic Inelastic Analyses of a Bridge Structure," Bulletin of the Seismological Society of America, Vol. 71, No. 2, April 1981, pp. 517-530.
27. Jennings, D.N., "Research Requirements Related to the Design of Seismic Resistant Highway Bridges," Bulletin of the New Zealand National Society for Earthquake Engineering, Vol. 15, No. 3, September 1982.
28. Roeder, C.W. and Stanton, J.F., "Elastomeric Bearings: State of the Art," Journal of Structural Engineering, Vol. 109, No. 12, December 1983.
29. Tseng, W.S. and Penzien, J., "Analytical Investigations of the Seismic Response of Long Multiple-Span Highway Bridges," Report No. EERC 73-12, Earthquake Engineering Research Center, University of California, Berkeley, CA, January 1974.
30. Chen, M.C. and Penzien, J., "Nonlinear Soil-Structure Interaction of Skew Highway Bridges," Report No. UCB/EERC-77/24, Earthquake Engineering Research Center, University of California, Berkeley, CA, August 1977.
31. Chen, M.C. and Penzien, J., "An Investigation of the Effectiveness of Existing Bridge Design Methodology in Providing Adequate Structural Resistance to Seismic Disturbances Phase III: Analytical Investigations of Seismic Response of Short-, Single-, or Multiple-Span Highway Bridges," Report No. FHWA-RD-75-10, October 1974.
32. Gates, J.H. and Imbsen, R.A., "Recent Innovations in Seismic Design and Analysis Techniques for Bridge Structures," Proceedings, 42nd Annual Convention, Structural Engineers Association of California, Coronado, CA, October 4-6, 1973.
33. Gates, J.H., "California's Seismic Design Criteria for Bridges," Journal, A.S.C.E., Structural Division ST-12, December 1976.
34. Gill, W., "Ductility of Rectangular Reinforced Concrete Columns with Axial Load," Research Report, Department of Civil Engineering, University of Canterbury, 1979.
35. Rojahn, C. and Raggett, J.D., "Guidelines for Strong-Motion Instrumentation of Highway Bridges," Report No. FHWA/RD-82/016, U.S. Department of Transportation, Federal Highway Administration.
36. Gates, J.H. and Smith, M.J., "Verification of Dynamic Modeling Methods by Prototype Excitation," Report No. FHWA/CA/SD-82/07, California Department of Transportation.

37. "Earthquake Resistance of Highway Bridges," Applied Technology Council, January 1979.
39. "Seismic Design Guidelines for Highway Bridges," Applied Technology Council, October 1981.
38. "Comparison of United States and New Zealand Seismic Design Practices for Highway Bridges," Applied Technology Council, August 1982.
40. Cal-Trans, "Standard Plans," January 1981.
41. "Seismic Design of Highway Bridges," Workshop Manual, Report No. FHWA-1P-81-2, U.S. Department of Transportation, Federal Highway Administration, January 1981.
42. Lambe, T.W. and Whitman, R.V. Soil Mechanics, John Wiley & Sons.
43. Scott, R.F., Foundation Analysis, Prentice-Hall.
44. Roark, R.J. and Young, W.C., Formulas for Stress and Strain, McGraw-Hill.
45. Boyce, W.E. and DiPrima, R.C., Elementary Differential Equations and Boundary Value Problems, John Wiley & Sons.
46. Wang, C.K. and Salmon, C.G., Reinforced Concrete Design, International Textbook Company.
47. Spiegel, M.R., Mathematical Handbook of Formulas and Tables, McGraw-Hill Book Company.
48. Grossman, S.I., Calculus, Academic Press

APPENDIX A

ESTIMATION OF ULTIMATE BENDING MOMENTS

1. ESTIMATION OF THE ULTIMATE BENDING MOMENTS IN THE Y-DIRECTION

The balanced condition (Ref. 46) is examined first. The forces taken by the reinforcement bars in this condition are shown in Table A.1. The total force taken by the reinforcement steel is equal to: $C_S = 402.01t$. The force taken by the concrete is $C_C = 1339.3t$. Adding, the ultimate capacity of the cross section in the balanced condition is 1741.35. This is bigger than the compressive force which acts on the cross section ($P_C = 965t$). Therefore, the capacity of the cross section is controlled by the tension in the reinforcement steel. By using the trial and error method, the width of the compression zone, which corresponds to a total compressive force close to $P_C = 965t$, is found to be $X_b \approx 0.591m$. In fact, the above value of X_b corresponds to an ultimate capacity in compression of $P_u = C_S + C_C = -51.33 + 1010.18 = 959.46 \approx 965t$. The forces taken by the reinforcement bars when $X_b = 0.591$ are shown in Table A.2 while the value of the compressive force taken by the concrete, along with its point of application, are shown in Fig. A.1a. For this distribution of forces, the ultimate moment capacity can be found:

$$M_{u,1} = 1315 \text{ tm.}$$

(The subscript 1 denotes the bottom cross section.)

Top Cross Section

Examination of the balanced condition shows again that the capacity of the cross section is controlled by tension in the reinforcement steel. Following the same procedure used in the case of the bottom cross section, one finds that a value of $X_b = 0.922$ gives an ultimate

capacity in compression of $P_u = C_s + C_c = -784.762 + 1730.92 = 946t$ which is close to the compressive force of 965t. Table A.3 and Fig. A.1b show the forces taken by the reinforcement bars and the concrete, respectively, when $X_b = 0.922$. The ultimate moment capacity in this case is found to be:

$$M_{u,2} = 3029.30 \text{ tm.}$$

2. EVALUATION OF THE ULTIMATE BENDING MOMENT IN THE X-DIRECTION

Bottom Cross Section

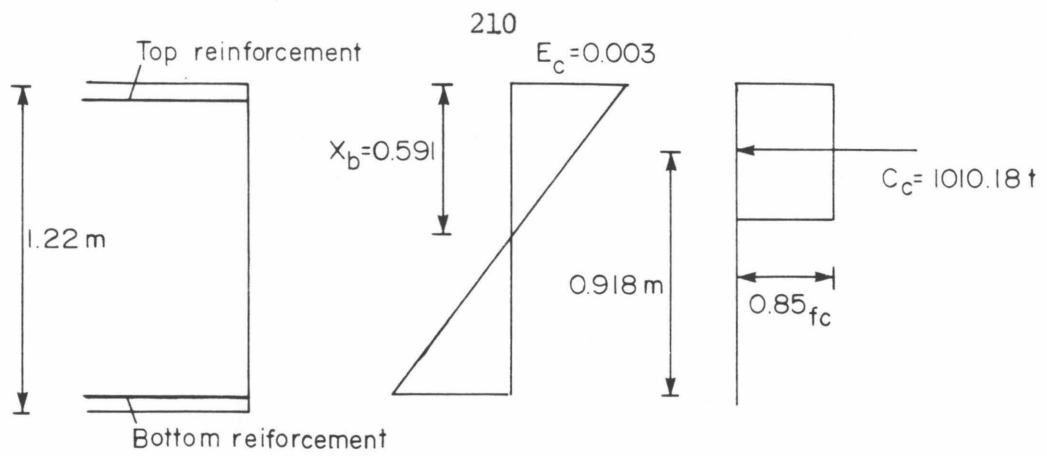
Due to the symmetry of the bottom cross section, its ultimate moment capacity for bending about the X-direction will be the same as the Y-direction, i.e.,

$$M_{u,1} = 1315 \text{ tm.}$$

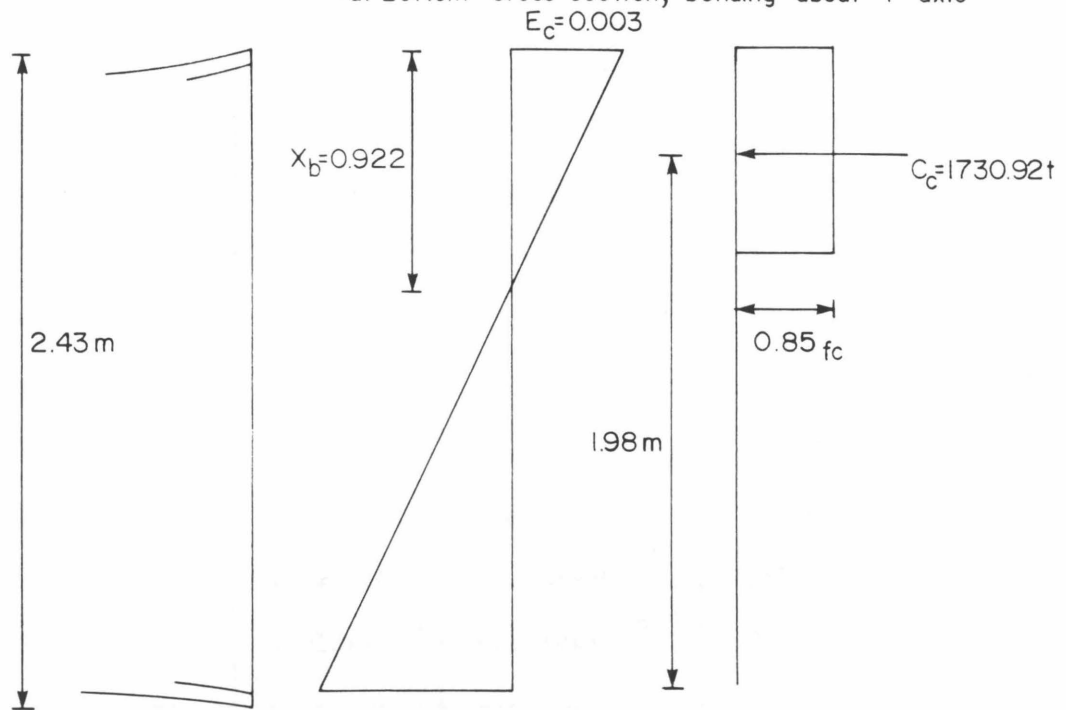
Top Cross Section

Choosing $X_b = 0.43$ gives an ultimate capacity in compression of $P_u = C_s + C_c = -623.85 + 1586.63 = 962.78 \approx 965t$. Table A.4 and Fig. A.1c show the forces of the reinforcement bars and the concrete, respectively. The ultimate moment capacity in this case is:

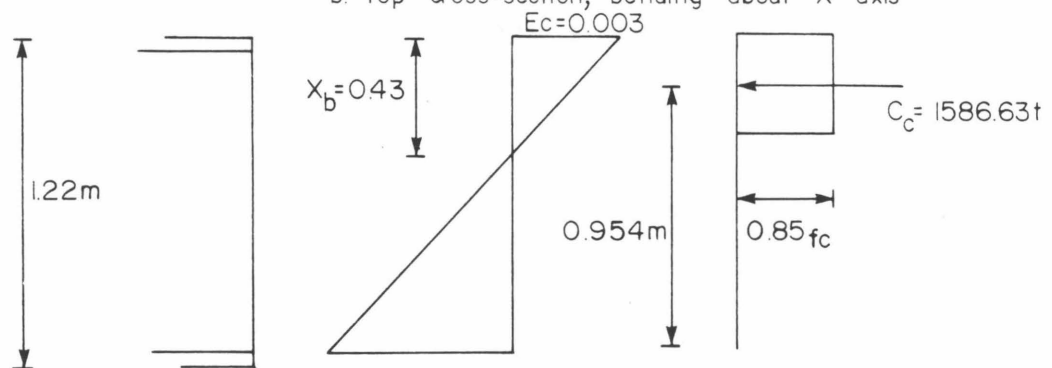
$$M_{u,2} = 1699 \text{ tm.}$$



a. Bottom cross-section, bending about Y axis



b. Top cross-section, bending about X axis



c. Top cross section, bending about X axis

FIG. A.1 MAGNITUDE AND POSITION OF CONCRETE FORCES

TABLE A.1: STRESSES OF REINFORCEMENT BARS IN BALANCED CONDITION				
Position of bar (Distance from the top of the cross section)	Area (m ²)	Deformation	Stress t/m ²	Force (t)
0.0508	2,013x10 ⁻³	2.79x10 ⁻³	35153.5	70.764
0.1438	4,026x10 ⁻³	2.7x10 ⁻³	35153.5	141.53
0.2368	4,026x10 ⁻³	2.043x10 ⁻³	35153.5	141.53
0.3298	4,026x10 ⁻³	1,667x10 ⁻³	33340	134.22
0.4228	4,026x10 ⁻³	1,291x10 ⁻³	25820	103.95
0.5158	4,026x10 ⁻³	0.91x10 ⁻³	18200	73.27
0.6088	4,026x10 ⁻³	0.54x10 ⁻³	10800	43.48
0.7018	4,026x10 ⁻³	0.1644x10 ⁻³	3288	13.23
0.7948	4,026x10 ⁻³	-0.21x10 ⁻³	-4200	-16.90
0.8878	4,026x10 ⁻³	-0.587x10 ⁻³	11740	-47.26
0.9808	4,026x10 ⁻³	-0.96x10 ⁻³	19200	-77.3
1.0738	4,026x10 ⁻³	-1.338x10 ⁻³	26760	-107.73
1.1668	2.013x10 ⁻³	-1.714x10 ⁻³	35153.5	-70.764

TOTAL FORCE

402.01t

TABLE A.2: BENDING ABOUT Y-AXIS—BOTTOM CROSS SECTION				
STRESSES OF THE REINFORCEMENT BARS WHEN $X_b = 0.591m$				
Position of bar (Distance from the top of the cross section)	Area (m^2)	Deformation	Stress t/m^2	Force (t)
0.0508	$2,013 \times 10^{-3}$	2.74×10^{-3}	35153.5	70.764
0.1438	$4,026 \times 10^{-3}$	$2,27 \times 10^{-3}$	35153.5	141.53
0.2368	$4,026 \times 10^{-3}$	1.79×10^{-3}	35153.5	141.53
0.3298	$4,026 \times 10^{-3}$	1.325×10^{-3}	26517.76	107.61
0.4228	$4,026 \times 10^{-3}$	0.85×10^{-3}	17076.14	69.3
0.5158	$4,026 \times 10^{-3}$	0.38×10^{-3}	7634.51	30.98
0.6088	$4,026 \times 10^{-3}$	-0.09×10^{-3}	-1807.1	-7.33
0.7018	$4,026 \times 10^{-3}$	-0.502×10^{-3}	-11248.73	-45.647
0.7948	$4,026 \times 10^{-3}$	-1.034×10^{-3}	-20690.35	-83.96
0.8878	$4,026 \times 10^{-3}$	-1.5×10^{-3}	-30131.97	-122.275
0.9808	$4,026 \times 10^{-3}$	-1.97×10^{-3}	-35153.5	-141.53
1.0738	$4,026 \times 10^{-3}$	-2.45×10^{-3}	-35153.5	-141.53
1.1668	2.013×10^{-3}	-1.714×10^{-3}	-35153.5	-70.765

TOTAL FORCE

-51.33

TABLE A.3: BENDING ABOUT Y-AXIS---TOP CROSS SECTION				
STRESSES OF REINFORCEMENT BARS WHEN $X_b = 0.922$				
Position of bar (Distance from the top of the cross section)	Area (m^2)	Deformation	Stress t/m^2	Force (t)
0.0508	0.001019	2.836×10^{-3}	35153.5	35.82
0.2522	0.001019	2.18×10^{-3}	35153.5	35.82
0.4536	0.001019	1.53×10^{-3}	30735.48	31.3194
0.655	0.00302	0.887×10^{-3}	17741.93	53.58
0.748	0.004058	0.587×10^{-3}	11741.93	47.64
0.841	0.004058	0.287×10^{-3}	5741.93	23.30
0.934	0.004058	-0.0129×10^{-3}	-258.064	-1.047
1.027	0.004058	-0.313×10^{-3}	-6258.064	-25.4
1.1248	0.004058	-0.613×10^{-3}	12258.064	-49.74
1.2178	0.004058	-0.90×10^{-3}	18064.51	-73.3058
1.306	0.004058	-1.213×10^{-3}	24258.064	-98.44
1.399	0.004058	-1.513×10^{-3}	30258.064	-122.78
1.4928	0.004058	-1.81×10^{-3}	35153.5	-142.65
1.585	0.004058	-2.113×10^{-3}	35153.5	-142.65
1.678	0.004058	-2.41×10^{-3}	35153.5	-142.65
1.777	0.00302	-2.73×10^{-3}	35153.5	-106.12
1.9744	0.001019	-3.37×10^{-3}	35153.5	-35.82
2.1758	0.001019	-4.018×10^{-3}	35153.5	-35.82
2.3772	0.001019	-4.67×10^{-3}	35153.5	-35.82

TOTAL FORCE

-784.761

TABLE A.4: BENDING ABOUT X-AXIS---TOP CROSS SECTION				
STRESSES OF REINFORCEMENT BARS WHEN $X_b = 0.43$				
Position of bar (Distance from the top of the cross section)	Area (m^2)	Deformation	Stress t/m^2	Force (t)
0.0508	0.00303224	2.64×10^{-3}	35153.5	106.59
0.144	0.004058	1.99×10^{-3}	35153.5	142.653
0.2372	0.004058	1.345×10^{-3}	26902.32	109.17
0.3304	0.004058	0.7×10^{-3}	13897.67	56.4
0.4236	0.004058	0.0446×10^{-3}	893.023	3.623
0.5168	0.004058	-0.60×10^{-3}	12111.62	-49.149
0.61	0.004058	-1.255×10^{-3}	25116.28	-101.92
0.7032	0.004058	-1.90×10^{-3}	35153.5	-142.90
0.7964	0.004058	-2.5×10^{-3}	35153.5	-142.65
0.8896	0.004058	-3.2×10^{-3}	35153.5	-142.65
0.9828	0.004058	-3.8×10^{-3}	35153.5	-142.65
1.076	0.004058	-4.5×10^{-3}	35153.5	-142.65
1.1692	0.00303224	-5.15×10^{-3}	35153.5	-106.59
0.1903	0.001019	1.67×10^{-3}	33446.51	34.093
0.3298	0.001019	0.7×10^{-3}	13981.4	14.25
0.5158	0.001019	-0.6×10^{-3}	11972.09	-12.2
0.7018	0.001019	-1.89×10^{-3}	35153.5	-35.83
0.8878	0.001019	-3.19×10^{-3}	35153.5	-35.83
1.0273	0.001019	-4.16×10^{-3}	35153.5	-35.83

TOTAL FORCE

-623.85

APPENDIX B

EVALUATION OF FOUNDATION SPRING CONSTANTS AND SOIL PROPERTIES

1. EVALUATION OF FOUNDATION SPRING CONSTANTS

The values of the foundation springs can be estimated by the formulas shown in Table B.1 (Ref. 41). These formulas are applicable to rectangular foundations, and values of the coefficients appearing in these formulas are given in Fig. B.1 (Ref. 41).

2. SOIL PROPERTIES

The properties of stiff soil, which were used in the example of Chapter 4, are shown in Table B.2 (personal communication with Professor R.F. Scott and Ref. 42).

TABLE B.1 SPRING CONSTANTS FOR RIGID RECTANGULAR BASE RESTING ON ELASTIC HALF-SPACE	
Motion	Spring Constant
Vertical	$k_Z = \frac{G}{1 - \mu} \beta_Z (BL)^{1/2}$
Horizontal	$k_X = 2(1 + \mu)G\beta_X (BL)^{1/2}$
Rocking	$k_\phi = \frac{G}{1 - \mu} \beta_\phi BL^2$

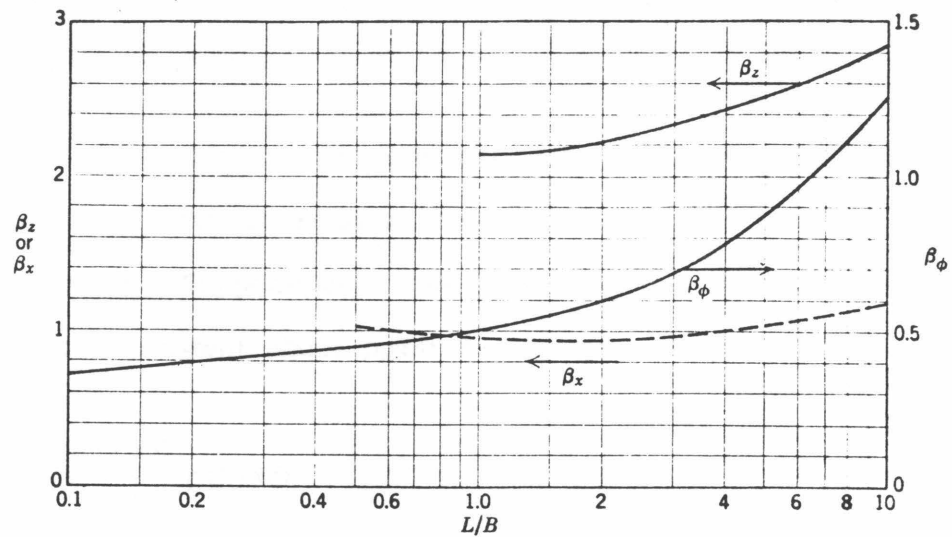


Fig. B.1 SPRING CONSTANT COEFFICIENTS FOR RECTANGULAR FOUNDATIONS (Ref. 42)

TABLE B.2 PROPERTIES OF STIFF SOIL	
Poisson Ratio (ν)	0.45
Shear Wave Velocity (V_S)	1500 f/sec = 457 m/sec
Unit Weight (γ_S)	125 p/f ³ = 2 t/m ³
Friction Angle (ϕ)	40°
Cohesion (c)	0 - 1000 p/f ² = 0 - 4.88 t/m ²
Subgrade Constants	
n_w (Ref. 43, pg. 259)	40 t/f ³ = 1412 t/m ³
k_o (Ref. 43, pg. 251)	3.8 t/f ³ = 135 t/m ³

3. EVALUATION OF THE TORSIONAL SOIL SPRING AT THE BOTTOM OF THE ABUTMENTS

The torsional soil spring at the bottom of the abutments, k_ϕ , can be approximately evaluated as follows. Let c be the total width of the abutment base. Suppose that the base rotates as shown in Fig. B.2. Then, the total moment about point A will be:

$$M = \int_0^c p(X)X dX \quad (B.1)$$

where

$$p(X) = kX \quad (B.2)$$

The value of k is assumed to be equal to the value of the horizontal subgrade reaction coefficient of the bottom of the abutment. Thus,

$$k = k_w + n_w \frac{z}{l} \Big|_{l=z}$$

or

$$k = k_w + n_w \quad (B.3)$$

Combining (B.1), (B.2), and (B.3) yields

$$M = (k_w + n_w) \frac{c^3}{3} \quad (B.4)$$

From (B.4), one gets:

$$k = (k_w + n_w) \frac{c^3}{3}$$

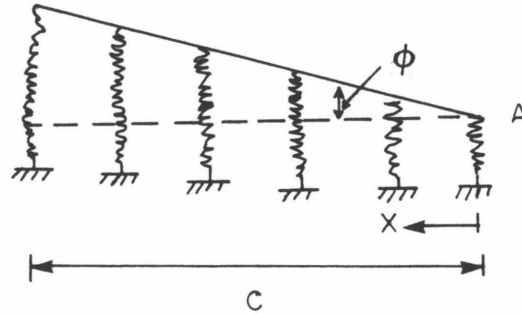


FIG. B.2 EVALUATION OF THE TORSIONAL SOIL SPRING AT THE BOTTOM OF THE ABUTMENTS